Radiolabelled Copper Complexes For Cancer Imaging

Rebekka Hueting

A thesis submitted in part fulfilment of the requirements for the degree of Doctor of Philosophy in Chemistry at the University of Oxford

Oriel College, Oxford

Trinity Term 2011

Author's Declaration

The work presented in this thesis was carried out in the Chemistry Research Laboratory at the University of Oxford between Michaelmas Term 2007 and Trinity Term 2011, under the joint supervision of Professor Véronique Gouverneur, Professor Jonathan R. Dilworth and Dr Martin Christlieb. All of the work is my own, except where stated otherwise, and has not been submitted for any other degree at this or any other university.

Rebekka Hueting

July 2011

Radiolabelled Copper Complexes for Cancer Imaging

Rebekka Hueting
Oriel College

submitted for DPhil
Trinity Term 2011

Chapter One introduces molecular imaging and the modalities available for oncological imaging. The radioisotopes and imaging agents for Positron Emission Tomography (PET) and Single Photon Emission Computed Tomography (SPECT) are discussed together with the bifunctional chelator approach for radiolabelling of biomolecules. Finally, the chemistry and radioisotopes of copper are described, and copper bis(thiosemicarbazonato) complexes introduced in the context of PET imaging.

Chapter Two describes the synthesis and characterisation of novel carboxylate- and maleimide-functionalised bis(thiosemicarbazonates) and their conjugation to biologically active molecules. Radiolabelling of a chelator-bombesin conjugate demonstrated site-specific labelling at room temperature and preliminary *in vitro* and *in vivo* studies confirmed its potential as an imaging agent. Bioconjugation to a model protein and subsequent radiolabelling was also investigated.

Chapter Three introduces molecular imaging of hypoxia with a focus on CuATSM. An overview of the currently accepted mechanism of hypoxia selectivity is presented. The emphasis is placed on the relationship between oxygenation status, uptake and retention which display cell- and tumour-line dependency.

Chapter Four presents the synthesis of copper bis(thiosemicarbazonates), radiolabelled either at the *metal* (^{64}Cu) or at the *ligand* (^{18}F or ^{123}I) for mechanistic studies. The physicochemical characteristics of the copper complexes were measured and the complexes evaluated for their *in vitro* hypoxia selectivity.

Chapter Five describes *in vitro* and *in vivo* studies of the orthogonally radiolabelled complexes, inclusive of control experiments with [^{64}Cu]CuATSM, the radiolabelled proligand and [^{64}Cu]Cu^{2+} salts. *In vitro* cellular assays, as well as *in vivo* biodistribution studies including dynamic PET and SPECT were performed. Stability studies contrasting the *in vitro* and *in vivo* behaviour were carried out. The collective data suggest that the currently proposed redox trapping mechanism might not provide a full understanding of the factors governing biodistribution and tumour uptake.

Chapter Six contains full experimental details for the work described in this thesis.

Acknowledgements

First and foremost I would like to thank my supervisors Jon, Veronique and Martin. It has been a privilege to study at Oxford and I am grateful for their continuous guidance and all they have taught me. I would like to thank Jon also for his support and encouragement not only during my DPhil, but throughout my entire undergraduate studies at Oxford.

I would like to acknowledge the Gray Lab Research Trust and GlaxoSmithKline for funding. In particular, I would also like to thank my industrial supervisors Prof Antony Gee and Dr Jan Passchier for invaluable discussions. Further, I would like to thank Prof Ruth Muschel, Prof Sir Mike Brady and Dr Sean Smart for their firm support of the project.

I am very grateful to Dr Veerle Kersemans and Dr Bart Cornelissen for the huge effort on the biological investigations. Without all your help and expertise and incredible teamwork, often late into the night, this thesis would be somewhat shorter. It has been a lot of fun working with you and more importantly having you as friends. Thank you!

My thanks go to Dr Parvinder Aley and Dr Grant Churchill for introducing me to microscopy and tissue culture. I would like to thank Dr Robert King, Miss Kamila Hussien and Dr Nadia Falzone for help with *in vitro* biological work and Dr Danny Allen for help with image processing. Thanks go to Dr Michael Jones for supervision in the lab, crystallography and EPR studies. I would like to thank Mrs Maria Marshall for help with HPLC, Dr Nick Rees and Dr Barbara Odell for NMR, Dr Robin Proctor and Mr Colin Sparrow for mass spectrometry.

I am grateful to Prof Dirk Tourwé and Dr Veronique Maes for the opportunity to work at Vrije Universiteit Brussels. Prof Roger Schibli and Dr Elisa Garcia-Garayoa are acknowledged for biological work on the bombesin project. I would also like to thank Dr Greg Mullen and Dr Richard Tavaré at KCL for the opportunity of participating with the C2A protein labelling.

I would like to thank the entire Dilworth and Gouverneur groups for being so helpful and making work in the Oxford Chemistry Laboratories so enjoyable. The entertaining dinners and ski-trips will not be forgotten!

Thanks to Antonia, Thomas and Dominik for your friendship and support and never being further than a phone call away. Thanks also go to Oriel College Womens' Boat Club for managing to occasionally drag me out of the lab.

A really huge thank you must go to Dr Matthew Tredwell for absolutely everything from marathon radiolabelling sessions to proof-reading this entire thesis, but more importantly for cuppas, owls and always being there.

I am very grateful to my brother Nikolai not only for 24 hour computer support, but also for fun times on holidays, days away in Bristol, and mostly for being a calming influence and having a brilliant sense of humour.

Finally, my thanks must go to my parents. Without all your love and continuous support none of this would have been possible.

„Da steh ich nun, ich armer Tor! Und bin so klug als wie zuvor.“

Johann Wolfgang von Goethe in *Faust I, 358*

Für Mama, Papa und Niko

Contents

Abbreviation	Meaning
A	Amps
Ar	aryl
Arg	arginine
BAM	biologically active molecule
BFC	bifunctional chelator
Boc	*tert*-butoxycarbonyl
BOP	Benzotriazol-1-yl-oxytris(dimethylamino)phosphonium hexafluorophosphate
btsc	*bis*(thiosemicarbazone)
calc.	calculated
COSY	correlation spectroscopy
cps	counts per second
CT	computed tomography
CV	cyclic voltammetry
DCC	*N*,*N'*-dicyclohexylcarbodiimide
DFT	density functional theory
DIPEA	Diisopropylethylamine
DMEM	Dulbecco's modified Eagle's Medium
DMF	*N*,*N*,-dimethylformamide
DMSO	dimethylsulfoxide
DOTA	1,4,7-10-tetraazacyclododecane-1,4,7,10-tetraacetic acid
DTPA	diethylenetetraamine pentaacetic acid
$E_{1/2}$	half wave potential
EC	electron capture
EDCI	1-ethyl-3-(3-dimethylaminopropyl)carbodiimide
EPR	electron paramagnetic resonance
ESI^+	positive ion electrospray
ESI^-	negative ion electrospray
Et	ethyl, CH_2CH_3
EtOAc	ethyl acetate
EtOH	ethanol
FBS	Foetal Bovine Serum
FDA	United Stated Food and Drug Administration
FDG	fluoro-deoxyglucose
FMISO	fluoromisonidazole
Fmoc	9-fluorenylmethoxycarbonyl
GBq	Gigabequerel
Glut	Glutamic acid
Gly	glycine
h	hours
His	histidine
HMBC	heteronuclear multiple bond correlation
HMQC	heteronuclear multiple quantum correlation

i_p	peak current
i.v.	intravenous
HPLC	high performance liquid chromatography
Leu	leucine
Log P	water/octanol partition coefficient
mg	milligram
MBq	Megabequerel
Me	methyl, CH_3
MeCN	acetonitrile
MeOH	methanol
MeV	megaelectron volts
Met	methionine
min	minutes
mL	millilitre
mM	millimolar
mmol	Millimoles
MRI	magnetic resonance imaging
NHE	normal hydrogen electrode
NHS	National Health Service, and *N*-hydroxysuccinimide
nm	nanometre
NMR	nuclear magnetic resonance
OAc	acetate
PET	positron emission tomography
Ph	phenyl
ppm	parts per million
rt	room temperature
R_t	retention time
RTM	tumour-to-muscle ratio
s	seconds
SCE	saturated calomel electrode
SOD	superoxide dismutase
SPECT	single photon emission computed tomography
t	time
TBAF	Tetrabutylammonium fluoride
TETA	1,4,8,11-tetraazacyclotetradecane-1,4,8,11-tetraacetic acid
TFA	trifluoroacetic acid
THF	tetrahydrofuran
TLC	thin layer chromatography
Trt	trityl, triphenylmethyl
UV	ultraviolet
V	volts
VEGF	vascular endothelial growth factor

Chapter 1
Introduction

1.1 Medical Imaging

1.1.1 Impact of Medical Imaging on Clinical Medicine

Many advances in modern medicine can be attributed to the success of proteomic and genomic research in identifying molecular and cellular changes that occur as a result of disease. Medical imaging provides non-invasive methods to detect, investigate and monitor disease specific aberrations. Since the accidental discovery of X-rays by Roentgen in 1895, conventional X-ray and X-ray computed tomography (CT) have become indispensable in routine clinical practice to provide anatomical information. These are now being complemented by so-called molecular imaging (MI) modalities. These enable "the visualization, characterization and measurements of biological processes at the molecular and cellular level in humans and other living systems".[1, 2] MI is non-invasive and yields information that may otherwise require tissue sampling, excision or fluid analysis. It also allows repeated imaging to monitor disease progression or treatment success. Since molecular imaging can be used to follow a suitably (radio-)labelled drug to and at its target sites *in vivo*, it has found also applications in drug development for determining a drug's mechanism of action, possible metabolites, dose regimens and treatment protocols.[3, 4]

1.2 Molecular Imaging in Cancer

1.2.1 Cancer Biology

Cancer is not a single disease but represents a collection of more than one-hundred different diseases that cause the transformation of normal cells into malignant neoplasm.[5] Carcinogenesis firstly involves changes at the genetic level (initiation). Genetic damage such as a point mutation, gene rearrangement or gene deletion occurs which causes cells to become cancerous (promotion).[5, 6] The cells can then undergo profound biochemical changes and become immortalized and evade surveillance by the human immune system (progression). Most cancers involve formation of solid mass lesions, whose size and location can be detected with radiological imaging (X-ray, CT, MRI, Ultrasound). However, anatomical imaging can miss small cancers and is unable to distinguish between benign and malignant lesions, or indeed lesion from normal tissue. Following the changes

in the genotype, so called phenotypic changes occur, such as increased glucose metabolism, angiogenesis and increased receptor expression (Table 1). These alterations often precede the formation of solid mass lesions. Molecular imaging techniques such as Positron Emission Tomography (PET) and Single Photon Emission Computerised Tomography (SPECT) offer the possibility of imaging these molecular and functional changes. Radiotracers are being developed that target a specific biological process and help to characterise the tumour biology. Nuclear medicine imaging techniques thus provide high sensitivity and specificity which complement the high resolution achieved through anatomic imaging. Diagnosis can thus be made earlier and more accurately than with anatomical techniques alone, facilitating individualised patient management.

Function	**Increased**	**Decreased**
Glucose metabolism	✓	
Amino Acid Transport	✓	
Protein Synthesis	✓	
DNA Synthesis	✓	
Blood Flow	✓	✓
Receptor Expression	✓	
Oxygen tension		✓
Hypoxia	✓	
Apoptosis	✓	✓
Angiogenesis, vascular density	✓	
Vascular permeability	✓	
Oncogene products	✓	
Many other genetic markers	✓	✓

Table 1 Molecular and functional alterations in cancer. Adapted from references. [5, 6]

A variety of targeting groups have been investigated as biomarkers to visualise the above disease characteristics. Radiolabelled amino-acids and sugars may be used in order to detect increased amino acid transport and increased glycolysis, whilst radiolabelled nucleosides analogues can interact in the DNA synthesis pathway and thus provide a non-invasive measure of proliferation.[7] Several cancers overexpress receptors either on the cell membrane (neuroendocrine tumours) or within the cells (oestrogen receptors in breast cancer) and radiolabelled variants of drug molecules and peptides that bind to these receptors can be used for imaging.[5, 6]

Larger radiolabelled biomolecules such as proteins and antibodies bind to tumour associated antigenic binding sites.[5, 8 9] Since a detailed discussion of imaging biomarkers is beyond the scope of this introduction, selected examples throughout will aim to highlight the application of such molecules to molecular imaging using PET and SPECT.

1.3 Molecular Imaging Modalities

A range of modalities is available for molecular imaging. Whilst each of the techniques summarised in Table 2 has its strengths, no single technique is universally suitable for all clinical applications. Hence, recent efforts have also considered dual modality approaches to improve diagnosis, for instance by combining the high resolution of MRI with the high sensitivity of PET and integrated whole-body PET/MRI scanners have already been used clinically.[10, 11] The work presented in this thesis relates to PET and SPECT. Therefore, CT and MRI are explained briefly in the context of anatomical referencing but due to space limitations, other techniques will not be discussed.

Technique	Resolution	Depth	Time	Imaging Agent	Target*	Rel. Cost
MR	10-100 µm	no limit	min-hours	Gd^{3+}, Fe^{3+}	A, P, M	£££
CT	50 µm	no limit	min	Iodine, Ba^{2+}	A, P	££
Ultrasound	50 µm	<10 cm	real-time	Microbubbles	A, P	££
PET	1-2 mm	No limit	min	^{18}F, ^{11}C, ^{15}O	P, M	£££
SPECT	1-2 mm	No limit	min	^{99m}Tc, ^{111}In, ^{123}I	P, M	££
Fluoroscopy	1 mm	No limit	real-time	Ba^{2+}	A, P	£

*A, anatomical; P, physiological; M, molecular.

Table 2 Overview of clinically used medical imaging techniques. Adapted from reference 3.

1.3.1 Single Photon Emission Computerised Tomography (SPECT)

SPECT imaging relies on the emissions of γ-rays from a radionuclide. The photons are detected using a gamma camera that collects multiple 2D images at several angles around the object, before tomographically reconstructing these into a 3D image. In order to accurately determine the origin of the γ-ray, collimators are fitted to exclude incident rays outside a small angular range. Collimators typically only detect 1 in 5000 photons which reduces signal intensity compared to

PET where no collimation is required. In contrast to PET, where resolution is governed by the positron range, resolution in SPECT is only limited by technology. New collimator designs, such as pinhole collimators can increase imaging resolution for small organs, human extremities and small animals to <1 mm, but depending on collimator design, these may compromise sensitivity and are not yet available for whole body human imaging. The use of combined SPECT/CT permits anatomical referencing of the SPECT image.

1.3.2 SPECT radionuclides

A range of SPECT radioisotopes that have been used clinically are summarised in Table 3.[12]

Radioisotope	Half life (h)	Production method	Emission Type	/ γ Energy (MeV)
^{123}I	13.2	Cyclotron ^{124}Xe (p,2p)	Electron Capture	/ 0.16 (see 1.3.2.2)
^{131}I	193	Reactor	β^- and γ	/ 0.364 γ, 0.6 β^-
^{99m}Tc	6	Generator ^{99}Mo (6d)	Isomeric Transition	/ 0.14
^{111}In	67.9	Cyclotron ^{109}Ag (α, 2n)	Electron Capture	/ 0.17/ 0.25
^{67}Ga	78.3	Cyclotron ^{65}Cu (α, 2n)	Electron Capture	/ 0.09/ 0.19/ 0.30

Table 3 Common SPECT radionuclides.[12]

1.3.2.1 Technetium-99m

Technetium-99m is often the SPECT isotope of choice as it is available at low cost and possesses favourable decay characteristics (140 keV, $t_{1/2}$ = 6.02 h) for imaging with commercially available γ-cameras. [^{99m}Tc]$TcO_4^-$$_{(aq)}$ is eluted from a ^{99}Mo/^{99m}Tc generator in saline for on-site radiopharmaceutical production using commercially available kits. The Tc is reduced to the required oxidation state in the presence of a ligand. The ^{99m}Tc-labelled complexes used in imaging can be divided into two categories. “Technetium essential” agents are those in which technetium incorporation determines the structure and physicochemical characteristics such as size, lipophilicity and charge that govern the biological behaviour. Neutral ^{99m}Tc-complexes are used for cerebral perfusion imaging, cationic for myocardial imaging and anionic for renal imaging; examples are depicted in Figure 1.

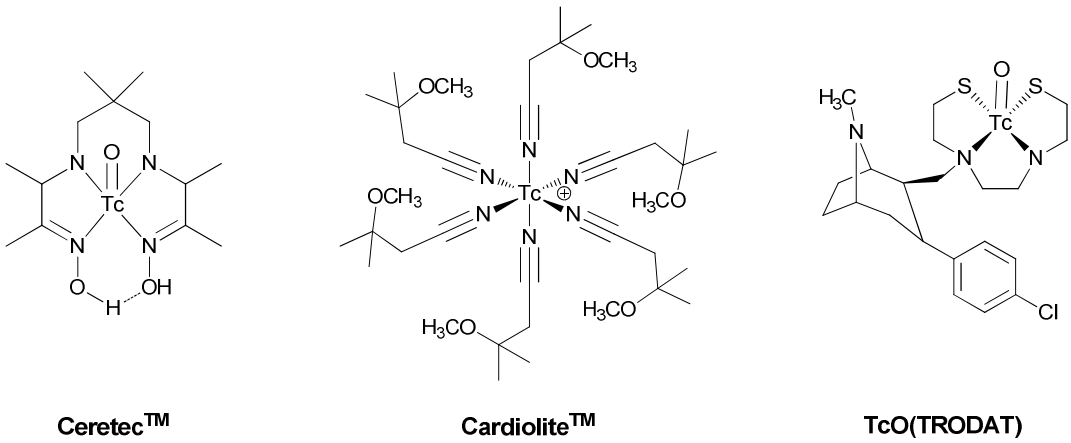

Figure 1 Structures of selected ^{99m}Tc radiopharmaceuticals.

An example of a technetium-tagged or "technetium non-essential" agent is [^{99m}Tc]Tc-Trodat, where a technetium chelator is conjugated to phenyltropane as a targeting vector for imaging dopamine receptors.

1.3.2.2 Iodine-123

^{123}I is most commonly produced by proton bombardment of ^{124}Xe using a medium sized biomedical cyclotron.[13] ^{123}Xe is formed and subsequently decays to elemental $^{123}I_2$ as shown in Scheme 1. ^{123}I is washed out of the target chamber as 123-iodide anion by elution with dilute sodium hydroxide in a halogen disproportionation reaction, before anion-exchange chromatography is used to concentrate the radioiodide and to harvest non-carrier added ^{123}I of high isotopic purity in 0.05 M NaOH. ^{123}I decays by electron capture with emission of γ radiation. The energy of the photons, 159 keV, is ideally suited to the excitation of the NaI (sodium iodide) crystal detector of current gamma cameras and for the pinhole collimators.[14]

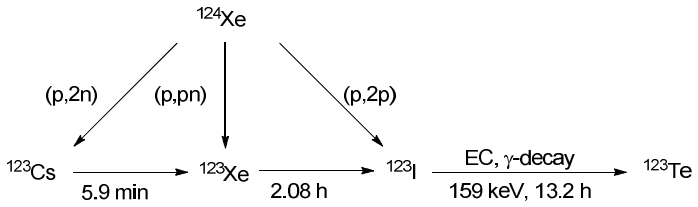

Scheme 1 (a) Decay scheme showing production and decay of ^{123}I SPECT isotope.[13]

^{123}I is not only more suitable for imaging purposes than the therapeutically used ^{131}I-isotope due to lower radiation burden, but allows higher count rates and better resolution,[15] and thus, its clinical use has increased in recent years. ^{123}I-ioflupane (DaTSCAN™) is used to differentiate essential tremor from Parkinsonian symptoms related to idiopathic Parkinson's Disease, as well as to distinguish dementia with Lewy bodies (DLB) from Alzheimer's disease.[16] [^{123}I]Metaiodobenzylguanidine (Adreview™) is a tracer that accumulates in adrenergic tissue and is used to identify neuroendocrine tumours, ischemic heart disease and drug-induced cardiotoxicity.[15, 17]

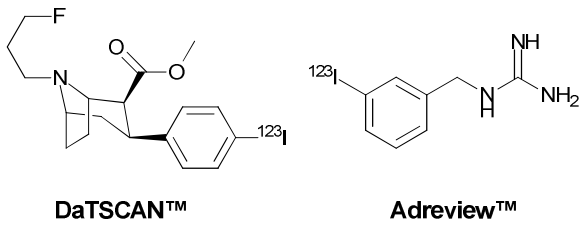

Figure 2 The clinically used ^{123}I-labelled radiotracers DaTSCAN™ and Adreview™.

1.3.3 Positron Emission Tomography (PET)

Positron Emission Tomography (PET) relies on the use of positron emitting isotopes. As the radionuclide decays, it ejects a positron from the nucleus that will travel a short distance depending on its kinetic energy before interacting with an electron. The resultant annihilation produces a pair of antiparallel 511 keV photons emitted at an angle of 179.5º – 180º that are detected by a circular array of detectors (Scheme 2).[5]

The detection method, known as annihilation coincidence detection (AOD), only detects (near) coincident pairs of photons, removing the need for mechanical collimation. This provides PET with higher resolution and increased sensitivity compared to its single-photon colleague SPECT. Typically, PET achieves a 2-3 mm resolution compared to 6-8 mm in SPECT.[18]

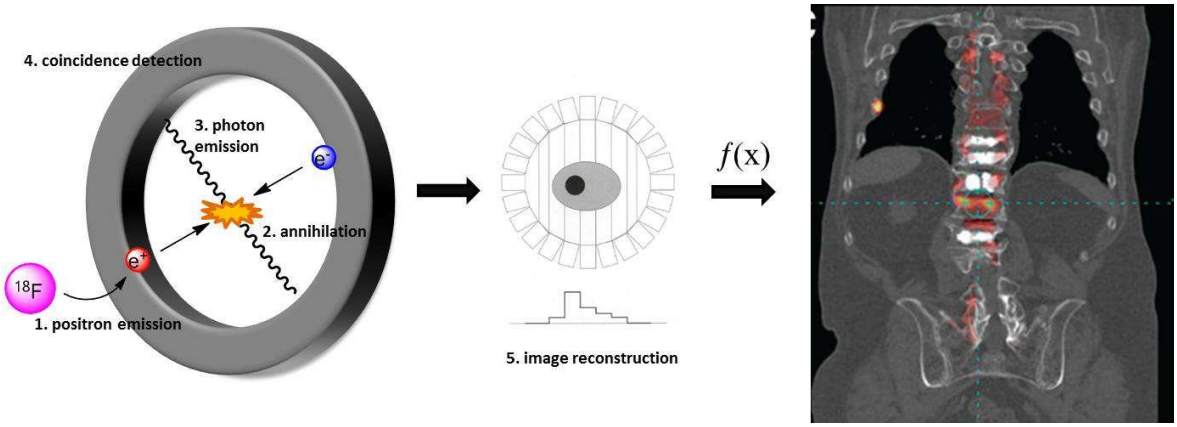

Scheme 2 Schematic representation of Positron Emission Tomography. The right image depicts a PET/CT image of an [^{18}F]NaF bone scan showing several compression fractures including the L1 superior endplate and right rib. Reprinted with permission from reference 19.

AOD determines a decay event within a line of response (LOR) along which the emission point is localised, tomographic reconstruction then calculates the point of emission to create a 3D image. Provided several corrections are applied (attenuation, scatter, random coincidences and dead time) PET can also provide quantitative information about regional radioactivity concentrations which enables kinetic modelling of the data.[6]

1.3.4 Conventional PET radionuclides

1.3.4.1 Fluorine-18

Fluorine-18 is the most widely used PET radionuclide and provides near ideal characteristics ($t_{1/2}$ = 110 min, β^+= 100%, 0.635 MeV) for high resolution PET. The accelerated use of PET and ^{18}F-PET in particular can attributed to the glucose metabolic tracer, [^{18}F]-2-fluoro-2-deoxy-D-glucose ([^{18}F]FDG), developed by Fowler and co-workers at Brookhaven.[20-22] [^{18}F]FDG is taken up into the cell *via* glucose transport proteins where it is phosphorylated to [^{18}F]FDG-6-phosphate. It cannot undergo glycolysis in the same manner as glucose-6-phosphate as the C-2 hydroxyl group essential for further metabolism has been replaced by ^{18}F, causing the tracer to become metabolically trapped. Although originally developed for imaging brain metabolism,[23] [^{18}F]FDG-PET has found applications mainly in oncology due to the increased glycolysis of cancer cells.

FDG is routinely used for diagnosis, staging and evaluating therapeutic response of cancers such as lymphoma, colorectal cancer, breast cancer and melanoma.[6, 24]

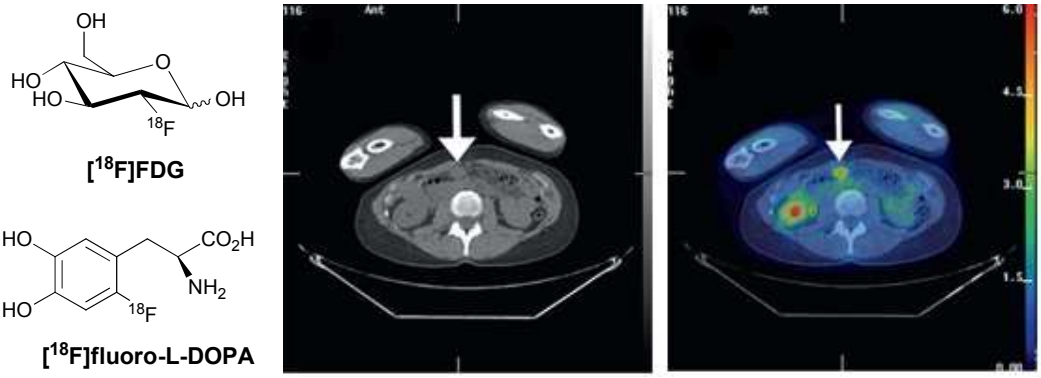

Figure 3 (left) Structures of [^{18}F]-2-fluoro-2-deoxy-D-glucose ([^{18}F]FDG) and [^{18}F]FDOPA (middle and right) CT and fused [^{18}F]FDG-PET/CT of a colorectal cancer patient with rising tumour markers as indicated by PET but negative conventional imaging (CT). Reprinted with permission from reference 25.

The synthesis of ^{18}F-labelled tracers can be broadly categorised into nucleophilic and electrophilic fluorination approaches.[26] Nucleophilic fluorination is the method of choice as it utilises high specific activity [^{18}F]fluoride that can be produced via the $^{18}O(p,n)^{18}F$ nuclear reaction on small biomedical cyclotrons. The fluoride is isolated in [^{18}O]H_2O and dried by azeotropic distillation with acetonitrile. Addition of a cryptand, such as the aminopolyether Kryptofix 2.2.2 ($K_{2.2.2}$), captures the metal cation (K^+) and separates it from the fluoride ion, thereby enhancing its nucleophilicity and solubilising it in a polar aprotic solvent (Scheme 3).

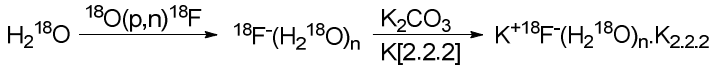

Scheme 3 Preparation of ^{18}F for nucleophilic fluorination reactions.

The resultant [^{18}F]F^- $K^+K_{2.2.2}$ complex can be used to introduce fluoride *via* nucleophilic aromatic substitution into aromatic rings, provided they possess good leaving groups (Cl < F < NO_2 < N^+Me_3) and are sufficiently activated by electron-withdrawing groups such as 3- or 4-NO_2, 4-Ac, 4-CHO, 4-CN or 4-CF_3.[27] Aliphatic nucleophilic substitution, employed for the synthesis of agents

such as [^{18}F]FDG and [^{18}F]FMISO (Chapter 3.2.2.2), requires good leaving groups such as triflate, tosylate, iodo or bromo, but does not rely on activating groups.[26, 27]

Electrophilic fluorination uses [^{18}F]F_2, which is produced through the addition of carrier F_2 (0.2 %) to the enriched [^{18}O]O_2 target, resulting in significantly lower specific activity (1GBq µmol^{-1}) than is achieved for nucleophilic [^{18}F]fluoride (up to 550 GBq µmol^{-1}). In addition, labelling with [^{18}F]F_2 often leads to fluorinated side products due to the reactivity of F_2. Nonetheless, certain PET tracers rely on electrophilic synthesis, such as [^{18}F]FDOPA and [^{18}F]fluoro-*m*-tyrosine, both of which are investigated for imaging the dopaminergic system in the diagnosis of Parkinson's disease. Recent efforts have improved electrophilic methods, for instance by producing high specific activity ^{18}F[F_2] in a post-target method from [^{18}F]fluoride.[28] Work by the Gouverneur group has used this to synthesise selective ^{18}F electrophilic fluorination reagents such as [^{18}F]Selectfluor and [^{18}F]NFSI.[29, 30]

Direct ^{18}F-fluorination requires substrates that tolerate anhydrous organic solvents or elevated temperatures. Hence, ^{18}F-labelling of sensitive biomolecules such as peptides and proteins is often accomplished by first labelling so-called prosthetic groups, which are then conjugated to the molecules of interest. A range of these ^{18}F-synthons has been reported, some of which are depicted in Figure 4.[26, 31, 32]

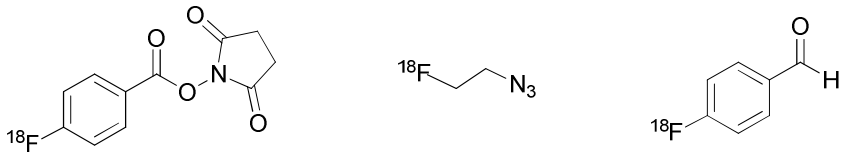

Figure 4 Commonly used prosthetic groups for the ^{18}F labelling of peptides and proteins.

1.3.4.2 Carbon, Oxygen and Nitrogen

Since carbon is abundant in natural products and drug molecules, the use of carbon-11 allows incorporation of a positron-emitting isotope without changing the chemical or biological properties of the compound. Carbon-11 is cyclotron produced (^{14}N(p,α)^{11}C) and isolated as [^{11}C]CO_2 or [^{11}C]CH_4 from the target. Normally it is converted to the most widely used precursors [^{11}C]methyliodide and [^{11}C]methyltriflate for methylation of C, N, O and S nucleophiles. The

20.4 min half-life generally limits synthetic procedures, but reactions such as ^{11}C methylation or metal-mediated ^{11}C carbonylation successfully introduce ^{11}C as the final radiolabelling step.[5, 26]

A widely investigated ^{11}C tracer synthesised *via* alkylation is L-[^{11}C-methyl]-methionine (Met). [^{11}C]Met images increased amino acid metabolism in tumours and has proven superior to ^{18}F[FDG] for the imaging of certain brain tumours (Figure 5).[33]

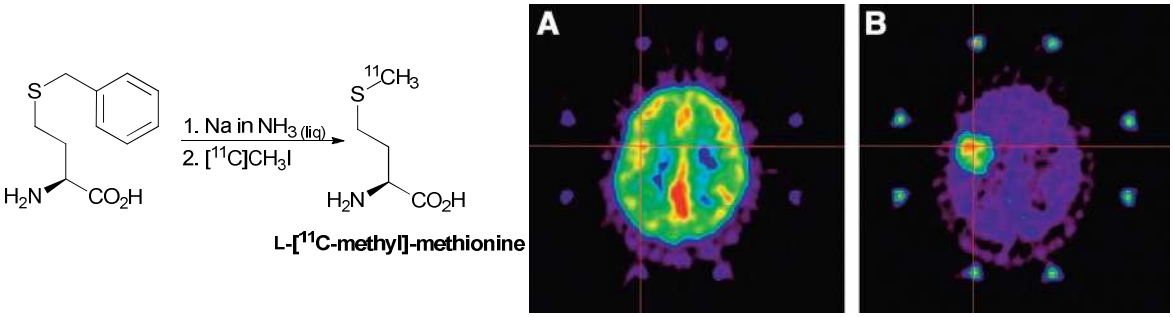

Figure 5 (left) Synthesis of [^{11}C]Met by alkylation on a sulphur nucleophile using [^{11}C]CH_3I [34] (right) PET performed with (A) ^{18}F[FDG] and (B) [^{11}C]Met in an anaplastic astrocytoma brain tumour patient. FDG tumour uptake was equivalent to that in cortical gray matter whereas tumour uptake of Met was higher than in the cortex, allowing definition of a target for biopsy. Reprinted with permission from Reference 35.

The extremely short half-lives of nitrogen-13 ($t_{1/2}$ = 10 min) and oxygen-15 ($t_{1/2}$ = 2 min) permit repeat PET procedures to be carried out within short time-periods but in turn restrict their use to single step synthetic procedures which somewhat limits their clinical utility. Both are generally used in the chemical form obtained from the cyclotron target or converted into simple products for inhalation or injection.[26] For instance, nitrogen-13 ($^{16}O(p,\alpha)^{13}N$) is obtained as nitrate/nitrite in water and reduced to [^{13}N]NH_3 for myocardial blood flow imaging. Oxygen-15, commonly generated via the $^{14}N(d,n)^{15}O$ nuclear reaction, is used as [^{15}O]CO_2 or [^{15}O]H_2O for imaging of cerebral blood flow.

1.3.5 Metallic PET Radionuclides

[^{18}F]NaF and [^{18}F]FDG are only two FDA approved PET radiotracers in oncology.[18] Whilst [^{18}F]FDG has dominated clinical applications of PET, there is a need for imaging molecular processes other than glucose metabolism, for instance, to measure tumour progression after surgery or to probe metabolically already very active tissues such as the brain. This requires disease-specific agents. Increasingly, PET is turning towards receptor targeted imaging that utilises peptides, proteins and antibodies that target receptors and antigens upregulated in disease with high specificity. Radiolabeled trace quantities of these biomarkers can monitor pathophysiological processes at doses free from pharmacological side effects. The traditional PET isotopes ^{18}F, ^{11}C, ^{15}O and ^{13}N are ideally suited for small molecule PET tracers with fast pharmacokinetics. Several ^{18}F-labelled peptides have been explored successfully in the clinic, but the short-lived radioisotopes generally do not cater for the biological half-lives and pharmacokinetics of larger biomolecular targeting vectors. In addition, their typical labelling conditions are not compatible with many sensitive biomolecules.

As an alternative, metallic PET radionuclides offer a range of different half-lives to match the pharmacokinetics and biological half-life of the targeting biomolecule (Table 4).

Radionuclide	Half-life	Production route	Decay mode (% branching ratio)	E(β^+) /keV	Human studies
^{68}Ga	68 min	^{68}Ge/^{68}Ga Generator	EC + β^+ (100) β^+ (89.14)	836.02	yes
^{64}Cu*	12.7 h	^{64}Ni(p,n)^{64}Cu Cyclotron	EC + β^+ (61.5) β^+(19) β^-(40)	278.2	yes
^{86}Y	14.7 h	^{86}Sr(p,n)^{86}Y Cyclotron	EC + β^+ (100) β^+ (31.9)	535	yes
^{89}Zr	78.4 h	^{89}Y(p,n)^{89}Zr cyclotron	EC + β^+ (100) β^+ (22.74)	395.5	yes

Table 4 Metallic PET radionuclides.[8, 18, 36]

For instance, radioimmunoPET with intact monoclonal antibodies (mAbs) requires several hours to days for antibody localization and clearance from background tissue in order to achieve good signals.[8] For instance, recent efforts have focused on the labelling of mAbs with long-lived ^{89}Zr to

* The complete set of copper radionuclides is discussed in section 1.5.1

target oncogenic markers such as Epidermal Growth Factor Receptor (EGFR),[37] carbonic anhydrase (CA-IX)[38] or Prostate-Specific Membrane Antigen (PSMA),[39] using Desferrioxamine (DFO) as a chelator for the Zr(IV) ion.[40]

Yttrium-86 has been explored primarily for dosimetry studies as an isotopic surrogate for the therapeutic isotope ^{90}Y, but several peptides and antibody based ^{86}Y-PET agents have recently been reported.[8] In contrast, short-lived ^{68}Ga is suited for labelling peptide and oligonucleotide based tracers. ^{68}Ga is currently the only readily available generator-produced PET radioisotope with short/intermediate half-life, offering a kit-based PET radiolabeling approach, such as that employed for clinically used ^{99m}Tc SPECT agents. Radiocopper offers a range of different half-lives. Copper-64 in particular has been investigated for labelling of small molecules as well as peptides and antibodies or antibody fragments.

1.3.6 CT and MRI for Hybrid Nuclear Imaging

Computed Tomography (CT) is based on a series of X-ray images taken at various angles around the object. The X-rays are attenuated to different extents by the bones and tissue. Computational processing then affords a 3-D image with sub-millimetre resolution.[5] In Magnetic Resonance Imaging (MRI), the patient is surrounded by an external magnetic field (1.5-14.1 Tesla). A radiofrequency field is then applied to cause a change in nuclear spin orientation of NMR active nuclei (^{1}H, ^{19}F or ^{31}P) so that they align with the magnetic field. Relaxation of the excited nuclei emits a radiofrequency signal whose intensity is characteristic for the nucleus, its concentration and the relaxation time T_1 and T_2 (where T_1 = spin lattice relaxation time constant and depends on the time taken to relax back to the ground state and T_2 = spin-spin relaxation time constant, determined by the time taken for the nuclei to de-phase). The detected signal is Fourier-transformed and a 3D image is produced. Since T_1 and T_2 are tissue dependent they are used to determine differences between ^{1}H nuclei in different environments. Whilst SPECT/CT is widely used clinically, dual PET/CT has also been implemented in clinical use since 2001.

1.3.7 Therapeutic applications of radionuclides

Radiotherapy relies on the use of high energy radiation from X-rays, γ-rays or particles in order to kill cancer cells.[41, 42] Several radionuclides emit radiation in the form of α or β^- particles or by means of Auger electron emission. ^{131}I has been routinely used in thyroid radiotherapy for over 50 years. ^{188}Re has been investigated for radiotherapy of larger tumour masses since its β-particles have a relatively long tissue range (10 -11 mm).[41] In contrast, Auger electrons emitted by ^{111}In have a μm range and are useful for damaging nuclear DNA,[42] as demonstrated by ^{111}In-DTPA-hEGF which has achieved tumour regression in mice bearing MDAMB-468 xenografts.[43] β-emitters have been investigated for therapy in the form of radiolabelled antibodies or peptides, such as ^{90}Y-Zevalin.[41]

1.4 Bifunctional chelator approach for metallic radionuclides

Non-metallic radionuclides may be incorporated into small molecule radiotracers by exchanging an isotopologue.[18] In the case of PET radiometals, the radionuclide usually requires complexation by a chelator. Unlike the metal-essential ^{99m}Tc agents, the majority of metallic PET radionuclides do not rely on the physicochemical properties of the metal complex alone, but are delivered by a biological targeting vector. In this 'bifunctional chelator approach', the radiometal is complexed by a suitable chelator that is attached *via* a covalent linker unit to the peptide, protein or antibody (Figure 6).

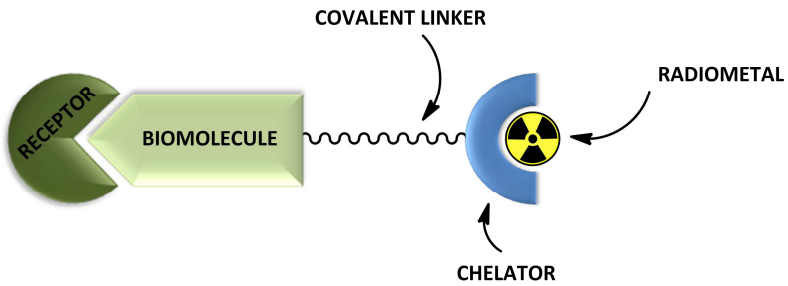

Figure 6 Representation of the bifunctional chelate approach.

Several factors must be considered when designing a bifunctional chelator to radiolabel a biomolecule. The metal-chelator complexes must be thermodynamically stable and equally importantly, kinetically inert in order to avoid dissociation *in vivo*.[36, 44-46] Often, macrocyclic chelators provide better thermodynamic and kinetic stability than acyclic chelators. This enhanced stability, known as the macrocyclic effect, may be attributed to the chelators improved preorganisation and lower solvation compared to acyclic systems, resulting in more favourable enthalpic and entropic contributions on chelation.[47]The chosen chelator must have the right coordination number, denticity and cavity size for the radiometal. For instance, both NOTA and DOTA have been successfully used for gallium, but NOTA has a higher stability constant (log K = 30.1) with ^{68}Ga than DOTA (log K = 21.3) since the coordination cavity of the latter N_4 macrocycle is less suitable for the Ga^{3+} ion.[48, 49]

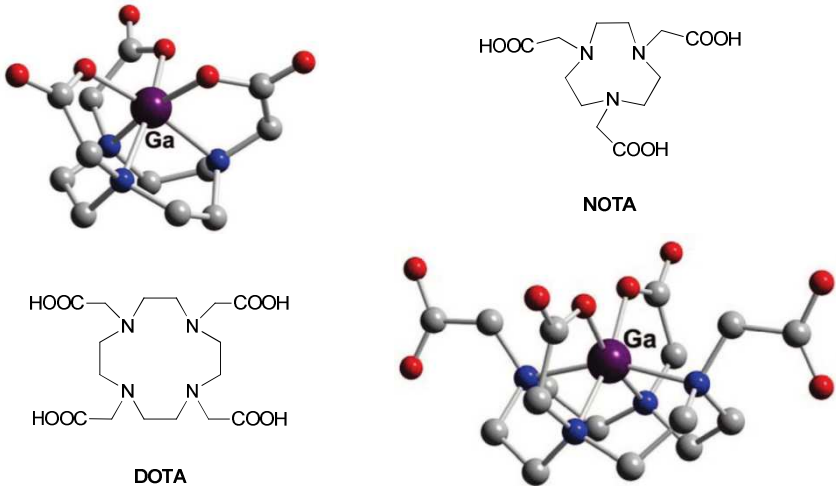

Figure 7 Structure of the macrocyclic chelators NOTA (top row) and DOTA (bottom row) and their respective Gallium complexes. Crystal structures were taken from reference 36.

Another important consideration is the efficiency (yield) of labelling. For radiolabelled peptides, a high ratio of labelled to unlabelled molecule is important to avoid receptor saturation with unlabelled compound which reduces contrast. For peptides and antibodies, large amounts of unlabelled compound can also lead to an immune response. Labelling kinetics depend on the radiometal and the structure and denticity of the chelator. Acyclic chelators often have faster labelling kinetics than macrocyclic chelators and they label at room temperature.

This is useful when labelling with short-lived radiometals such as ^{68}Ga or when labelling sensitive biomolecules. Acyclic chelators such as DFO or DTPA have been explored for the ^{68}Ga-labelling of peptides and antibodies within minutes at room temperature.[18, 50]

In the case of acyclic chelation of ^{86}Y by DTPA, the stability of the chelate could be improved by optimising the denticity and increasing the rigidity of the chelator. Whilst the heptadentate DTPA, using one carboxyl for conjugation proved unsuitable for *in vivo* use,[51, 52] an octadentate and semi-rigid derivative CHX-A"-DTPA forms complexes stable enough for antibody imaging.[53, 54]

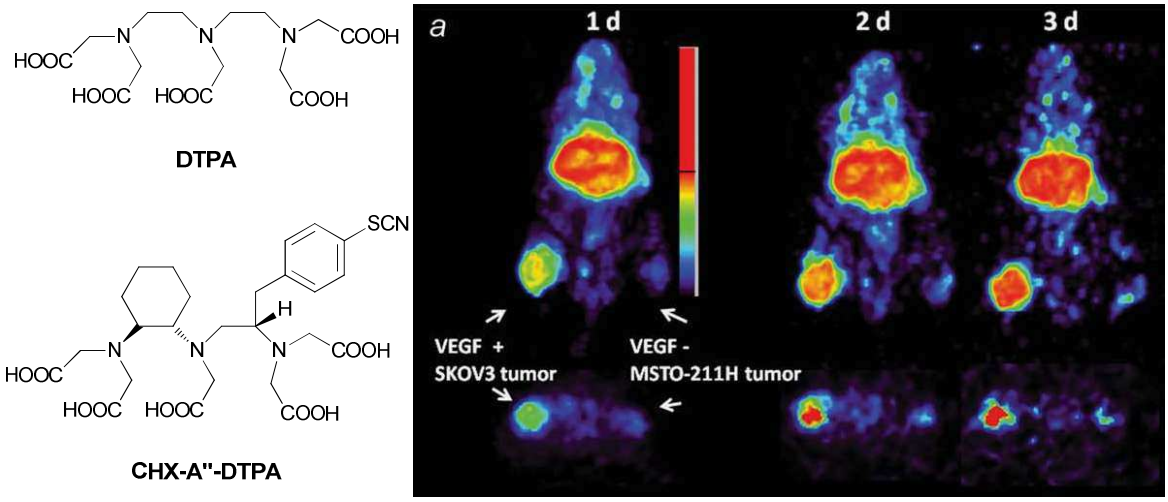

Figure 8 (left) Structures of acyclic DTPA derivatives (right) PET imaging of tumour angiogenesis using the ^{86}Y-labelled VEGF-specific antibody ^{86}Y-CHX-A"-DTPA-bevacizumab. The mouse bears a VEGF-A–positive human ovarian carcinoma SKOV3 xenograft on one leg and VEGF-A–negative human biphasic mesothelioma MSTO-211H on the other leg. Reprinted with permission from reference 53.

Another important consideration is the nature of the linker, the conjugation groups, and the site of attachment on the biomolecule. The functionality used to connect the bifunctional chelator generally needs to be reactive towards pendant nucleophilic groups on the protein, such as NH_2, OH or SH. The optimal bioconjugation reaction should be fast, use mild conditions in the case of proteins and, if possible, require minimal purification.[55] Commonly used bioconjugation methods are depicted in Figure 9. The conjugation site and the number of chelators per biomolecule may influence the *in vivo* affinity of the targeted radiopharmaceutical since too heavy substitution may result in a loss of affinity of the biomolecule for the target site.[56] Since the appended metal complex can also affect the overall pharmacokinetics of the biological vector, selective modification of the

bioconjugate can be achieved by using differently charged bifunctional chelators or introducing different charges and spacers into the linker construct. For instance, the introduction of aliphatic, aromatic and polyethylene glycol spacers in the covalent linker unit has been widely investigated to alter the pharmacokinetics of radiolabelled bombesin and GRP peptides which are used to image the gastrin-releasing peptide receptor overexpressed in several cancers.[57-59]

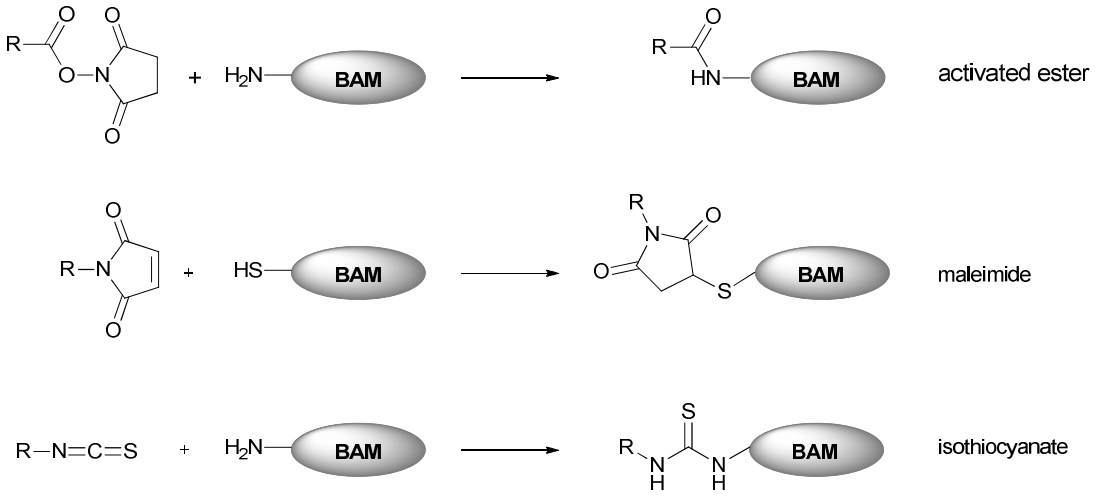

Figure 9 Different bioconjugation strategies used in the bifunctional chelator approach.[41]

Finally, it is important to consider that downstream optimisations of the bifunctional chelator-bioconjugate may be necessary following preliminary *in vitro* and *in vivo* studies, [55] and designing chelating systems that can easily be trialed with different functional groups and linkers units accelerates these translational processes.

1.5 Copper radiopharmaceuticals

1.5.1 Copper radionuclides

The transition metal copper offers a useful range of radioisotopes with a variety of half-lives and decay characteristics summarised in Table 5. The short-lived isotopes $^{60\text{-}62}$Cu decay by electron capture (EC) and β^+ emission, making them useful for tomographic imaging, ^{67}Cu decays exclusively by β^- emission and is thus suitable for radiotherapy. ^{64}Cu in particular is a versatile radionuclide due to its intermediate 12.7 h half-life. It combines all three decay modes (β^+, β^- and EC). Electron capture also results in Auger electron emission, which increases the therapeutic potential of radiocopper deposited in the cell nucleus.[60] The spatial image resolution of ^{64}Cu is comparable to that of ^{18}F so that the existing PET systems require no alteration.[41] With the exception of the generator produced ^{62}Cu, the copper radioisotopes are commonly produced on a small biomedical cyclotron by bombardment of an enriched Nickel target.[61] ^{64}Cu, produced *via* the ^{64}Ni(p,n)^{64}Cu nuclear reaction, has been reported to have a specific activity ranging from 10–470 GB μmol^{-1}.[61, 62]

Isotope	Half-life	Production	Emission Type (%)	$E_{\beta+}$ (MeV)
^{60}Cu	23.4 min	Cyclotron, ^{60}Ni(p,n)^{60}Cu	β^+ (93%) EC (7%)	2.0, 3.92, 3.0
^{61}Cu	3.32 h	Cyclotron, ^{61}Ni(p,n)^{61}Cu	β^+ (60%) EC (40%)	1.22
^{62}Cu	9.76 min	^{62}Zn/^{62}Cu Generator	β^+ (97%) EC (2%)	2.91
^{64}Cu	12.7 h	Cyclotron, ^{64}Ni(p,n)^{64}Cu	β^- (39.6%) β^+(17.4%) EC (41%)	0.655
^{67}Cu	62.0 h	Accelerator ^{67}Zn(n,p)^{67}Cu	β^- (100%)	0.395, 0.484, 0.577

Table 5 Summary of copper radionuclides used for imaging and therapy.[60, 63]

1.5.2 Copper chelation chemistry

Copper chelation chemistry is limited to three accessible oxidation states (I-III). Cu^{3+} is only rarely found and requires strong π-donor ligands.[60] The Cu^{+} oxidation state forms complexes with soft, polarisable ligands such as phosphines, nitriles, thioethers, thiolates or cyanide. Since it has no metal imposed preference for geometry it therefore often selects tetrahedral geometry to minimise steric interactions between ligands. Due to the absence of any crystal field stabilisation energy, Cu(I) complexes are often kinetically labile if not stabilised with polydentate soft ligands. Thus, they are generally not suitable for radiopharmaceutical applications so that the predominant oxidation state for radiocopper chemistry in protic media remains Cu^{2+}.[36, 62, 63] In contrast to xenobiotic radiometals such as ^{89}Zr and ^{99m}Tc, copper plays an active role in many biological processes and its homeostasis is tightly regulated in the human body.[64] *In vivo* it is protein bound as Cu(II) by extracellular (albumin, ceruloplasmin) and intracellular (cytochrome C oxidase, superoxide dismutase, metallothioneins) proteins. These biochelators are present at significantly higher concentrations than the injected radiocopper complexes. Copper radiopharmaceuticals therefore need to be not only thermodynamically stable but kinetically inert to avoid *in vivo* transchelation. Cu(II) forms complexes with coordination numbers from 4-6 displaying a range of geometries that are often influenced by Jahn Teller distortions. Tetradentate chelators, such as Schiff base and amino acid derivatives employ an N_2X_2 donor set and form complexes with square-planar, tetrahedral or intermediate geometries. In contrast, copper (II) complexes of hexadentate chelators are commonly distorted octahedral.

Both acyclic and macrocyclic chelators have been explored for radiopharmaceutical applications, but efforts generally have focused on the latter. Systems such as polyazamacrocycles with pendant arms benefit from increased stability through the macrocyclic and chelate effects.[62] Functionalised DOTA, NOTA (Figure 7) and TETA (Figure 10) ligands have been extensively explored as bifunctional chelators for ^{64}Cu labelling of peptides, proteins and antibodies.[62, 65-67] These show superior stability to acyclic systems but still suffer from liver uptake *in vivo* which is believed to result from transchelation to ceruloplasmin.[45, 46]

Recent efforts have examined cross-bridged cyclams and cage-like sepulchrate/sarcophagine ligands such as DiamSar and SarAr (Figure 10). The sarcophagines aim to increase *in vivo* stability by steric shielding and charge effects, the cage like structures restrain the coordination environment of the Cu^{2+} should temporary partial ligand dissociation occur. Several functionalised variants have been synthesised.

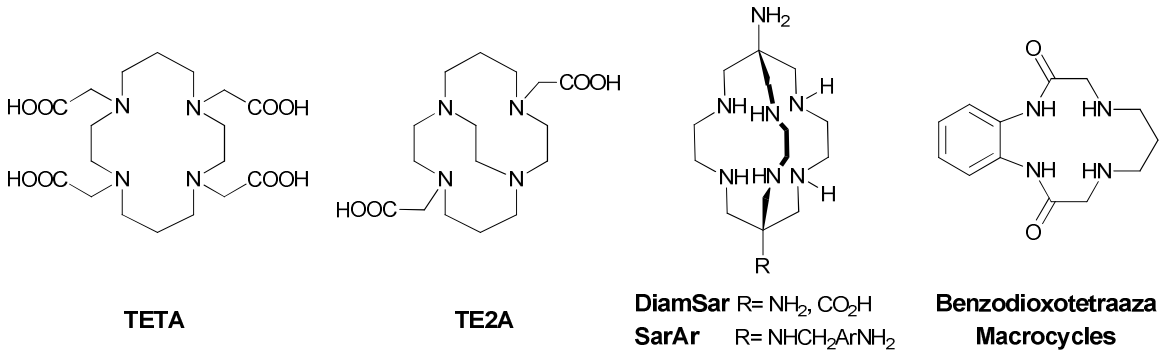

Figure 10 Macrocyclic chelators explored for use in copper radiopharmaceuticals.

The cross bridged cyclams chelators adopt a *cis*-folded confirmation. In the case of systems with pendant carboxyl arms such as CuCB-TE2A the coordination environment is further completed by two carboxymethyl arms to achieve a six-coordinate distorted octahedron. Cu-CB-TE2A displayed high kinetic inertness in acid. Use of one carboxylate arm for peptide conjugation caused a slight reduction in acid decomplexation half-life, but *in vivo* comparison of TETA and TE2A somatostatin analogues still demonstrated that Te2A was superior in significantly reducing liver uptake and interestingly also displayed a greater tumour affinity. Increased *in vivo* stability has also been sought by control of redox chemistry as demonstrated by a benzodiazamacrocycle reported by the Dilworth and Maecke groups (Figure 10). The complex had a biologically inaccessible Cu(II)/Cu(I) reduction potential of E_P = -1.84 V.[68, 69]

1.6 Bis(thiosemicarbazones)

Thiosemicarbazones and bis(thiosemicarbazones) have been investigated for their biological activity since the 1950s as antiviral, antifungal, antitumour and antimalarial agents.[70] The ligands are formed by acid catalysed condensation of a thiosemicarbazide with an aldehyde/ketone or dicarbonyl to give a thiosemicarbazone or bis(thiosemicarbazone) respectively.[71-73]

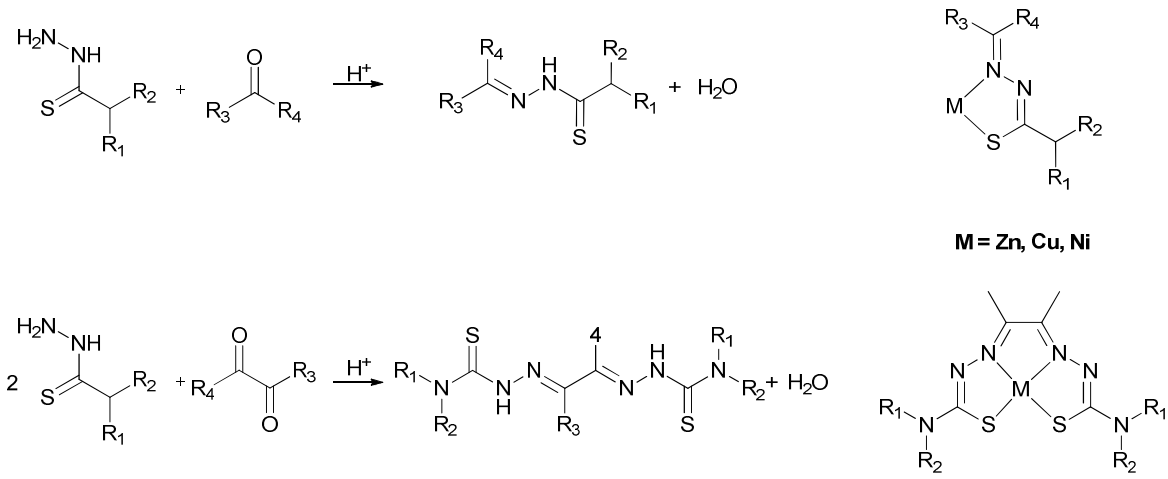

Figure 11 (top) Synthesis of thiosemicarbazone and ligand binding in a metal thiosemicarbazone (bottom) Synthesis of a 1,2 bis(thiosemicarbazone) and structure of its corresponding neutral metal(II) complex.

They act as ligands for most first row and some second and third row transition metal ions by incorporating them in a 5-membered chelate ring through the sulphur atom and the azomethinic nitrogen. In the case of bis(thiosemicarbazones), the sulphur coordinates in its monoanionic form as a "masked thiolate". Since two thiosemicarbazone groups are available they provide a tetradentate N_2S_2 donor system for complexation of the metal (II) ion.

1.6.1 Copper bis(thiosemicarbazonates)

Originally, ligands such as H_2GTS and H_2KTS† were investigated as antitumour agents,[74, 75] but research quickly revealed that their antineoplastic activity was connected to their ability to chelate Cu.[76, 77] The exact mechanism of antitumour activity has not been fully elucidated but studies

† The nomenclature used for these ligands will be explained in Chapter Two

suggested that after cellular uptake, the metal complex is reduced by intracellular thiol groups, leading to dissociation from the ligand and intracellular hyperaccumulation of copper. This results in disruption of DNA synthesis, oxidative phosphorylation and oxidation of thiols to disulfides, as well as causing cellular poisoning.[78] Recent work by Donnelly and co-workers has explored Cu(GTSM) for the controlled intracellular delivery of Cu to treat Alzheimer's disease.[79, 80] The increased intracellular availability of Cu was suggested to activate neuroprotective pathways, resulting in improved cognition in animals with AD.[80, 81]

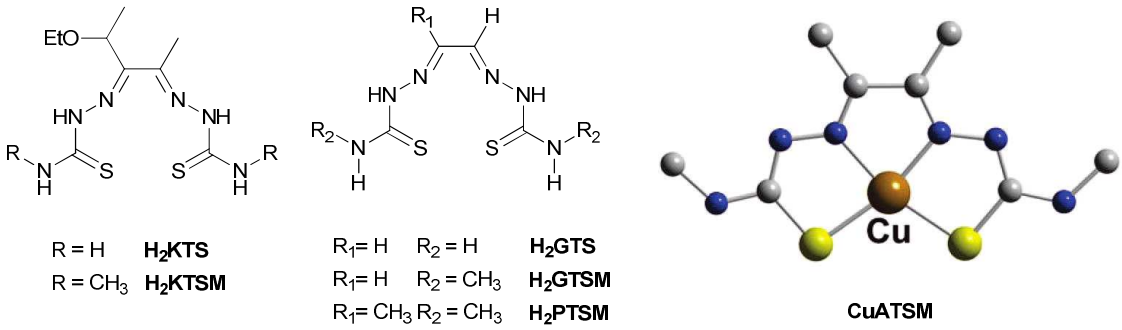

Figure 12 (left) Structures of selected bis(thiosemicarbazone) ligands (right) Crystal structure of Cu(II)ATSM.[36]

The ability of the stable lipophilic copper complexes to diffuse across cell membranes led to the investigation of radiolabelled copper bis(thiosemicarbazonato) complexes as perfusion tracers. The highly membrane permeable $^{62/67}$Cu-labelled Cu(PTSM) has been investigated for cerebral and myocardial perfusion imaging, it efficiently crosses the blood-brain barrier and its reduction results in good tissue retention. This created an interest in applications of radiolabelled copper bis(thiosemicarbazones) in other contexts. Fujibayashi *et al* reported selective uptake of copper(II)-diacetyl-bis(N^4-methylthiosemicarbazone), Cu(ATSM) in ischaemic heart tissue.[82] In contrast to the other complexes discussed above which are reduced in all cells, the Cu(II)/Cu(I) reduction potential of Cu(ATSM) was significantly lower and it was found to be selectively retained only in highly reducing environments such as hypoxic cells.[83, 84] Experiments revealed that the reduction potentials of the complexes were governed by the substitution pattern of the diimine backbone, whereas changing the substitution pattern on the N*4* terminal had little effect on the hypoxia selectivity. DFT calculations further proposed that H_2ATSM is more efficient at stabilising the

Cu(I) ion than ligands such as H_2PTSM or H_2GTSM.[85, 86] The detailed structure-activity studies and biological tests that were performed to investigate the basis of CuATSM as a hypoxia imaging agent are discussed in Chapter 3.

The tetradentate bis(thiosemicarbazone) ligands form kinetically and thermodynamically stable complexes ($K_a = 10^{18}$). Since CuATSM is only reduced intracellularly in a hypoxic environment, frameworks that retain the core dimethyl backbone motif should be suitable for other *in vivo* imaging applications.

1.7 Project Aims

The work in this thesis concerns two aspects of using copper bis(thiosemicarbazonates) as radiopharmaceuticals in cancer imaging.

Part I- Bis(thiosemicarbazones) as bifunctional chelators

- The synthesis and characterisation of new bis(thiosemicarbazones) as bifunctional chelators for the room-temperature copper radiolabelling of biomolecules.
- Potential of the chelators for use with peptides and proteins and biological evaluation

Part II- Orthogonal radiolabelling of copper bis(thiosemicarbazonates) for mechanistic studies

- The synthesis and physicochemical characterisation of a suitable pair of copper bis(thiosemicarbazonato) complexes radiolabelled at the metal and at the ligand
- Use of these complexes to study the mechanism of hypoxia selectivity of the class of hypoxia selective copper (II) bis(thiosemicarbazonates)
    - *In vitro* and *in vivo* studies and comparison to the parent compound Cu(ATSM)
    - Evaluation of the orthogonally labelled derivatives as new hypoxia selective tracers if applicable

1.8 References for Chapter I

1. T. E. Peterson and H. C. Manning, *J. Nucl. Med. Technol.*, 2009, **37**, 151-161.
2. A. Mankoff David, *J. Nucl. Med.*, 2007, **48**, 18N, 21N.
3. M. Rudin and R. Weissleder, *Nat. Rev. Drug Discovery*, 2003, **2**, 123-131.
4. J. K. Willmann, N. van Bruggen, L. M. Dinkelborg and S. S. Gambhir, *Nat. Rev. Drug Discovery*, 2008, **7**, 591-607.
5. S. Vallabhajosula, *Molecular Imaging for PET and SPECT*, 1 Edition edn., Springer, 2009.
6. R. L. Wahl, *Principles and Practice of PET and PET/CT*, 2nd Edition edn., Lippincott Williams & Wilkins, 2009.
7. T. Saga, M. Koizumi, T. Furukawa, K. Yoshikawa and Y. Fujibayashi, *Cancer Sci.*, 2009, **100**, 375-381.
8. T. K. Nayak and M. W. Brechbiel, *Bioconjugate Chem.*, 2009, **20**, 825-841.
9. V. Tolmachev and S. Stone-Elander, *Biochim. Biophys. Acta, Gen. Subj.*, 2010, **1800**, 487-510.
10. C. Catana, A. van der Kouwe, T. Benner, C. J. Michel, M. Hamm, M. Fenchel, B. Fischl, B. Rosen, M. Schmand and A. G. Sorensen, *J. Nucl. Med*, 2010, **51**, 1431-1438.
11. A. Drzezga, M. Souvatzoglou, A. Beer, S. Ziegler, S. Furst, S. Nekolla and M. Schwaiger, *Society of Nuclear Medicine Annual Meeting Abstracts*, 2011, **52**, 262.
12. S. L. Pimlott and A. Sutherland, *Chem. Soc. Rev.*, 2011, **40**, 149-162.
13. J. L. H. Eersels, M. J. Travis and J. D. M. Herscheid, *J. Labelled Compd. Radiopharm.*, 2005, **48**, 241-257.
14. H.-M. Park, *J. Nucl. Med.*, 2002, **43**, 77-78.
15. S. Shirkare, T. Kuwert, M. Weckesser, N. Czech, K. J. Langen and H. W. Muller-Gartner, *Localization of a pheochromocytoma using I-123 MIBG adrenal scintigraphy*, Institut fur Medizin, Forschungszentrum, Julich, Germany, India, 1994.
16. J. Booij and P. Kemp, *Eur. J. Nucl. Med. Mol. Imaging*, 2008, **35**, 424-438.
17. V. Camacho and I. Carrio, *Curr. Opin. Biotechnol.*, 2007, **18**, 60-64.
18. B. M. Zeglis and J. S. Lewis, *Dalton Trans.*, 2011, DOI: 10.1039/C0DT01595D.
19. L. Bridges Robert, R. Wiley Chris, C. Christian John and P. Strohm Adam, *An introduction to Na(18)F bone scintigraphy: basic principles, advanced imaging concepts, and case examples*, Alaska Open Imaging Center, Anchorage, Alaska 99504, USA, United States, 2007.
20. S. Fowler Joanna and T. Ido, *Semin. Nucl. Med*, 2002, **32**, 6-12.
21. J. S. Fowler and T. Ido, *Handb. Radiopharm.*, 2003, 307-321.
22. M. Reivich, D. Kuhl, A. Wolf, J. Greenberg, M. Phelps, T. Ido, V. Casella, J. Fowler, E. Hoffman and et al., *Circ. Res.*, 1979, **44**, 127-137.
23. M. E. Phelps, S. C. Huang, E. J. Hoffman, C. Selin, L. Sokoloff and D. E. Kuhl, *Ann. Neurol.*, 1979, **6**, 371-388.
24. B. Beuthien-Baumann, K. Hamacher, F. Oberdorfer and J. Steinbach, *Carbohydr. Res.*, 2000, **327**, 107-118.
25. U. Chowdhury Fahmid, N. Shah, F. Scarsbrook Andrew and M. Bradley Kevin, *Postgrad. Med. J.*, 2010, **86**, 174-182.
26. P. W. Miller, N. J. Long, R. Vilar and A. D. Gee, *Angew. Chem., Int. Ed.*, 2008, **47**, 8998-9033.
27. L. Cai, S. Lu and V. W. Pike, *Eur. J. Org. Chem.*, 2008, 2853-2873.
28. J. Bergman and O. Solin, *Nucl. Med. Biol.*, 1997, **24**, 677-683.
29. H. Teare, G. Robins Edward, E. Arstad, K. Luthra Sajinder and V. Gouverneur, *Chem. Commun.*, 2007, 2330-2332.
30. H. Teare, E. G. Robins, A. Kirjavainen, S. Forsback, G. Sandford, O. Solin, S. K. Luthra and V. Gouverneur, *Angew. Chem., Int. Ed.*, 2010, **49**, 6821-6824, S6821/6821-S6821/6819.
31. H. J. Wester and M. Schottelius, *Ernst Schering Res. Found. Workshop*, 2007, **62**, 79-111.

32. T. Ramenda, T. Kniess, R. Bergmann, J. Steinbach and F. Wuest, *Chem. Commun.*, 2009, 7521-7523.
33. W. Chen, *J. Nucl. Med.*, 2007, **48**, 1468-1481.
34. B. Langstrom and H. Lundqvist, *Int. J. Appl. Radiat. Isot.*, 1976, **27**, 357-363.
35. B. Pirotte, S. Goldman, N. Massager, P. David, D. Wikler, A. Vandesteene, I. Salmon, J. Brotchi and M. Levivier, *J. Nucl. Med.*, 2004, **45**, 1293-1298.
36. T. J. Wadas, E. H. Wong, G. R. Weisman and C. J. Anderson, *Chem. Rev.*, 2010, **110**, 2858-2902.
37. L. R. Perk, G. W. M. Visser, M. J. W. D. Vosjan, M. Stigter-van Walsum, B. M. Tijink, C. R. Leemans and G. A. M. S. van Dongen, *J. Nucl. Med.*, 2005, **46**, 1898-1906.
38. B. A. W. Hoeben, J. H. A. M. Kaanders, G. M. Franssen, E. G. C. Troost, P. F. J. W. Rijken, E. Oosterwijk, G. A. M. S. van Dongen, W. J. G. Oyen, O. C. Boerman and J. Bussink, *J. Nucl. Med.*, 2010, **51**, 1076-1083.
39. J. P. Holland, V. Divilov, N. H. Bander, P. M. Smith-Jones, S. M. Larson and J. S. Lewis, *J. Nucl. Med.*, 2010, **51**, 1293-1300.
40. P. K. E. Börjesson, Y. W. S. Jauw, R. de Bree, J. C. Roos, J. A. Castelijns, C. R. Leemans, G. A. M. S. van Dongen and R. Boellaard, *J. Nucl. Med.*, 2009, **50**, 1828-1836.
41. S. Bhattacharyya and M. Dixit, *Dalton Trans.*, 2011, DOI: 10.1039/C1DT10379B
42. B. Cornelissen and K. A. Vallis, *Curr. Drug Discovery Technol.*, 2010, **7**, 263-279.
43. R. M. Reilly, D. A. Scollard, J. Wang, H. Mondal, P. Chen, L. A. Henderson, B. M. Bowen and K. A. Vallis, *J. Nucl. Med.*, 2004, **45**, 701-708.
44. C. J. Anderson and M. J. Welch, *Chem. Rev.*, 1999, **99**, 2219-2234.
45. L. A. Bass, M. Wang, M. J. Welch and C. J. Anderson, *Bioconj. Chem.*, 2000, **11**, 527-532.
46. C. A. Boswell, X. Sun, W. Niu, G. R. Weisman, E. H. Wong, A. L. Rheingold and C. J. Anderson, *J. Med. Chem.*, 2004, **47**, 1465-1474.
47. D. K. Cabbiness and D. W. Margerum, *J. Am. Chem. Soc.*, 1969, **91**, 6540-6541.
48. R. Delgado and J. J. R. Frausto da Silva, *Talanta*, 1982, **29**, 815-822.
49. E. T. Clarke and A. E. Martell, *Inorg. Chim. Acta*, 1991, **181**, 273-280.
50. B. Koop, S. N. Reske and B. Neumaier, *Radiochim. Acta*, 2007, **95**, 39-42.
51. H.-J. Wester, J. Brockmann, F. Roesch, W. Wutz, H. Herzog, P. Smith-Jones, B. Stolz, C. Bruns and G. Stoecklin, *Nucl. Med. Biol.*, 1997, **24**, 275-286.
52. R. M. Sharkey, C. Motta-Hennessy, O. A. Gansow, M. W. Brechbiel, I. Fand, G. L. Griffiths, A. L. Jones and D. M. Goldenberg, *Int. J. Cancer*, 1990, **46**, 79-85.
53. T. K. Nayak, K. Garmestani, K. E. Baidoo, D. E. Milenic and M. W. Brechbiel, *Int. J. Cancer*, 2010, **128**, 920-926.
54. L. Camera, S. Kinuya, K. Garmestani, C. Wu, M. W. Brechbiel, L. H. Pai, T. J. McMurry, O. A. Gansow, I. Pastan and et al., *J. Nucl. Med.*, 1994, **35**, 882-889.
55. M. D. Bartholoma, A. S. Louie, J. F. Valliant and J. Zubieta, *Chem. Rev.*, 2010, **110**, 2903-2920.
56. B. K. Giersing, M. T. Rae, M. CarballidoBrea, R. A. Williamson and P. J. Blower, *Bioconjugate Chem.*, 2001, **12**, 964-971.
57. C. J. Smith, W. A. Volkert and T. J. Hoffman, *Nucl. Med. Biol.*, 2005, **32**, 733-740.
58. J. C. Garrison, T. L. Rold, G. L. Sieckman, F. Naz, S. V. Sublett, S. D. Figueroa, W. A. Volkert and T. J. Hoffman, *Bioconjugate Chem.*, 2008, **19**, 1803-1812.
59. T. J. Hoffman, H. Gali, C. J. Smith, G. L. Sieckman, D. L. Hayes, N. K. Owen and W. A. Volkert, *J. Nucl. Med.*, 2003, **44**, 823-831.
60. P. J. Blower, J. S. Lewis and J. Zweit, *Nucl. Med. Biol.*, 1996, **23**, 957-980.
61. P. Burke, O. Golovko, J. C. Clark and F. I. Aigbirhio, *Inorg. Chim. Acta*, 2010, **363**, 1316-1319.
62. T. J. Wadas, E. H. Wong, G. R. Weisman and C. J. Anderson, *Curr. Pharm.*, 2007, **13**, 3-16.
63. C. J. Anderson and R. Ferdani, *Cancer Biother. Radiopharm.*, 2009, **24**, 379-393.
64. M. C. Linder, L. Wooten, P. Cerveza, S. Cotton, R. Shulze and N. Lomeli, *Am. J. Clin. Nutr.*, 1998, **67**, 965S-971S.

65. G. R. Mirick, R. T. O'Donnell, S. J. DeNardo, S. Shen, C. F. Meares and G. L. DeNardo, *Nucl. Med. Biol.*, 1999, **26**, 841-845.
66. G. W. Philpott, S. W. Schwarz, C. J. Anderson, F. Dehdashti, J. M. Connett, K. R. Zinn, C. F. Meares, P. D. Cutler, M. J. Welch and B. A. Siegel, *J. Nucl. Med.*, 1995, **36**, 1818-1824.
67. M. R. Lewis, C. A. Boswell, R. Laforest, T. L. Buettner, D. Ye, J. M. Connett and C. J. Anderson, *Cancer Biother. Radiopharm.*, 2001, **16**, 483-494.
68. P. J. Barnard, J. P. Holland, S. R. Bayly, T. J. Wadas, C. J. Anderson and J. R. Dilworth, *Inorg. Chem.*, 2009, **48**, 7117-7126.
69. P. Antunes, R. Delgado, M. G. B. Drew, V. Felix and H. Maecke, *Inorg. Chem.*, 2007, **46**, 3144-3153.
70. G. Pelosi, *Open Crystallogr. J.*, 2010, **3**, 16-28.
71. P. S. Donnelly, *Dalton Trans.*, 2011.
72. M. Christlieb and J. R. Dilworth, *Chem.-Eur. J.*, 2006, **12**, 6194-6206.
73. B. M. Paterson and P. S. Donnelly, *Chem. Soc. Rev.*, 2011, **40**, 3005-3018.
74. H. G. Petering, H. H. Buskirk and G. E. Underwood, *Cancer Res.*, 1964, **24**, 367-372.
75. F. A. French and B. L. Freedlander, *Cancer Res.*, 1960, **20**, 505-538.
76. H. G. Petering, H. H. Buskirk and J. A. Crim, *Cancer Res.*, 1967, **27**, 1115-1121.
77. B. A. Booth and A. C. Sartorelli, *Nature*, 1966, **210**, 104-105.
78. C. H. Chan-Stier, D. Minkel and D. H. Petering, *Bioinorg. Chem.*, 1976, **6**, 203-217.
79. P. J. Crouch, L. W. Hung, P. A. Adlard, M. Cortes, V. Lal, G. Filiz, K. A. Perez, M. Nurjono, A. Caragounis, T. Du, K. Laughton, I. Volitakis, A. I. Bush, Q.-X. Li, C. L. Masters, R. Cappai, R. A. Cherny, P. S. Donnelly, A. R. White and K. J. Barnham, *Proc. Natl. Acad. Sci..*, 2009, **106**, 381-386.
80. P. S. Donnelly, A. Caragounis, T. Du, K. M. Laughton, I. Volitakis, R. A. Cherny, R. A. Sharples, A. F. Hill, Q.-X. Li, C. L. Masters, K. J. Barnham and A. R. White, *J. Biol. Chem.*, 2008, **283**, 4568-4577.
81. K. A. Price, A. Caragounis, B. M. Paterson, G. Filiz, I. Volitakis, C. L. Masters, K. J. Barnham, P. S. Donnelly, P. J. Crouch and A. R. White, *J. Med. Chem.*, 2009, **52**, 6606-6620.
82. Y. Fujibayashi, H. Taniuchi, Y. Yonekura, H. Ohtani, J. Konishi and A. Yokoyama, *J. Nucl. Med.*, 1997, **38**, 1155-1160.
83. J. S. Lewis, D. W. McCarthy, T. J. McCarthy, Y. Fujibayashi and M. J. Welch, *J. Nucl. Med.*, 1999, **40**, 177-183.
84. A. L. Vavere and J. S. Lewis, *Dalton Trans.*, 2007, 4893-4902.
85. J. P. Holland, J. C. Green and J. R. Dilworth, *Dalton Trans.*, 2006, 783-794.
86. R. I. Maurer, P. J. Blower, J. R. Dilworth, C. A. Reynolds, Y. Zheng and G. E. D. Mullen, *J. Med. Chem.*, 2002, **45**, 1420-1431.

Chapter 2

Bis(thiosemicarbazones) as bifunctional chelators for the 64-copper labelling of biomolecules

2.1 Introduction

The successful exploitation of metallic radioisotopes for PET relies on the development of suitable bifunctional chelators for the radiometal. The use of radiocopper for the labelling of peptides, proteins and antibodies in particular requires several important factors to be considered. Since the number of receptors at the *in vivo* target site is limited in many cases, high specific activity bioconjugates are needed to achieve good contrast. This reduces the amount of non-radiolabelled biomolecule injected, thus lowering the risk of immune response to the peptide or antibody. In order to achieve a high ratio of labelled to unlabelled bioconjugate with copper radioisotopes, the use of high specific activity radiocopper should be combined with a chelator that labels with high efficiency. In addition separation of the labelled biomolecule from any excess, unlabelled form must be carried out, frequently *via* HPLC methods. As outlined in Chapter 1, kinetic inertness of the copper complex *in vivo* is crucial and the possibility of *in vivo* Cu(II)/Cu(I) redox chemistry and transchelation also need to be considered.[1-3] Although the latest generation macrocyclic chelators have demonstrated excellent stability *in vivo*, nearly all require elevated temperatures or non-physiological pH ranges over prolonged periods for efficient labelling. Radiolabelling at ambient temperatures is possible, but often requires extended labelling times, resulting in lower radiochemical yields and needs addition of scavenger ligand to remove unbound radiocopper as illustrated in Table 1. A chelating system with fast labelling kinetics that achieves high radiochemical yields under biocompatible conditions therefore would provide advantages for the radiolabelling of sensitive biomolecules.

Ref.	Chelator	Target/biomolecule	Radiometallation
4	DOTA	PSMA/antibody	^{64}Cu in NH_4OAc, pH 5.5, 40°C, 40 min quenched with DTPA
5	NOTA	GRPR/peptide	^{64}Cu in NH_4OAc, pH 7, 70°C, 60 min quenched with DTPA
6	Diamsar	GRPR/peptide	^{64}Cu in NH_4OAc, pH 5.5, 40°C, 60 min
7	Te2A	$\alpha_v\beta_3$ peptide	^{64}Cu in NH_4OAc, pH 8, 95°C, 60 min

Table 1 Typical copper-64 radiolabelling conditions for different macrocyclic chelator systems.

An alternative approach for the labelling of sensitive peptides and proteins could be based on a bifunctional bis(thiosemicarbazone). As discussed in Chapter 1.6, N_2S_2 bis(thiosemicarbazones) form neutral and stable complexes with Cu(II).[3, 8] Due to the reduction potential of Cu(II)ATSM, reduction is believed to occur only in a hypoxic intracellular environment.[9, 10] Due to their modest size and rapid labelling, chelates based on the core CuATSM should not damage or compromise the protein or peptide or reduce receptor binding.[11] Copper radiolabelling of bis(thiosemicarbazones) occurs instantly at room temperature and near physiological pH and radiochemical yields are typically >95%.[3, 12-14] Recent efforts by the Dilworth group have demonstrated that bis(thiosemicarbazonate) systems also offer advantages for practical kit formulation. Synthesis and purification of ^{64}Cu-bis(thiosemicarbazonates) was achieved *via* transmetallation of the corresponding Zn(II) bis(thiosemicarbazonate) bound to a polymer support via its fifth coordination site.[15] Addition of aqueous radiocopper only liberates radiolabelled compound in solution.

Bis(thiosemicarbazones) have already been explored as bifunctional chelators prior to their use in hypoxia imaging.[3] Complexes such as **(1)** and **(2)** incorporated carboxylic acid linker moieties into the complex backbone (Figure 1),[16-19] but they suffered from poor radiochemical yields and were not stable *in vivo* due to demetallation.

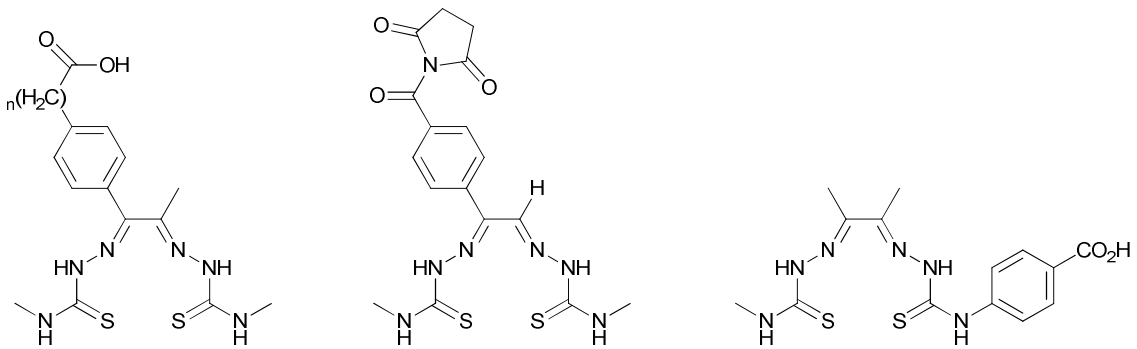

(1) n = 1-5 **(2)** **(3)**

Figure 1 Previously reported bis(thiosemicarbazonate) ligands bearing a COOH functional group.

In order to retain the favourable stability and redox properties of Cu(II)ATSM, work by Heslop *et al*. maintained the dimethyl backbone motif and introduced an aromatic carboxylic acid at the terminal *N*4 substituent (Structure **(3)**, Figure 1).[20] Although this derivative was successfully conjugated to octreotide, it suffered from solubility and purification problems.

As part of a research programme to provide improved hypoxia tracers of the CuATSM family, work in the Dilworth group has yielded bifunctional derivatives bearing a hydrazinic nitrogen group (H_2ATSR/A)[13] at the *N*-terminus as depicted in Figure 2.[13]

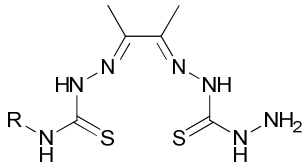

H_2ATSR/A

R= Et, Me, Allyl

Figure 2 H_2ATSR/A ligand

These bis(thiosemicarbazones) were used to prepare small molecule derivatives of the CuATSM family as hypoxia selective tracers (see Chapter 4). The copper (II) complexes maintained the favourable Cu(II)/Cu(I) reduction potential, showed good stability in serum, hypoxia selectivity *in vitro*, and demonstrated *in vivo* tumour uptake of radiocopper. For the radiolabelling of biomolecules however, a chelator with an acid functionality would be advantageous. Solid phase peptide synthesis is often carried out in a *C*- to *N*-terminus fashion since some peptides require *C*-terminus conservation to preserve biological function. Furthermore, protein conjugation frequently is performed *via* pendant amine residues. It was therefore of interest to synthesise new bifunctional bis(thiosemicarbazones) that bear pendant COOH groups for the radiolabelling of sensitive peptides and proteins.

2.2 Aims

The aim of this chapter was to synthesise functionalised bis(thiosemicarbazones) bearing pendant COOH groups based on the H_2ATSR/A proligand. Particular objectives were:

(i) The evaluation of suitable aliphatic and aromatic spacers for functionalisation

(ii) The synthesis of chelators with more than one functional group for derivatisation

(iii) ^{64}Cu and ^{99m}Tc radiolabelling

(iv) Evaluation of the derivatives for use with solid phase peptide synthesis and solution phase protein coupling conditions, using suitable model systems

(v) Biological evaluation of the peptide and protein bioconjugates

2.3 Nomenclature

An abbreviated naming system for bis(thiosemicarbazone) ligands and metal complexes based on the R_1-R_4 ligand substituents, as shown in the general structure in Figure 3, has now been widely adopted. The first letter designates the substitution pattern of the backbone, where for instance A= dialkyl, G= glyoxal and P = pyruvaldehyde. The middle letters TS denote thiosemicarbazone. The R_3 and R_4 substituents on the terminal nitrogen atoms are indicated by single letters such as M = methyl, E = ethyl, P = phenyl. In the case of asymmetrical ligands, both halves are indicated by a forward slash, for instance H_2ATSM/A. The abbreviated names of key derivatives in this thesis, illustrated for the ligand structures, are summarised by the Table of Figure 3 below. Where this facilitates discussion for biological work, derivatives will be discussed based on this naming system with an appropriate extension as defined for each compound.

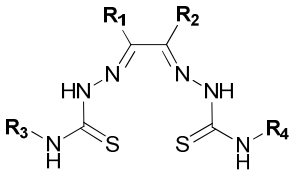

[H_2ATSR$_3$/R$_4$]

Ligand	R_1	R_2	R_3	R_4
H_2ATSM	Me	Me	Me	Me
H_2PTSM	Me	H	Me	Me
H_2GTS	H	H	H	H
H_2ATSM/A	Me	Me	Me	NH_2
H_2ATSE/A	Me	Me	Et	NH_2
H_2ATSMen	Me	Me	Me	$(CH_2)_2NH_2$

Figure 3 Nomenclature of symmetrical and assymetrical bis(thiosemicarbazone) ligands.

2.4 Ligand synthesis

2.4.1 Imine conjugates

Several previous ATSR (where R is a functionalised substituent) derivatives were synthesised *via* the Zn complex rather than the proligand, since the former displays better solubility. The Zn complexes may be transmetallated quantitatively to the corresponding copper complexes. To explore both routes for synthesising a pendant COOH derivative, the ligands **2.03** (H_2ATSM/A) and **2.04** (H_2ATSE/A) and their corresponding Zn complexes **2.05** and **2.06** were synthesised from the half ligands **2.01** and **2.02** as previously reported (Scheme 1).[13, 21]

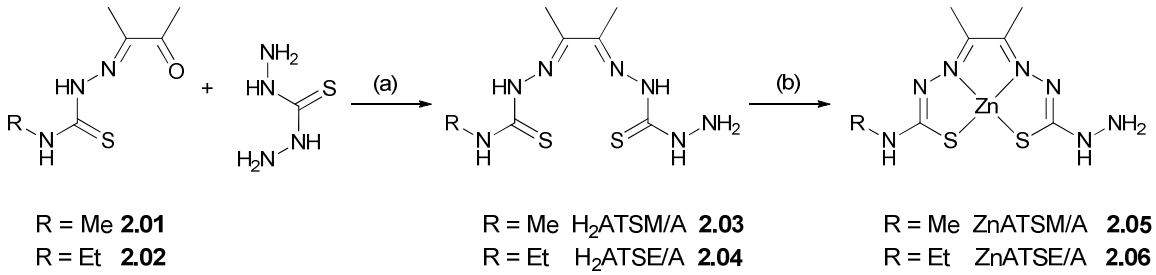

Scheme 1 Synthesis of asymmetrical H_2ATSR/A ligands and corresponding Zn complexes.[13] (a) 10% HCl (aq) catalyst, ethanol, 50°C, 5 h (b) $Zn(OAc)_2 \cdot 2H_2O$, methanol, reflux, 4 h.

In order to synthesise a conjugate bearing an aliphatic spacer unit, simple ring opening of succinic anhydride to form **2.07** was first explored. Reaction of ZnATSM/A with succinic anhydride resulted in a mixture of unidentified products over a range of temperatures (ambient to reflux) in THF, MeOH or DMF. Similarly, reaction of H_2ATSM/A with succinic anhydride at room temperature was unsuccessful. Reaction at higher temperatures in MeOH resulted in a sparingly soluble precipitate. ESI-MS and ^{1}H NMR analysis revealed formation of a ring closed product **2.08**, as indicated by an *m/z* of 342 and a singlet resonance with integral of 4 hydrogens for the succinimide ring methylene protons at 2.8 ppm. However, the extremely low solubility of the substance prevented further characterisation or its use in further chemistry.

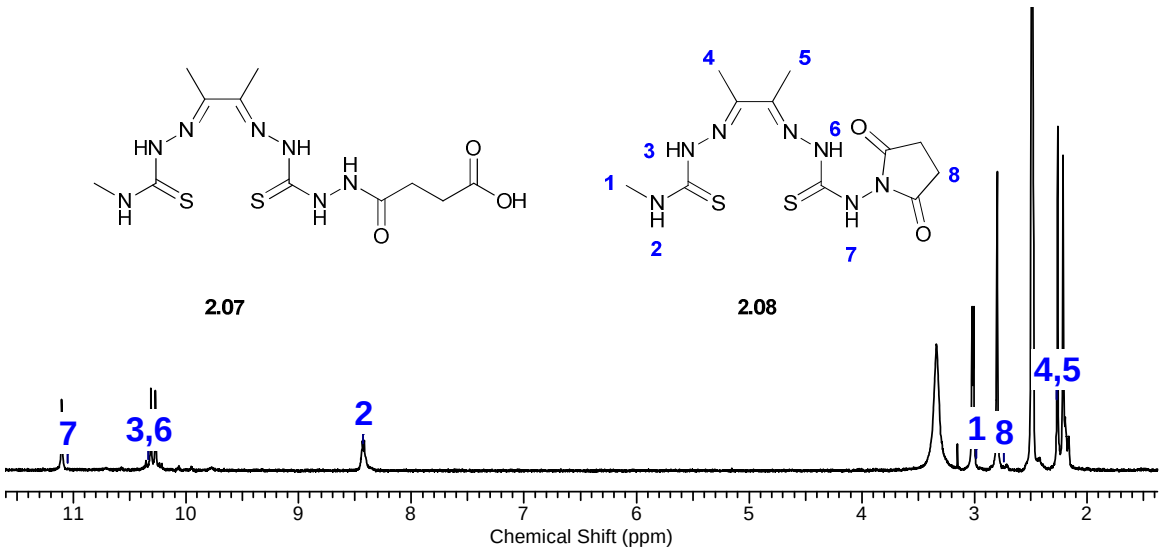

Figure 4 ^{1}H NMR (DMSO-d_6) of product **2.08**, obtained from reaction of H_2ATSM/A with succinic anhydride . The desired product **2.07** was not observed.

Previous H_2- or ZnATSR/A derivatives have been successfully obtained by condensation with an aldehyde or ketone.[21, 22] Since derivatives of aliphatic carbonyls are reported to be unstable,[21] aromatic imine conjugates were investigated. Interestingly, reaction of the Zn complex **2.06** with 2- or 4-carboxybenzaldehyde yielded multiple products based on ^{1}H NMR and HPLC analysis. In contrast, trial conjugations with the protected *p*-methyl ester proceeded cleanly. This suggests that the problems may be attributed to the free acid group which could coordinate to the free apical fifth coordination site on the Zn during reaction or analysis. This route was not further pursued since transformation of the free H_2ATSE/A proligand to the imine conjugates **2.09** and **2.10** proceeded in yields of 70 - 85% (Scheme 2). Ligands were fully characterised by ^{1}H and^{13}C NMR, ESI-MS and elemental analysis as summarised in Table 2.

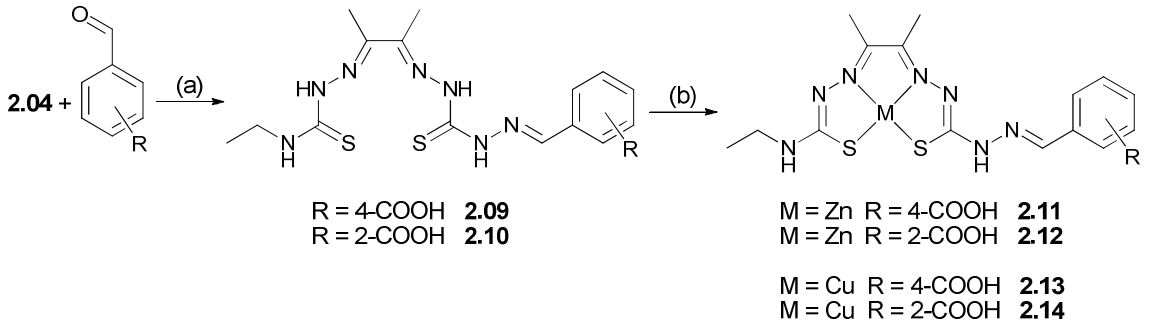

Scheme 2 Synthesis of imine bonded functionalised ligands and metal complexes from the H_2ATSE/A proligand. (a) 1.2 eq aldehyde, MeOH, room temperature, 16 h, 82% (b) 1.1 eq $Zn(OAc)_2 \cdot 2H_2O$ or $Cu(OAc)_2 \cdot H_2O$, MeOH, rt, 30 min, 85-96%.

Previous reports carried out these imine condensations at reflux, however it is noteworthy that reaction of H_2ATSE/A with 2- and 4-carboxybenzaldehyde in methanol proceeded cleanly when carried out at room temperature overnight or at 40°C for 6 h. Reaction at room temperature also avoided ligand self-cyclisation, which has been reported previously for reactions of the H_2ATSM/A ligand at higher temperatures.[13] The copper complexes **2.13** and **2.14** were formed by complexation of the ligand with $CuCl_2$ in methanol. Although the Zn complexes were not required as synthetic precursors, it was of interest to synthesise these with respect to the solid supported radiolabelling method. Remarkably, **2.11** and **2.12** could be formed by reaction of the proligands with $ZnCl_2$, confirming that the problems encountered with **2.06** may be attributed to reactions of the free

carboxyl group with free or complexed zinc. Although a single peak HPLC spectra and HRMS analysis could be obtained for **2.11**, repeated efforts showed low C and N values in elemental analysis. These could be indicative of the presence of water as has been previously observed.[20]

Compound	m/z calc $(M-H)^-$	m/z found	R_t (min, M_1)	Elemental Analysis C, H, N
2.09	406.1125	406.1137	11.85	47.2 (47.2), 5.1 (5.2), 24.0 (24.1)
2.10	406.1125	406.1123	12.05	47.1 (47.2), 5.1 (5.2), 24.0 (24.1)
2.11	468.0260	468.0267	11.75	35.5 (40.8), 3.2 (4.1), 16.8 (20.8)
2.12	468.0260	468.0259	11.75	40.9 (40.8), 4.1 (4.1), 20.8 (20.8)
2.13	467.0265	467.0253	12.25	41.0 (41.1), 4.1 (4.0), 20.9 (20.9)
2.14	467.0265	467.0255	12.05	40.9 (41.1), 4.0 (4.0), 20.9 (20.9)

Table 2 Analysis data for imine conjugated bis(thiosemicarbazone) ligands and their Zn and Cu complexes.

Initially, imine condensations conducted in this chapter also included the use of the H_2ATSM/A derivative. However, transformations of the H_2ATSE/A ligand generally proceeded more cleanly than those of H_2ATSM/A. Where purification was required, derivatives of the ethyl ligand also proved easier to recrystallize, presumably due to their slightly improved solubility in DMSO as well as protic solvents (MeOH, EtOH) at elevated temperatures. Further efforts therefore focused mainly on the ethyl derivatives.

2.4.2 Amide conjugates

Since aromatic imine derivatives may be prone to hydrolysis in aqueous conditions, amide linked derivatives were also investigated for improved stability. To avoid the possibility of obtaining further cyclised derivatives such as **2.08**, aromatic dicarboxylate motifs were used. Previous amide conjugation reactions in the group employed activated NHS esters of an aliphatic carboxylic acid.[23] Initially therefore, the reaction of the *N*-hydroxysuccinimide (NHS) activated esters of the monoprotected (as the esters CO_2Me or CO_2Et) aromatic dicarboxylates with H_2ATSE/A was attempted. However, the use of aromatic activated esters resulted in incomplete reaction or formation of side products. Coupling of the monoprotected acid using EDCI was also unsuccessful. Efficient coupling could be achieved using the BOP coupling agent and DIPEA base in combination with 4-(*tert*-butoxy-carbonyl)benzoic acid as the dicarboxylate. This was more suitable than the mono Me- or Et-esters as these were found to partially hydrolyse during the

coupling procedure, leading to a mixture of products. Couplings were conducted in the minimum amount of DMF at room temperature over 4 h and best results were achieved when using a 0.1 eq excess of acid (with respect to the ligand), coupling agent and base to achieve **2.15** in 96% yield (Scheme 3). Addition of water followed by sonication of the suspension resulted in formation of a fine precipitate which was isolated by filtration. Subsequently, the precipitate was washed with water and EtOH to remove the by-products liberated by the coupling agent.

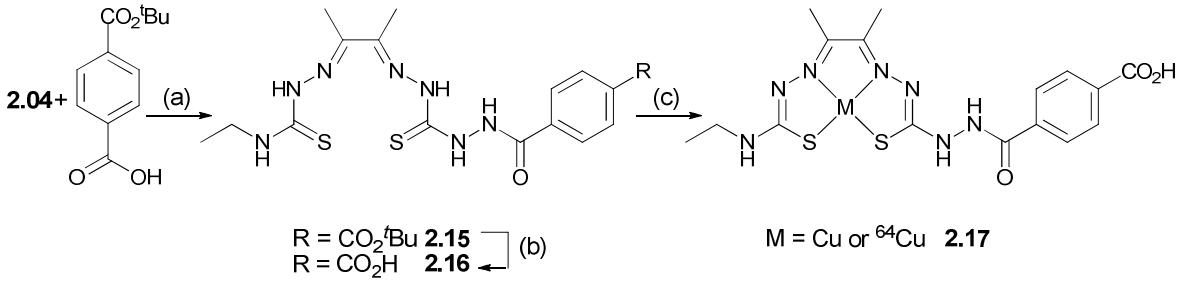

Scheme 3 Synthesis of amide bonded ligand **2.16** from the H_2ATSE/A proligand (a) 1.1 eq BOP, 1.1 eq DIPEA, DMF, rt, 4 h, 96% (b) trifluoroacetic acid (TFA), rt, 2.5 h, 65% (c) $Cu(OAc)_2$, MeOH, rt, 30 min 85% or $[^{64}Cu]Cu(OAc)_2$ (see 2.4.5).

Deprotection of **2.15** gave **2.16** in 65% yield using neat TFA over 2.5 h at room temperature. The volume of TFA was decreased *in vacuo* before addition of Et_2O and isolation of the product by filtration. The products were fully characterised by ESI-MS, ^1H and ^{13}C NMR and elemental analysis, as summarised in Table 3. Noteably, the bis(thiosemicarbazone) ligand was stable in neat TFA for periods of up to 4 h.

Compound	m/z calc $(M-H)^-$	m/z found	R_t (min)	Elemental Analysis C, H, N
2.15	502.1666 †	502.1667	13.18 (M_2)	50.0 (50.1), 6.0 (6.1), 20.4 (20.4)
2.16	422.1075	422.1076	10.35 (M_1)	45.3 (45.5), 5.0 (5.0), 23.2 (23.2)
2.17	483.0214	483.0213	10.30 (M_1)	39.6 (39.6), 4.0 (4.0), 20.1 (20.2)

Table 3 ESI-MS data, † denotes $(M+Na)^+$, HPLC retention times (methods M_1 and M_2) and elemental analysis data found (calc.) for **2.15**-**2.17**.

2.4.3 Solution phase conjugation and extended linker synthesis

The suitability of the new set of carboxyl functionalised bis(thiosemicarbazones) for coupling to peptides and proteins under aqueous conditions was assessed. Glycine and triglycine were chosen as amino acid and peptide sequence mimic respectively. The NHS activated ester of **2.09** was formed readily using EDCI in DMF, but the activated ester of **2.16** was not detected by ESI-MS. The low solubility of the imine activated ester required its use *in situ*. An aliquot of the DMF solution was added to an equimolar amount of glycine or triglycine in PBS. Regrettably, the active ester showed slight precipitation and was recovered unchanged at the end of the 6 h incubation. To investigate whether the lack of reactivity was due to the low solubility of the derivatives, the water-soluble sulfo-NHS ester was synthesised and used *in situ*. No desired product was detected. It seemed possible that this may be caused by a decreased reactivity of the aromatic NHS esters, further enhanced by a stabilising conjugation with the ATSE ligand system.

We surmised that the reactivity and solubility could be improved by breaking the conjugation *via* the introduction of a further aliphatic spacer. Despite the lack of reactivity of the NHS ester, coupling of the pendant aromatic COOH group of **2.16** to glycine(*tert*butylester) was accomplished using the BOP coupling protocol to afford conjugate **2.18** in 98% yield (Scheme 4). TFA deprotection analogous to that applied to **2.15** afforded the extended linker **2.19**.

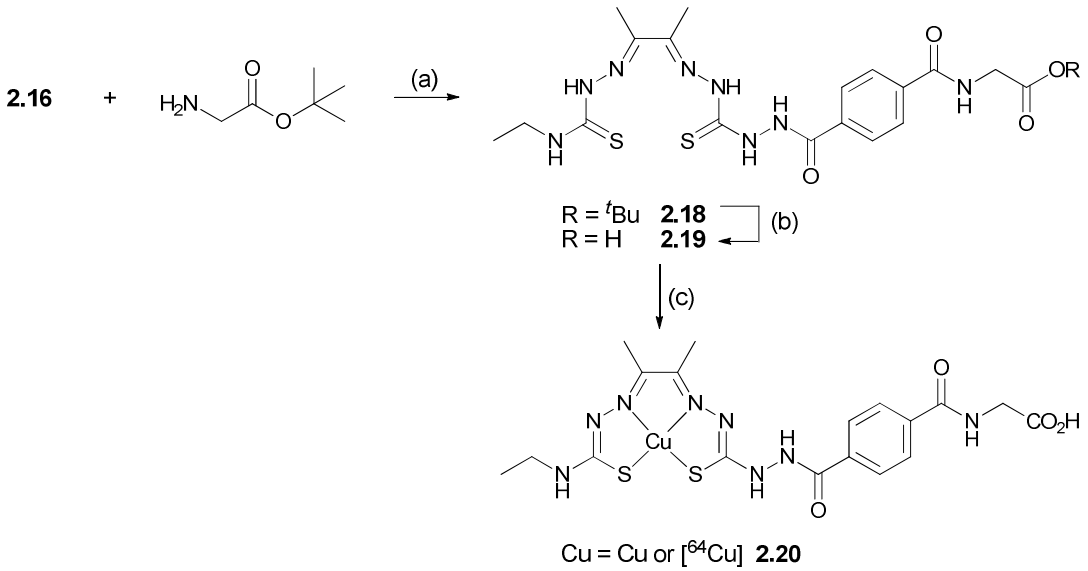

Scheme 4 (a) 1.1 eq glycine tertbutyl ester, 1.1 eq BOP, 1.1 eq diisopropylethylamine, DMF, rt, 4 h, 98% (b) trifluoroacetic acid, rt, 2.5 h, 71% (c) $Cu(OAc)_2 \cdot H_2O$, MeOH, rt, 30 min, 96% or $[^{64}Cu]Cu(OAc)_2$ (see 2.4.5).

The TFA deprotection conditions were deemed unsuitable for the imine conjugate. The extended aldehyde linker methyl 2-(4-formylbenzamido)acetate (**2.21**)[24] was synthesised first and then condensed with H_2ATSE/A to afford **2.22** in 68% yield (Scheme 5). The ligands were fully characterised by ESI-MS, ^{1}H and ^{13}C NMR and elemental analysis. Figure 5 and 6 depict the ^{1}H and ^{13}C NMR spectra of **2.22**. Copper complexation of both extended linkers to give **2.20** and **2.23** was achieved using $Cu(OAc)_2{\cdot}2H_2O$ or $CuCl_2$ in MeOH at room temperature.

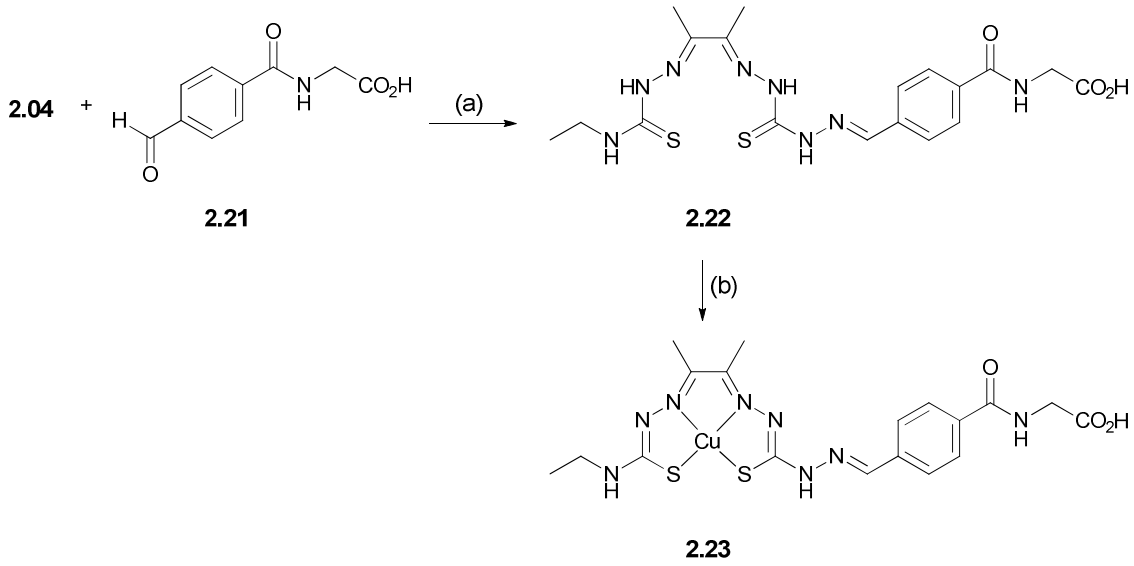

Scheme 5 Synthesis of extended imine-conjugated ligand **2.22** and its copper complex **2.23.** (a) MeOH, rt, 16 h then 50°C, 2 h, 68% (b) $Cu(OAc)_2.H_2O$, MeOH, rt, 30 min, 76%.

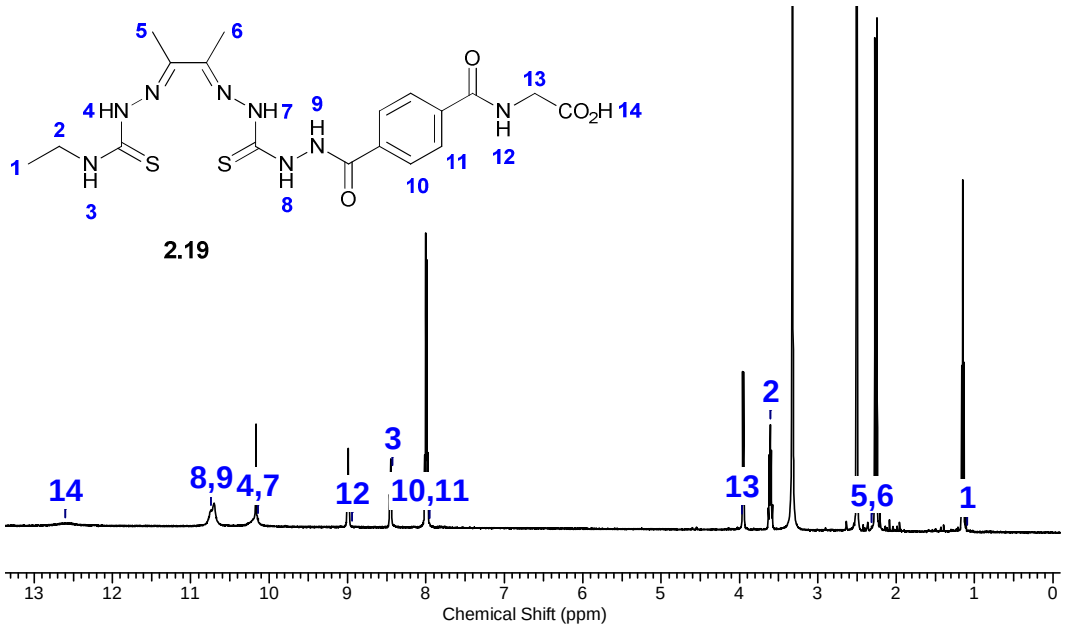

Figure 5 ^{1}H NMR spectrum of **2.19** in DMSO-d_6.

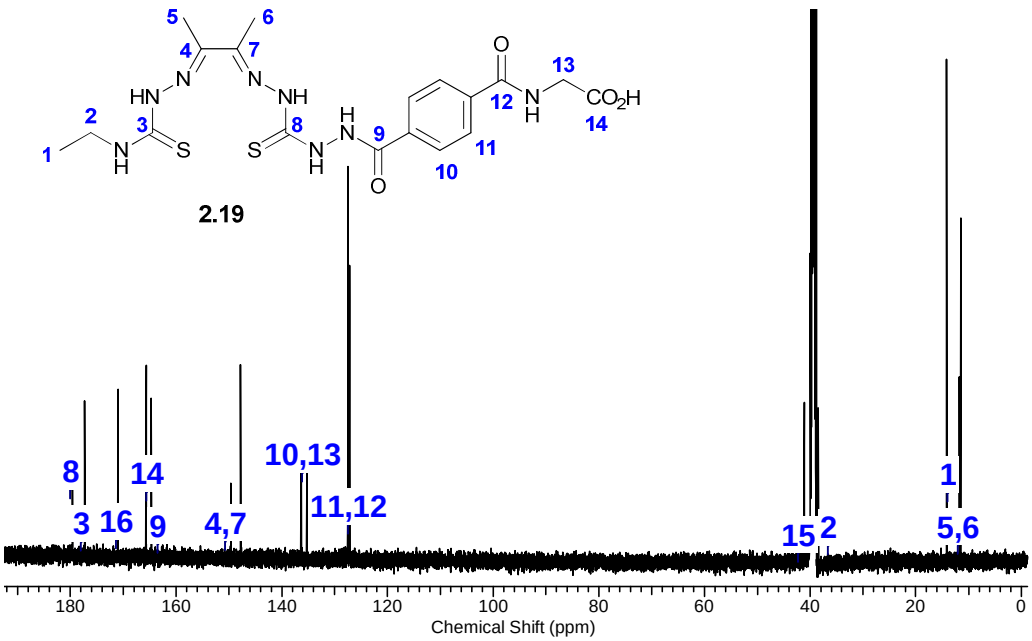

Figure 6 ^{13}C NMR spectrum of **2.19** in DMSO-d_6

In order to prevent further solubility problems as those encountered with the NHS activated ester of **2.09**, only the water soluble sulfo-NHS analogues of the extended linker ligands were synthesised using EDCI and sulfo-NHS in DMSO. The esters were used *in situ* and reacted with triglycine in DMSO or PBS. Product formation in these trial reactions was detected by ESI-MS. After 1 h, the desired conjugates **2.24** and **2.25** could be detected, after 12 h only product and residual acid (if conducted in water) were detected. These preliminary experiments demonstrate that the extended linkers should in principle be suitable for conjugation to proteins under aqueous conditions using a frequently employed EDC/sulfo-NHS approach.[25]

Compound	Corresponding activated ester	Activated ester *m/z* found (calc)	Triglycine conjugate	*m/z* found (calc)
2.09	NHS	503.1 (503.1)		not detected
2.09	sulfo-NHS	583.09 (583.09)		not detected
2.16	NHS	not detected		-
	sulfo-NHS	not detected		-
2.19	sulfo-NHS	679.09 (679.09)	**2.25**	593.17 (593.17)
2.22	sulfo-NHS	640.12 (640.12)	**2.24**	634.19 (634.19)

Table 4 ESI-MS ($(M-H)^-$) data for activated ester formation and reaction.

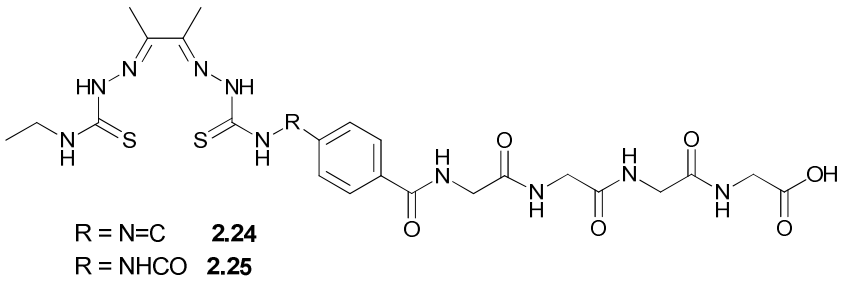

Figure 7 Products of the reaction of the sulfo-NHS esters of **2.19** and **2.22** with triglycline.

2.4.4 Bifunctional derivatisation- conjugation with glutamic acid

The preparation of a bifunctional chelator that can accommodate another orthogonal attachment site, in addition to that conjugated to a targeting biomolecule, was investigated next. This allows the bis(thiosemicarbazone) chelator to accommodate a second diagnostic label for multimodal imaging or a pharmacokinetic modifier. In addition, it offers the possibility to incorporate the radiotracer at any given point within a peptide sequence. In order to enhance the solubility of the bis(thiosemicarbazone), the derivative was based on an aliphatic construct, using glutamic acid with orthogonally-protected NH_2 and CO_2H groups as depicted in Scheme 6. **2.03** was conjugated to FmocGlu(O^{t}Bu)OH using the previous BOP coupling protocol (Scheme 4). The resultant product was recrystallised from EtOH to achieve **2.26** in 59% yield.

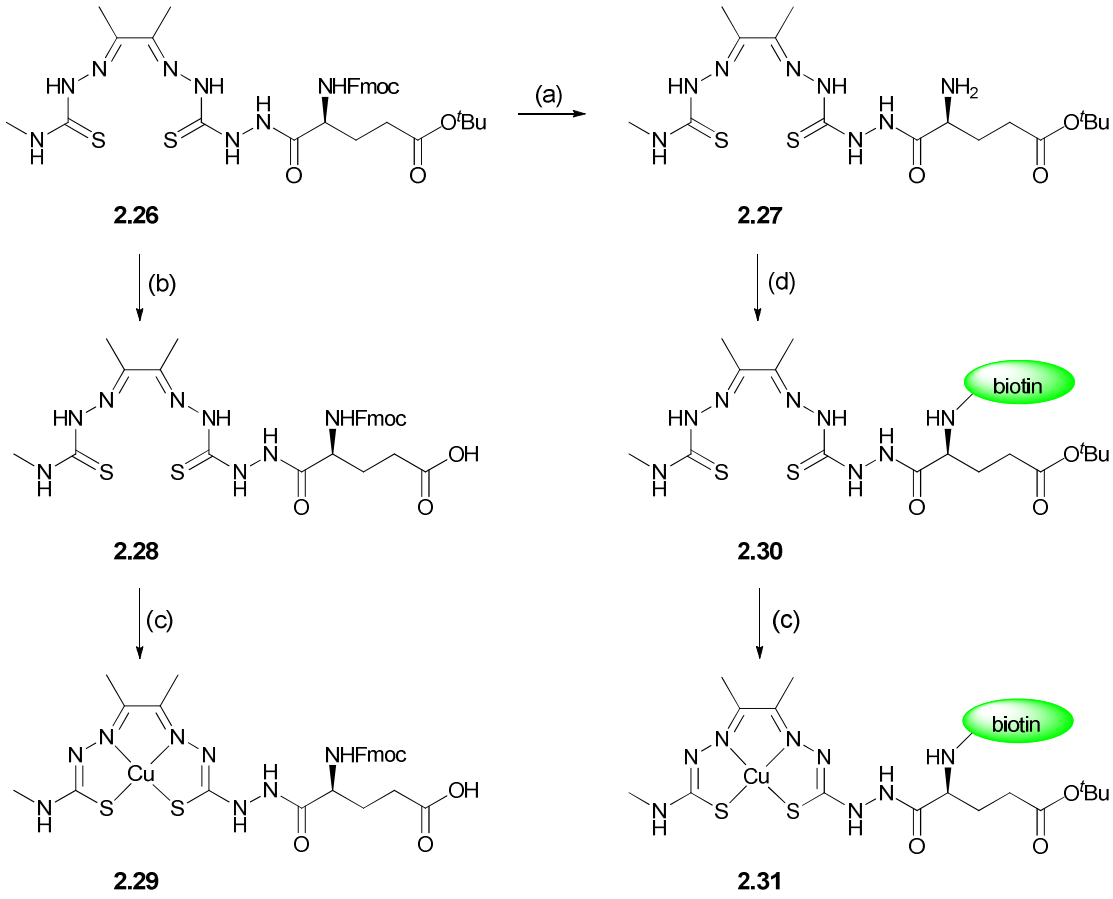

Scheme 6 Synthesis, selective deprotection and bioconjugation of an aliphatic linked bis(thiosemicarbazone) bifunctional chelator. **2.26** and **2.30** were prepared under the same conditions as for **2.19** using BOP. (a) 20% piperidine, DMF, 45 min then H_2O, then Et_2O, 60% (b) TFA, 3 h, rt, then Et_2O, 59% (c) $Cu(OAc)_2 \cdot H_2O$, MeOH, rt, 30 min, 77% for **2.29** and 96% for **2.31** (d) Biotin, BOP, DIPEA, DMF, 4 h, 63%.

Selective deprotection of the functional groups was achieved using standard Fmoc/^{t}Bu deprotection methods. Reaction with 20% piperidine in DMF afforded **2.27** bearing a free amine group whereas deprotection in neat TFA over 3 h gave **2.28** followed by Cu-complexation to give **2.29**. As a proof-of-principle, **2.27** was conjugated to the commonly used biomarker biotin to obtain ligand **2.30** which was fully analysed by NMR, ESI-MS, HPLC and elemental analysis. Subsequent Cu-complexation to form **2.31** proceeded with a 96% yield. Elemental analysis data for the Cu complex indicated low values for C and N but a single peak HPLC and high resolution mass were successfully obtained.

Compound	m/z calc $(M+Na)^+$	m/z found	R_t (min)	Elemental Analysis C, H, N (calc)
2.26	691.2455	691.2437	14.55	55.6 (55.7), 5.9 (5.9), 16.6 (16.6)
2.27	447.1955*	447.1964	12.40	42.9 (43.0), 6.8 (6.8), 25.0 (25.1)
2.28	613.2010*	613.1989	12.45	52.9 (52.9), 5.2 (5.3), 18.2 (18.3)
2.29	672.1004	672.0983	12.40	48.0 (48.1), 4.6 (4.5), 16.6 (16.6)
2.30	695.2550	695.2554	11.26	46.4 (46.4), 6.5 (6.6), 20.9 (20.8)
2.31	756.1690	756.1691	11.84	39.6 (42.5), 3.2 (5.8), 15.7 (19.1)

Table 5 ESI-MS, HPLC and elemental analysis data for **2.26-2.31**. *denotes $(M+H)^+$.

2.4.5 ^{64}Cu Radiolabelling

The ligands **2.09**, **2.16**, **2.19** and **2.22** were selected for copper-64 radiolabelling experiments. These were performed at the Siemens Oxford Molecular Imaging Laboratory. Copper-64 was purchased either from Mr Paul Burke at the Wolfson Brain Imaging Centre, Cambridge, or from Dr Rowena Paul at St. Thomas' Hospital, King's College London. The radioisotope was prepared by the ^{64}Ni(p,n)^{64}Cu nuclear reaction on a medical cyclotron by bombarding an enriched ^{64}Ni electroplated gold target.[26] [^{64}Cu]Cu^{2+}(aq) was extracted from the target in HCl and separated from [^{64}Ni]Ni^{2+} using ion exchange chromatography. [^{64}Cu]Cu^{2+} was obtained as aqueous [^{64}Cu]$CuCl_2$ in 0.1 M HCl. The stock solution of copper was reformulated to [^{64}Cu]$Cu(OAc)_{2(aq)}$ by addition of 0.2 M sodium acetate buffer (pH = 5.5) and this solution was used for radiolabelling reactions. The ^{64}Cu-complexes were prepared from the corresponding ligands as reported for previous systems.[13] A 1 mg mL^{-1} solution of the relevant ligand was prepared in DMSO. For these small scale

reactions, 10 - 20 µL of [^{64}Cu](OAc)$_2$(aq) (<10 MBq) was added to 50 µL of the ligand solution and 150 µL DMSO. Reaction mixtures were left to stand at room temperature for 5 min before 25 µL of the reaction solution was analysed by reverse-phase radio-HPLC and radio-TLC.

As anticipated for bis(thiosemicarbazones), labelling of **2.09**, **2.16**, **2.19** and **2.22** to give [^{64}Cu]**2.13**, [^{64}Cu]**2.17**, [^{64}Cu]**2.20** and [^{64}Cu]**2.23** respectively occurred virtually instantaneously at room temperature. Radio-HPLC and radio-TLC confirmed that all four complexes were obtained in high radiochemical yield (RCY) (typically > 98%) and high radiochemical purity (> 95%) as summarised in Table 6. Figure 8 depicts the radio-HPLC of [^{64}Cu]**2.23**.

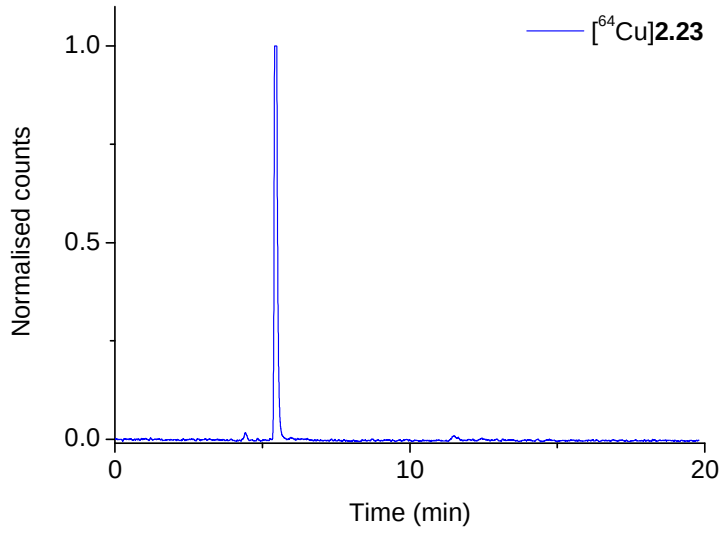

Figure 8 Radio-HPLC trace of [^{64}Cu]**2.23**.

Although these derivatives were not yet conjugated to a targeting biomolecule, it was of interest to get a first indication to what the extent they bind to serum proteins, since binding to the protein fraction in blood *in vivo* can affect biodistribution and availability.[27, 28] To this end, [^{64}Cu]**2.13**, [^{64}Cu]**2.17**, [^{64}Cu]**2.20** and [^{64}Cu]**2.23** were incubated in fresh mouse serum *in vitro*, and aliquots were removed up to 120 min post incubation for analysis. The amount of protein bound radioactivity was determined by the ethanol precipitation method (for a detailed discussion of this method, see Chapter 5.6). At 120 min, around 20% of the activity was bound for all derivatives. Significantly, the amount of activity bound remained constant over time, suggesting little or no

decomposition over the course of incubation. This is comparable to what has previously been observed for [^{64}Cu]CuATSM and related derivatives.[12, 22, 23]

Compound	RCY	Serum binding	Log P
[^{64}Cu]**2.13**	>98%	18%	1.36
[^{64}Cu]**2.17**	>98%	20%	1.48
[^{64}Cu]**2.20**	>99%	19%	0.88
[^{64}Cu]**2.23**	>99%	22%	0.94

Table 6 Radiolabelling yields (determined by radio-TLC (EtOAc/MeOH 95:5) of [^{64}Cu]**2.13**, [^{64}Cu]**2.17**, [^{64}Cu]**2.20** and [^{64}Cu]**2.23** and a comparison of serum binding and log P values for the derivatives.

2.5 Applications to the ^{64}Cu-radiolabelling of peptides

Following the successful synthesis and ^{64}Cu-radiolabelling of the COOH-functionalised ligands it was decided to test their suitability for the radiolabelling of a peptide model system. In particular, the ability to survive standard solid phase peptide synthesis conditions is important if the chelator is to be incorporated into a peptide sequence. The stable amide bonded chelators **2.16** and **2.19** were deemed most suitable for this purpose.

2.5.1 Bombesin

One of the most widely investigated radiolabelled peptide targeting vectors is Bombesin (BBN).[29, 30] The 14-amino acid sequence is the amphibian homologue of the gastrin releasing peptide (GRP). Gastrin releasing peptide receptors (GRPR) are highly overexpressed on a variety of human tumour cells in prostate cancer,[31] breast cancer[32] and small cell lung cancer tissues.[33] BBN sequences have been extensively radiolabelled with various radionuclides, such as ^{18}F, ^{67}Ga, ^{99m}Tc and ^{177}Lu and ^{64}Cu, for diagnostic PET and SPECT imaging as well as targeted radiotherapy.[34-38] In particular, BBN sequences have been investigated with ^{64}Cu using several DOTA and NOTA type macrocycles[34] and should therefore serve as a suitable benchmark to investigate bis(thiosemicarbazonate) peptide conjugates, providing a platform for *in vitro* and *in vivo* comparison.

The exact peptide sequence was chosen in collaboration with the group of Prof Dirk Tourwé at Vrije Universiteit Brussels. The chosen sequence was the minimum active sequence BBS(7-14) that had been optimised to achieve enhanced pharmacokinetics. The amino acids Leu[13] and Met[14] are replaced by Cha and Nle respectively and the sequence bears a β^3AspβAlaβAla spacer between the peptide and chelator.[39, 40] These modifications have been shown to increase stability and confer higher tumour uptake when radiolabelled with ^{99m}Tc using an N$^{\alpha}$HisAc chelator.[41, 42]

2.5.2 Conjugation to Bombesin

Peptide conjugation was carried out at the Department of Organic Chemistry at Vrije Universiteit Brussels, Belgium under the supervision of Prof Dirk Tourwé and Dr Veronique Maes.

The protected peptide, kindly provided by Dr Maes, was synthesised on a rink amide resin using the Fmoc-strategy previously described.[40] All couplings were carried out in duplicate using 4 eq of Fmoc-amino acid, 4 eq of DIC and 4 eq of HOBt in DMF. The synthesis of the conjugate is outlined in Scheme 7.

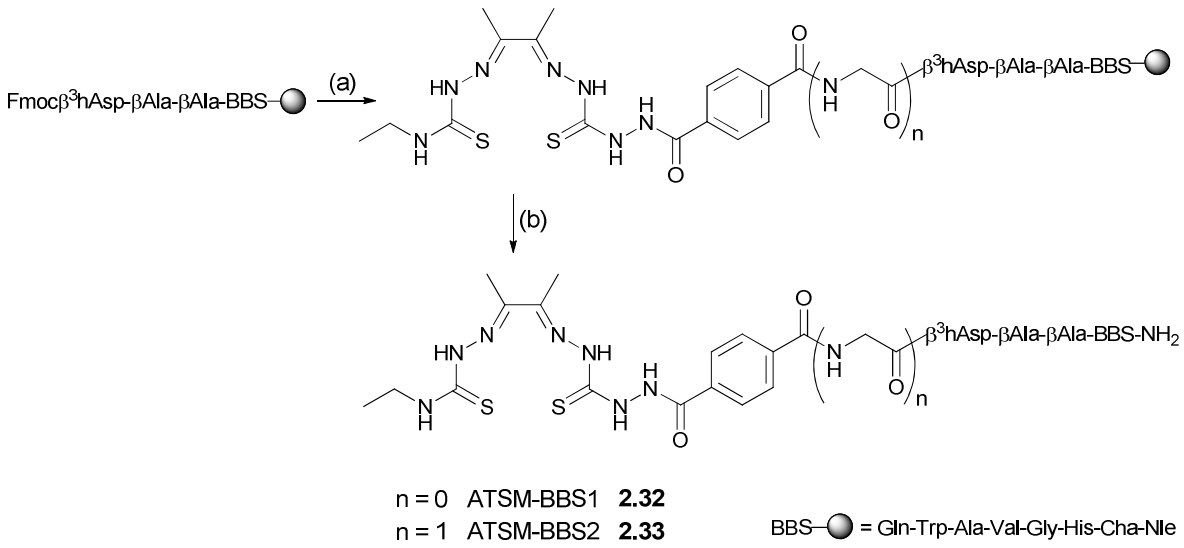

Scheme 7 Solid phase synthesis of the bis(thiosemicarbazone)-BBS conjugates. Reagents and Conditions (a) 1ml 25% 4-methylpiperidine in DMF, 2 × 10 min, rt then ATSM-BBS1: 2 eq BOP, DIPEA, DMF, rt, 8 h; ATSM-BBS2: 2 eq DIC, HOBt, 3 h, rt (b) thioanisole (TA)/ethanedithiol (EDT) 7:3 in TFA, 3.5 h, rt.

Immediately prior to conjugation with chelator **2.16** and **2.19**, the terminal Fmoc group was removed from the resin-bound peptide by treatment with 4-methylpiperidine in DMF. As anticipated from the solution phase coupling experiments in section 2.4.3, chelator **2.16** required activation with BOP coupling agent and DIPEA base over 8 h to achieve conjugation. Chelator **2.19** coupled readily over 3 h using the standard DIC and HOBt protocol employed for the Tc chelators. Prior to peptide cleavage, the resin was washed with CH_2Cl_2, Et_2O and dried *in vacuo*. Global cleavage and deprotection was performed using TFA as described in Scheme 7. The solution was then added to Et_2O to precipitate the peptide which then was lyophilised to afford the conjugates **2.32** (designated as ATSM-BBS1) and **2.33** (ATSM-BBS2) respectively. Both conjugates were purified by preparative HPLC and lyophilisation. During preparative HPLC, not all of the material was recovered from the column. This was attributed to the slightly low solubility of the conjugates in the solvent system. Attempts to use other systems were unsuccessful. The purities of the isolated conjugates compared well to the previously reported systems as summarised in Figure 9.[43]

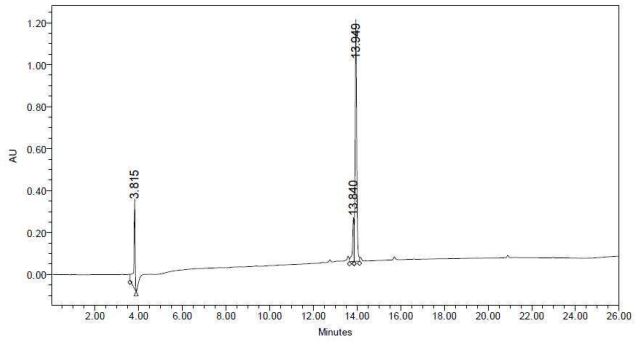

Ligand	ATSM-BBS1	ATSM-BBS2
m/z found	1638.6	1694.7
(calc)	(1637.8)	(1694.8)
yield	53.4%	19.4%
purity	94%	95%
HPLC R_t	14.1 min	14.0 min

Figure 9 (left) HPLC of the bis(thiosemicarbazone) bombesin conjugate ATSM-BBS1 after preparative HPLC purification (R_t = 4 min = solvent peak) (right) Chemical characterisation data of both conjugates.

2.5.3 EPR studies

The backbone-functionalised bis(thiosemicarbazone) systems previously reported suffered from significant non-specific copper protein binding.[3] Before proceeding with radiolabelling experiments, it was therefore decided to establish whether metal binding at ambient temperature would still result in specific copper complexation at the chelator site, rather than unspecific binding to the peptide sequence. For this purpose, both the unconjugated chelator **2.16** and the ATSM-BBS1 sequence **2.32** were titrated with 1 eq of $Cu(OAc)_2 \cdot 2H_2O$ at room temperature to form the corresponding copper complexes **2.17** and **2.34** (designated as CuATSM-BBS1). EPR analysis was then used to analyse the copper species formed. Spectra were recorded by Dr Michael Jones.

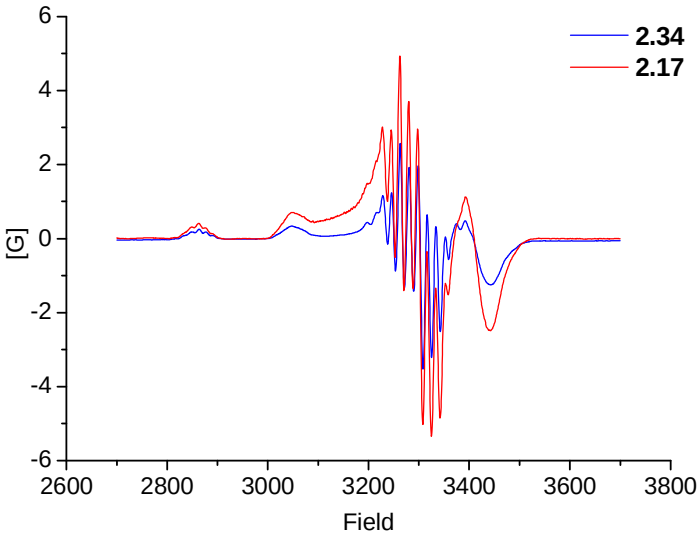

Figure 10 X-band EPR spectra of **2.17** and **2.34** in anhydrous DMF/ethylene glycol 4:1 at 60K.

As can be seen from Figure 10, the EPR spectra of both **2.17** and **2.34** indicated that a single Cu(II) species had been formed.[44-48] The copper is d^9 square planar and the EPR spectra at X-band bear close similarity to other Cu(II)ATSM derivatives previously studied.[44] This confirms that in the conjugates the copper is bound exclusively in the bis(thiosemicarbazone) ligand as there are no signals attributable to copper bound to the protein. This in line with the clean radio-HPLC traces that were observed for the ^{64}Cu-labelled complexes (see sections 2.4.5 and 2.5.4).

2.5.4 ^{64}Cu-radiolabelling of ATSM-BBS conjugates

Copper-64 radiolabelling and biological investigations of the ATSM-BBS conjugates were carried out at the Centre of Radiopharmaceutical Sciences of the Paul Scherrer Institut, Switzerland. Radiolabelling of the conjugates for biological investigations was performed by Mr Alain Blanc. Biological tests were conducted by Dr Elisa García-Garayoa.

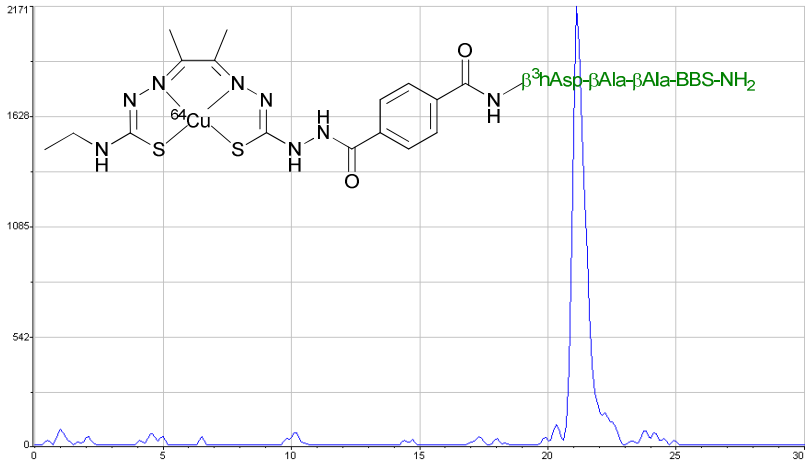

Figure 11 Radio-HPLC of [^{64}Cu]CuATSM-BBS1 radiolabelled at rt after Sep-pak purification.

Copper radiolabelling of ATSM-BBS1 and ATSM-BBS2 to give [^{64}Cu]CuATSM-BBS1 ([^{64}Cu]**2.34**) and [^{64}Cu]CuATSM-BBS2 ([^{64}Cu]**2.35**) was performed in ammonium acetate buffer at pH 5.5 at room temperature. The radiochemical yield of [^{64}Cu]CuATSM-BBS2 (91%) was slightly higher than that for [^{64}Cu]CuATSM-BBS1 (85%).[*] Simple purification by Sep-pak cartridge proved sufficient to obtain radiochemically pure complexes. Interestingly, when the labelling was done at 75°C, yields were > 90-95 %. Radio-HPLC analysis after 24 h revealed that the complexes were stable in saline solution. Log *P* values were determined as described earlier and found to be 0.42 ± 0.04 and 0.39 ± 0.01 for [^{64}Cu]CuATSM-BBS1 and [^{64}Cu]CuATSM-BBS2 respectively. Figure 11 depicts the HPLC chromatogram of [^{64}Cu]CuATSM-BBS1 after purification.

[*] The radiocopper used at PSI for peptide labelling and *in vitro* and *in vivo* experiments contains small amounts of ^{67}Cu. Pure ^{64}Cu was used for all other labelling work in this thesis.

2.5.5 Receptor binding and internalisation studies

Receptor binding is an important prerequisite for high tumour affinity *in vivo* and therefore the receptor binding affinity of the ligand peptide conjugates was verified prior to *in vivo* investigations. Binding studies were performed on human prostate adenocarcinoma cells (PC3) that express a high level of GRPR. A competition assay was performed on adherent cells using a previously reported procedure with the non-labelled ATSM analogues and [^{125}I-Tyr^{4}]BBS.[49] IC_{50} values, determined from the replacement curves shown in Figure 12, were 2.9 nM and 3.8 nM for ATSM-BBS1 and ATSM-BBS2 respectively. The bis(thiosemicarbazone) conjugates therefore displayed affinities in the range of the analogous (N^{α}His)chelator containing sequence previously used for chelation of ^{99m}Tc (5.1 nM) and compared well to that of natural bombesin (1.9 nM).[41, 42]

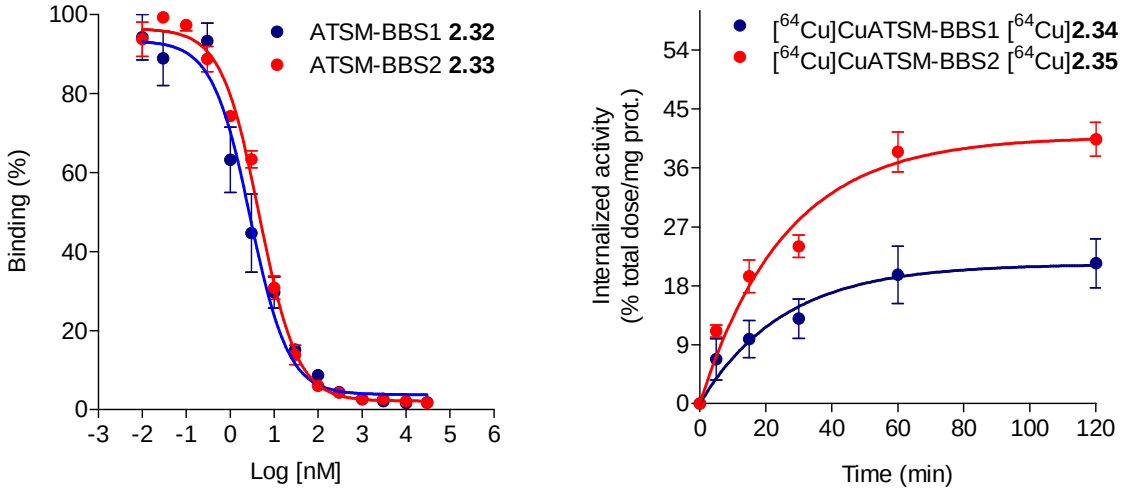

Figure 12 (left) Displacement curves of ATSM-BBS1 and ATSM-BBS2 in PC-3 cells. (right) Time course internalisation of the ^{64}Cu-labelled analogues in PC3 cells. The percentage of internalised activity is given relative to the total activity added to the cells.

Receptor internalisation assays with the radiolabelled conjugates [^{64}Cu]**2.34** and [^{64}Cu]**2.35** showed that internalisation was somewhat slower for the [^{64}Cu]CuATSM-BBS conjugates than for the comparable ^{99m}Tc(N^{α}His) system which showed close to 80% internalization after 30 min.[41] Overall, [^{64}Cu]CuATSM-BBS2 showed much better internalisation than [^{64}Cu]CuATSM-BBS1.

2.5.6 *In vivo* biodistribution

Since [^{64}Cu]CuATSM-BBS2 ([^{64}Cu]**2.35**) displayed better internalisation and lower non-specific binding, this derivative was chosen for preliminary *in vivo* evaluation. Biodistribution studies were performed in female CD-1 nu/nu mice bearing PC-3 tumour xenografts. Mice were injected intravenously with 100 kBq of [^{64}Cu]CuATSM-BBS2 and sacrificed at 1 or 24 h post injection (p.i.). Organs were harvested and counted in a γ-counter to determine the percentage of the injected dose per gram of tissue (%ID/g).

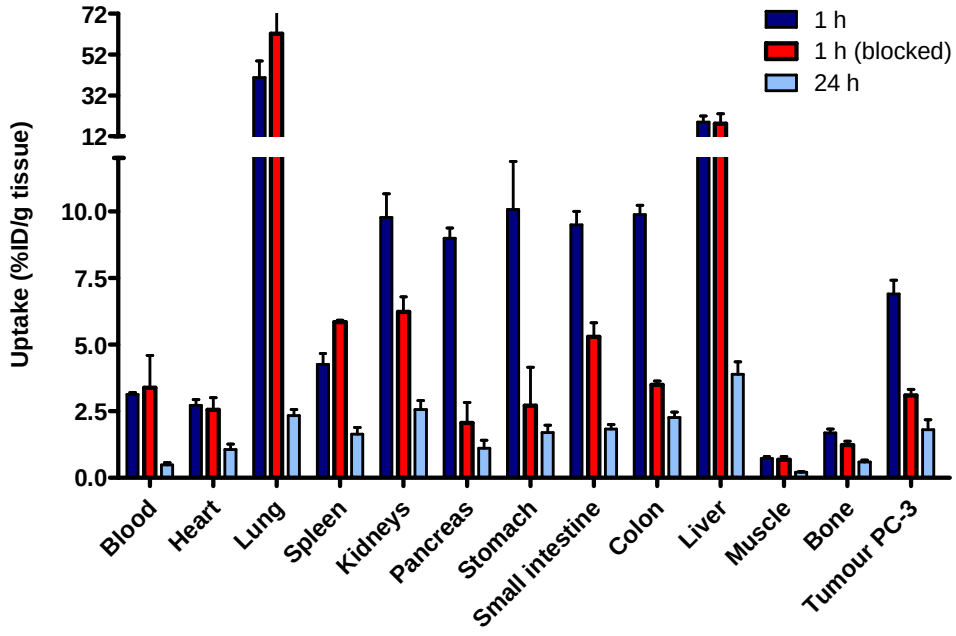

Figure 13 Biodistribution by dissection of [^{64}Cu]CuATSM-BBS2 ([^{64}Cu]**2.35**) in nude mice with PC3 tumour xenografts.

From the dissection data in Figure 13, it can be seen that [^{64}Cu]CuATSM-BBS2 showed rapid blood clearance, with 3% ID/g at 1 h and less than 0.5% ID/g remaining in the blood at 24 h p.i. Interestingly, lung uptake was very high at the early time point but was cleared at 24 h. This is in contrast to what has been observed for the ^{99m}Tc derivatives previously (<1% ID/g). It was suspected that this may be due to the low solubility of the conjugate in aqueous media. The high pancreatic and gastrointestinal uptake is consistent with the high receptor expression in these organs. These values could be significantly reduced in blocking studies, where mice were

administered a co-injection of 100 µg of unlabelled peptide. Liver uptake was high which is in accordance with the high lipophilicity of the derivative. However it is highly likely that this arises from copper being sequestered from the ATSM ligand (see discussions in Chapter 5 on the *in vivo* stability of CuATSM). Further *in vivo* experiments would be needed to determine the precise origin of this high liver uptake.

Significantly however, tumour uptake of [$^{64/67}$Cu]CuATSM-BBS2 was high, displaying tumour-to-muscle ratios (RTM) of 9.6:1 at 1h p.i. A direct comparison with other ^{64}Cu systems is hampered as data for this exact peptide sequence labelled with another copper chelator is not yet available. However, the uptake observed was significantly higher than for other copper chelators with a comparable bombesin motif, where tumour uptake for DOTA and NOTA labelled derivatives was 4%ID/g.[50] Importantly, tumour uptake of [$^{64/67}$Cu]CuATSM-BBS2 was significantly reduced in blocking studies which confirms the specificity of the uptake.

2.6 Applications to the ^{64}Cu-radiolabelling of proteins

The peptide conjugation and room temperature ^{64}Cu-radiolabelling of the carboxylate functionalised bis(thiosemicarbazones) in section 2.5 demonstrated that these are in principle suitable bifunctional chelators for the ^{64}Cu-labelling of biomolecules. Thus it was decided to investigate the potential of the bis(thiosemicarbazone) motif for the radiolabelling of heat-sensitive proteins. Besides accomplishing a mild, high specific activity radiolabelling approach, site specific attachment of the label is crucial for certain proteins to retain their specific targeting. Traditionally, radiolabels are attached *via* the thiol groups of cysteine residues or, most commonly, *via* the ε-amine of lysine residues.[25] Whilst this is readily achieved, the abundance of these residues means that the protein could be modified at, or close to, its active or binding site, potentially rendering the bioconjugate biologically inactive. One way to address this concern is to provide a bio-orthogonal conjugation site for the chelator on the protein.

The aim of this section was to investigate the suitability of functionalised copper bis(thiosemicarbazonates) for the mild, site specific ^{64}Cu-radiolabelling of a genetically engineered C2A domain of rat synaptotagmin I, which was selected for proof-of-concept experiments.

2.6.1 C2A and cell death

The regulation of cellular death is critical to maintain normal physiology in the body. The two main forms of cell death are apoptosis (programmed cell death) and necrosis (accidental, non-regulated cell death).[51] Dysregulation of these pathways, in particular with respect to apoptosis, is central to many diseases. Unwanted apoptosis for instance occurs during myocardial infarction or immune rejection following an organ transplant.[52] In contrast, many cancers acquire resistance to apoptosis and chemotherapeutic treatments and radiotherapy are aimed at inducing apoptotic cell death.[53] Hence, the non-invasive imaging of cell death is an important clinical objective to assess the extent of disease or to monitor treatment progress. A common characteristic of apoptosis is the externalisation of phosphatidylserine (PS), a component of the inner leaflet cell membrane, which acts as a molecular flag for phagocytes.[54] There are several proteins that have a high affinity for

phosphatidylserine, examples include Annexin V and the C2A domain of Synaptotagmin I that both bind to PS in a Ca^{2+} dependent manner. Radiolabelled, these may serve as proteinogenic imaging agents. Annexin V, radiolabelled with ^{99m}Tc and ^{18}F has been widely investigated in preclinical and early stage clinical PET and SPECT imaging of cell death in myocardial infarction and cancer.[55-57] Likewise, the ~16 kDa protein C2A has been labelled with ^{99m}Tc for SPECT.[58] A recent report comparing fluorescently labelled C2A and Annexin V suggests that C2A has reduced binding to viable cells, resulting in up to 4-fold more specific binding to necrotic and apoptotic cells when compared to Annexin V.[59] Similar to Annexin V however, C2A is vulnerable to non-site specific modification and it has been demonstrated that labelling *via* the lysine residues surrounding the C2A site causes a decrease in PS affinity.[60] Recently, Tavaré *et al*. reported an engineered C2AcH protein that incorporates a free cysteine (for site-specific covalent modification) and a hexahistidine tag (for site-specific radiolabeling with $[^{99m}Tc(CO)_3(OH_2)_3]^+$) in the C-terminal with excellent PS affinity. A second derivative, C2Ac, includes only the C-terminal cysteine.

Although ^{18}F-radiolabelled C2A has been investigated,[61] there are to date no reports of any site specifically labelled analogues for PET. To the best of our knowledge, the use of ^{64}Cu has not been explored and it was decided to investigate the use of a functionalised bis(thiosemicarbazone) for the mild, site specific ^{64}Cu-radiolabelling of this biomarker.

2.6.2 Synthesis of maleimide functionalised bis(thiosemicarbazones)

Conjugation to the pendant thiol group of C2Ac may be achieved *via* introduction of a maleimide group on the bis(thiosemicarbazone) chelator. In a pH range of 6.5-7.5, the maleimide undergoes alkylation with the thiol to form a stable thioether bond. In order to introduce an exocyclic maleimide onto the bis(thiosemicarbazone), we first explored the use of maleic anhydride in a cyclisation reaction on the pendant hydrazine of H_2ATSE/A. A range of reaction conditions resulted in sparingly soluble products that could not be analysed further.

Instead, the use of H_2ATSM/en, a more highly alkylated and more soluble proligand previously reported by this group, was explored. (For synthesis and a detailed discussion of the reactivity of this proligand and its Cu-complex, see chapter 4.3). Regrettably, reaction of H_2ATSM/en or its Zn complex ZnATSM/en with maleic anhydride resulted in formation of untractable side products (Scheme 8). In the reaction of ZnATSM/en, the open chain maleamic acid derivative **2.39** was detected by ESI-MS, but attempts to drive the reaction towards the ring-closed product were unsuccessful.

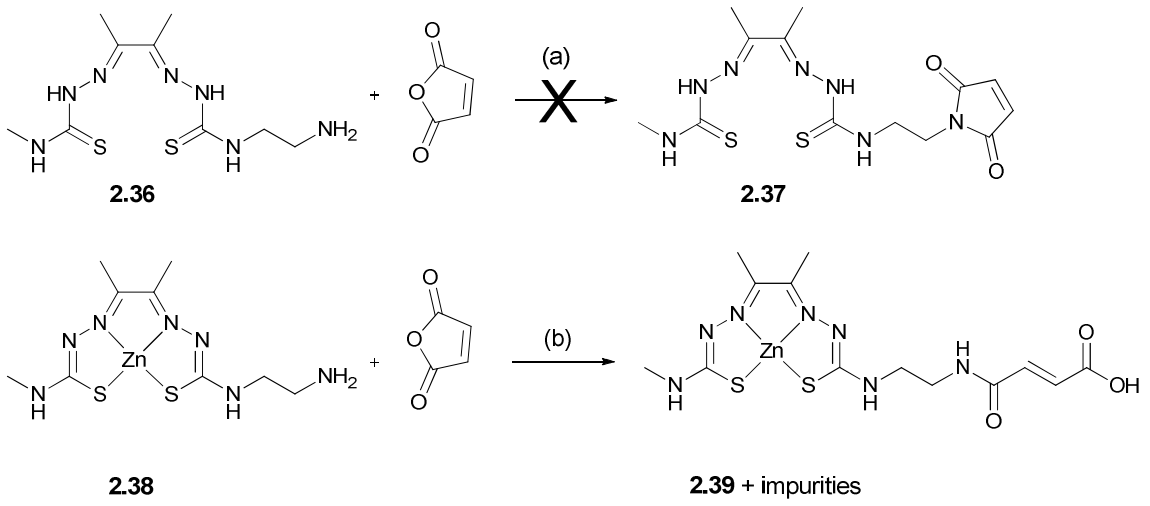

Scheme 8 Attempted synthesis of maleimide functionalised bis(thiosemicarbazones) via direct reaction of amine functionalised H_2ATSM/en or ZnATSM/en with maleic anhydride under a range of reaction conditions (a) MeOH, molecular sieve, 50°C (b) MeOH or THF, molecular sieve, 50°C - reflux *or* MeOH, AcOH, reflux.

Consequently, the pendant maleimide group was introduced *via* the previous successful peptide coupling strategy, attaching the bis(thiosemicarbazone) ligand to a maleimide functionalised

carboxylic acid. As depicted in Scheme 9, coupling of H_2ATSE/A (**2.04**) to 3-maleimidopropionic acid and 3-maleimidobenzoic acid afforded **2.40** (H_2ATSE/A-ALmal) and **2.42** (H_2ATSE/A-ARmal), bearing aliphatic and aromatic linkers respectively between the ligand core and the maleimide functionality. Use of commercially available 3-maleimidopropionic acid resulted in formation of inseparable side-products, hence the maleimide had to be purified by Kugelrohr distillation before use.[62] The ligands were isolated in >95% purity. Attempts to recrystallise either ligand (from DMSO/H_2O or DMSO/EtOH) did not improve the purity and resulted in decomposition of the product when heat was applied. Subsequently, both ligands were purified by preparative HPLC. Removal of the MeCN/H_2O solvent system *in vacuo* on a rotary evaporator caused the off-white solids to turn yellow and impurities were detected in the HPLC. Instead, the ligands were successfully isolated when the MeCN was evaporated at room temperature *in vacuo* followed by lyophilisation.

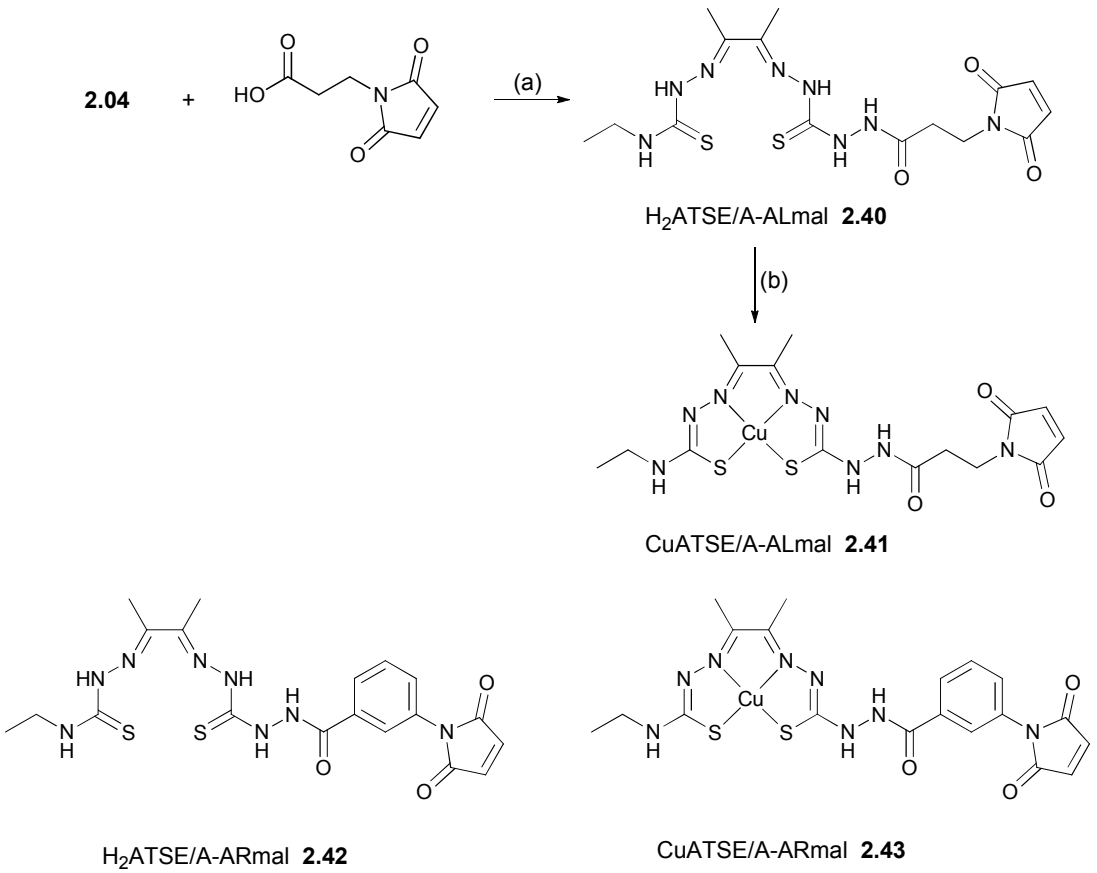

Scheme 9 Synthesis of the maleimide functionalised ligands **2.40** and **2.42** and their copper complexes **2.41** and **2.43**. The synthetic route is outlined for the aliphatic linker-based derivatives and was analogous for the chelator and complex bearing the aromatic linker units. (a) BOP, DMF, DIPEA, 4 h, rt, 94% (**2.40**) and 98% (**2.42**) (b) $Cu(OAc)_2 \cdot H_2O$, MeOH, rt, 5 min, 71% (**2.41**) and 65% (**2.43**).

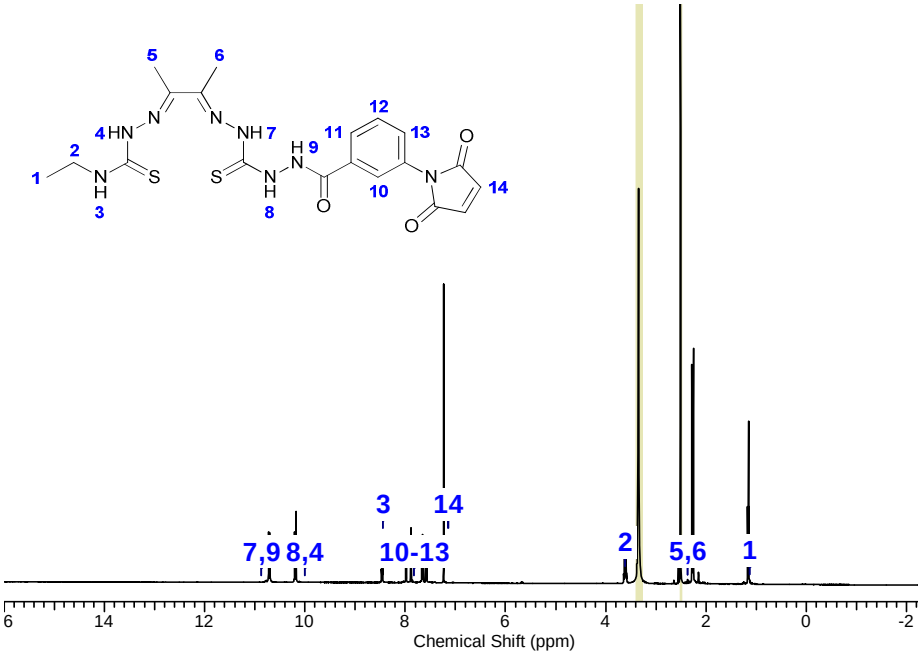

Figure 14 ^{1}H NMR spectrum of **2.42** in d_6-DMSO.

Synthesis of the copper complexes **2.41** (CuATSE/A-ALmal) and **2.43** (CuATSE/A-ARmal) was achieved using $Cu(OAc)_2$ and standard procedures. Table 7 summarises the elemental analysis and mass spectrometry data for **2.40**-**2.43**. Elemental analysis values for C, H, N for **2.43** were low, again probably due to the presence of water as this ligand could not be dried under heat *in vacuo*. Single peaks in HPLC and radio-HPLC (see section 2.6.3) were obtained however and the accurate mass agreed very closely with the proposed structure.

	Compound	***m/z* calc.**	***m/z* found**	**R_t (min)**	**Elemental analysis C, H, N**
2.40	H_2ATSE/A-ALmal	449.1148	449.1137	9.25	42.2 (42.2), 5.2 (5.2), 26.2 (26.3)
2.41	CuATSE/A-ALmal	510.0288	510.0283	9.54	37.0 (36.9), 4.1 (4.1), 22.8 (23.0)
2.42	H_2ATSE/A-ARmal	529.1411*	529.1412	10.94	48.0 (48.1), 4.6 (4.7), 23.7 (23.6)
2.43	CuATSE/A-ARmal	534.0323	534.0322	11.55	37.6 (42.6), 3.7 (3.7), 17.4 (20.9)

Table 7 ESI-MS data (corresponding to $(M + H)^+$, $(M + Na)^+$ or $*(M+Na+CH_3OH)^+$, HPLC retention times (M_2), and elemental analysis data found (calc.) for **2.40**-**2.43**.

2.6.3 Radiolabelling

Both ligands **2.40** and **2.42** were successfully radiolabelled by reaction with [^{64}Cu](OAc)$_2$ using the standard procedures outlined in section 2.4.5.[12] As anticipated from the carboxylic acid functionalised ligands, ^{64}Cu-complexation proceeded at room temperature. Radio-HPLC and radio-TLC analysis within a few minutes of labelling indicated formation of [^{64}Cu]**2.41** and [^{64}Cu]**2.43** with high radiochemical yields (> 95%) and radiochemical purities (> 97%) as determined by radio-TLC and radio-HPLC. Figure 15 depicts the radio-HPLC traces of both complexes.

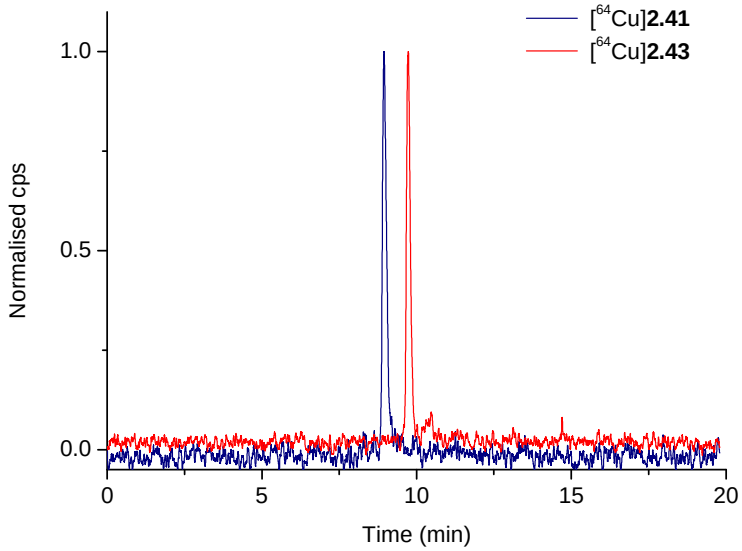

Figure 15 Radio-HPLC traces of [^{64}Cu]**2.41** and [^{64}Cu]**2.43**

2.6.4 Reactivity towards thiols

Prior to protein conjugation, the reactivity of **2.40**-**2.43** towards thiols was verified. For this purpose, a stock solution of ligand or copper complex in DMSO was added to PBS at pH 7.4 (1:3 DMF:PBS), containing an equimolar amount of cysteine ethyl ester as a model thiol. The solutions were screened for product formation after 30 min incubation by ESI-MS. *m/z* Data is shown in Table 8 and agreed with the proposed products depicted in Figure 16.

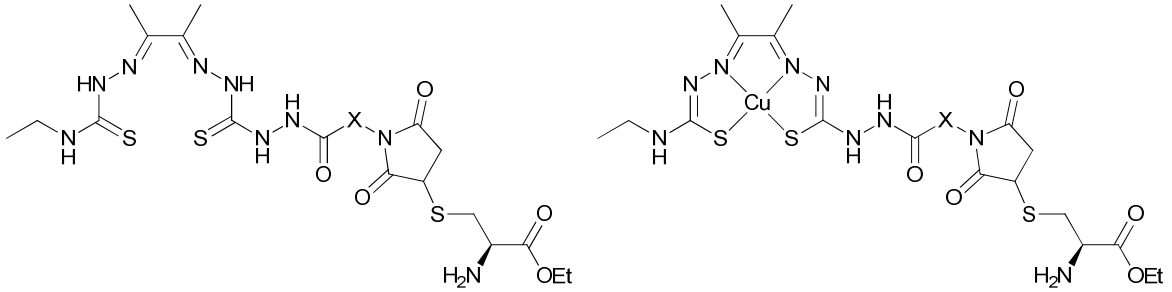

Figure 16 Structures of cysteine-ethyl ester conjugated proligands **2.44** and **2.46** and their corresponding conjugated Cu-complexes **2.45** and **2.47**.

No	Product	*m/z* calculated	*m/z* found
2.44	H_2ATSE/A-ALmalCysOEt	598.1659 $[M+Na]^+$	598.1663
2.45	CuATSE/A-ALmalCysOEt	659.0798 $[M+Na]^+$	659.0808
2.46	H_2ATSE/A-ARmalCysOEt	646.1659 $[M+Na]^+$	646.1655
2.47	CuATSE/A-ARmalCysOEt	707.0798 $[M+Na]^+$	707.0796

Table 8 Results of ESI-MS screening of **2.40**-**2.43** reacting with HCysOEt.HCl in DMF/PBS to give **2.44**-**2.47** as detected by ESI-MS.

2.6.5 ^{64}Cu-labelling of C2Ac *via* bis(thiosemicarbazone)-maleimide derivatives

Having established the reactivity of **2.40** and **2.42** towards thiol, conjugation to C2Ac was explored for mild postlabelling of the protein with ^{64}Cu.

Work in this section was performed in collaboration with the group of Dr Greg Mullen at the Department of Imaging Sciences, King's College London. Conjugation experiments were performed under the supervision of Dr Richard Tavaré, protein expression and radiolabelling experiments were conducted by Dr Richard Tavaré.

2.6.5.1 Conjugation of maleimide functionalised bis(thiosemicarbazones) to C2Ac

C2Ac protein was expressed and purified as previously described.[63] Bioconjugation was performed as outlined in Scheme 10. To 1 mL of C2Ac protein (2 mg mL^{-1} in PBS) was added a 3-fold molar excess of chelator **2.40** or **2.42** dissolved in 100 µL DMSO. The pH was adjusted to 8 and the solution was incubated for 4 h at room temperature.

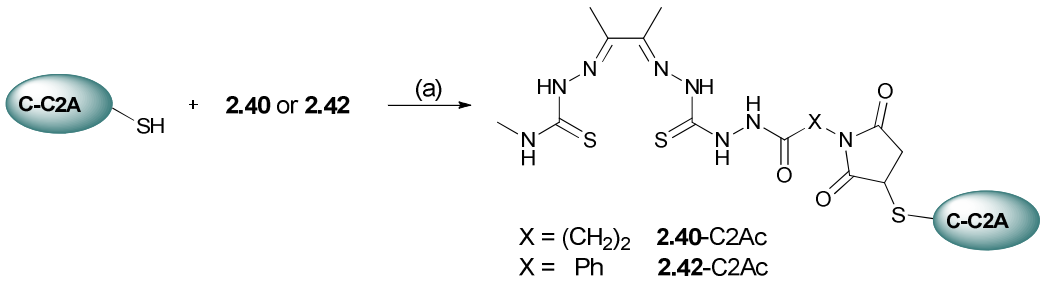

Scheme 10 Conjugation of C2Ac to maleimide functionalised bis(thiosemicarbazone) proligands **2.40** and **2.42** (a) 3 eq of chelator were dissolved in DMSO and incubated with C2Ac in PBS at pH 8 for 4 h at rt to afford the **2.40**-C2Ac and **2.42**-C2Ac chelator-protein conjugates.

During the incubation of C2Ac with **2.42**, formation of a fine precipitate was observed, indicating that the solubility of **2.42** in aqueous media may be problematic. After incubation, the excess chelator was removed by size exclusion chromatography using a PD-10 column pre-equilibrated with PBS. PD-10 fractions were monitored by UV-vis absorption for the presence of the protein (280 nm).[63] LC-MS was used to confirm formation of the C2Ac-chelator conjugates as summarised in Table 9. The data indicated formation of the **2.40**-C2Ac and **2.42**-C2Ac conjugates as shown by peaks at 15424.7 and 15472.2 Da respectively. For **2.42**-C2Ac, a second peak was detected at 15491.0 (+18.8 Da) which could not be further identified. Owing to precipitate formation and the presence of this unidentified by-product, **2.42** and **2.42**-C2Ac were not investigated further and efforts focused on the more soluble chelator **2.40** bearing the aliphatic linker.

Protein/Conjugate	***m/z* expected**	***m/z* found**
C2Ac	14998.0 $[M+H]^+$	14998.4
2.40-C2Ac	15425.1 $[M+H]^+$	15424.7
2.42-C2Ac	15472.5	15472.2, 15491.0

Table 9 Summary of ESI-MS data for C2Ac and the **2.40**-C2Ac and **2.42**-C2Ac protein conjugates.

2.6.5.2 ^{64}Cu-radiolabelling of 2.40-C2Ac *via* post-labelling approaches

Firstly, **2.40**-C2Ac was radiolabelled by addition of aqueous [^{64}Cu]$Cu(OAc)_2$ at pH 6.2 at room temperature. Radio-TLC analysis indicated that 80% of the conjugate was already labelled after 5 min incubation. Following a total incubation time of 30 min, the labelled [^{64}Cu]**2.41**-C2Ac

conjugate was purified by PD-10 fractionation using the procedure applied for the **2.40**-C2Ac chelator conjugate. The PD-10 elution profile, depicted in Figure 17A, confirmed that 81% of the activity was associated with the protein-containing fractions (1 and 2). However, radio-TLC of the main protein containing fraction 2 indicated that free ^{64}Cu was still present as shown by the activity detected in the 40-50 mm region (Figure 17B).

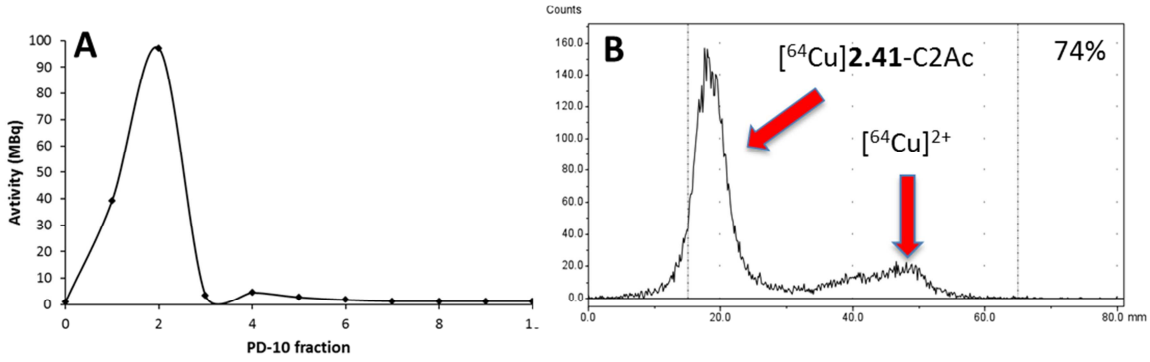

Figure 17 (A) PD-10 fractionation after 30 min incubation of **2.40**-C2Ac with [^{64}Cu]Cu(OAc)$_2$, with the protein contained in fractions 1 and 2 (right) Radio-TLC (10% ammonium acetate:methanol 1:1) of fraction 2 indicates a 74% radiochemical purity, with the presence of [^{64}Cu]**2.41**-C2Ac (20 mm) and a further peak found in the region of the ^{64}Cu-copper ion (40-50 mm).

Since PD-10 size exclusion chromatography would be expected to separate the low molecular weight ^{64}Cu from the radiolabelled 15 kDa protein, it was considered whether the free ^{64}Cu-activity observed in the radio-TLC may be due to the protein binding Cu^{2+} and competing with the chelator for $^{64}Cu^{2+}$. This could then cause leaking of the non-tightly chelated activity later on during size exclusion treatment or radio-TLC. Indeed, a single report suggests that Ca^{2+} binding sites in C2A bind Cu^{2+} with an affinity suspected to be in the nanomolar range.[64] C2Ac contains 3 Ca^{2+} binding sites composed of Asp residues that approach a hexadentate or heptadentate coordination environment.[59, 65]

Thus it was considered how any non-bis(thiosemicarbazonate) bound activity, which may be associated with the protein, could be removed. Donnelly *et al.* previously compared the Cu^{2+} binding properties of CuATSM and EDTA.[66] The authors found that a direct titration of a H_2ATSM:EDTA (1:2) mixture did not result in formation of Cu(ATSM) as detected by UV-vis. In contrast, Cu(ATSM) was stable overnight in 1000 equiv of EDTA. The experiments indicated that

EDTA binds Cu^{2+} more rapidly than H_2ATSM but the copper ion does not exchange between the two ligands, reflecting the kinetic stability of CuATSM once formed. Thus, it was anticipated that addition of excess EDTA after the radiolabelling step might remove non-specifically bound activity.

Incubation of the **2.40**-C2Ac conjugate with [^{64}Cu]Cu(OAc)$_2$ was repeated and followed by radio-TLC analysis. Radio-TLCs for the [^{64}Cu]Cu(OAc)$_2$ reference and the [^{64}Cu]**2.41**-C2Ac conjugate at 5, 15, 30 and 120 min post labelling were obtained with EDTA included in the running buffer (10% ammonium acetate:methanol 1:1+25mM EDTA). Again, inspection of the radio-TLCs indicated that ~80% of the activity was associated with the conjugate at 5 min, this decreased slightly to 75% at 120 min (Figure 18A), with the remainder of the activity being free (or EDTA-bound) [^{64}Cu]Cu^{2+}. At 120 min post incubation with the radioisotope, 200 µL of 50 mM EDTA were added to the conjugate solution to chelate any free or non-specifically protein-bound ^{64}Cu. The [^{64}Cu]**2.41**-C2Ac conjugate was purified by PD-10 size exclusion as before (Figure 18B).

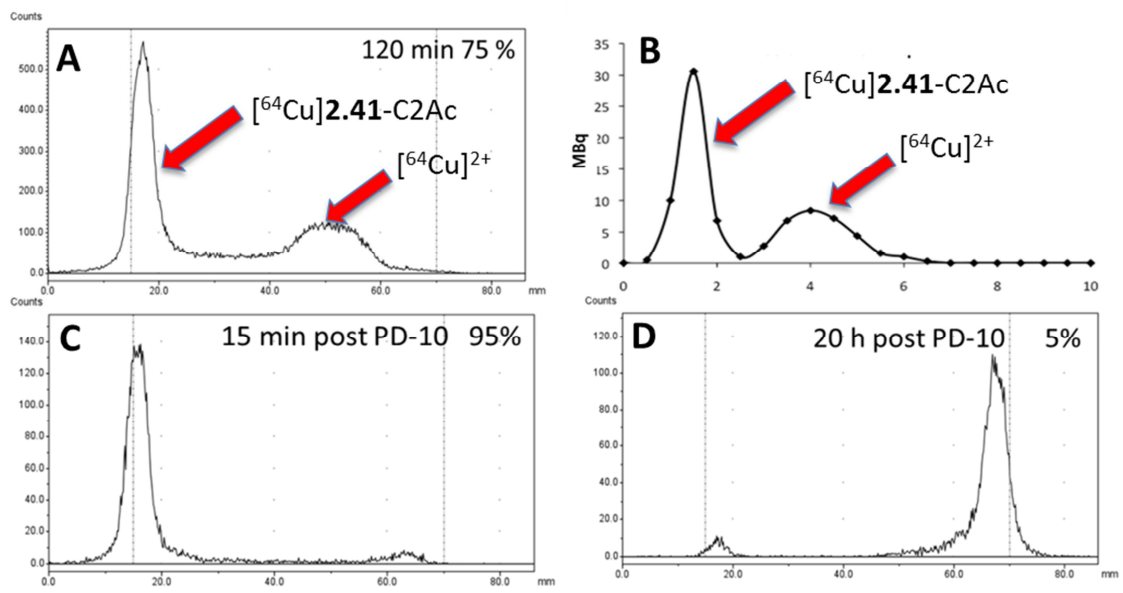

Figure 18 (A) Radio-TLC (10% ammonium acetate:methanol 1:1+25 mM EDTA) of [^{64}Cu]**2.41**-C2Ac at 120 min post labelling (B) PD-10 fractionation at 120 min post labelling (C) and (D) radio-TLCs at 15 min and 20 h post PD-10 purification. At 20 h post incubation, 95% of the activity is found in the region of [^{64}Cu]Cu(OAc)$_2$, indicating the activity is no longer associated with the protein-chelator conjugate.

The elution profile revealed that 66% of the activity was found in the protein fractions 1, 1.5 and 2. The remainder was associated with lower molecular mass fractions (fraction 3-6), indicating either free [^{64}Cu]Cu or [^{64}Cu]CuEDTA. The main [^{64}Cu]**2.41**-C2Ac containing fraction 1.5 was monitored by radio-TLC to assess the stability of [^{64}Cu]**2.41**-C2Ac in PBS over time. Radio-TLC at 5, 15 min (Figure 18C) and 150 min indicated that ~90-95% of the conjugate remained intact. In contrast, radio-TLC at 20 h showed that only 5% of the complex remained intact (Figure 18D).

2.6.5.3 Pre-labelling approach

The leaking of activity from the protein fraction at later time-points (Figure 18D) raised the possibility that the Ca^{2+} binding sites in C2A may effectively compete with the bis(thiosemicarbazone) for Cu^{2+} chelation. In order to ascertain whether there was indeed protein binding of [^{64}Cu]Cu^{2+}, or whether the leaking was due to inherent instability of the ^{64}Cu-labelled chelate, a pre-labelling approach was performed for comparison. Labelling of chelator **2.40** with [^{64}Cu]$Cu(OAc)_2$ (Figure 19A) was performed using standard procedures as reported in section 2.4.5. [^{64}Cu]**2.41** was purified on a C-18 Sep-Pak cartridge and reformulated into EtOH.

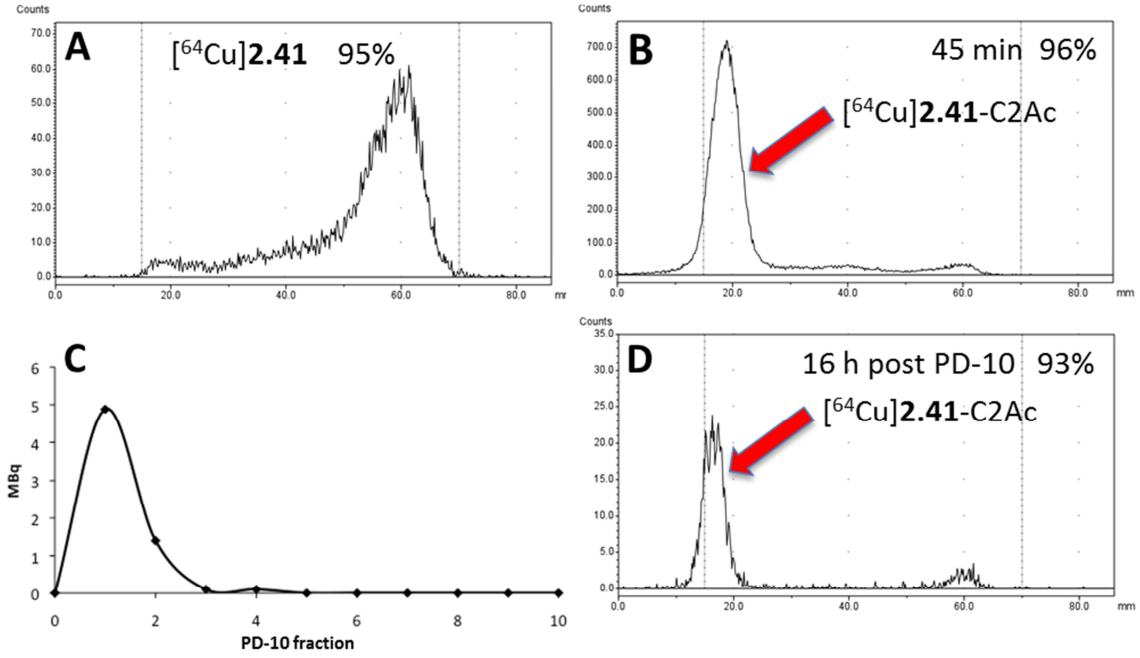

Figure 19 Post-labelling approach by conjugation of [^{64}Cu]**2.41** to C2Ac. (A) radio-TLC of [^{64}Cu]**2.41** before conjugation (EtOAc:MeOH 95:5) (B) radio-TLC of [^{64}Cu]**2.41**-C2Ac (10% ammonium acetate:methanol 1:1+25 mM EDTA) at 45 min post conjugation (C) PD-10 elution profile of [^{64}Cu]**2.41**-C2Ac at 45 min post conjugation (D) radio-TLC (10% ammonium acetate:methanol 1:1+25 mM EDTA) of [^{64}Cu]**2.41**-C2Ac at 16 h post incubation in PBS (37°C).

The ethanolic solution was concentrated under a stream of nitrogen before addition to C2Ac in PBS (pH 8) for conjugation.

Radio-TLC after 45 min incubation at room temperature indicated that [^{64}Cu]**2.41**-C2Ac conjugate formation was already complete (Figure 19B). PD-10 fractionation was performed to remove any unconjugated [^{64}Cu]**2.41** and revealed that 88% of the activity was conjugated to the protein (fractions 1 and 2, Figure 19C). [^{64}Cu]**2.41**-C2Ac from fraction 1 was then monitored over time as previously to determine the stability of the conjugate in PBS solution. In contrast to the results obtained for the one-step labelling approach, 93% of the conjugate was still intact after 16 h incubation in PBS at 37°C as determined by the radio-TLC analysis (Figure 19D). The contrasting results for the post- and prelabelling approaches investigated suggest that C2A effectively competes with the bis(thiosemicarbazone) moiety for ^{64}Cu.

2.6.5.4 Serum stability of [^{64}Cu]2.41-C2Ac

Since the behaviour of [^{64}Cu]**2.41**-C2Ac (formed *via* pre-labelling) suggested formation of a stable conjugate, the copper bis(thiosemicarbazonato)-protein conjugate was investigated further. The *in vitro* stability in serum was determined by incubating [^{64}Cu]**2.41**-C2Ac in human serum. Aliquots were withdrawn at 1, 2, 6 and 20 h post incubation and monitored by radio-TLC as before. Since serum proteins such as ceruloplasmin or human serum albumin are able to sequester Cu^{2+}, radio-TLC was complemented by gel analysis to test for the presence of other radiocopper-containing protein. Samples from each experiment were ran on SDS-PAGE and analysed by autoradiography as depicted in Figure 20. Analysis of the percentage activity in each lane revealed that 81.7±1.9% and 97.9±1.8% remained associated with the C2Ac protein fraction (15 kDa) for samples incubated for 20 h in serum or PBS respectively. The serum stability observed is therefore slightly lower than for the SPECT analogue [^{99m}Tc]AcH-C2A (94%, 16 h).[63] Since the remainder of the activity was seen at higher molecular weight bands, some activity may indeed be sequestered by serum proteins able to bind copper, such as albumin or ceruloplasmin.

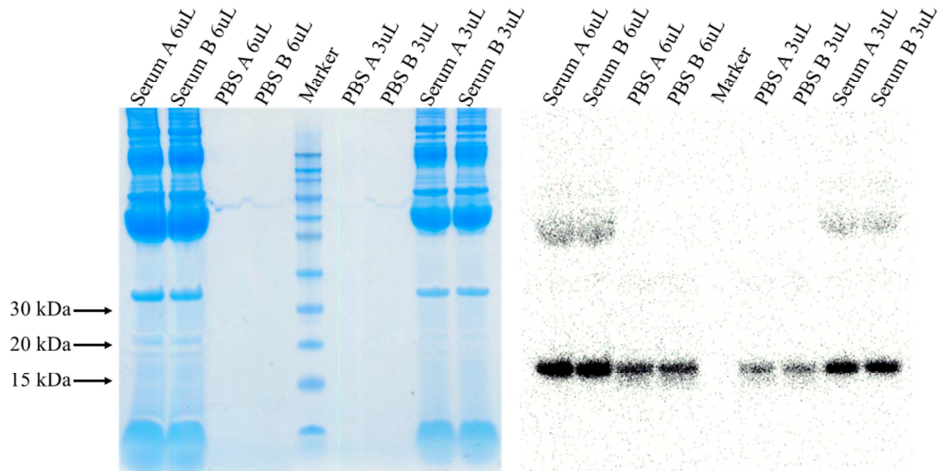

Figure 20 SDS/PAGE gel of [^{64}Cu]**2.41**-C2Ac samples after overnight incubation in PBS or serum. A and B represent duplicate measuring points.

2.6.5.5 Preliminary results for binding of [^{64}Cu]2.41-C2Ac to PS on red blood cells

In order to establish whether the [^{64}Cu]**2.41**-C2Ac conjugate (formed via the pre-labelling approach) retained affinity for phosphatidylserine on red blood cells. In contrast to fresh red blood cells, phosphatidylserine is exposed in preserved red blood cells, allowing Annexin V or C2A to bind in a calcium dependent manner. A literature reported binding assay previously applied for fluorescently labelled Annexin V and ^{99m}Tc-labelled C2AcH was performed.[67] Full results have not been obtained to date, but preliminary experiments revealed increasing binding of the [^{64}Cu]**2.41**-C2Ac conjugate to PS with increasing calcium concentrations, suggesting that the site specifically attached copper-bis(thiosemicarbazonate) did not adversely affect the binding affinity of the protein.

2.7 Discussion of peptide and protein labelling results

The synthesis, characterisation and radiolabelling of the COOH functionalised and maleimide functionalised bis(thiosemicarbazone) derivatives demonstrate that the H_2ATSR/A proligand can readily be functionalised for bioconjugation. Successful solid phase peptide synthesis and bioconjugation under aqueous conditions at room temperature further support their suitability as bifunctional chelators. Whilst radiolabelling of the peptide was readily achieved, in the first instance, investigation of the postlabelling approach for proteins appeared to be impeded by the chosen protein's ability to bind copper. Control experiments seem to confirm this, since [^{64}Cu]**2.41**-C2Ac, formed *via* the pre-labelling approach, displayed acceptable serum stability and maintained protein affinity in preliminary binding assays. This suggests that indeed C2Ac competes to some extent with the bis(thiosemicarbazone) moiety for [^{64}Cu]Cu^{2+} in the direct post-labelling approach. The facile pre-labelling and fast conjugation suggest that the maleimide-functionalised bis(thiosemicarbazone) provides a viable route for the [^{64}Cu]-radiolabelling of C2Ac, which has not previously been successfully labelled with ^{64}Cu. However, a two-step approach is also achieveable with macrocyclic chelators that confer higher in vivo stability. *In vivo* investigations are therefore needed to evaluate the [^{64}Cu]**2.41**-C2Ac conjugate and whether there are any particular advantages of bis(thiosemicarbazones) for use in a pre-labelling approach.

Nonetheless, the room-temperature labelling properties of the bis(thiosemicarbazone) motif, combined with the good binding affinity of the pre-labelled conjugate, suggest that bis(thiosemicarbazones) may serve for the facile ^{64}Cu-radiolabelling of other heat or pH sensitive proteins that require postlabelling, where no competition from the protein is expected.

The preliminary *in vivo* biodistributions of the [^{64}Cu]ATSM-BBS2 peptide conjugate revealed high liver and lung uptake. Lung uptake may be due to microprecipitation, since the low solubility of the peptide conjugates already presented problems during the purification. The high amount of non-specific binding also requires further investigation. *In vitro* and *in vivo* experiments, in particular with respect to metabolite and stability studies, are required to determine whether non-target uptake is a result of the clearance pathway of the biomolecule or whether it is solely due to lack of stability

of the bis(thiosemicarbazone) *in vivo*. However, [^{64}Cu]ATSM-BBS2 revealed higher tumour uptake than other copper-chelators with comparable peptide motifs and significantly, the uptake was specific and could be blocked. Approaches to address the above concerns about stability could involve modification of the chelator to increase kinetic stability. Work within the group has already explored chelators with modified donor groups that still label at room temperature, for instance by replacing one of the sulphur donors with a pyridine or carbonyl moiety to yield asymmetric donor systems[68] Another possibility would be to increase the steric bulk of the chelator at the backbone or pendant arms in order to enhance kinetic stability and minimise any possible transchelation *in vivo*.

2.7.1 Increasing the steric bulk of the ligand

In preliminary experiments, the introduction of adamantyl substituents was investigated to increase the steric bulk of the bis(thiosemicarbazone) ligand. 4-(2-Adamantyl)thiosemicarbazide **2.48** was synthesised following a previously reported procedure.[69] The thiosemicarbazide was then reacted with 2,3-butanedione to afford ligand **2.49**. Reaction with $Zn(OAc)_2 \cdot H_2O$ in 7:3 $CHCl_3$:MeOH afforded the Zn-complex **2.50** in 80% yield. **2.49** and **2.50** were fully characterised by NMR, ESI-MS and elemental analysis.

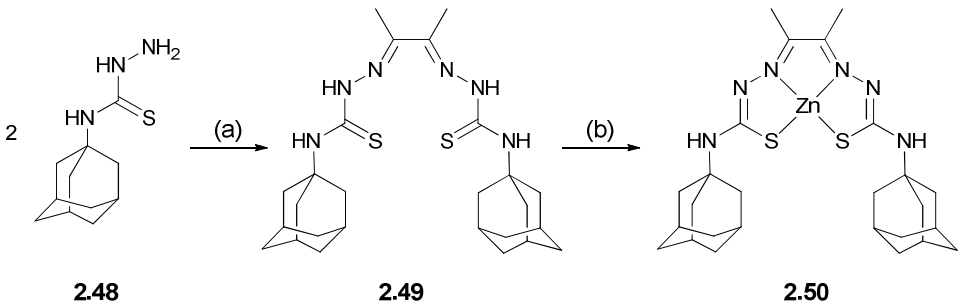

2.48 **2.49** **2.50**

Scheme 11 Synthesis of bis(thiosemicarbazone) ligand and corresponding Zn-complex bearing adamantyl substituents on the exocyclic nitrogen. (a) 2,3-butanedione, conc. H_2SO_4, EtOH, rt, 16 h, 54% (b) $Zn(OAc)_2 \cdot 2H_2O$, CH_3Cl/MeOH, 50°C, 2 h, 79%.

Crystals of **2.50** suitable for single crystal X-ray analysis were grown by slow evaporation of a concentrated DMSO solution of the complex.

The crystal structure was recorded and resolved by Dr Amber Thompson and Dr Michael Jones.

The crystal was initially solved as triclinic in the space group P_{-1} with a Z prime of 4 but as this was unusual, alternative symmetry was considered and it was found that the correct unit cell was in fact monoclinic with the space group of $C_{2/c}$ and Z prime of 2. Attempts were made to model the partially occupied, diffuse, disordered DMSO molecules also present in the structure, but a stable model could not be reached with these in it, so SQUEEZE was required to provide a sensible solution.[70] The solved structure was very similar to previously published examples of zinc(II) bis(thiosemicarbazonato) complexes which are 5-coordinate distorted square based pyramidal and withdrawn in the order of 0.43-0.52 Å out of the SNNS plane by a monodentate ligand in the apical site.[13, 15, 71, 72] This case is comparable, with a molecule of dimethylsulfoxide coordinated *via* the O to the Zn in the apical site, resulting in Zn sitting 0.521 Å above the SNNS plane.

The majority of the bond lengths and angles do not differ significantly from the ZnATSM·DMSO structure that was reported by Christlieb *et al.*, and the respective DFT calculated distances.[71]

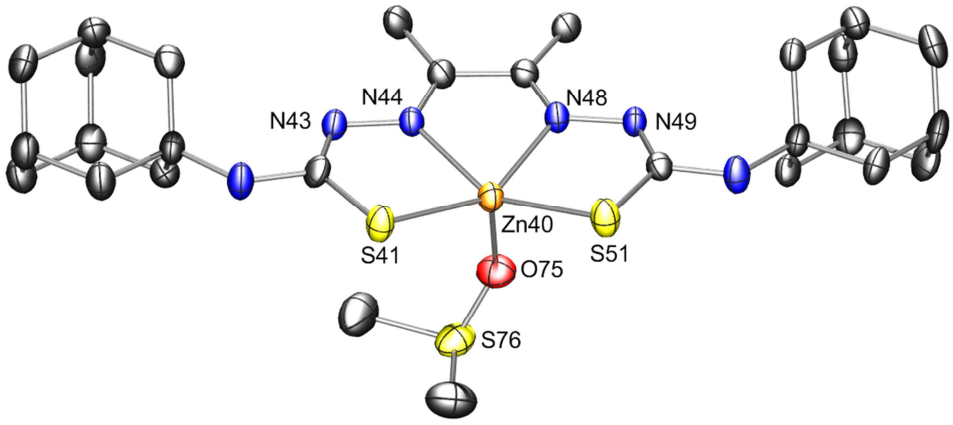

Figure 21 ORTEP[73, 74] plot of the X-ray crystal structure of **2.50** with the thermal ellipsoids drawn at 30% probability and hydrogen atoms removed for clarity.

Molecule 1		**Molecule 2**	
Zn1 . S2	2.329(2)	Zn40 . S41	2.331(2)
Zn1 . N5	2.133(7)	Zn40 . N44	2.132(7)
Zn1 . N8	2.102(8)	Zn40 . N48	2.079(8)
Zn1 . S11	2.340(3)	Zn40 . S51	2.336(3)
Zn1 . O36	2.061(5)	Zn40 . O75	2.075(5)
S2 . Zn1 . N5	80.28(19)	S41 . Zn40 . N44	79.7(2)
S2 . Zn1 . N8	147.53(18)	S41 . Zn40 . N48	147.92(19)
N5 . Zn1 . N8	75.0(3)	N44 . Zn40 . N48	75.3(3)
S2 . Zn1 . S11	111.57(9)	S41 . Zn40 . S51	111.57(10)
N5 . Zn1 . S11	149.55(16)	N44 . Zn40 . S51	149.82(16)
N8 . Zn1 . S11	82.0(2)	N48 . Zn40 . S51	82.5(2)
S2 . Zn1 . O36	110.22(14)	S41 . Zn40 . O75	109.64(15)
N5 . Zn1 . O36	96.6(2)	N44 . Zn40 . O75	96.37(19)
N8 . Zn1 . O36	93.45(19)	N48 . Zn40 . O75	92.99(19)
S11 . Zn1 . O36	104.56(15)	S51 . Zn40 . O75	105.15(15)
Zn1 . S2 . C3	97.3(3)	Zn40 . S41 . C42	96.6(3)
N4 . N5 . Zn1	123.1(5)	N43 . N44 . Zn40	123.5(6)
Zn1 . N5 . C6	116.3(6)	Zn40 . N44 . C45	115.3(6)
Zn1 . N8 . C7	117.3(6)	Zn40 . N48 . C47	118.9(7)
Zn1 . N8 . N9	120.8(6)	Zn40 . N48 . N49	120.0(7)
C10 . S11 . Zn1	93.9(4)	C50 . S51 . Zn40	93.2(4)
Zn1 . O36 . S37	134.5(3)	Zn40 . O75 . S76	135.3(3)

Table 10 Key bond lengths and angles of the X-ray crystal structure of **2.50**.

Overlays of the two molecules in the asymmetric unit using Mercury 2.4, indicated that the two forms (depicted in green and blue in Figure 22) were very similar, with no significantly different conformational orientations observed in any parts of the molecule. In addition, the respective atomic distances vary only within experimental uncertainty.

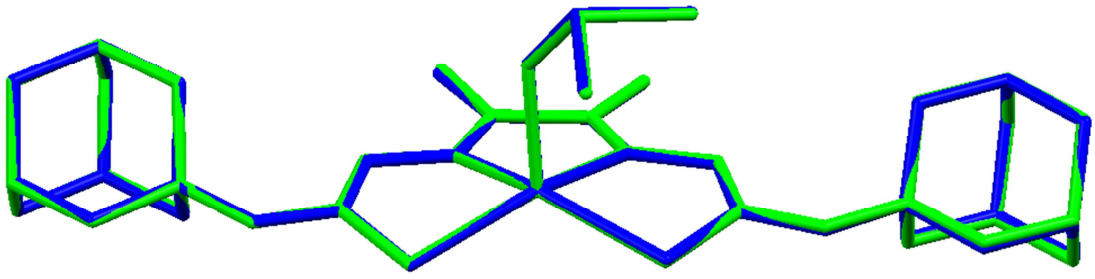

Figure 22 Overlay of the two molecules (green and blue) in the asymmetric unit for the X-ray crystal structure of **2.50**.

2.8 Conclusion

A series of bis(thiosemicarbazone) bifunctional chelators bearing aromatic and aliphatic linker units with pendant COOH and maleimide groups have been developed. The ligands were radiolabelled rapidly at room temperature with high radiochemical yields and purities. Solution phase coupling experiments have demonstrated a superior reactivity for aliphatic over aromatic COOH groups.

Two pendant COOH group chelators have been conjugated to a peptide using standard solid phase peptide synthesis conditions. Room temperature radiolabelling, EPR characterisation, *in vitro* binding assays and preliminary *in vivo* biodistributions revealed that rapid, site specific labelling and target affinity are maintained when the bis(thiosemicarbazone) is conjugated to a peptide.

Reaction of the maleimide functionalised ligand with a thiol-bearing protein demonstrate that conjugation under aqueous conditions is feasible. Post-labelling was complicated by the intrinsic copper binding properties of the protein chosen. Nonetheless, experiments with the pre-labelled analogue demonstrated that the conjugate retained good stability in serum and preliminary measurements suggest that the bis(thiosemicarbazone) moiety did not adversely affect the protein's target affinity.

Further *in vivo* work is needed to obtain a full evaluation of these derivatives as bifunctional chelators. Further synthetic work could involve modification of the ligand structures to optimise *in vivo* behaviour and to increase stability of the conjugates whilst maintaining the favourable rapid labelling properties at room temperature.

2.9 References for Chapter 2

1. G. Crisponi, V. M. Nurchi, D. Fanni, C. Gerosa, S. Nemolato and G. Faa, *Coord. Chem. Rev.*, 2010, **254**, 876-889.
2. T. J. Wadas, E. H. Wong, G. R. Weisman and C. J. Anderson, *Chem. Rev.*, 2010, **110**, 2858-2902.
3. P. J. Blower, J. S. Lewis and J. Zweit, *Nucl. Med. Biol.*, 1996, **23**, 957-980.
4. U. Elsaesser-Beile, G. Reischl, S. Wiehr, P. Buehler, P. Wolf, K. Alt, J. Shively, M. S. Judenhofer, H.-J. Machulla and B. J. Pichler, *J. Nucl. Med.*, 2009, **50**, 606-611.
5. A. F. Prasanphanich, P. K. Nanda, T. L. Rold, L. Ma, M. R. Lewis, J. C. Garrison, T. J. Hoffman, G. L. Sieckman, S. D. Figueroa and C. J. Smith, *Proc. Natl. Acad. Sci.*, 2007, **104**, 12462-12467.
6. H. Cai, Z. Li, C.-W. Huang, A. H. Shahinian, H. Wang, R. Park and P. S. Conti, *Dalton Trans*. 2010, **21**, 1417-1424.
7. L. Wei, Y. Ye, T. J. Wadas, J. S. Lewis, M. J. Welch, S. Achilefu and C. J. Anderson, *Nucl. Med. Biol.*, 2009, **36**, 277-285.
8. M. A. Green, D. L. Klippenstein and J. R. Tennison, *J. Nucl. Med.*, 1988, **29**, 1549-1557.
9. A. L. Vavere and J. S. Lewis, *Dalton Trans.*, 2007, 4893-4902.
10. K. A. Wood, W. L. Wong and M. I. Saunders, *Nucl. Med. Biol.*, 2008, **35**, 393-400.
11. B. M. Paterson and P. S. Donnelly, *Chem. Soc. Rev.*, 2011, **40**, 3005-3018.
12. S. R. Bayly, R. C. King, D. J. Honess, P. J. Barnard, H. M. Betts, J. P. Holland, R. Hueting, P. D. Bonnitcha, J. R. Dilworth, F. I. Aigbirhio and M. Christlieb, *J. Nucl. Med.*, 2008, **49**, 1862-1868.
13. J. P. Holland, F. I. Aigbirhio, H. M. Betts, P. D. Bonnitcha, P. Burke, M. Christlieb, G. C. Churchill, A. R. Cowley, J. R. Dilworth, P. S. Donnelly, J. C. Green, J. M. Peach, S. R. Vasudevan and J. E. Warren, *Inorg. Chem.*, 2007, **46**, 465-485.
14. J. P. Holland, P. J. Barnard, S. R. Bayly, H. M. Betts, G. C. Churchill, J. R. Dilworth, R. Edge, J. C. Green and R. Hueting, *Eur. J. Inorg. Chem.*, 2008, 1985-1993.
15. H. M. Betts, P. J. Barnard, S. R. Bayly, J. R. Dilworth, A. D. Gee and J. P. Holland, *Angew. Chem., Int. Ed.*, 2008, **47**, 8416-8419.
16. *Application: EP Pat.*, 1988-307510, 306168, 1989.
17. D. W. McPherson, G. Umbricht and F. F. Knapp, Jr., *J. Labelled Compd. Radiopharm.*, 1990, **28**, 877-899.
18. Y. Arano, A. Yokoyama, Y. Magata, H. Saji, K. Horiuchi and K. Torizuka, *Int. J. Nucl. Med. Biol.*, 1986, **12**, 425-430.
19. Y. Arano, A. Yokoyama, T. Furukawa, K. Horiuchi, T. Yahata, H. Saji, H. Sakahara, T. Nakashima, M. Koizumi and et al., *J. Nucl. Med.*, 1987, **28**, 1027-1033.
20. A. R. Cowley, J. R. Dilworth, P. S. Donnelly, J. M. Heslop and S. J. Ratcliffe, *Dalton Trans.*, 2007, 209-217.
21. P. D. Bonnitcha., DPhil Thesis, University of Oxford, 2010
22. P. D. Bonnitcha, A. L. Vavere, J. S. Lewis and J. R. Dilworth, *J. Med. Chem.*, 2008, **51**, 2985-2991.
23. H. M. Betts, DPhil Thesis, University of Oxford, 2009.
24. S.-A. Poulsen, *J Am Soc Mass Spectrom.*, 2006, **17**, 1074-1080.
25. G. T. Hermanson and Editor, *Bioconjugate Techniques*, 1995.
26. P. Burke, O. Golovko, J. C. Clark and F. I. Aigbirhio, *Inorg. Chim. Acta*, 2010, **363**, 1316-1319.
27. N. E. Basken, C. J. Mathias, A. E. Lipka and M. A. Green, *Nucl. Med. Biol.*, 2008, **35**, 281-286.
28. N. E. Basken and M. A. Green, *Nucl. Med. Biol.*, 2009, **36**, 495-504.
29. C. J. Smith, W. A. Volkert and T. J. Hoffman, *Nucl. Med. Biol.*, 2005, **32**, 733-740.
30. N. Gonzalez, T. W. Moody, H. Igarashi, T. Ito and R. T. Jensen, *Curr. Opin. Endocrinol., Diabetes Obes.*, 2008, **15**, 58-64.
31. H. Reile, P. E. Armatis and A. V. Schally, *Prostate*, 1994, **25**, 29-38.

32. S. Giacchetti, C. Gauville, P. De Cremoux, L. Bertin, P. Berthon, J. P. Abita, F. Cuttitta and F. Calvo, *Int. J. Cancer*, 1990, **46**, 293-298.
33. M. H. Corjay, D. J. Dobrzanski, J. M. Way, J. Viallet, H. Shapira, P. Worland, E. A. Sausville and J. F. Battey, *J. Biol. Chem.*, 1991, **266**, 18771-18779.
34. T. J. Hoffman and C. J. Smith, *Nucl. Med. Biol.*, 2009, **36**, 579-585.
35. T. J. Hoffman, H. Gali, C. J. Smith, G. L. Sieckman, D. L. Hayes, N. K. Owen and W. A. Volkert, *J. Nucl. Med.*, 2003, **44**, 823-831.
36. H. Zhang, J. Chen, C. Waldherr, K. Hinni, B. Waser, J. C. Reubi and H. R. Maecke, *Cancer Res.*, 2004, **64**, 6707-6715.
37. I. Dijkgraaf, O. C. Boerman, W. J. G. Oyen, F. H. M. Corstens and M. Gotthardt, *Anti-Cancer Agents Med. Chem.*, 2007, **7**, 543-551.
38. S. M. Okarvi, *Med. Res. Rev.*, 2004, **24**, 357-397.
39. V. Maes, E. Garcia-Garayoa, P. Blaeuenstein and D. Tourwe, *J. Med. Chem.*, 2006, **49**, 1833-1836.
40. E. Garcia Garayoa, C. Schweinsberg, V. Maes, D. Ruegg, A. Blanc, P. Blauenstein, D. A. Tourwe, A. G. Beck-Sickinger and P. A. Schubiger, *Q J Nucl Med Mol Imaging*, 2007, **51**, 42-50.
41. C. Schweinsberg, V. Maes, L. Brans, P. Blauenstein, D. A. Tourwe, P. A. Schubiger, R. Schibli and E. G. Garayoa, *Bioconjugate Chem.*, 2008, **19**, 2432-2439.
42. E. Garcia Garayoa, C. Schweinsberg, V. Maes, L. Brans, P. Blauenstein, D. A. Tourwe, R. Schibli and P. A. Schubiger, *Bioconjugate Chem.*, 2008, **19**, 2409-2416.
43. L. Brans, V. Maes, E. Garcia-Garayoa, C. Schweinsberg, S. Daepp, P. Blauenstein, P. A. Schubiger, R. Schibli and D. A. Tourwe, *Chem. Biol. Drug Des.*, 2008, **72**, 496-506.
44. L. E. Warren, S. M. Horner and W. E. Hatfield, *J. Amer. Chem. Soc.*, 1972, **94**, 6392-6396.
45. R. Pogni, M. C. Baratto, A. Diaz and R. Basosi, *J Inorg Biochem*, 2000, **79**, 333-337.
46. J. P. Holland, J. C. Green and J. R. Dilworth, *Dalton Trans.*, 2006, 783-794.
47. S. Lim, K. A. Price, S.-F. Chong, B. M. Paterson, A. Caragounis, K. J. Barnham, P. J. Crouch, J. M. Peach, J. R. Dilworth, A. R. White and P. S. Donnelly, *J. Biol. Inorg. Chem., 2010,* **15**, 225-235
48. D. Kivelson and R. Neiman, *J. Chem. Phys.*, 1961, **35**, 149-155.
49. E. Garcia Garayoa, D. Ruegg, P. Blauenstein, M. Zwimpfer, I. U. Khan, V. Maes, A. Blanc, A. G. Beck-Sickinger, D. A. Tourwe and P. A. Schubiger, *Nucl. Med. Biol.*, 2007, **34**, 17-28.
50. S. D. Voss, S. V. Smith, N. Dibartolo, L. J. McIntosh, E. M. Cyr, A. A. Bonab, J. L. J. Dearling, E. A. Carter, A. J. Fischman, S. T. Treves, S. D. Gillies, A. M. Sargeson, J. S. Huston and A. B. Packard, *Proc. Natl. Acad. Sci.*, 2007, **104**, 17489-17493.
51. G. Kroemer, L. Galluzzi, P. Vandenabeele, J. Abrams, E. S. Alnemri, E. H. Baehrecke, M. V. Blagosklonny, W. S. El-Deiry, P. Golstein, D. R. Green, M. Hengartner, R. A. Knight, S. Kumar, S. A. Lipton, W. Malorni, G. Nunez, M. E. Peter, J. Tschopp, J. Yuan, M. Piacentini, B. Zhivotovsky and G. Melino, *Cell Death Differ.*, 2009, **16**, 3-11.
52. S. L. Wolters, M. F. Corsten, C. P. M. Reutelingsperger, J. Narula and L. Hofstra, *Eur. J. Nucl. Med. Mol. Imaging*, 2007, **34**, S86-S98.
53. D. Hanahan and R. A. Weinberg, *Cell*, 2000, **100**, 57-70.
54. B. Verhoven, R. A. Schlegel and P. Williamson, *J. Exp. Med.*, 1995, **182**, 1597-1601.
55. X. Li, J. M. Link, S. Stekhova, K. J. Yagle, C. Smith, K. A. Krohn and J. F. Tait, *Bioconjugate Chem.*, 2008, **19**, 1684-1688.
56. J. F. Tait, C. Smith and F. G. Blankenberg, *J. Nucl. Med.*, 2005, **46**, 807-815.
57. H. H. Boersma, B. L. J. H. Kietselaer, L. M. L. Stolk, A. Bennaghmouch, L. Hofstra, J. Narula, G. A. K. Heidendal and C. P. M. Reutelingsperger, *J. Nucl. Med.*, 2005, **46**, 2035-2050.
58. F. G. Blankenberg, *J. Nucl. Med.*, 2008, **49**, 81S-95S.
59. I. S. Alam, A. A. Neves, T. H. Witney, J. Boren and K. M. Brindle, *Bioconjugate Chem.*, 2010, **21**, 884-891.
60. S. Krishnan Anant, A. Neves Andre, M. de Backer Maaike, D.-E. Hu, B. Davletov, I. Kettunen Mikko and M. Brindle Kevin, *Radiology*, 2008, **246**, 854-862.

61. F. Wang, Z. Wang and W. Qu, *Society of Nuclear Medicine Annual Meeting Abstracts*, 2009, **50**, 385.
62. R. M. de Figueiredo, P. Oczipka, R. Froehlich and M. Christmann, *Synthesis*, 2008, 1316-1318.
63. R. Tavare, R. Torres Martin De Rosales, P. J. Blower and G. E. D. Mullen, *Bioconjugate Chem.*, 2009, **20**, 2071-2081.
64. D. Rajalingam, T. K. S. Kumar and C. Yu, *Biochemistry*, 2005, **44**, 14431-14442.
65. R. B. Sutton, B. A. Davletov, A. M. Berghuis, T. C. Sudhof and S. R. Sprang, *Cell*, 1995, **80**, 929-938.
66. Z. Xiao, P. S. Donnelly, M. Zimmermann and A. G. Wedd, *Inorg. Chem.*, 2008, **47**, 4338-4347.
67. J. F. Tait, D. F. Gibson and C. Smith, *Anal. Biochem.*, 2004, **329**, 112-119.
68. M. B. M. Theobald, University of Oxford, 2010.
69. A. Kreutzberger, H. H. Schroeders and J. Stratmann, *Arch. Pharm.*, 1984, **317**, 767-771.
70. L. Palatinus and G. Chapuis, *J. Appl. Crystallogr.*, 2007, **40**, 786-790.
71. M. Christlieb, J. P. Holland and J. R. Dilworth, *Inorg. Chim. Acta*, 2010, **363**, 1133-1139.
72. M. Christlieb, A. R. Cowley, J. R. Dilworth, P. S. Donnelly, B. M. Paterson, H. S. R. Struthers and J. M. White, *Dalton Trans.*, 2007, 327-331.
73. L. J. Farrugia, *J. Appl. Crystallogr.*, 1997, **30**, 565.
74. C. L. Barnes, *J. Appl. Crystallogr.*, 1997, **30**, 568.

Chapter 3

Introduction to molecular imaging of hypoxia and CuATSM

3.1 Tumour hypoxia

Hypoxia is a pathological condition of insufficient oxygen supply. It occurs when the vascular supply to tissue is interrupted, as in myocardial infarction or stroke, in diabetes mellitus following poor perfusion of limbs, or in certain types of cancer.[1]

When cells are suddenly deprived of oxygen, various chemosensory systems act to reinstate the oxygen supply by modulating pulmonary circulation, perfusion and blood circulation.[2] If the oxygen requirement for oxidative phosphorylation cannot be met, cells normally die by apoptosis (programmed cell death) or necrosis (accidental cell death).[1, 3]

Cancer cells, however, can respond differently to hypoxia by adapting their metabolism to survive the low oxygen environments. Hypoxia is a typical characteristic of advanced solid tumour growth and significantly alters the biology of the cancer cell.[4, 5] In tumours, perfusion limited or acute hypoxia can arise from limited oxygen delivery caused by deficits in perfusion of the tumour microenvironment. Chronic hypoxia arises from increased diffusion distances between tumour cells and their nutritive blood vessels, as encountered when tumours outgrow their vascular supply.[1, 6] A variety of changes in protein and gene expression occur and there are many characteristic pathological markers of hypoxia.[2, 4] For instance, cells compensate their nutrient deprivation by enhancing glucose uptake via hypoxia induced expression of glucose transporters and a switch from aerobic to anaerobic metabolism (glycolysis). Hypoxia also mediates the production of growth factors that induce angiogenesis (the formation of new blood vessels) to assist oxygen delivery. Furthermore, hypoxia can cause proliferation and metastasis, initiated by cell migration and regeneration after acute or chronic hypoxia damage. Hypoxia can also incur genetic instability and immortalisation of cells. These further contribute to the tumour's aggressiveness by providing a natural selection of tumour cells that are fit to survive the specific tumour microenvironment.[7]

A major mechanism governing the adaptive responses to a lack of oxygen is the regulation of transcription by the transcription factors Hypoxia Inducible Factors (HIFs).[4] More than 100 proteins are upregulated as a response to hypoxia by HIFs, in particular Hypoxia Inducible Factor 1 (HIF-1).[8] HIF-1 is a heterodimeric protein composed of an oxygen sensitive 1α unit and a 1β

subunit. As depicted in Scheme 1, under normoxia, HIF-1α is hydroxylated by the prolyl hydroxylases and targeted for proteasomal degradation, using oxygen as a co-factor. In the absence of oxygen, HIF-1α concentration increases and dimerises with the 1ß subunit to form HIF-1. The heterodimer binds to the core DNA-binding sequence 5"RCGTG-3" of target genes and activates transcription of hundreds of proteins, including those essential to promote angiogenesis, glycolysis, invasion and metastasis.[9]

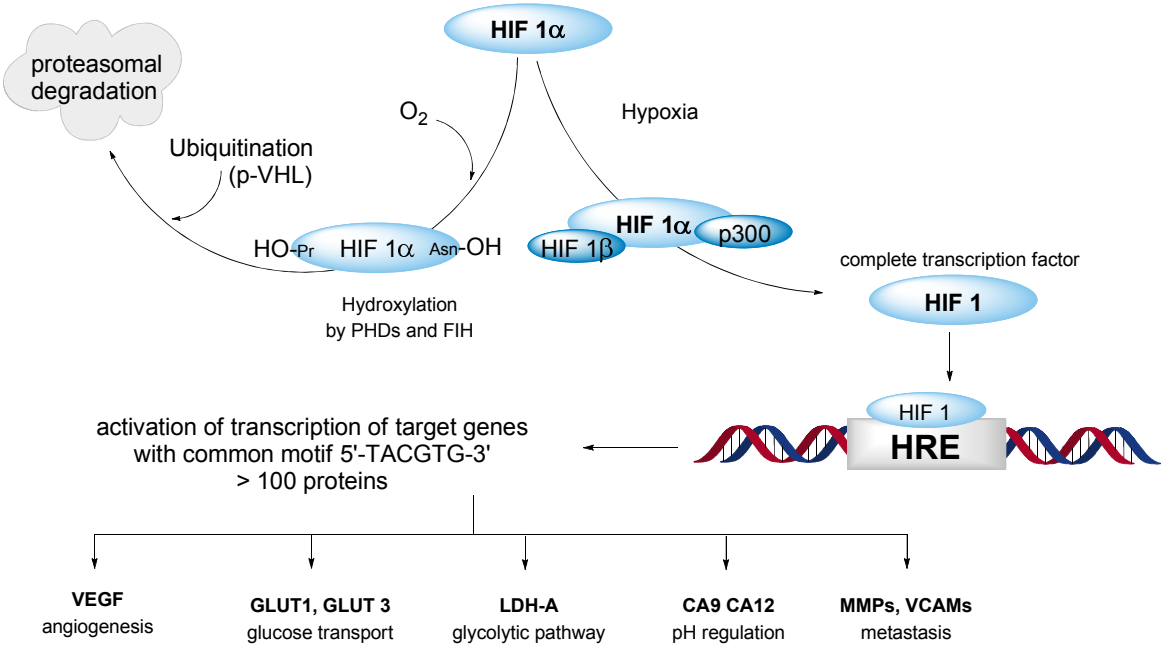

Scheme 1 Schematic representation of HIF-1 pathway. Under normoxic conditions, HIF-1α is hydroxylated, preventing binding to its cofactors and enabling targeting by the von Hippel-Lindau factor for ubiquitination and proteasomal degradation. Under hypoxic conditions, it can interact with its cofactors to form a heterodimer that binds to hypoxia response elements and activates transcription of proteins to promote survival of the cancer cell.

These adaptations equip cancer cells to better survive in their hypoxic environment and thus promote tumour survival. Clinically, this results in increased tumour aggressiveness and resistance to radiation- and chemotherapy. As illustrated by Figure 1, hypoxia in tumours has a negative effect on prognosis due to higher recurrence rate and metastasis.[1] Starting from the pioneering work of Gray[10] over fifty years ago, numerous studies have shown the role of hypoxia in resistance to radiation therapy. Ionising radiation is most effective when leading to irreparable DNA double strand breaks. Oxygen is a potent radiosensitiser as primary radicals react with O_2 to form

secondary free radicals that cause permanent DNA damage which cannot be repaired by intracellular thiols. Hence the increased resistance to radiation therapy is directly related to the lack of intracellular O_2.[5, 10] In normal tissue, oxygen tension shows a Gaussian distribution with a median of 40-60 mmHg and ranges from 20-80 mmHg. Hypoxic tumours have a median of 10 mmHg and this value has been associated with the onset of resistance to radiotherapy. Full resistance occurs in tissues of < 0.5 mmHg.[11] Hypoxia also influences chemotherapy. Most chemotherapeutics function as antiproliferative agents and are thus less effective on tumour cells that have slowed their growth rate as a response to hypoxia.[6, 12] In addition, reduced perfusion rates and increased distances to tumour vasculature limit the therapeutics' access to the tumour, and thus shield cells from the cytotoxic effects.[6, 11]

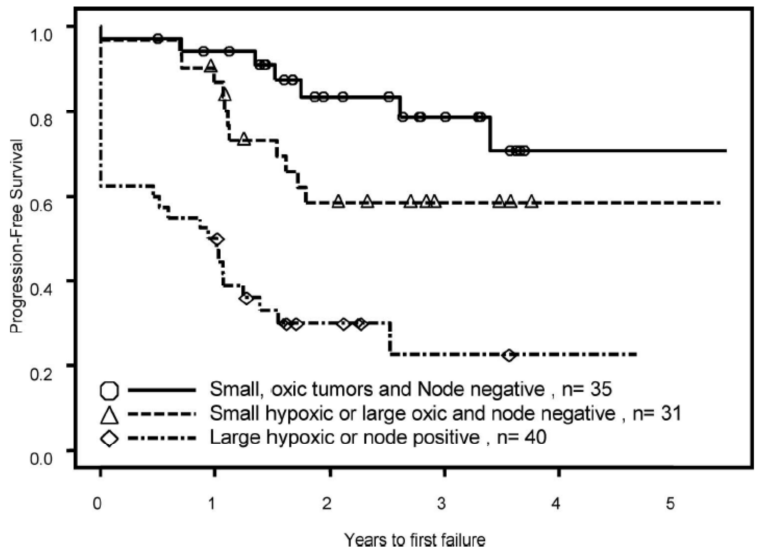

Figure 1 Kaplan-Meier analysis showing the influence of hypoxia on disease free survival. Prognostic groups were created by assigning patients to groups according to tumour size, hypoxia and nodal status of the tumour. Reprinted with permission from reference 13.

These aspects demonstrate that tumour hypoxia is a negative prognostic factor and the identification of hypoxic regions has become an important goal in tumour staging and disease planning. A reliable diagnostic method to determine the location and volume of hypoxic fractions in tumours will greatly assist in radiotherapy planning or help to determine the most suitable chemotherapeutic treatment. However, it could also be used to determine where a palliative approach may be more appropriate.

3.2 Measurement of tumour hypoxia

3.2.1 Invasive methods

To date, there have been several approaches to measure and quantify tumour hypoxia in the clinic.[1] The "gold standard" remains the use of a polarographic oxygen sensitive needle electrode to directly measure pO_2 in tumours *in vivo*, with a good correlation between results and response to therapy and patient prognosis.[12, 14, 15] However, this invasive approach requires accessible tumour sites and damages tissues, further it is prone to sampling errors and relies on CT or ultrasound guided placement.[16] Immunohistochemical methods are often used to detect and quantify tumour hypoxia. A nitroimidazole compound, such as pimonidazole or EF5 is administered as a hypoxia marker prior to biopsy (for mechanism and structure, see section 3.2.2). Immunohistochemical staining of the sample with an antibody binding to the hypoxia marker is then performed.[17-20] These invasive methods have severe drawbacks. Serial biopsies to monitor tumour oxygenation pre- and post-therapy are painful and impracticable. In addition, tumours often are spatially and temporally heterogeneous with well-perfused areas co-existing along those of severe hypoxia. Representative sampling thus only gives information on a small fraction of the tumour.

To plan and monitor treatment, a non-invasive method that permits serial assessment of hypoxia is highly desirable and functional molecular imaging offers possible alternatives.

3.2.2 Methods for Molecular Imaging of Hypoxia

Molecular imaging methods such as PET, SPECT or MRI have the potential to delineate tumour hypoxia *in vivo*. Several tumour locations can be assessed simultaneously and the possibility to repeat measurements allows therapeutic progress to be monitored. Oxygen electrode measurements merely provide a pO_2 value, molecular imaging agents can provide further distinction by delineating only viable, hypoxic tissue, since most of the agents discussed below are not targeted to necrotic tissue. Hence, molecular imaging agents can provide near real-time, dynamic data with spatial resolution capable of assessing regional heterogeneity.

A range of molecular imaging modalities has been investigated for *in vivo* measurement of hypoxia that rely either on direct measure of intrinsic oxygen concentration or on a surrogate marker that responds to, or becomes activated within, hypoxic cells.

3.2.2.1 MRI

MRI provides several approaches to measure tumour hypoxia. ^{19}F-MRI oximetry uses perfluorocarbons (PFCs) as oxygen-sensitive reporter molecules.[21] A linear relationship exists between the ^{19}F MR spin-lattice relaxation rate ($R_1=1/T_1$) of PFCs and oxygen tension. *In vivo* measurements of R_1 can be converted into pO_2 maps using *in vitro* calibration curves[22] with compounds such as hexafluorobenzene (see Figure 2). PFCs are biologically inert and exhibit low toxicity, but a severe drawback is the need for intratumoural injection of the agent to avoid sequestering in liver and spleen. Blood oxygen level dependent (BOLD) MRI is an alternative and measures blood oxygenation based on the paramagnetism of deoxyhaemoglobin (oxyhaemoglobin is diamagnetic) in order to reflect changes in tumour oxygenation.[23] BOLD allows a high temporal and spatial resolution but is not quantitative.[24] The bioreductive 2-nitroimidazole EF5 (Figure 2 and section 3.2.2.2) has also been investigated as a ^{19}F-NMR probe. Since ^{19}F-MRI suffers from a lack of ^{19}F-MR facilities capable of imaging humans alternative pO_2 probes based on ^{1}H-NMR are being investigated.[21]

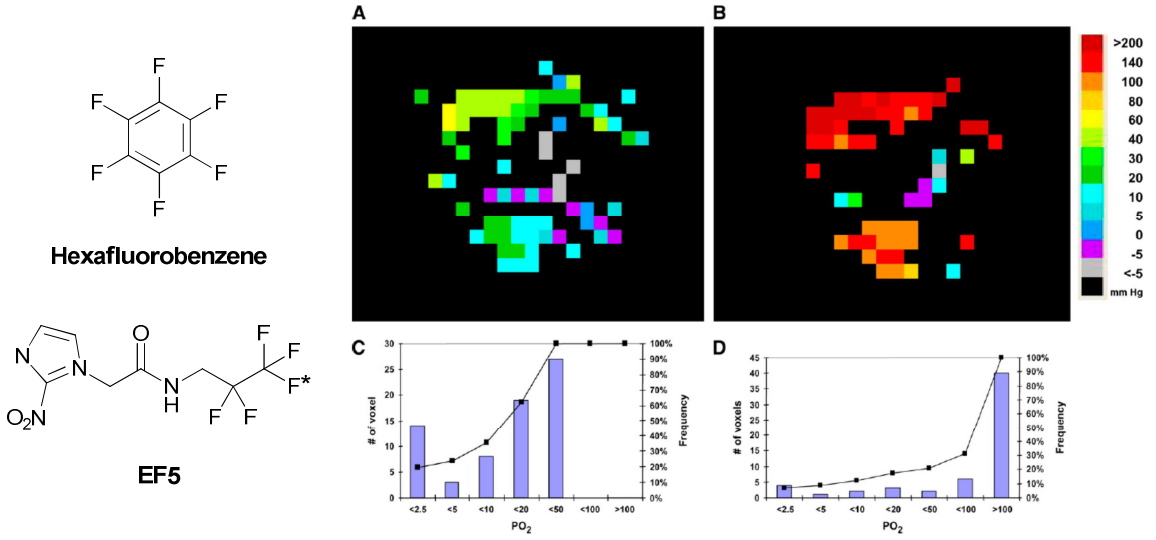

Figure 2 (left) structure of HFB and EF5 used in ^{19}F-MRI. [^{18}F]EF5 (F*=^{18}F) is also used in PET (right) ^{19}F MRI oximetry using HFB to image a H460 tumour xenograft in a nude rat (0.57 cm^3 tumour xenograft) to acquire pO_2 maps with an in-plane resolution of 1.25 mm while the rat breathed air (left) or oxygen (right). The corresponding histograms below depict the number of voxels exhibiting a defined pO_2 range during air or oxygen breathing, respectively. Diagram reprinted with permission from reference 1.

3.2.2.2 PET and SPECT

Several PET and SPECT agents have been explored for imaging hypoxia.[16, 25] A large proportion of these are based on compounds bearing a 2-nitroimidazole group as the targeting moiety. The mechanism of hypoxia selectivity is thought to involve an intracellular, enzyme-mediated, series of one-electron reductions as shown in Scheme 2. For 2-nitroimidazoles, the initial one-electron reduction is biologically accessible and reversible. Hence, in the presence of sufficient O_2, the initial radical anion is reoxidised to the original neutral tracer which can diffuse back out of the cell. In the absence of O_2, reoxidation is slow and further reductions can lead to a highly reactive hydroxylamine or amine derivative that results in covalent intracellular binding.[26]

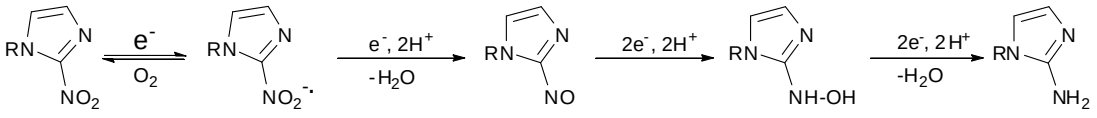

Scheme 2 Series of one-electron reductions for the proposed intracellular trapping of nitroimidazoles.[27]

Chapman *et al.* first investigated ^{14}C labelled misonidazole in spheroids to define the hypoxic tumour microenvironment.[28] Since then, several nitroimidazoles have been labelled with both metallic and non-metallic radionuclides, as depicted in Figure 3. For instance, BMS 181321 is an agent based on a ^{99m}Tc-amineoxime chelate linked to a 2-nitroimidazole but this tracer was too lipophilic and showed poor hepatic clearance.[29, 30] Another amine-oxime ligand, based on a four-carbon backbone is [^{99m}Tc]HL91m. Interestingly, the control ligand [^{99m}Tc]HL91 which lacks the nitroimidazole group, was found to have the higher hypoxia selectivity but its mechanism of action is still uncertain.[31, 32] Iodine-labelled 2-nitroimidazoles, such as [^{123}I]IAZA[33] for SPECT and [^{125}I]IAZA[33], [^{18}F]FAZA and [^{124}I]AZG[33, 34] for PET have also been reported. An ^{18}F-radiolabelled variant of EF5 (see 3.2.2.1) has also been investigated.[35]

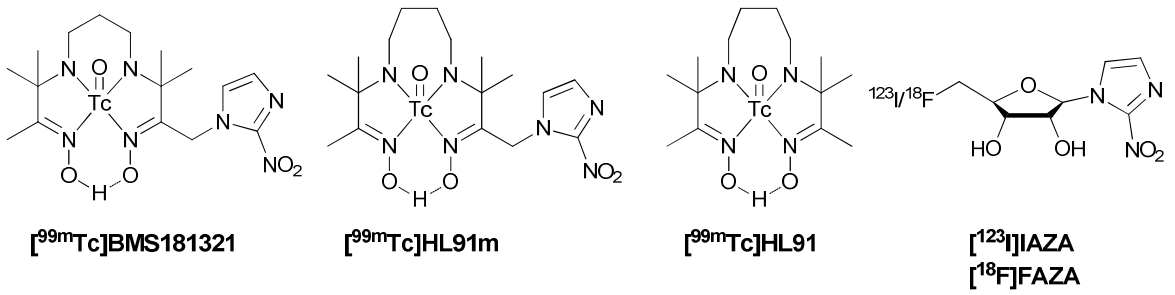

Figure 3 Technetium and iodine based agents investigated for imaging of hypoxia.

The most widely studied PET imaging agent for hypoxia is [^{18}F]FMISO whose synthesis is depicted in Scheme 3. The lipophilic tracer (log P = 2.6) is thought to diffuse readily through cell membranes. FMISO is directly affected by tumour oxygenation and hypoxic regions require pO_2 levels below 2-3 mmHg to cause significant retention.[36] Preclinical[37, 38] and clinical studies[39] have demonstrated successful assessment of tumour hypoxia with a direct correlation between the volume of the hypoxic fractions and [^{18}F]FMISO uptake. Pre-therapy FMISO-imaging in patient studies was predictive of radiotherapy outcome in head and neck cancer patients[40] and higher hypoxic volumes and tumour-blood ratios were associated with shorter time to progression and survival in glioblastoma patients.[41] However, FMISO presents several major limitations. Tumour-to-blood ratios are <1.2 and the limited contrast ratio reflects the low *in vivo* uptake. The problem

is enhanced due to slow clearance which delays imaging for up to 3 h after injection which is suboptimal for the short ^{18}F half-life.

To improve the low count rate and image quality, new derivatives such as ^{18}F-fluoroazomycin arabinoside, [^{18}F]FAZA, have been investigated which showed superior blood clearance when compared to [^{18}F]FMISO.[42] So far, the above mentioned agents have all been investigated in the clinic but have received mixed reports, limited in part by strong background signals due to slow clearance[43] and some tumour line dependency.[44]

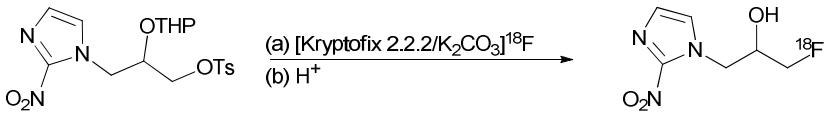

Scheme 3 Radiosynthesis of the hypoxia tracer [^{18}F]FMISO.

An alternative approach to the radiolabelling of nitroimidazoles is to use a complex where the radionuclide constitutes a part of the construct that conveys the hypoxia targeting properties. One such agent is the copper (II) complex copper(II)-diacetyl-bis(*N*^{4}-methylthiosemicarbazone), Cu(ATSM). Cu(ATSM) rapidly delineates tumour hypoxia with high tumour to muscle ratios. As discussed below, the redox properties of the copper are thought to be key to the mode of hypoxia selectivity, but the currently accepted mechanism is not consistent with certain aspects of its observed *in vitro* and *in vivo* behaviour and the exact mode of selectivity is still not fully understood.

3.3 CuATSM

As outlined in Chapter 1, copper(II)bis(thiosemicarbazonato) complexes were first evaluated in the 1990s as an alternative to [^{18}F]FMISO for the PET imaging of hypoxia. Fujibayashi *et. al.* observed hypoxia selective uptake of CuATSM in an *ex-vivo*, isolated rat heart model of ischemia.[45] A reductive retention mechanism mediated by NADH-dependent enzymes of the electron transport chain in mitochondria was proposed. Specifically, it was suggested that Cu(II)ATSM is only reduced to become irreversibly trapped under hypoxia, as a result of abnormally reduced mitochondria, as depicted in Scheme 4.

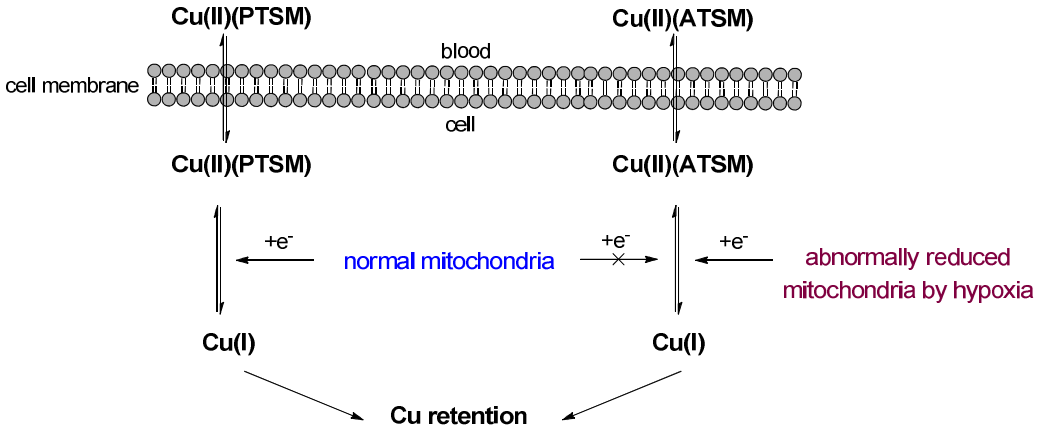

Scheme 4 Original mechanism of hypoxia selectivity of Cu(II)ATSM, proposed by Fujibayashi and supported by Obata.

In hypoxic cells, electron flow is disturbed due to hyper-reduction of NADH dehydrogenase, also called Complex I. Reduced Complex I is thought to use NADH as a two-electron donor to reduce Cu(II)ATSM. In normoxic cells, undisturbed Complex I is incapable of accessing the redox potential of Cu(II)ATSM. This is in contrast to CuPTSM, which has a less negative reduction potential and is non-selectively trapped in all cells.[45]

Obata *et al.* conducted additional studies in subcellular fractions of Ehrlich ascites tumour cells to show that reductive metabolism occurred in the microsome/cytosol fraction rather than in the mitochondria.[46] They demonstrated that the reductive process was heat-sensitive and could be enhanced by exogenous NAD(P)H. Reductase inhibition studies of NADH:cytochrome b5- and

NADPH:cytochrome P450 reductase further indicated their involvement in the reductive retention of Cu(II)ATSM. The retention mechanism in tumour cells was compared to that in normal cells and it was found that the enzymatic reduction of Cu(II)ATSM was enhanced under hypoxia.

3.3.1 *In vitro* and mechanistic studies

Dearling *et al.* investigated the dependence of the redox potential on the hypoxia selectivity of CuATSM by conducting detailed *in vitro* structure activity relationship studies.[47] The reduction potential of a series of copper bis(thiosemicarbazonates) was found to be altered by the alkylation pattern of the ligand backbone.[48, 49] The presence of two alkyl groups gave complexes with redox potentials in the range of -0.57 to -0.59 V[1] which showed varying degrees of hypoxia selectivity in *in vitro* cellular uptake assays. In contrast, complexes with one or no alkyl groups had less negative potentials (-0.42 V to – 0.53 V) and showed no oxygen dependent uptake in cells, as illustrated in Figure 4.

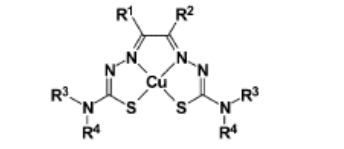

	R^1	R^2	R^3	R^4
GTS	H	H	H	H
GTSM	H	H	CH_3	H
PTS	CH_3	H	H	H
PTSM	CH_3	H	CH_3	H
$PTSM_2$	CH_3	H	CH_3	CH_3
PTSE	CH_3	H	C_2H_5	H
PTSP	CH_3	H	C_6H_5	H
ATS	CH_3	CH_3	H	H
ATSM	CH_3	CH_3	CH_3	H
CTS	C_2H_5	CH_3	H	H
CTSM	C_2H_5	CH_3	CH_3	H
DTS	C_2H_5	C_2H_5	H	H
DTSM	C_2H_5	C_2H_5	CH_3	H

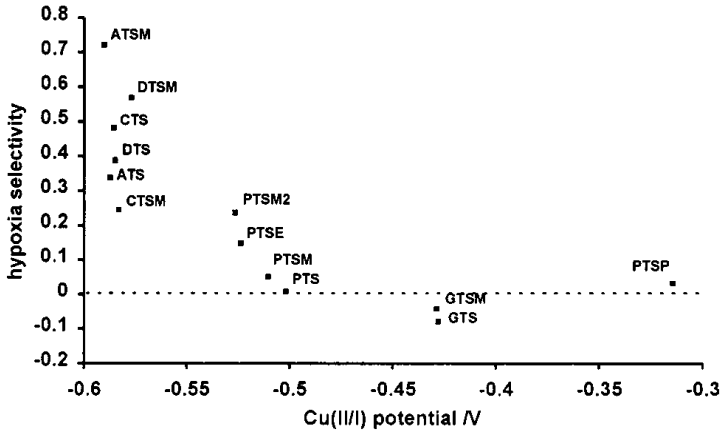

Figure 4 (left) Nomenclature for copper(II) bis(thiosemicarbazonato) complexes (right) Plot of hypoxia selectivity of copper(II) complexes in relation to their Cu(II/I) redox potential measured versus the standard Ag/AgCl electrode. Reprinted with permission from reference 48.

[1] The reduction potentials in references 48-50 are reported *vs.* Ag/AgCl electrode, where the Cu(II)/Cu(I) reduction potential of CuATSM is -0.59 V. Ag/AgCl has a potential of +0.197 V *vs.* NHE (normal hydrogen electrode) and the saturated calomel electrode (SCE) has a potential of +0.242 V *vs.* NHE, giving a difference of 0.045. Electrode potentials in this thesis have been reported versus the SCE, $E_{1/2}$(SCE), for ease of comparison with previous work within the group.

McQuade *et al.* further reported that CuATSE, bearing two exocyclic ethyl- instead of methyl groups as in CuATSM, had elevated uptake in *in vitro* cellular assays over a wider range of oxygen conditions and showed increased *in vivo* tumour uptake. This suggested that subtle modification may enable ligand tuning for imaging of different levels of hypoxia.

Whilst the structure-activity relationships elucidated the structural dependence of hypoxia selectivity of copper-bis(thiosemicarbazonates), the mechanism proposed by Obata and Fujibayashi however was at variance with cellular uptake and wash-out studies performed by Lewis *et al.*,[50] who compared uptake of CuATSM, CuPTSM and FMISO under varying degrees of hypoxia in EMT6 cells. CuATSM exhibited more efficient uptake and superior washout kinetics in hypoxic and normoxic cells compared to FMISO and suggested that it would offer superior PET imaging of hypoxia. The study showed oxygen dependent uptake for both CuATSM and FMISO whereas CuPTSM showed high uptake independent of oxygen concentration. In the washout studies, cells were incubated under various pO_2 for 60 min and subsequently resuspended in fresh medium at 20% O_2 for 60 min. The studies showed that little (~10%) washout was observed from cells that had been incubated with CuPTSM under normoxia or hypoxia, suggesting that CuPTSM was reduced efficiently in all cells. For cells incubated with CuATSM however, over 40% washout was observed from normoxic cells over 1h incubation in fresh medium, whereas only 27% of CuATSM was washed out from cells that had previously experienced hypoxia. In conjunction with Fujibayashi's results, the authors suggested that the retention of CuATSM is a reversible phenomenon, depending only on pO_2. Enzymatic reduction (most probably by Complex I) occurs in all cells rather than being a result of cellular damage, but is upregulated in hypoxic cells that contain Complex I with particularly high electron and/or NADH concentrations. These observations led to a revised mechanism by Dearling *et al.* [48, 49] and Maurer *et al.*,[51] who proposed that reduction in both normoxic and hypoxic cells led to the $[Cu(I)ATSM]^-$ species. The unstable Cu(I) complex could then either slowly dissociate, leading to irreversible trapping of Cu(I), or be reoxidised in the presence of oxygen to Cu(II)ATSM and diffuse back out of the cell. The authors suggested that the stability of CuATSM is the main feature that determined the hypoxia selectivity of CuATSM. Density functional theory and cyclic voltammetry with variable pH and UV/visible

spectroscopy monitoring were used to investigate the fate of the Cu(I) species.[27, 51] It was found that the reduction of the perfusion marker Cu(II)PTSM and Cu(II)GTS became irreversible in the presence of weak acid whilst Cu(II)ATSM seemed to remain unaffected. The Cu(I)ATSM species was proposed to be more resistant to acid catalysed dissociation than the non-hypoxia selective complexes CuGTS or CuPTSM, which increases the chance of reoxidation to Cu(II)ATSM when molecular oxygen is present.

The results are at variance with studies by Holland *et. al.* who carried out further spectroelectrochemical and computational studies on a series of copper(bisthiosemicarbazonates) to elucidate the exact role of the pK_a and protonation of both the Cu(II) species and reduced Cu(I) species.[52] Spectroelectrochemistry demonstrated that molecular oxygen can re-oxidise $[Cu(I)ATSM]^-$ extremely rapidly. The reduction of the copper(II)bis(thiosemicarbazonato) complexes investigated was shown to be highly pH dependent and a combined revised mechanism confirms previous findings that the one-electron reduction potential and rate of reoxidation are structure dependent as illustrated in Scheme 5.

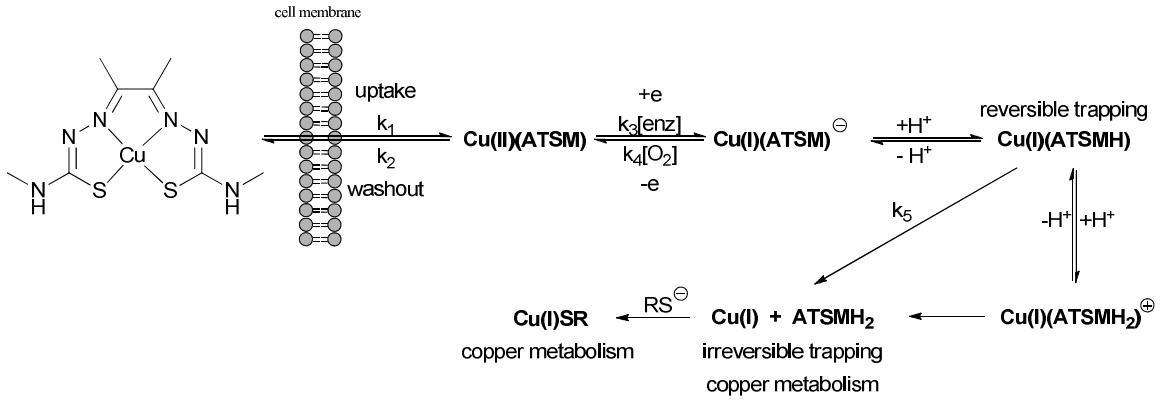

Scheme 5 Revised mechanism proposed by Holland et al.[52] The scheme shows the proposed mechanistic pathways involved in the hypoxia selective uptake and retention of Cu(ATSM). The simulated rate constants (k_1 = 9.8(±0.59)×10^{-4}s^{-1}, k_2 = 2.9(±0.17)×10^{-3}s^{-1}, k_3 = 5.2(±0.31)×10^{-2}s^{-1}, k_4 = 2.2(±0.13) mol^{-1}dm^3, k_5 = 9(±0.54)×10^{-5}s^{-1}) shown were based on a fit between the proposed mechanism and experimental cellular uptake and washout data by Lewis.[50]

It was also proposed that Cu(I)ATSM and Cu(I)PTSM both are stable towards ligand dissociation in the absence of a proton source, whilst high acid concentration encouraged the dissociation of copper (I) ions from the ligand. At low acid concentration, a range of protonated intermediate species were observed, with the equilibrium between the different protonated species also being structure dependent. The particular hypoxic selectivity of CuATSM arises from a "delicate balance between enzyme mediated one-electron reduction and subsequent oxidation by dioxygen versus protonation and ligand dissociation".[52] For CuATSM, the rates of reduction, reoxidation and protonation are fast relative to the rate of pH-mediated ligand dissociation. The individual equilibrium for the species involved is dependent on the electron donating or withdrawing nature of the ligand backbone. These results were also found to be consistent with the *in vitro* cellular uptake and the washout studies by Lewis *et al.* Holland and Lewis subsequently published estimated rate constants based on a simulation between the revised mechanism and the observed *in vitro* uptake and washout data reported, as depicted in Scheme 5.[50, 53, 54]

3.3.2 Nomenclature

In discussing *in vitro* and in *vivo* literature work in this chapter, [^{64}Cu]CuATSM uptake designates [^{64}Cu] radioactivity resulting from [^{64}Cu]CuATSM administration where the cited work does not distinguish between intact complex and other forms of radiocopper. Literature work customarily refers to CuATSM 'uptake' and the author's terminology generally has been preserved in this introduction. In Chapter 5, the word 'uptake' is replaced with 'retention'. The exact processing of radiocopper is not known and the radioactivity measured in our studies may be the balance of both uptake and efflux of radioactivity. Retention describes the net result of these processes.

3.3.3 Preclinical work

The *in vitro* cellular uptake and washout studies by Lewis *et al.* discussed in section 3.3.1 were accompanied by *in vivo* biodistribution studies which showed equal retention of CuATSM and CuPTSM at 1, 5, 10, 20 and 40 min p.i. in EMT-6 tumour bearing mice. *Ex vivo* autoradiography was undertaken on tumour slices from animals that had received a co-injection of [^{64}Cu]CuATSM and [^{60}Cu]CuPTSM. The authors reported that for [^{64}Cu]CuATSM, uptake was heterogeneous in tumours known to contain hypoxic fractions whilst for [^{60}Cu]CuPTSM demonstrated a homogenous distribution. In a 9L glioma rat model, they showed that for CuATSM, retention was found to correlate with tumour pO_2 as measured by a needle oxygen electrode. The oxygen levels in tumours were manipulated by administration of hydralazine (to increase tumour hypoxia) or varying the inhaled oxygen levels (atmospheric air, 100 % O_2). Visual examination of the autoradiography data indicated that the high tumour uptake seen for CuATSM was relatively homogeneous in hydralazine treated animals. Untreated animals showed less and heterogeneous uptake, consistent with hypoxic and normoxic areas expected in the control tumours. In a further study in canine myocardium, [$^{64/62/61}$Cu]CuATSM was taken up in hypoxic and ischemic tissue within 20 min of administration, and the activity was not retained in necrotic tissue.[55] [$^{64/62/61}$Cu]CuATSM uptake kinetics were seemingly independent of blood flow, indicating that the tracer may potentially be used clinically to detect myocardial hypoxia.

Further work evaluated the spatial correlation of activity with regions of hypoxia, as determined by autoradiography and immunohistochemistry. Yuan *et al.* investigated the spatial correlation of [^{64}Cu]CuATSM and the hypoxia marker EF5 by performing PET imaging and comparing autoradiographic distributions and immunohistochemical staining on R3230Ac, FSA and 9L tumours in rats at 1h p.i.[56] Higher RTM were observed for FSA compared with R3230Ac and 9L. [^{64}Cu]CuATSM autoradiography and immunohistochemistry images also varied between the tumour types: whilst R3230Ac and 9L showed a close spatial correlation between [^{64}Cu]CuATSM and EF5 hypoxia staining, FSA tumours showed no correlation. Results were confirmed by further

controls with the hypoxia markers pimonidazole and carbonic anhydrase IX. Breathing carbogen significantly decreased tumour hypoxia in FSA-bearing animals as measured by EF5 staining, but did not affect [^{64}Cu]CuATSM uptake. Tumour line dependent uptake of [^{64}Cu]CuATSM was also observed by O'Donoghue *et al.* who compared the intratumoural distribution of [^{64}Cu]CuATSM, [^{18}F]FMISO, pimonidazole and the perfusion marker dye Hoechst-33342 in rats bearing R3327AT prostate tumours and FaDu squamous cell carcinomas (Figure 5).[57] The study found that [^{18}F]FMISO uptake was similar between 30 min-4 h p.i. in both tumour types. In FaDu, serial PET imaging showed similar early and late [^{64}Cu]CuATSM PET images that corresponded to [^{18}F]FMISO scans and electrode measurements. In R3327AT tumours, [^{64}Cu]CuATSM uptake showed a temporal evolution over 0.5-20 h p.i. For early time-points, a negative correlation between ^{64}Cu and hypoxia (pimonidazole), and a positive correlation with perfusion (Hoechst staining) was observed as depicted in Figure 5. Only at late time points did [^{64}Cu]CuATSM correspond to [^{18}F]FMISO PET images, autoradiographic distribution and colocalisation with pimonidazole.

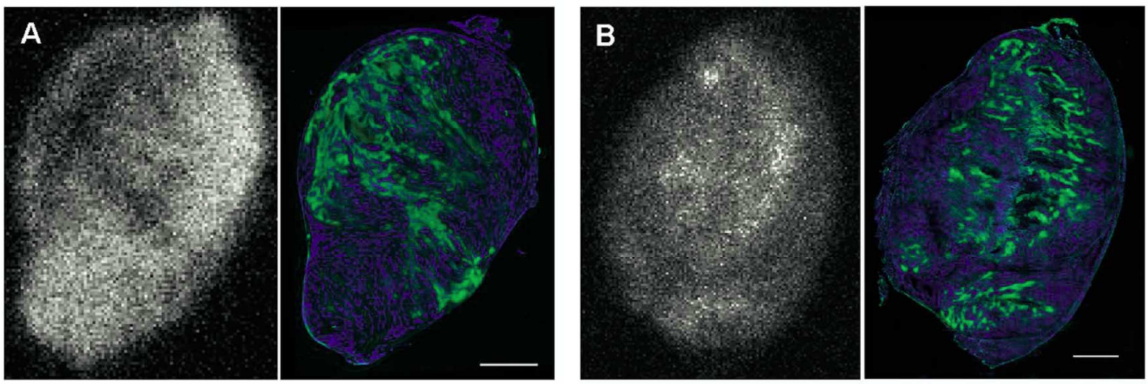

Figure 5 R3327-AT tumour slices of a rat killed (A) 1 h and (B) 24 h post [^{64}Cu]CuATSM administration. The black and white images show the digital autoradiograph of ^{64}Cu distribution (light = high counts, dark = low counts). The fluorescence microscopy overlay images shows distribution of perfusion determined by Hoechst 33342 dye (blue) and hypoxia as defined by pimonidazole-associated immunofluorescence (green). The images shows correlation of ^{64}Cu activity with perfusion at the 1h time point in (A), whereas ^{64}Cu correlates with regions of hypoxia at later timepoints as shown by (B). Visual comparison is confirmed by the correlation coefficients obtained from scatter diagrams of autoradiography pixel count versus fluorescent intensity. Reprinted with permission from reference 57.

Subsequently, Burgman *et al.* investigated uptake of [^{64}Cu]CuATSM as a function of oxygen concentration in two rodent and four human tumour cell lines *in vitro*.[58] ^{64}Cu accumulation was

rapid during the first 0.5-1 h of incubation and was always highest in anoxic cells, but lower and dependent on cell type in hypoxic cells. The initial uptake kinetics were also highly cell-line dependent. The metabolism of CuATSM by the cells was also investigated *via* octanol extraction (see Chapter 5.6). Within 2 h under hypoxic conditions, no intact [^{64}Cu]CuATSM was detected anymore, whereas the amount of intact compound recovered under normoxia was one fifth. The metabolised [^{64}Cu]CuATSM activity was also taken up when incubated in fresh cells, albeit at a slower rate. In addition, the authors observed strongly cell-line dependent efflux of activity.

More recent investigations underlined the tumour specificity. [^{64}Cu]CuATSM uptake in SCCVII squamous cell carcinoma bearing mice did not vary with increasing tumour oxygenation, whilst [^{18}F]FMISO uptake decreased with increasing tumour oxygenation.[59] Tumour uptake of [^{64}Cu]CuATSM could also not be changed if the tumour was re-oxygenated by carbogen inhalation 90 min post-injection. This was interpreted as further evidence of irreversible cellular trapping of the [^{64}Cu]CuATSM.

A dual tracer autoradiography study by Dence *et al* in 9L glioma compared the distribution of [^{64}Cu]CuATSM, [^{18}F]FDG and [^{18}F]FLT.[60] [^{18}F]FMISO and [^{64}Cu]CuATSM demonstrated excellent regional correlation at 10 min and 24 h post injection. The proliferation marker [^{18}F]FLT also showed a strong correlation with [^{64}Cu]CuATSM, implying that hypoxic regions were also high in proliferation. No regional correlation between the uptake of [^{64}Cu]CuATSM and [^{18}F]FDG was found. Obata *et al.* compared [^{64}Cu]CuATSM and [^{18}F]FDG in VX2 tumour bearing white rabbits.[61] The major accumulation of [^{64}Cu]CuATSM occurred in the active, outer rim cells of the tumour whereas [^{18}F]FDG was distributed in the pre-necrotic inner regions. Oh *et al.* confirmed that FDG was also not positively correlated with [^{64}Cu]CuATSM uptake in a Lewis lung carcinoma tumour mouse model.[62] There was no correlation with pimonidazole uptake; at 1h p.i. the activity was found to accumulate on the outer edges of the tumour. In contrast, pimonidazole staining occured in the inside tumour regions and showed some overlap with [^{18}F]FDG. Immunohistochemical analysis with different proliferation markers revealed that [^{64}Cu]CuATSM accumulated in quiescent, but clonogenic cells, indicating that they continued DNA synthesis.

The authors suggested that regions of pimonidazole uptake were severely hypoxic, whereas the regions of high [^{64}Cu]CuATSM accumulation were mildly hypoxic and merely highly reducing due to a high NADH/NADPH concentration. The article proposes that the differing uptake of [^{64}Cu]CuATSM and pimonidazole are a result of their different retention mechanisms and therefore [^{64}Cu]CuATSM and the nitroimidazole based agents may image different aspects of hypoxia.

3.3.4 CuATSM for radiotherapy

The efficiency of radiotherapy is dependent upon the oxygen enhancement effect as a higher O_2 concentration increases DNA damage by generating oxygen free radicals. ^{64}Cu, as well as being a positron emitter, also emits medium energy β particles and high LET Auger electrons. These have a subcellular range and deposit their energy extremely close to the site of decay, and, if deposited close to the nucleus, can cause DNA damage. Since this occurs independent of oxygen concentration, a few studies have evaluated the potential of [^{64}Cu]CuATSM as a radiotherapeutic agent to localize [^{64}Cu] in potential hypoxic tumour regions. Lewis *et al.* have shown that administration of a therapeutic dose (4-10 mCi) of [^{64}Cu]CuATSM significantly increased the survival time of hamsters bearing human GW39 tumours with no acute toxicity.[63] One group of animals had also been given hydralazine to induce transient hypoxia, however this did not increase the therapeutic effect. The study was also able to use PET and MRI with a therapeutic dose of [^{64}Cu]CuATSM to monitor tumour volume over time and to determine tumour dose accurately, which may have important applications for dosimetry calculations and real-time PET monitoring of therapy in the clinical setting. Further studies demonstrated that pre-treatment of mice bearing EMT6 tumours with 2-deoxyglucose (2-DG) led to increased uptake of [^{64}Cu]CuATSM compared to non-treated mice. Tumour growth was inhibited by ~60% and survival was increased by ~50% when compared to untreated mice or ones which had only received one of the agents. To evaluate the molecular basis of using [^{64}Cu]CuATSM as a radiotherapy agent, Obata *et al.* carried out clonogenic survival, cell growth and comet assays in cells that had been incubated with [^{64}Cu]CuATSM under hypoxia.[64] [^{64}Cu]CuATSM uptake was able to induce DNA damage and cell

proliferation was inhibited after 24 h. Subcellular localisation data revealed that ^{64}Cu activity was primarily found in the microsomal/cytosol fraction, but a transition to the nuclear fraction was observed with time. Interestingly, comparative data obtained for [^{64}Cu]CuPTSM indicated no significant differences in localisation as depicted in Figure 6 below.

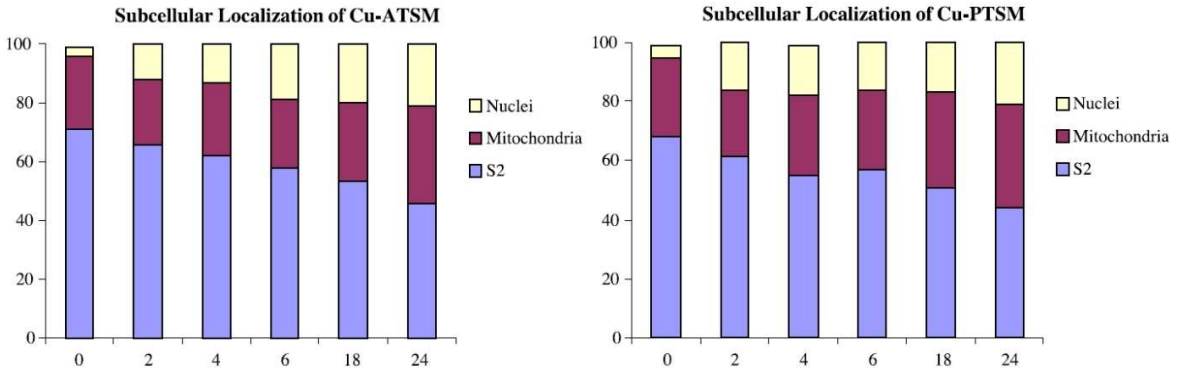

Figure 6 (left) Bar chart showing the subcellular distribution (mean % of total radioactivity) of ^{64}Cu following treatment of cells with [^{64}Cu]CuATSM and [^{64}Cu]CuPTSM. S2 is the cellular residue after removal of nuclei and mitochondria. With time, a relocalisation from S2 and the mitochondrial to nuclear fraction is observed for both compounds. Data reprinted with permission from reference 64.

Weeks *et al.* investigated the correlation between cellular hypoxia and DNA damage/cytotoxicity induced by [^{64}Cu]CuATSM.[65] They confirmed that DNA damage induced was attributable to the radioactive emissions from ^{64}Cu, and further showed that the toxicity experienced was a result of increased [^{64}Cu]CuATSM uptake alone under hypoxic conditions rather than a synergy between radiation and hypoxia. As the intracellular extent of hypoxia is difficult to determine, the authors monitored HIF-1α expression as an indicator of hypoxia and found a strong correlation between HIF-1α and [^{64}Cu]CuATSM uptake. The combined results further underlined the potential of [^{64}Cu]CuATSM as a therapeutic drug for the delivery of radiotoxic ^{64}Cu to radiation resistant tumours.

3.3.5 Clinical studies

A limited number of clinical PET imaging studies of solid tumours in humans have been conducted to date with [$^{60/62/64}$Cu]CuATSM.[53, 66] The studies primarily assessed the relationship between tumour uptake of CuATSM and survival/response to therapy. The first study published in 2000 observed intense uptake of [^{62}Cu]CuATSM in patients with lung cancer.[67] A negative correlation with blood flow was also observed, suggesting that low flow enhanced uptake of CuATSM and the distribution of radioactivity was different to that of [^{18}F]FDG. A further study in non-small-cell lung cancer (NSCLC) patients investigated whether pre-treatment tumour uptake of [^{60}Cu]CuATSM could predict response to therapy.[68] Tumour uptake was variable and tumour-to-muscle ratio (RTM) threshold could be used to distinguish responders to radio-/chemotherapy with a RTM <3.0 from non-responders that had a RTM ≥3.0. Tumour SUVs however did not correlate with therapy response or survival and the tumour uptake of FDG was not significantly different in responders and non-responders. Further studies of uterine cervical cancers confirmed CuATSM uptake to be inversely related to progression-free survival and response to therapy.[69-71]

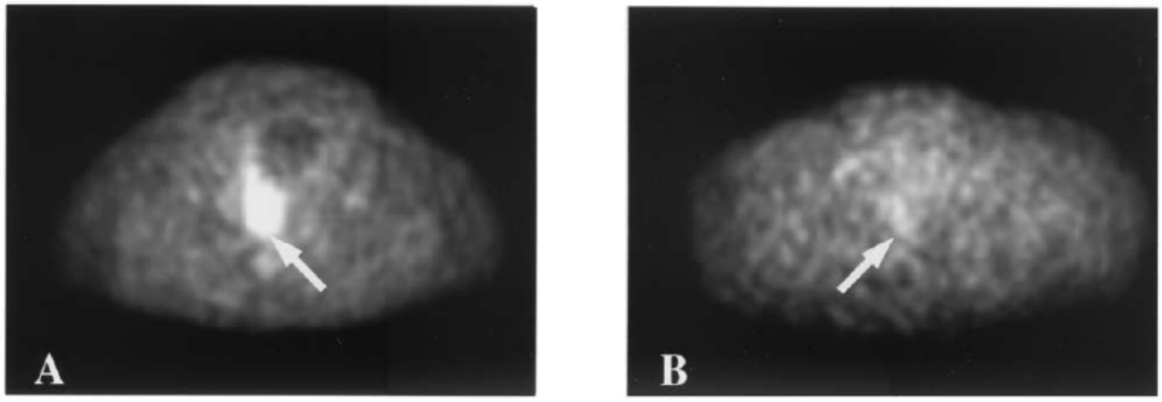

Figure 7 Transaxial PET images of the pelvis representing summed data obtained 30–60 min after injection of [^{60}Cu]CuATSM of patients with primary cervical tumours. There is intense [^{60}Cu]CuATSM uptake (RTM = 5.1) in Patient A who developed recurrent disease at 6 months. In patient B, low [^{60}Cu]CuATSM uptake is visible (RTM = 2.3) in the primary tumour and the patient remained free of disease at 23 months. Reprinted with permission from reference 69.

Dehdashti *et al.* determined a correlation between molecular markers of hypoxia and CuATSM uptake. The study used immunohistochemical methods to stain for VEGF, EGFR, COX-2 and CA-9 in cervical biopsy samples.[71] Patients with high CuATSM uptake were found to overexpress

VEGF, EGFR and COX-2. A noticeable common feature of all the above clinical studies is that they compare tumour uptake of CuATSM with response to therapy, rather than with direct tissue oxygenation measurements using polarography oxygen electrodes as discussed in section 3.1.1. This was in part justified by the inaccessibility of these tumours, as is the case in NSCLC.[68]

At the time of writing, further clinical studies are underway or recruiting patients, for instance to quantify the reproducibility of CuATSM uptake in pre-treatment CuATSM PET scans and to evaluate CuATSM for identifying hypoxic atherosclerotic plaque.[72]

3.3.6 CuATSM and copper metabolism

Whilst clinical studies have demonstrated that CuATSM is able to provide a prediction of treatment response, it remains unclear why preclinical studies correlating CuATSM with hypoxia in several tumour types have shown such varied results. It is thus uncertain whether the uptake is a universal reflection of tumour hypoxia in terms of pO_2 or whether the uptake and retention of CuATSM involves other biochemical mechanisms that have either resulted from hypoxia, or are even independent of it. The authors that report cell and tumour-line dependent variations suggest that the observed differences may be the result of differing cellular metabolism. The efflux of ^{64}Cu after the initial incubation in certain cell lines under hypoxia and anoxia cannot be accounted for by the mechanisms proposed in section 3.1.5. When the [^{64}Cu]Cu(I) becomes subject to cellular metabolism at these later time points, cellular levels of ^{64}Cu are reflecting the active transport of ^{64}Cu metabolites rather than uptake of [^{64}Cu]CuATSM.

Cellular Cu homeostasis is maintained by an array of Cu transporters and Cu chaperones.[73, 74] The primary transporters for copper into the cell are the plasma membrane copper transporters Ctr1 and Ctr2. Ctr1 transports Cu with high affinity in a time-dependent and energy-independent manner and it has also been shown to facilitate the transport of the anticancer drugs cisplatin, carboplatin and oxaliplatin.[75] Once copper is in the cytoplasm, copper chaperones deliver copper to target enzymes such as Cu/Zn superoxide dismutase (SOD1) in the cytoplasm, and cytochrome C oxidase (CCO)

in the mitochondria. Another target for delivery are ATP7A and ATP7B which function primarily as Cu exporters. ATP7A supplies copper to other enzymes which are secreted from the cell or are placed in vesicles, but it can also export Cu when cytoplasmic levels are too high. All of these Cu transporters are specific to Cu(I). Burgman *et al.* and Donogue *et al.* postulated that these transporters may be involved in the active transport of Cu metabolites, and that the cell/tumour-line dependent retention of ^{64}Cu is governed by the balance of Cu(I) import and export in each cell line.[57, 58] This has been supported recently by Dearling and Packard, who suggest that the trapping mechanism of CuATSM is biphasic.[76] The first phase is the reduction/oxidation equilibrium involving molecular oxygen and thiols. The second step is the interaction of the copper ion with the intracellular proteins. The authors postulate that this second step can be complicated by the changes in cellular biochemistry and cell proteomes as a result of hypoxia, leading to differences in the extent of uptake and retention between different cell lines. Interestingly, hypoxia has been found to stimulate copper uptake and to increase the expression of Ctr1 transporter in macrophage cells, which in turn increased transport to ATP7A and to the secretory pathway.[77] To date, however, little is known in general about the effects of pathophysiological conditions- such as hypoxia- on intracellular copper homeostasis.[77]

	Reference	Animal/cell/tumour model	Comparative marker	Correlation	Technique	Comment/Conclusion
In vitro	Lewis 1999[50]	EMT6	FMISO/CuPTSM (pO_2 medium)	Yes	suspension/adherent cellular uptake assays	O_2 dependent cellular uptake of CuATSM FMISO binding at higher pO_2 than CuATSM % uptake of FMISO lower than CuATSM
	Burgman 2005[58]	rodent: R3327-AT, FSaII human:MDA468, MCF7, DU145, FaDu	N/A (pO_2 medium)	Yes	adherent cellular uptake assays under anoxia, hypoxia and normoxia	Oxygen dependent decomposition of CuATSM Oxygen dependent uptake cell line dependent ^{64}Cu efflux cell line dependent
PRECLINICAL	Lewis 1999 [50]	Balb/c mice EMT6	CuPTSM / AR (1h)	N/A	PET/ dual tracer AR	heterogeneous CuATSM distribution homogeneous CuPTSM distribution
	Lewis 2001[78]	Fischer 344 rat /9L glioma	Needle oxygen electrode	Yes N/A	pO_2 hydralazine	CuATSM uptake increased with lower pO_2 hydralazine increased CuATSM uptake
	O'Donoghue 2005[57]	Fischer Cpn rat /R3327AT /R3327AT /FaDu /FaDu	FMISO (CuATSM 1h) FMISO (CuATSM 24h) FMISO (CuATSM 1h) FMISO (CuATSM 24h) pimonidazole	No Yes Yes Yes	PET/AR/pO_2 dual tracer AR	R3327AT: CuATSM correlates with FMISO at late timepoints, confirmed by AR/IHC. FaDu: correlation between early/late CuATSM and FMISO, confirmed by AR/IHC
	Yuan 2006[56]	Fischer 344 rat /R3230 /FSA /9L glioma	EF5 (1h) FSA only: pimonidazole/CA IX	Yes No Yes	AR	R323aAc and 9L: correlation of CuATSM and EF5 IHC. FSA: no correlation with pimonidazole and CAIX IHC
	Matsumoto 2008[59]	C3H mice/SCCVII	FMISO CuATSM	Yes No	Dynamic PET/AR/IHC	small but significant paradoxical increase in CuATSM tumour uptake for animals breathing air or carbogen compared to 10% oxygen.
	Dence 2008[60]	Fischer 344 rat/ 9L	FMISO (CuATSM 10 min) FMISO (CuATSM 24 h) FDG (CuATSM 10 min) FLT (CuATSM 10 min)	Yes Yes No Yes	PET/ dual tracer AR glucose metabolism	confirmed 9L results by Yuan et al. regions of high hypoxia as defined by CuATSM are highly proliferative but have varied glucose metabolism activity
	Oh 2009[62]	C57BL/6 mice / LLC1	FDG (CuATSM 1h) Pimonidazole Ki 67/BrDu (proliferation)	No/in part No/Yes	dual tracer AR/IHC proliferation	CuATSM accumulated in quiescent but clonogenic tumor cell regions under mild hypoxia
CLINICAL	Grigsby[71] 2007	cervical tumour patients	VEGF antibody COX-2 antibody CA-IX antibody EGFR antibody	Yes Yes Yes Yes	PET/cervival biopsy/IHC	Increased [^{60}Cu]CuATSM uptake was correlated with overexpression of molecular markers of hypoxia

Table 1 Overview of *in vitro*, preclinical and clinical studies that compare CuATSM to other biomarkers of hypoxia using PET imaging, Immunohistochemistry (IHC) and autoradiography (AR).

3.4 Outlook

Table 1 summarizes key studies to date that compared CuATSM with other hypoxia biomarkers in *in-vitro*, preclinical and clinical settings. Further studies also investigated CuATSM in the context of fatty acid synthase expression[79], cancer stem cells[80] and HIF1α/CaIII expression of hypoxic muscle tissue[81]. The literature demonstrates that CuATSM holds great potential as a hypoxia selective imaging agent, but also serves as a reminder that it remains to some extent a "prototype". The investigations discussed demonstrate that although hypoxia selectivity for CuATSM has been proven *in vitro* and *in vivo*, the relationship between oxygenation status, uptake and retention is not universal but tumour and cell line dependent. This raises concerns about its ability to delineate hypoxia in all tumour types. Reports on the spatial correlation with nitroimidazole-based markers are also variable and suggest time-dependence. Additional caveats are that CuATSM responds only to regions much more hypoxic than is clinically important for the onset of radioresistance and the tracer displays high uptake in some non-target organs such as the liver.

As discussed in this chapter, the currently proposed models are based predominantly on the chemical and electrochemical experiments that were carried out alongside *in vitro* and preclinical investigations. However, further investigations are needed to complete or amend the mechanism to elucidate the anomalies observed *in vitro* and *in vivo* to date. This will help to evaluate CuATSM and related bis(thiosemicarbazone) biomarkers in terms of their clinical potential, improve the interpretation of the imaging outcome and potentially help to design an improved tracer.

In vivo studies so far have focused mainly on detecting the amount and distribution of tumoural radiocopper activity. Few investigations pay attention to the nature of the Cu species involved or on the intracellular metabolism. One aspect hardly investigated is the uptake, distribution and metabolism of the bis(thiosemicarbazone) ligand. The following chapters are aimed at designing and applying a new mechanistic probe that enables a comparison of the metabolic fate of the metal and the ligand of a copper bis(thiosemicarbazonate), both in the *in vitro* and *in vivo* setting.

3.5 References for Chapter 3

1. K. A. Krohn, J. M. Link and R. P. Mason, *J. Nucl. Med.*, 2008, **49**, 129S-148S.
2. C. Michiels, *Am. J. Pathol.*, 2004, **164**, 1875-1882.
3. G. Kroemer, L. Galluzzi, P. Vandenabeele, J. Abrams, E. S. Alnemri, E. H. Baehrecke, M. V. Blagosklonny, W. S. El-Deiry, P. Golstein, D. R. Green, M. Hengartner, R. A. Knight, S. Kumar, S. A. Lipton, W. Malorni, G. Nunez, M. E. Peter, J. Tschopp, J. Yuan, M. Piacentini, B. Zhivotovsky and G. Melino, *Cell Death Differ.*, 2009, **16**, 3-11.
4. A. L. Harris, *Nat. Rev. Cancer*, 2002, **2**, 38-47.
5. D. Hanahan and R. A. Weinberg, *Cell*, 2000, **100**, 57-70.
6. P. Vaupel and L. Harrison, *Oncologist*, 2004, **9 Suppl 5**, 4-9.
7. M. Weinmann, C. Belka and L. Plasswilm, *Onkologie*, 2004, **27**, 83-90.
8. G. L. Semenza, *Oncogene*, 2010, **29**, 625-634.
9. C. J. Schofield and P. J. Ratcliffe, *Biochem. Biophys. Res. Commun.*, 2005, **338**, 617-626.
10. L. H. Gray, A. D. Conger, M. Ebert, S. Hornsey and O. C. A. Scott, *Br. J. Radiol.*, 1953, **26**, 638-648.
11. J. M. Brown, *Cancer Res.*, 1999, **59**, 5863-5870.
12. M. Hoekel, K. Schlenger, B. Aral, M. Mitze, U. Schaeffer and P. Vaupel, *Cancer Res.*, 1996, **56**, 4509-4515.
13. A. Fyles, M. Milosevic, D. Hedley, M. Pintilie, W. Levin, L. Manchul and R. P. Hill, *J Clin Oncol*, 2002, **20**, 680-687.
14. M. Nordsmark, M. Overgaard and J. Overgaard, *Radiother Oncol*, 1996, **41**, 31-39.
15. D. M. Brizel, S. P. Scully, J. M. Harrelson, L. J. Layfield, R. K. Dodge, H. C. Charles, T. V. Samulski, L. R. Prosnitz, M. W. Dewhirst and et al., *Cancer Res.*, 1996, **56**, 5347-5350.
16. S. J. Chitneni, G. M. Palmer, M. R. Zalutsky and M. W. Dewhirst, *J. Nucl. Med.*, 2011, **52**, 165-168.
17. J. Lee, D. W. Siemann, C. J. Koch and E. M. Lord, *Int. J. Cancer*, 1996, **67**, 372-378.
18. C. J. Koch, *http://www.hypoxia-imaging.org/v2/methods/ef5manual.htm*, Accessed 21/01/2011, 2011.
19. E. G. C. Troost, P. Laverman, J. H. A. M. Kaanders, M. Philippens, J. Lok, W. J. G. Oyen, A. J. Van Der Kogel, O. C. Boerman and J. Bussink, *Radiother. Oncol.*, 2006, **80**, 157-164.
20. J. H. A. M. Kaanders, K. I. E. M. Wijffels, H. A. M. Marres, A. S. E. Ljungkvist, L. A. M. Pop, F. J. A. Van den Hoogen, P. C. M. De Wilde, J. Bussink, J. A. Raleigh and A. J. Van der Kogel, *Cancer Res.*, 2002, **62**, 7066-7074.
21. J. Pacheco-Torres, P. López-Larrubiaa, P. Ballesterosb and S. Cerdána, *NMR in Biomedicine*, 2011, **24**, 1-16.
22. R. P. Mason, H. Shukla and P. P. Antich, *Magn. Reson. Med.*, 1993, **29**, 296-302.
23. M. Rodrigues Loreta, A. Howe Franklyn, R. Griffiths John and P. Robinson Simon, *J Magn Reson Imaging*, 2004, **19**, 482-488.
24. C. Baudelet and B. Gallez, *Magn. Reson. Med.*, 2002, **48**, 980-986.
25. G. Mees, R. Dierckx, C. Vangestel and C. Van de Wiele, *Eur. J. Nucl. Med. Mol. Imaging*, 2009, **36**, 1674-1686.
26. A. Nunn, K. Linder and H. W. Strauss, *Eur. J. Nucl. Med.*, 1995, **22**, 265-280.
27. P. J. Blower, J. R. Dilworth, R. I. Maurer, G. D. Mullen, C. A. Reynolds and Y. Zheng, *J. Inorg. Biochem.*, 2001, **85**, 15-22.
28. J. D. Chapman, A. J. Franko and J. Sharplin, *Br. J. Cancer*, 1981, **43**, 546-550.
29. K. E. Linder, Y. W. Chan, J. E. Cyr, M. F. Malley, D. P. Nowotnik and A. D. Nunn, *J. Med. Chem.*, 1994, **37**, 9-17.
30. J. R. Dilworth and S. J. Parrott, *Chem. Soc. Rev.*, 1998, **27**, 43-55.
31. R. D. Okada, G. Johnson, III, K. N. Nguyen, B. Edwards, C. M. Archer and J. D. Kelly, *Circulation*, 1997, **95**, 1892-1899.
32. M. Tatsumi, K. Yutani, H. Kusuoka and T. Nishimura, *Eur. J. Nucl. Med.*, 1999, **26**, 91-94.
33. R. H. Mannan, V. V. Somayaji, J. Lee, J. R. Mercer, J. D. Chapman and L. I. Wiebe, *J Nucl Med.*, 1991, **32**, 1764-1770.

34. P. Zanzonico, J. O'Donoghue, J. D. Chapman, R. Schneider, S. Cai, S. Larson, B. Wen, Y. Chen, R. Finn, S. Ruan, L. Gerweck, J. Humm and C. Ling, *Eur. J. Nucl. Med. Mol. Imaging*, 2004, **31**, 117-128.
35. L. S. Ziemer, S. M. Evans, A. V. Kachur, A. L. Shuman, C. A. Cardi, W. T. Jenkins, J. S. Karp, A. Alavi, W. R. Dolbier and C. J. Koch, *Eur. J. Nucl. Med. Mol. Imaging*, 2003, **30**, 259-266.
36. J. S. Rasey, N. J. Nelson, L. Chin, M. L. Evans and Z. Grunbaum, *Radiat. Res.*, 1990, **122**, 301-308.
37. J. S. Rasey, W. J. Koh, J. R. Grierson, Z. Grunbaum and K. A. Krohn, *Int. J. Radiat. Oncol., Biol., Phys.*, 1989, **17**, 985-991.
38. J. S. Rasey, J. J. Casciari, P. D. Hofstrand, M. Muzi, M. M. Graham and L. K. Chin, *Radiat. Res.*, 2000, **153**, 84-92.
39. J. S. Rasey, W. J. Koh, M. L. Evans, L. M. Peterson, T. K. Lewellen, M. M. Graham and K. A. Krohn, *Int. J. Radiat. Oncol. Biol. Phys.*, 1996, **36**, 417-428.
40. J. G. Rajendran, D. L. Schwartz, J. O'Sullivan, L. M. Peterson, P. Ng, J. Scharnhorst, J. R. Grierson and K. A. Krohn, *Clin. Cancer Res.*, 2006, **12**, 5435-5441.
41. A. M. Spence, M. Muzi, K. R. Swanson, F. O'Sullivan, J. K. Rockhill, J. G. Rajendran, T. C. H. Adamsen, J. M. Link, P. E. Swanson, K. J. Yagle, R. C. Rostomily, D. L. Silbergeld and K. A. Krohn, *Clin. Cancer Res.*, 2008, **14**, 2623-2630.
42. A. L. Vavere and J. S. Lewis, *Dalton Transactions*, 2007, 4893-4902.
43. D. J. Chapman, *J. Nucl. Med.*, 2001, **42**, 1653-1655.
44. R. C. Urtasun, M. B. Parliament, A. J. McEwan, J. R. Mercer, R. H. Mannan, L. I. Wiebe, C. Morin and J. D. Chapman, *Br. J. Cancer Suppl.*, 1996, **27**, S209-212.
45. Y. Fujibayashi, H. Taniuchi, Y. Yonekura, H. Ohtani, J. Konishi and A. Yokoyama, *J. Nucl. Med.*, 1997, **38**, 1155-1160.
46. A. Obata, S. Kasamatsu, J. S. Lewis, T. Furukawa, S. Takamatsu, J. Toyohara, T. Asai, M. J. Welch, S. G. Adams, H. Saji, Y. Yonekura and Y. Fujibayashi, *Nucl. Med. Biol.*, 2005, **32**, 559.
47. J. L. J. Dearling, J. S. Lewis, G. E. D. Mullen, M. T. Rae, J. Zweit and P. J. Blower, *Eur. J. Nucl. Med.*, 1998, **25**, 788-792.
48. J. L. J. Dearling and P. J. Blower, *Chem. Commun.*, 1998, 2531-2532.
49. J. L. J. Dearling, J. S. Lewis, G. E. D. Mullen, M. J. Welch and P. J. Blower, *J. Biol. Inorg. Chem.*, 2002, **7**, 249-259.
50. J. S. Lewis, D. W. McCarthy, T. J. McCarthy, Y. Fujibayashi and M. J. Welch, *J. Nucl. Med.*, 1999, **40**, 177-183.
51. R. I. Maurer, P. J. Blower, J. R. Dilworth, C. A. Reynolds, Y. Zheng and G. E. D. Mullen, *J. Med. Chem.*, 2002, **45**, 1420-1431.
52. J. P. Holland, P. J. Barnard, D. Collison, J. R. Dilworth, R. Edge, J. C. Green and E. J. L. McInnes, *Chem.-Eur. J.*, 2008, **14**, 5890-5907.
53. J. P. Holland, J. S. Lewis and F. Dehdashti, *Q. J. Nucl. Med. Mol. Imaging*, 2009, **53**, 193-200.
54. J. P. Holland, J. H. Giansiracusa, S. G. Bell, L.-L. Wong and J. R. Dilworth, *Phys. Med. Biol.*, 2009, **54**, 2103-2119.
55. S. Lewis Jason, P. Herrero, L. Sharp Terry, A. Engelbach John, Y. Fujibayashi, R. Laforest, A. Kovacs, J. Gropler Robert and J. Welch Michael, *J Nucl Med*, 2002, **43**, 1557-1569.
56. H. Yuan, T. Schroeder, J. E. Bowsher, L. W. Hedlund, T. Wong and M. W. Dewhirst, *J. Nucl. Med.*, 2006, **47**, 989-998.
57. J. A. O'Donoghue, P. Zanzonico, A. Pugachev, B. Wen, P. Smith-Jones, S. Cai, E. Burnazi, R. D. Finn, P. Burgman, S. Ruan, J. S. Lewis, M. J. Welch, C. C. Ling and J. L. Humm, *Int. J. Radiat. Oncol., Biol., Phys.*, 2005, **61**, 1493-1502.
58. P. Burgman, J. A. O'Donoghue, J. S. Lewis, M. J. Welch, J. L. Humm and C. C. Ling, *Nucl. Med. Biol.*, 2005, **32**, 623-630.

59. K.-I. Matsumoto, L. Szajek, M. C. Krishna, J. A. Cook, J. Seidel, K. Grimes, J. Carson, A. L. Sowers, S. English, M. V. Green, S. L. Bacharach, W. C. Eckelman and J. B. Mitchell, *Int. J. Oncol.*, 2007, **30**, 873-881.
60. C. S. Dence, D. E. Ponde, M. J. Welch and J. S. Lewis, *Nucl. Med. Biol.*, 2008, **35**, 713-720.
61. A. Obata, M. Yoshimoto, S. Kasamatsu, H. Naiki, S. Takamatsu, K. Kashikura, T. Furukawa, J. S. Lewis, M. J. Welch, H. Saji, Y. Yonekura and Y. Fujibayashi, *Nucl. Med. Biol.*, 2003, **30**, 529-534.
62. M. Oh, T. Tanaka, M. Kobayashi, T. Furukawa, T. Mori, T. Kudo, S. Fujieda and Y. Fujibayashi, *Nucl. Med. Biol.*, 2009, **36**, 419-426.
63. J. S. Lewis, R. Laforest, T. L. Buettner, S.-K. Song, Y. Fujibayashi, J. M. Connett and M. J. Welch, *Proc. Natl. Acad. Sci.*, 2001, **98**, 1206-1211.
64. A. Obata, S. Kasamatsu, J. S. Lewis, T. Furukawa, S. Takamatsu, J. Toyohara, T. Asai, M. J. Welch, S. G. Adams, H. Saji, Y. Yonekura and Y. Fujibayashi, *Nucl. Med. Biol.*, 2005, **32**, 21-28.
65. A. J. Weeks, R. L. Paul, P. K. Marsden, P. J. Blower and D. R. Lloyd, *Eur. J. Nucl. Med. Mol. Imaging*, 2010, **37**, 330-338.
66. M. P. S. Dunphy and J. S. Lewis, *J. Nucl. Med.*, 2009, **50**, 106S-121S.
67. N. Takahashi, Y. Fujibayashi, Y. Yonekura, M. J. Welch, A. Waki, T. Tsuchida, N. Sadato, K. Sugimoto and H. Itoh, *Ann. Nucl. Med.*, 2000, **14**, 323-328.
68. F. Dehdashti, M. A. Mintun, J. S. Lewis, J. Bradley, R. Govindan, R. Laforest, M. J. Welch and B. A. Siegel, *Eur. J. Nucl. Med. Mol. Imaging*, 2003, **30**, 844-850.
69. F. Dehdashti, P. W. Grigsby, J. S. Lewis, R. Laforest, B. A. Siegel and M. Welch, *J. Nucl. Med.*, 2008, **49**, 201-205.
70. F. Dehdashti, W. Grigsby Perry, A. Mintun Mark, S. Lewis Jason, A. Siegel Barry and J. Welch Michael, *Int. J. Radiat. Oncol. Biol. Phys.*, 2003, **55**, 1233-1238.
71. W. Grigsby Perry, S. Malyapa Robert, R. Higashikubo, K. Schwarz Julie, J. Welch Michael, C. Huettner Phyllis and F. Dehdashti, *Mol. Imaging Biol.*, 2007, **9**, 278-283.
72. U. N. I. o. Health, http://clinicaltrials.gov/.
73. G. Crisponi, V. M. Nurchi, D. Fanni, C. Gerosa, S. Nemolato and G. Faa, *Coord. Chem. Rev.*, 2010, **254**, 876-889.
74. S. La Fontaine, M. L. Ackland and J. F. B. Mercer, *Int. J. Biochem. Cell Biol.*, 2010, **42**, 206-209.
75. S. Ishida, J. Lee, D. J. Thiele and I. Herskowitz, *Proc. Natl. Acad. Sci.*, 2002, **99**, 14298-14302.
76. J. L. J. Dearling and A. B. Packard, *Nucl. Med. Biol.*, 2010, **37**, 237-243.
77. C. White, T. Kambe, Y. G. Fulcher, S. W. Sachdev, A. I. Bush, K. Fritsche, J. Lee, T. P. Quinn and M. J. Petris, *J. Cell Sci.*, 2009, **122**, 1315-1321.
78. J. S. Lewis, T. L. Sharp, R. Laforest, Y. Fujibayashi and M. J. Welch, *J. Nucl. Med.*, 2001, **42**, 655-661.
79. A. L. Vavere and J. S. Lewis, *Nucl. Med. Biol.*, 2008, **35**, 273-279.
80. Y. Yoshii, T. Furukawa, Y. Kiyono, R. Watanabe, A. Waki, T. Mori, H. Yoshii, M. Oh, T. Asai, H. Okazawa, M. J. Welch and Y. Fujibayashi, *Nucl. Med. Biol.*, 2010, **37**, 395-404.
81. D. Skovgaard, M. Kjaer, J. Madsen and A. Kjaer, *J. Nucl. Med.*, 2009, **50**, 950-958.

Chapter 4

Orthogonal labelling of bis(thiosemicarbazones) for mechanistic studies

4.1 Introduction

As described in Chapter 3, the currently accepted mechanism of hypoxia selectivity of CuATSM involves cellular uptake of the compound followed by enzyme mediated reduction to a $[Cu(I)ATSM]^-$ species. This either dissociates (under hypoxia) or is reoxidised to Cu(II)ATSM (under normoxia), enabling it to pass back out of the cell. The hypoxia selectivity depends on the redox potential and lipophilicity of the ligand, which in turn is governed by the backbone substituents. The detailed structural dependence of the Cu(II)/Cu(I) reduction, the relative stability of the Cu(I) species and the pH dependence of the process have since been further investigated.

To date, biological investigations involving the copper-radiolabelled complex, such as *in vitro* uptake in cells and *in vivo* studies in rodents have only been able to monitor the fate of the *radiometal*. Investigations on the subcellular distribution, cell line- and tumour line dependence and tumour oxygenation status have provided data on the absolute uptake and distribution of the Cu* activity. However, the studies did not distinguish between intact complex and Cu* bound to protein or other biological ligands. In particular, there is little information to indicate if the free bis(thiosemicarbazone) ligand is retained in the cell when CuATSM dissociates. Valuable mechanistic information on the mode of activity of biomarkers belonging to the CuATSM family could be gained from independent *in vivo* tracking of both the metal and the ligand. The design and synthesis of a suitable mechanistic probe would give information on the fate of the bis(thiosemicarbazone) ligand of copper-bis(thiosemicarbazonates) *in vitro* and *in vivo*.

4.1.1 Orthogonal labelling

In order to investigate the fate of the bis(thiosemicarbazone) ligand, we decided to employ a novel strategy termed Orthogonal Labelling. The concept, illustrated in Scheme 1, involves the synthesis of a pair of structurally identical radiotracers- one bears the radiolabel at the metal core (^{64}Cu), whilst the other contains a radiolabel (^{18}F or ^{123}I) attached to a specific position in the ligand. The two orthogonally labelled tracers then allow the ligand and the radiometal to be tracked independently. Mechanistic information can be obtained from *in vitro* cellular uptake experiments as well as *in vivo* biodistributions and dynamic PET or SPECT imaging.

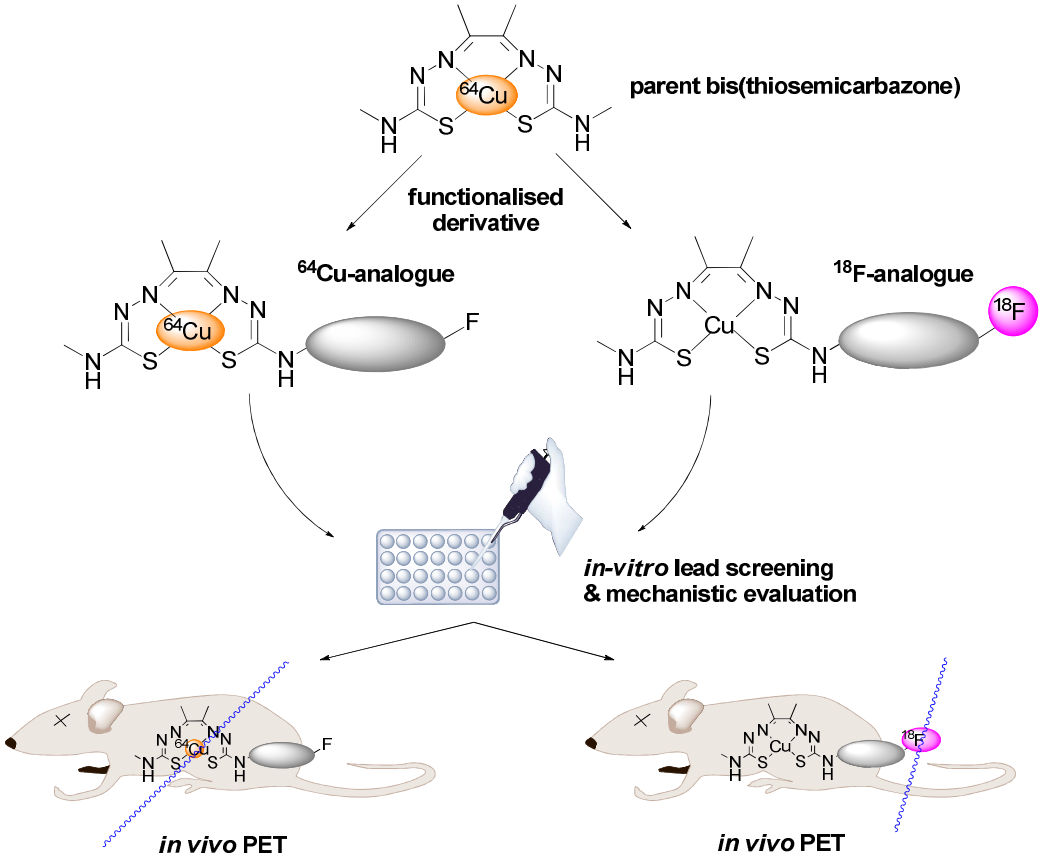

Scheme 1 Schematic of the orthogonal radiolabelling approach (illustrated for ^{18}F) for a pair of structurally identical copper-bis(thiosemicarbazonates). The analogues, labelled either with ^{64}Cu or ^{18}F, are designed to determine the fate of the metal or ligand respectively. Screening of the copper-complexes identifies leads with suitable electrochemical profile and *in vitro* cellular uptake. The corresponding orthogonal pair is then used to obtain *in-vitro* and *in-vivo* mechanistic information about the mechanism of hypoxia selectivity.

The orthogonally labelled tracers should provide complementary information about the role and the fate of the ligand. This may help to design a second generation of bis(thiosemicarbazone) ligands to

address current problems such as high hepatointestinal uptake. Should the orthogonally labelled tracers maintain hypoxia selectivity, such that the ligand is retained inside the cell in a similar manner to the radiocopper, this would also enable the use of alternative radioisotopes for the radiolabelling of copper-bis(thiosemicarbazonates). ^{64}Cu is not routinely produced in many locations, whereas ^{18}F for instance is widely available at low cost and several iodine radioisotopes are also in routine clinical use. The hypoxia selective complex could thus be radiolabelled at the ligand according to radioisotope availability.

In the literature, the concept of orthogonal labelling is mainly limited to the labelling of known tracers with a different half-life radioisotope. For instance, an azomycin arabinoside derivative has been labelled with both iodine and fluorine to give [$^{124/123}$I]IAZA and [^{18}F]IAZA. There are a few other examples of orthogonal radiolabelling for mechanistic investigations, such as studies with [^{3}H]FMISO which has been used for delayed tissue autoradiography in an animal stroke model to understand the role of cellular hypoxia in stroke.[1]

4.1.2 Functionalisation of Cu(ATSM)

As discussed in Chapters 1 and 3, mechanistic investigations have shown that the hypoxia selectivity is primarily governed by the reduction potential and the alkylation pattern of the backbone. Research within the Dilworth group[2-4] and elsewhere has demonstrated that, using the pendant amine substituents H_2ATSR/A[4] and H_2ATSRen[3] described in Chapter 2.4.1 and 2.6.2, it is possible to synthesise bis(thiosemicarbazones) that retain the dimethyl backbone but are functionalised on one exocyclic nitrogen without compromising the redox potential or the hypoxia selectivity of the complex. Some of these complexes are depicted in Scheme 2.

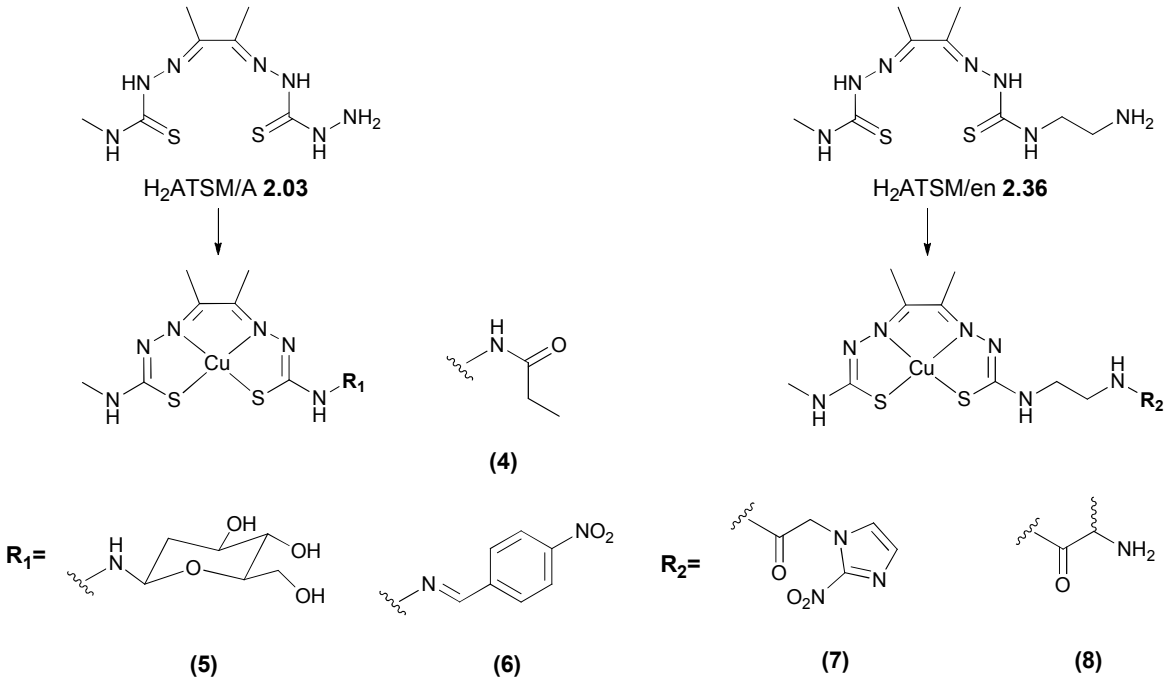

Scheme 2 Copper bis(thiosemicarbazonates), based on the H_2ATSM/A and H_2ATSM/en motif, previously investigated as hypoxia selective ^{64}Cu-labelled radiotracers.

In vivo biodistributions of a water soluble glucose conjugate **(5)**[4, 5] revealed a shift from hepatointestinal to partial renal excretion compared to CuATSM, but the overall biodistribution was largely unaffected.[6] The imine condensation of H_2ATSM/A to 4-nitrobenzaldehyde to form **(6)** or to an aldehyde bearing a nitroimidazole group (not shown) resulted in highly lipophilic conjugates with good *in vitro* and *in vivo* hypoxia selectivity. These derivatives however suffered from large liver uptake.[2] Less lipophilic variants, such as derivative **(7)**, were achieved by amide coupling of H_2ATSM/en to nitroimidazoles bearing carboxylic acid groups. These agents had improved uptake differentials between normoxic and hypoxic cells *in vitro* and significantly lower non-target organ uptake *in vivo* than derivatives based on H_2ATSM/A. The above examples illustrate that functionalisation *via* the exocyclic nitrogen is possible without compromising the hypoxia selectivity of the bis(thiosemicarbazonato) complex. It further demonstrates that the linker and the conjugate group can have a significant impact on both the hypoxia selectivity and the biodistribution.

4.1.3 Previous strategies for ^{18}F- and ^{64}Cu-orthogonally labelled bis(thiosemi-carbazonato) complexes

The derivatives discussed in 4.1.2 retained *in vitro* hypoxic selectivity and *in vivo* tumour uptake. Therefore modification *via* the exocyclic nitrogen presents a viable approach for ligand functionalisation. Work carried out simultaneously within our groups has produced two orthogonally ^{18}F- and ^{64}Cu-labelled derivatives (Scheme 2).

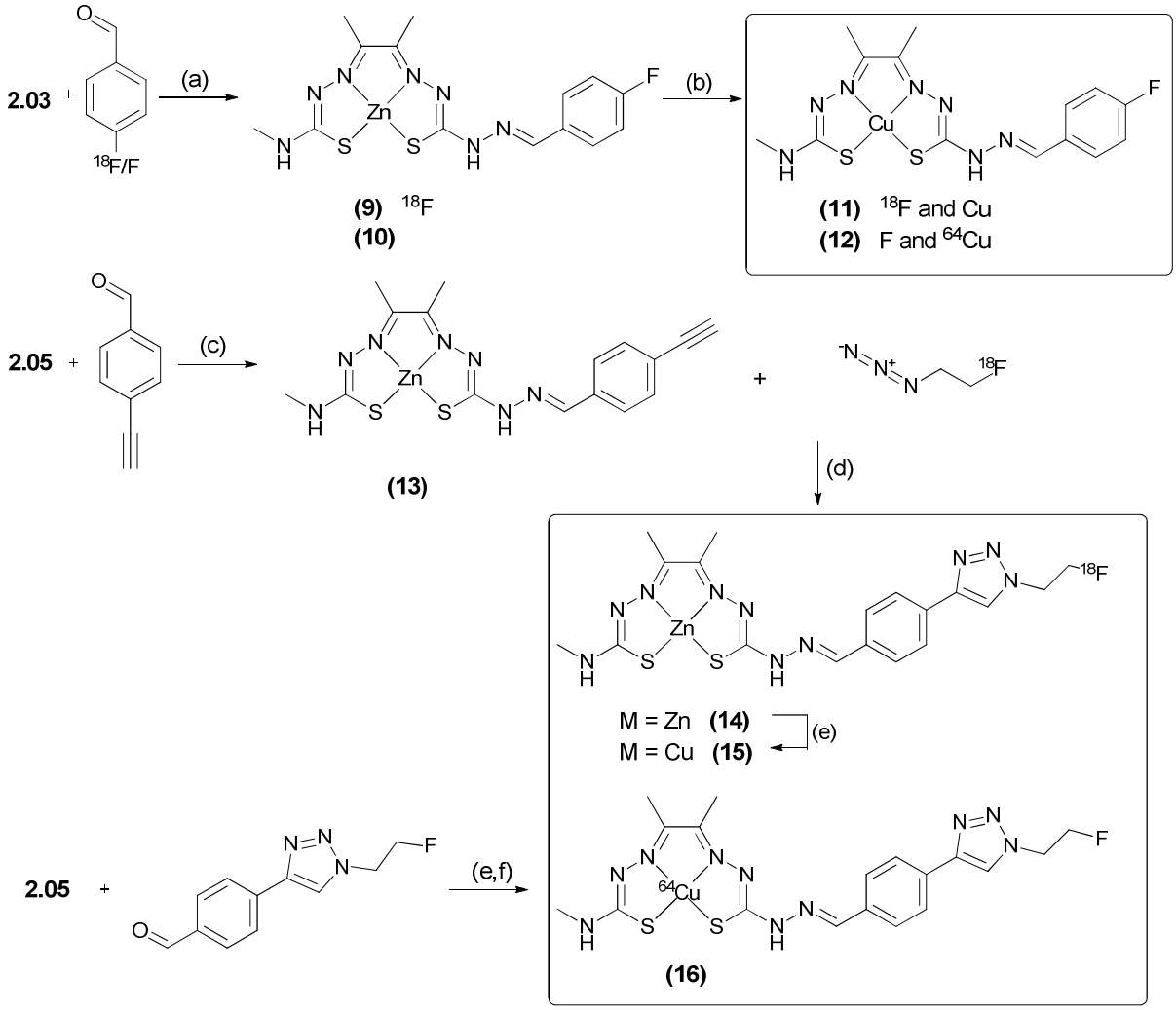

Scheme 3 (a) 4-fluorobenzaldehyde, MeCN, 80°C, 15 min, 56% RCY (b) $Cu(OAc)_2$ or $[^{64}Cu]Cu(OAc)_2$, DMF/H_2O, rt, 5 min, quantitative (c) MeOH, 65°C, 2 h, 80% (d) $CuSO_4$, Na-ascorbate, DMSO, 100°C, 15 min, 84% RCY (e) $Cu(OAc)_2$, DMF, rt, 5 min, 88% (f) MeOH, 65°C, $CuSO_4$, Na-ascorbate, rt, 4 h, 38% (g) $[^{64}Cu]Cu(OAc)_2$, DMF/H_2O, rt, 5 min, quantitative.

ZnATSM/A was transformed in an imine condensation with 4-fluorobenzaldehyde to give **(11)** or **(12)** and a Huisgen 1,3-dipolar cycloaddition with [^{18}F]2-fluoro-1-azidoethane to give **(15)** or **(16)**.[7] The cold complexes **(12)** and **(16)** showed similar redox potentials (-0.60 V and -0.64 V) compared to the parent Cu(ATSM) (-0.65 V). Unfortunately, *in vitro* cellular uptake assays revealed that neither **(12)** nor **(16)** showed sufficient *in vitro* hypoxia selectivity.

In contrast, a further amide-bonded derivative **(17)** had a sufficiently large hypoxic differential *in vitro* for further *in vivo* investigations. Substrate **(17)** was synthesised *via* peptide coupling of H_2ATSM/A to 4-fluorobenzoic acid as depicted in Scheme 4.

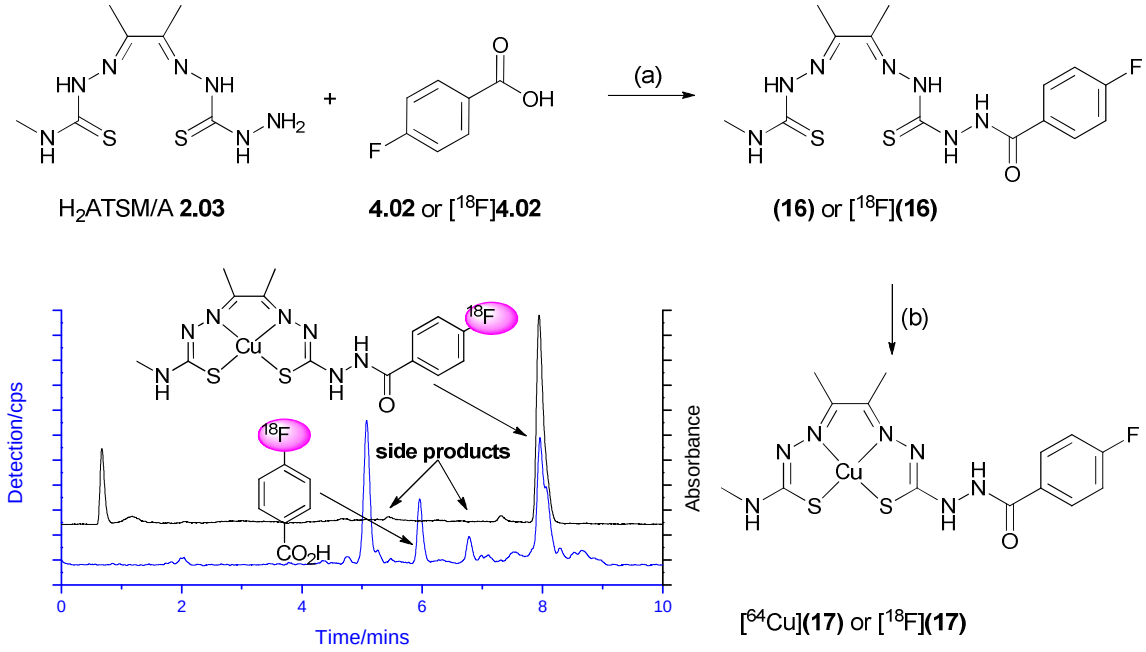

Scheme 4 Synthesis of amide-bonded orthogonally-labelled derivatives [^{18}F]**(17)** and [^{64}Cu]**(17)**.[7] (a) BOP, MeCN, DIPEA, 80°C, 15 min, 32% decay-corrected RCY from $^{18}F^-$ (b) [^{64}Cu]$Cu(OAc)_2$ or $Cu(OAc)_2$, DMF/H_2O, rt, 5 min, both quantitative. [^{18}F]-4-Fluorobenzoic acid was synthesised according to reference 8.

Whilst it was possible to synthesise [^{18}F]**(17)** in small quantities, the chosen route presented significant problems. The reaction required a two-step synthesis of [^{18}F]fluorobenzoic acid.[8] Subsequent coupling of the acid to H_2ATSM/A ligand using BOP coupling agent resulted in poor yields due to the formation of by-products containing ^{18}F, as shown by the radio-HPLC trace in Scheme 4. Previous work within the Dilworth group and within this thesis had shown that

couplings of a functionalised ligand are most successful when using stoichiometric amounts of ligand, coupling agent, a non-nucleophilic base and coupling partner.[9-11] These conditions are not easily reproduced on a radiochemical scale as an excess of ligand and coupling agent is inevitably present compared to the labelled prosthetic group and this leads to the formation of side-products. In addition, the use of heat when coupling bis(thiosemicarbazone) ligands to shorten the reaction times for compatibility with the ^{18}F- half-life can also lead to unwanted side products. Consequently, it was unfortunately not technically possible to produce enough of the labelled derivative for *in vitro* or *in vivo* investigations.

4.2 Aims

This chapter concerns the design and synthesis of a second generation of orthogonally-labelled derivatives for mechanistic studies. In order to serve as suitable mechanistic probes, the lead compounds are required to maintain the favourable physicochemical and biological characteristics of the parent compound, while simultaneously providing feasible radiosynthetic routes to provide sufficient quantities of the orthogonally labelled derivatives for preclinical studies.

The following changes from the ^{18}F-labelling approach discussed in section 4.2 have been employed:

(i) The use of a different functionalised bis(thiosemicarbazone) core for the ^{18}F-labelling and conjugation

(ii) The synthesis of derivatives orthogonally labelled with ^{123}I and ^{64}Cu to provide a longer half-life to facilitate synthesis of the orthogonal derivatives and provide time for transportation of the labelled compounds for *in vivo* imaging

4.3 Second generation of orthogonal ^{18}F and ^{64}Cu-labelled copper bis(thiosemicarbazonato) complexes based on the ATSM/en motif

We wished to explore a new approach to orthogonally labelled bis(thiosemicarbazonato) complexes that uses the ATSM/en core introduced in section 2.6.2 to obtain CuATSMenF (**4.03**) depicted in Figure 1. We opted to persist with the 4-fluorobenzoic acid motif as the hydrazinic functionalised tracer [^{64}Cu]**(17)** displayed favourable physicochemical and *in vitro* properties.

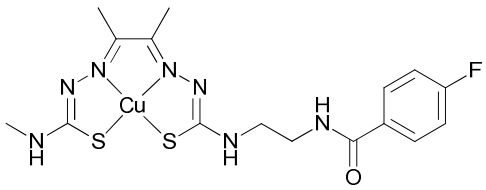

CuATSMenF **4.03**

Figure 1 Structure of proposed second generation fluorinated derivative for orthogonal labelling

The synthesis of the proligand H_2ATSM/en (**2.36**) and its corresponding Cu complex CuATSMen (**4.08**) has previously been developed within the group and is depicted in Scheme 5.[12] Monoprotected ethylene diamine is reacted with carbon disulphide, followed by methyl iodide. The resultant dithiocarbamate **4.05** is then reacted with hydrazine to afford thiosemicarbazide **4.06**.

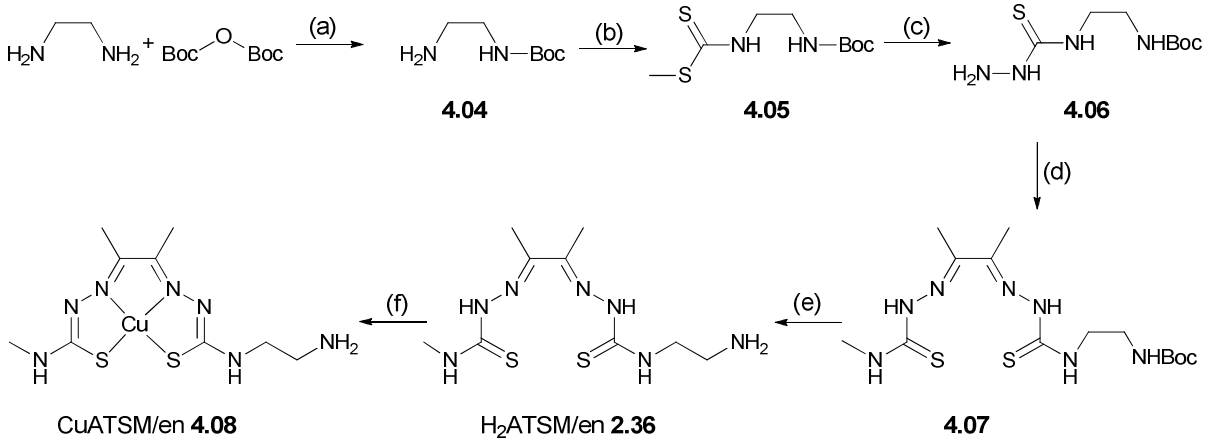

Scheme 5 Synthesis of the H_2ATSMen ligand **2.36** and the CuATSMen complex **4.08** (a) $CHCl_3$, 0°C (b) NEt_3, CS_2 then MeI, EtOH 20°C (c) $NH_2NH_2{\cdot}H_2O$, EtOH, reflux (d) 4-*N*-ethyl-3-thiosemicarbazone, cat. HCl, EtOH, 45°C (e) TFA, rt (f) $Cu(OAc)_2{\cdot}2H_2O$.

Imine condensation with the Me half ligand **2.01** followed by Boc-deprotection in neat TFA gave the desired proligand **2.36**.

Besides potentially improved *in vivo* profiles (section 4.1.2), bis(thiosemicarbazones) based on the alkylamino derivative H_2ATSM/en also offer synthetic advantages. The reactivity of hydrazine is normally enhanced over other amine nucleophiles due to the α-effect. The lone pairs in the two adjacent nitrogen atoms interact to increase their relative energies to result in a more nucleophilic species. This effect would be expected to operate in the hydrazine moiety of the H_2ATSR/A proligand and metal complexes, however these both proved to be much less nucleophilic than expected. This is due to substantial delocalisation of the lone pair of the nitrogen adjacent to the chelate ring. This is confirmed by X-ray crystallography for the free H_2ATSM ligand in the two structures in Figure 2 below.

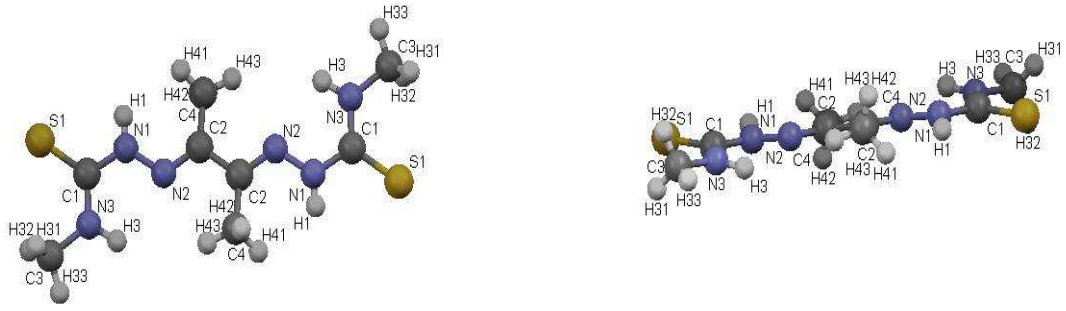

Figure 2 Two views of the ORTEP representations of the structure of H_2ATSM showing the planarity of the N3 exocyclic nitrogen. Relevant bond distances (in Å): C1-N1 = 1.368, C1-N3 = 1.323, C2-N2 = 1.292, C3-N3 = 1.455.

The side elevation of the structure on the right shows that N3 is essentially planar due to delocalisation of the lone pair. The bond distances also confirm this with the C1-N3 distance being intermediate between the values for a C=N bond (C2-N2 = 1.292 Å) and a C-N single bond (C3-N3=1.323 Å). Although this structure is for ATSM, analogous delocalisation will occur for H_2ATSM/A and this will have the consequence of also reducing the electron density on the terminal exocyclic NH_2 group.

As a consequence of the above, reactions of both hydrazinic derivatives H_2ATSR/A and ZnATSR/A with activated aromatic esters resulted in incomplete reaction and the formation of side products as already discussed in Chapter 2.

A potential solution to this would be to insulate the lone pair of the pendant amine from the delocalisation by use of the aminoethyl linker H_2ATSM/en and its Cu complex.

Conjugations of the H_2ATSM/en proligand with activated esters have proved faster and proceeded cleaner in higher yield, whilst BOP couplings of the ligand were also successful.[11] Use of the ATSM/en motif also provides further synthetic pathways that can be explored. It has previously been shown that attempts to synthesise unconjugated CuATSM/A from H_2ATSM/A does not yield a stable species.[9, 13] In contrast, CuATSM/en is stable and this opens another one step pre-conjugation route to CuATSM/en with a pre-labelled prosthetic group. Use of the metal complex instead of the ligand would allow elevated temperatures to be used to speed up the reaction whilst the presence of the metal would avoid the previously observed ligand cyclisation reactions.

4.3.1 CuATSMenF

Before attempting the routes for the ^{64}Cu and ^{18}F-labelled compounds, the cold fluorinated reference ligand **4.09** and copper complex **4.03** were synthesised by the standard coupling strategy employed in Chapter 2.4, using BOP coupling agent and DIPEA base in DMF at room temperature as depicted in Scheme 6.

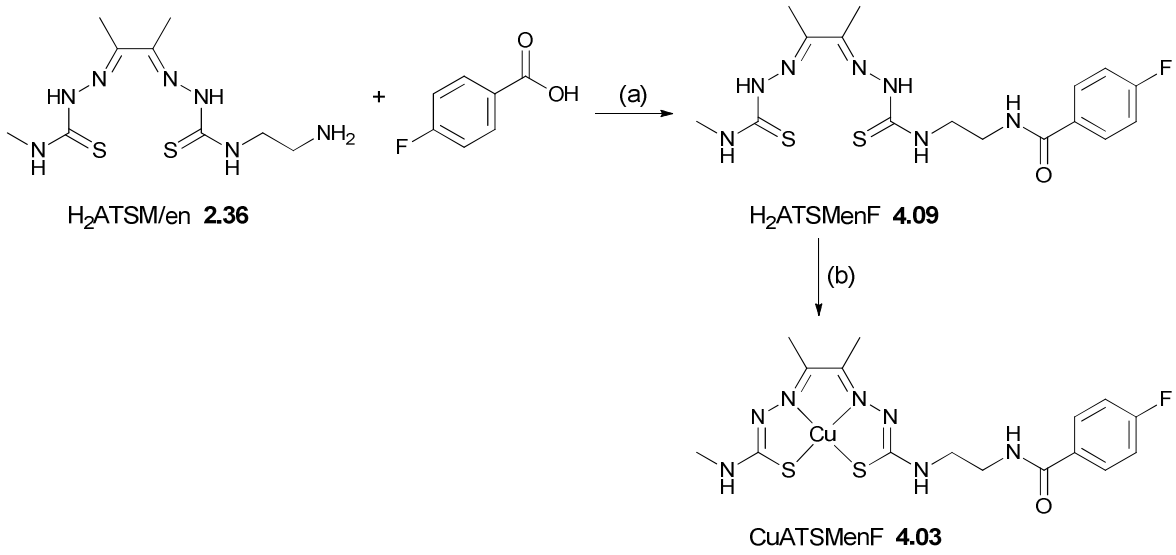

Scheme 6 Synthesis of H_2ATSMenF (**4.09**) and CuATSMenF (**4.03**) (a) BOP, DIPEA, DMF, 4 h, rt, 70% (b) $Cu(OAc)_2 \cdot 2H_2O$, MeOH, 15 min, 81%.

Compound **4.09** was purified by sonication in water and cold EtOH and fully analysed by NMR, HRMS and elemental analysis. NMR spectra were recorded in DMSO-d_6. Figure 3 shows the assigned ^{1}H spectrum of **4.09**. The assignment was confirmed by HMQC and HMBC, and both ^{1}H and ^{13}C NMR were in agreement with the proposed structure. Complexation with cold copper to obtain **4.03** was carried out by addition of 1.2 eq of $Cu(OAc)_2 \cdot H_2O$ to a suspension of the ligand in methanol and the reaction was complete within 15 min at room temperature. The copper(II) complex was considerably more soluble in methanol and methanol-water mixtures than the CuATSM/A fluorobenzoic acid derivative **(17)**. Thus the solvent had to be removed completely *in vacuo* before washing the remaining residue with H_2O to remove the excess copper acetate salt. This increased solubility is an additional advantage of using the ethylenediamine based linker.

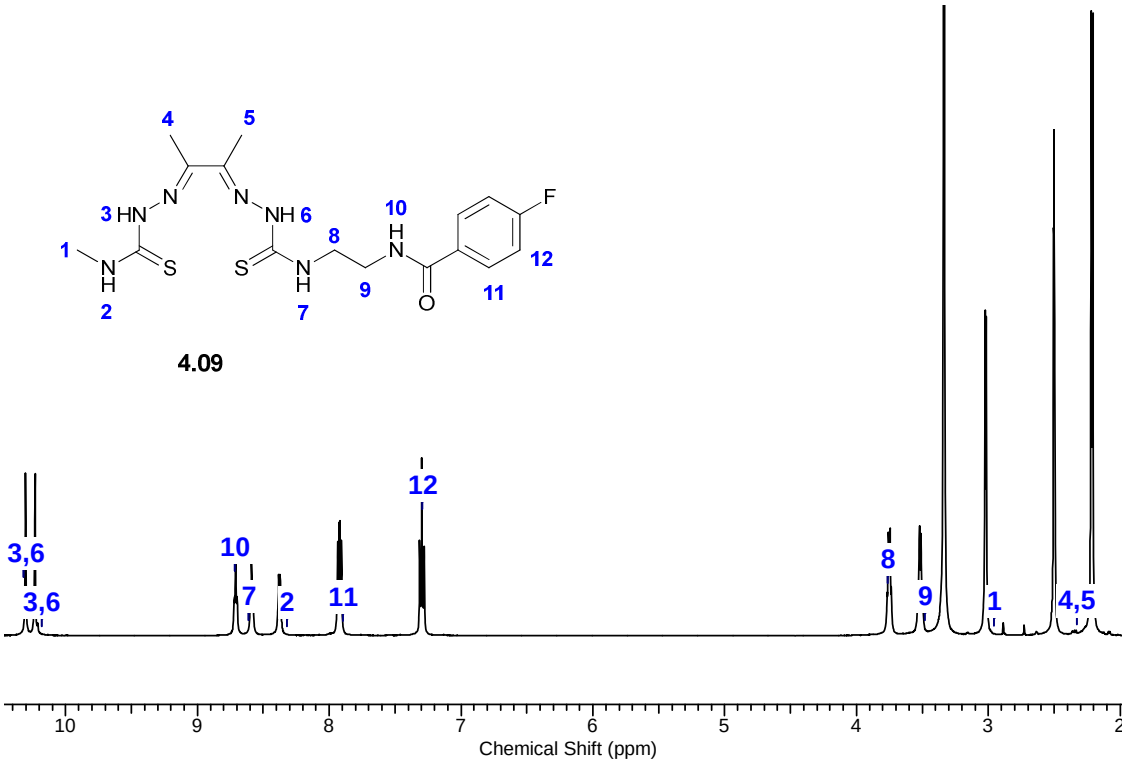

Figure 3 ^{1}H NMR spectrum of **4.09** in DMSO-d_6.

4.3.1.1 [^{64}Cu]CuATSMenF

The ^{64}Cu-labelling of all derivatives in this chapter was carried out by the same method, either by transmetallation from the Zn-bis(thiosemicarbazone) complex or by direct addition of radiocopper to the bis(thiosemicarbazone) ligand. [^{64}Cu]Cu(OAc)$_2$ (10-150 MBq) was added to a stock solution of ligand or Zn complex in DMSO (50 µL of 1mg ml^{-1}). The solution was left to stand for 10 min before purification. The compounds were purified by placing them on a pre-conditioned C-18 Sep-pak cartridge and any unchelated [^{64}Cu]Cu^{2+} is then removed by flushing with water before eluting the compound in ethanol. [^{64}Cu]CuATSMenF ([^{64}Cu]**4.03**) was prepared in this way from **4.09** in > 95% RCY and > 99% RCP, as determined by radio-HPLC and radio-TLC. Figure 4 depicts the radio-HPLC trace of [^{64}Cu]**4.03** confirming formation of a single species.

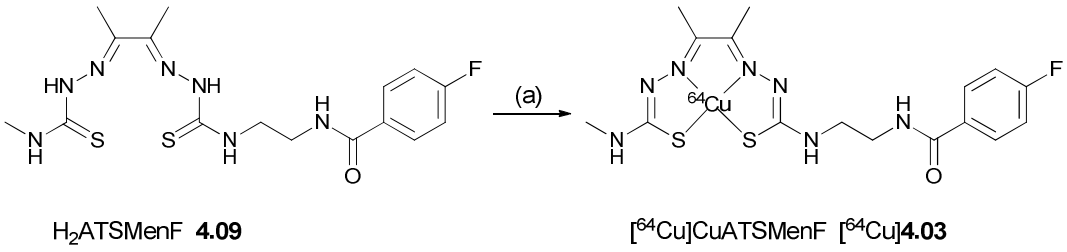

Scheme 7 Synthesis of [^{64}Cu]CuATSMenF. (a) [^{64}Cu]Cu(OAc)$_2$, DMSO/H_2O, 95% RCY.

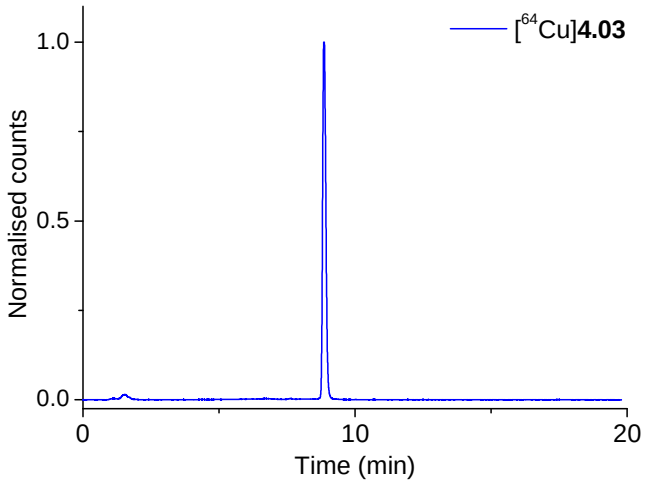

Figure 4 Radio-HPLC trace of [^{64}Cu]**4.03** ([^{64}Cu]CuATSMenF).

Before proceeding with the synthesis of the ^{18}F-labelled analogue, the electrochemical and *in vitro* behaviour of the complex was investigated. **4.03** had a Cu(II)/Cu(I) reduction potential close to that of CuATSM (-0.649 V and -0.646 V respectively). *In vitro* cellular uptake experiments confirmed its hypoxic selectivity and the results of both these measurements are detailed in sections 4.4.6-4.4.8.

4.3.1.2 [^{18}F]CuATSMenF

We anticipated that CuATSM/en, displaying better reactivity than H_2ATSE/A or ZnATSE/A, could be reacted with the activated ester, 4-fluorosuccinimidylbenzoate (FSB) as shown in Scheme 8.

In order to synthesise the orthogonally-labelled [^{18}F]CuATSMenF ([^{18}F]**4.03**) the reaction was first verified non-radiochemically, employing CuATSM/en and *N*-succinimidyl 4-fluorobenzoate

(**4.10**).[14, 15] CuATSM/en[13] was dissolved in DMSO and a stoichiometric amount of **4.10**[14] and Et_3N were added. The reaction was stirred at 60°C for 1h and, monitored by UV-HPLC and ESI-MS, gave quantitative conversion to the product. Pleasingly, a shortened reaction time of 15 min at 80°C achieved similar results, so these conditions were chosen for the hot synthesis.

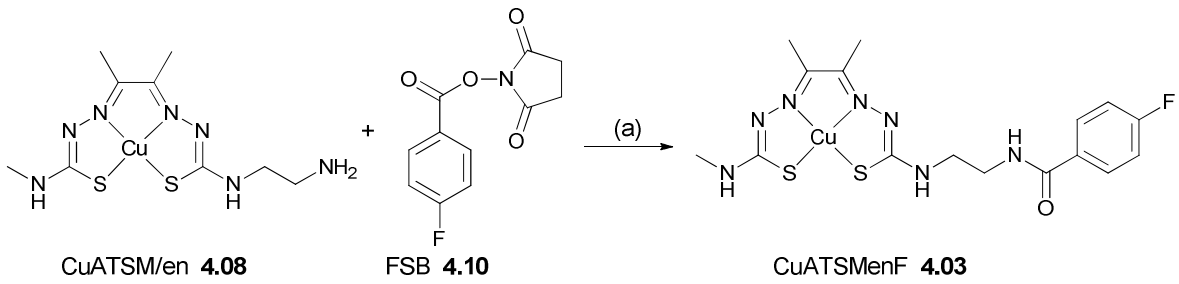

Scheme 8 Synthesis of **4.03** (CuATSMenF) by reaction of CuATSM/en with the FSB activated ester (a) Et_3N, 80°C, 15 min, quantitative conversion by HPLC.

The synthesis of radiolabelled activated ester [^{18}F]**4.10** was carried out on an automated Scintomics synthesis unit as depicted in Figure 5. To dry the aqueous ^{18}F-fluoride, it was first passed onto a QMA anion exchange resin cartridge to remove the $H_2{}^{18}O$ and eluted into the first reactor vial with a solution of Kryptofix 222 and K_2CO_3 in acetonitrile/water (vial A). The resulting K^{18}F/Kryptofix 222 complex was dried by azeotropic distillation at 110°C with 3 × 0.5 mL acetonitrile under a stream of N_2 before the resultant dry complex was dissolved in anhydrous acetonitrile. Reactants were either added to reactor 1 (from vial C or D) or the liquid was dispensed into reaction vials for external, manual synthesis. Transfer into the second reactor allowed an interim C-18 purification and further synthesis (reactants/solvents from vial F and G). [^{18}F]FSB has been widely used for the fluorine-labelling of peptides and proteins.[16] All current protocols require a three-step radiosynthesis in several reactors, with exception of a three-step one-pot procedure and a two-step procedure recently developed by Tang[17] and Glaser[18] respectively. Both these methods are in theory compatible with the two-reactor set-up of the Scintomics Synthesis Unit.

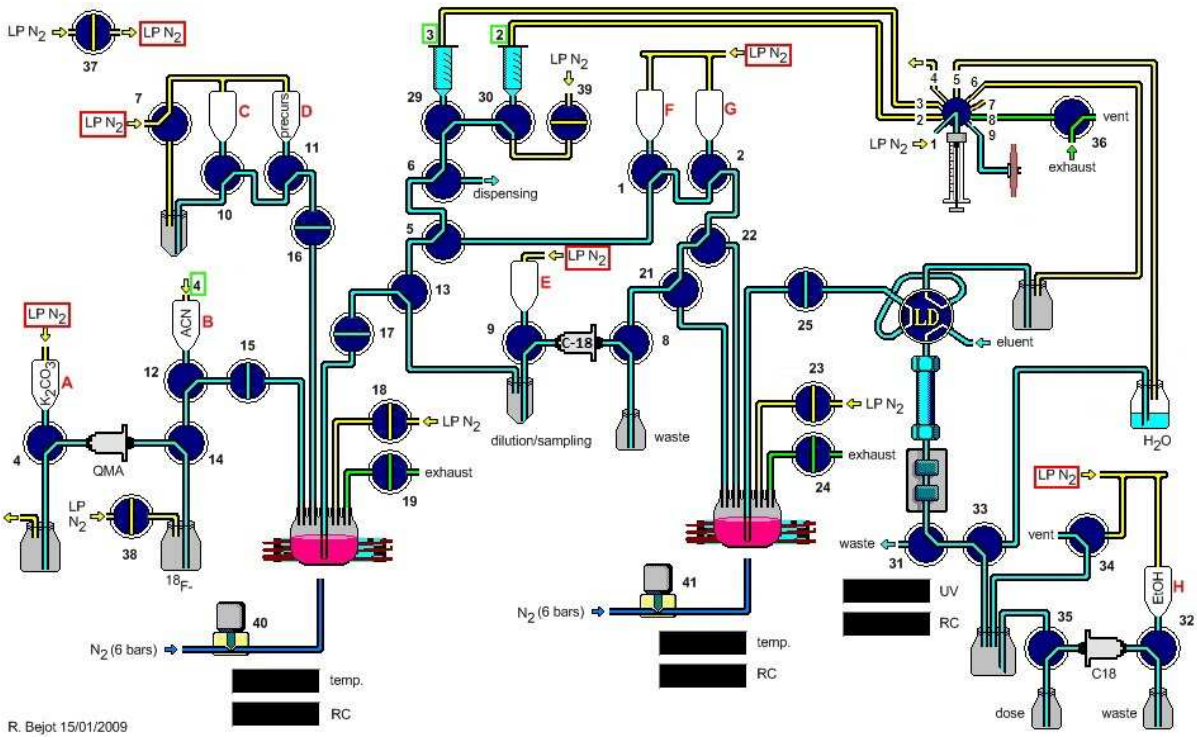

Figure 5 Scintomics Synthesis Unit.

The method of Tang was attempted first and involved ^{18}F-fluorination of ethyl 4-(trimethylammonium triflate)benzoate (**4.11**), followed by saponification of [^{18}F]-ethyl-4-fluorobenzoate (**4.12**) with tetrapropylammonium hydroxide to yield the [^{18}F]-4-fluorobenzoate salt **4.13**. This was converted to [^{18}F]**4.10** by treatment with *N*,*N*,*N*',*N*'-tetramethyl-O-(*N*-succinimidyl)uranium tetrafluoroborate (TSTU). Following the above steps, the product was passed through a C-18 cartridge into reactor 2 containing copper complex **4.08** in DMSO for conjugation. An equimolar amount of triethylamine was added and the reaction was heated at 80°C for 15 min. Unfortunately, no [^{18}F]**4.03** could be isolated; sampling of reactor 1, reactor 2 and the final product post preparative HPLC purification showed that only small amounts of [^{18}F]-4-fluorobenzoate had in fact been formed.

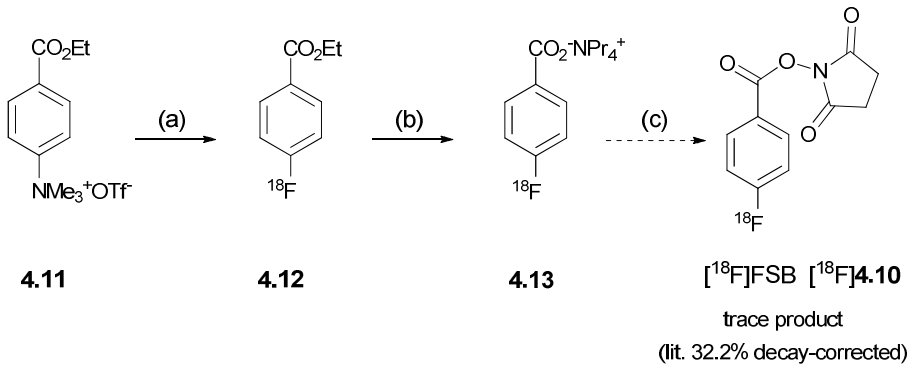

Scheme 9 Attempted synthesis of [^{18}F]FSB on the Scintomics system using the method of Tang. (a) [^{18}F]K[2.2.2]/K_2CO_3, 10 min, 90°C (b) N(C_3H_7)OH, MeCN, 120°C, 3 min (c) TSTU, MeCN, 90°C, 5 min. steps (a)-(b) were not isolated from the synthesis unit, trace product was detected in (c).

Attempts to employ the method by Glaser were more successful. [^{18}F]fluorobenzaldehyde (**4.01**) was synthesised *via* a previously reported procedure (Scheme 10).[8] Disappointingly, the compound was only isolated in a RCY of 10%. The subsequent direct oxidative conversion of **4.01** to [^{18}F]**4.10** using diacetoxyiodobenzene and NHS is thought to involve the reaction of aldehyde with diacetoxyiodobenzene and NHS via formation of PhI(OAc)NHS *in situ*.[19] This step had to be optimised to replace EtOAc with a water miscible solvent to comply with local rules of our radiosynthesis laboratory. Cold trial reactions showed that DMSO was unsuitable whereas reaction in MeCN afforded the desired activated ester quantitatively from 4-fluorobenzoate.

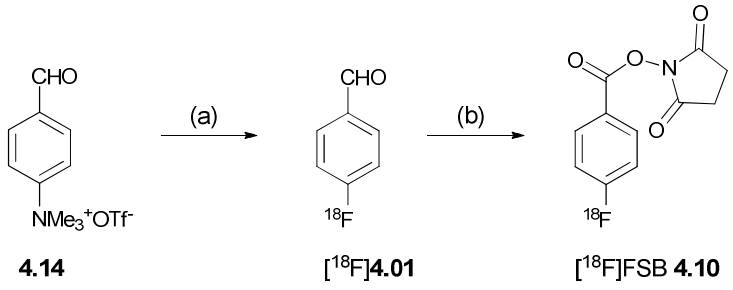

Scheme 10 Synthesis of [^{18}F]FBA[8] followed by [^{18}F]FSB synthesis (method of Glaser[18]) (a) [^{18}F]K[2.2.2]/K_2CO_3, 15 min, 90°C, 10% RCY (lit. 60%) (b) $PhI(OAc)_2$, NHS, MeCN 20% RCY (from FBA).

The method by Glaser suggests that it is essential to carry out this step at 0°C, so reactor 2 containing solid diacetoxyiodobenzene was fitted with an ice bath prior to starting use of labelled material. [^{18}F]**4.01** and NHS in MeCN were added to reactor 2 and the reaction was kept at 0°C for 15 min, followed by 5 min at room temperature. Purification by preparative HPLC and

reformulation into MeCN afforded 18 MBq of [^{18}F]**4.10** (20% non-decay corrected RCY from [^{18}F]**4.01**).

The ester was removed from the Scintomics unit, added manually to the functionalised copper complex **4.08** in DMSO and reacted at 80°C for 15 min (Scheme 11). The crude reaction mixture was analysed by radio-HPLC. Figure 6 shows the crude radio-HPLC trace of [^{18}F]**4.03** compared to the cold **4.03** UV reference sample and [^{18}F]**4.10** starting material.

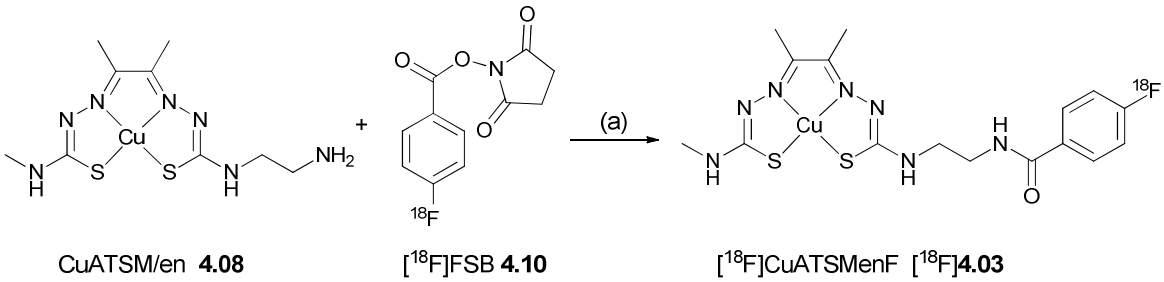

Scheme 11 Conjugation of [^{18}F]FSB to CuATSM/en to form [^{18}F]**4.03** (a) DMSO, 80°C, Et_3N, 15 min quantitative conversion by HPLC.

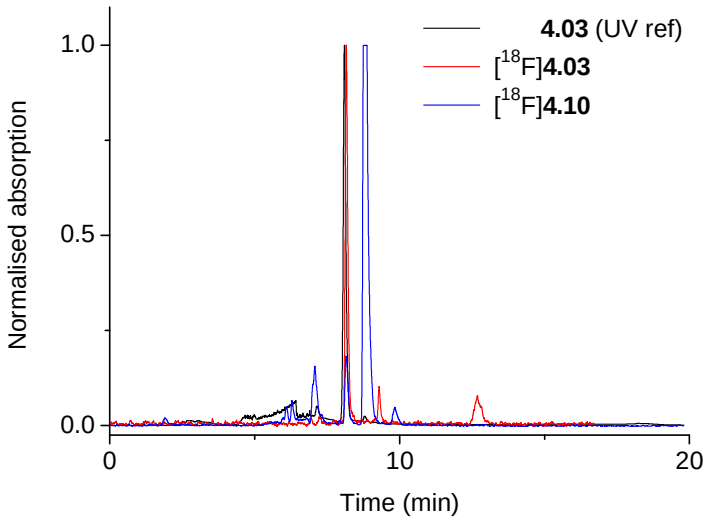

Figure 6 Radio-HPLC spectra of [^{18}F]**4.10** activated ester, [^{18}F]**4.03** and the cold **4.03** UV reference spectrum.

The trace confirms that the activated ester [^{18}F]**4.10** is almost quantitatively converted to [^{18}F]**4.03** by HPLC, with only minor trace impurities formed that could be removed by preparative HPLC. The crude product was not further purified due the low levels of activity (< 10 MBq) isolated.

The successful reaction of [^{18}F]**4.03** proves that coupling of the aminoethyl derivative CuATSM/en to [^{18}F]**4.10** provides a valid alternative for orthogonal labelling of the CuATSM core and does not generate the unwanted side-products encountered in the coupling of H_2ATSM/A to [^{18}F]4-fluorobenzoic acid. However, the difficulties in producing large amounts of [^{18}F]FSB from our permitted activity limit have prevented the synthesis of sufficient quantities of [^{18}F]**4.03** for *in vivo* work. This is carried out at the Churchill hospital and transport takes at least an hour so with the short half-life of ^{18}F it is necessary to be able to make at least 30 MBq of labelled product to obtain an adequate PET image.

4.4 Orthogonal radiolabelling approaches using Iodine-123

The work by Carroll *et al.*[7] and the second generation derivatives discussed above show that a prosthetic group approach for the ^{18}F-orthogonal labelling of bis(thiosemicarbazones) is in principle successful but suffers from a limited starting activity of ^{18}F labelled prosthetic group. Therefore, to produce enough activity for *in vivo* work within our current technical limits, we considered an alternative approach using the longer-lived SPECT isotope, ^{123}I, for a third generation of orthogonal tracers. Besides assisting synthesis, the intermediate-length half-life allows longitudinal imaging to study pharmacokinetics over longer time periods than can be done with short-lived radiopharmaceuticals. This could be important for mechanistic studies, since some reports claim that CuATSM is best imaged after 24 h (see Chapter 3). Should the ligand be retained in the tumour, these derivatives could also offer a hypoxia selective SPECT imaging agent. This alternative to the expensive ^{64}Cu-parent compound could utilise the SPECT cameras and infrastructure already present in most hospitals. Furthermore, iodine offers a range of radioisotopes with different half-lives both for SPECT (^{123}I, $t_{1/2}$ = 13.2 h) and PET (^{124}I, $t_{1/2}$ = 4.2 days, ^{125}I, $t_{1/2}$ = 59.4 days) imaging as well as radiotherapy (^{131}I, $t_{1/2}$ = 8 days) and these could be useful in the further development of hypoxia imaging and therapy using bis(thiosemicarbazonato) complexes.

4.4.1 Radioiodination methods

In general, the radioiodination routes can be divided into nucleophilic and electrophilic substitution reactions.[20, 21] The nucleophilic substitution pathway is dominated by halogen-halogen exchange reactions (Scheme 12). The isotopic or non-isotopic exchange catalysed by ammonium sulphate or copper (I) in acidic, aqueous medium. It can be applied to activated or non-activated arenes, and has for instance been used for the radiosynthesis of MIBG mentioned in Chapter 1.3.2.

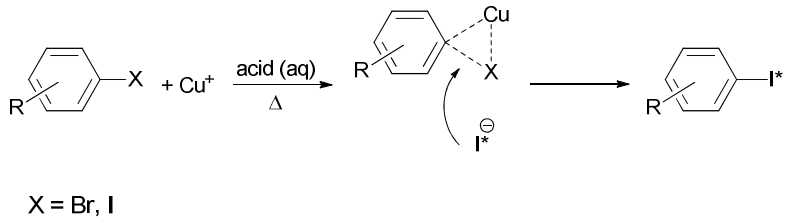

Scheme 12 Nucleophilic radioiodination *via* halogen exchange.[20]

Electrophilic radioiodination is the overall preferred route due to the facile and rapid oxidation of I^- to an electropositive form of iodine I* (HOI*, H_2OI^*) under mild conditions.[22] Oxidants such as chloramine-T, *N*-chloro- or bromosuccinimide or peracetic acid are used *in situ*.

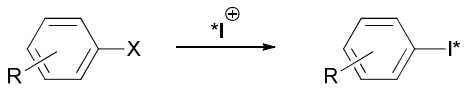

Scheme 13 Electrophilic radioiodination.[20]

In order to limit oxidative side reactions when labelling sensitive substrates such as proteins, immobilized forms of the *N*-chlorosubstrates are employed: Iodobeads® are non-porous polystyrene beads derivatised with *N*-chlorobenzenesulfonamide (sodium salt) and iodogen®, containing four functional chlorine atoms is coated on a reaction vessel.[23] The electrophilic iodine species generated can then react either directly with the aromatic substrate *via* electrophilic aromatic substitution or in a demetallation reaction with an organometallic species (Scheme 13). Trialkyltin compounds are often the precursor of choice as radioiododestannylation proceeds in high radiochemical yields and high regioselectivity using small amounts of precursor.

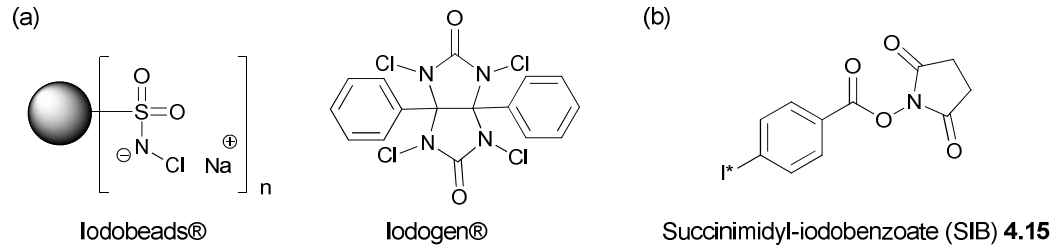

Figure 7 (a) solid phase oxidising agents Iodobead® and Iodogen® (b) the *p*-succinimidyl-iodobenzoate prosthetic group SIB.

Direct electrophilic radioiodination is readily achieved in proteins for instance on tyrosine residues by substituting a hydrogen for an iodine *ortho* to an aromatic hydroxyl group. Due to their similarity to thyroid hormones however, these are prone to *in vivo* deiodination by specific enzymes whilst other proteins are altogether unsuitable for direct iodination. For this reason, prosthetic groups, such *N*-succinimidyl-iodobenzoate (SIB) shown in Figure 7, have been developed.[24, 25] The *N*-succinimidyl ester derivatives will react with free amine residues such as lysine. The SIB acylating agent is reported to have a greater stability than the phenolic iodide and can be prepared either *via* the above mentioned iododestannylation (vide infra) or isotopic exchange, when high specific activity is not required.[25-28] Prosthetic group labelling of proteins can successfully reduce *in vivo* deiodination and prolong plasma half-life.[26 29]

4.4.2 Strategies for iodinated copper bis(thiosemicarbazonato) complexes

The first objective was the synthesis and ^{64}Cu-radiolabelling of potential iodinated bis(thiosemicarbazone) derivatives to determine their suitability in terms of physicochemical characteristics and *in vitro* hypoxia selectivity. This was followed by an investigation of the synthetic feasibility towards the radioiodinated routes. In an analogy to the orthogonally labelled ^{18}F-fluorinated tracers, the synthesis of the iodinated bis(thiosemicarbazonato) complexes in Figure 8 was investigated.

Radioiodine incorporation is preferred at an sp^2 hybridised carbon, since both the vinylic and aromatic carbon-iodine bond strengths are higher (268-297 kJ/mol) than the relatively weak aliphatic bond (222 kJ/mol); this prevents *in vivo* deiodination by S_N2 substitution or β-elimination.[30,20] Therefore, a click-compound analogous to [^{18}F/^{64}Cu]**(16)** was omitted.

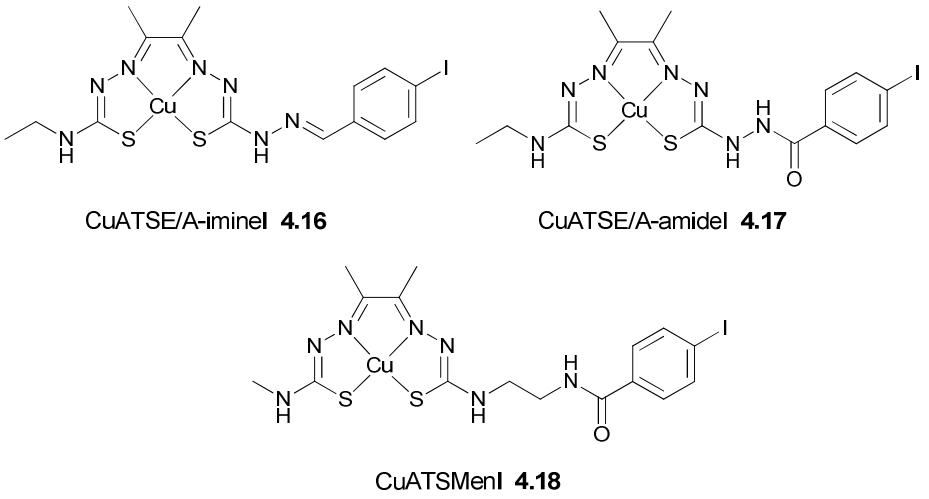

Figure 8 Structures of the proposed iodinated copper bis(thiosemicarbazonato) complexes for orthogonal ^{123}I- and ^{64}Cu-radiolabelling.

4.4.3 Synthesis of imine-based conjugate: CuATSE/A-imineI

Despite the ^{64}Cu-labelled fluorinated orthogonal tracer **(12)** (section 4.1.3) having low *in vitro* hypoxia selectivity, we decided it worthwhile to pursue an analogous iodinated derivative CuATSE/A-imineI (**4.16**) since all other imine-bonded derivatives synthesised within the group previously had shown hypoxia-selectivity. Further information would also be available on whether the lack of hypoxia selectivity effect was specific to the H_2ATSM/A-imine fluorine derivative.

We pursued derivatives based on H_2ATSE/A rather than the methyl derivative, as we surmised that these should be easier to purify, based on the findings outlined in Chapter 2.4.

The desired iodinated ligand H_2ATSE/A-imineI (**4.19**) and zinc complex ZnATSE/A-imineI (**4.20**) were successfully synthesised by conjugation with 4-iodobenzaldehyde as shown in Scheme 14. The condensation reaction of ZnATSE/A with iodobenzaldehyde was carried out in MeOH at 50°C for 3 h, whilst H_2ATSE/A, as expected from Chapter 2, did not tolerate heat and required reaction at room temperature overnight.

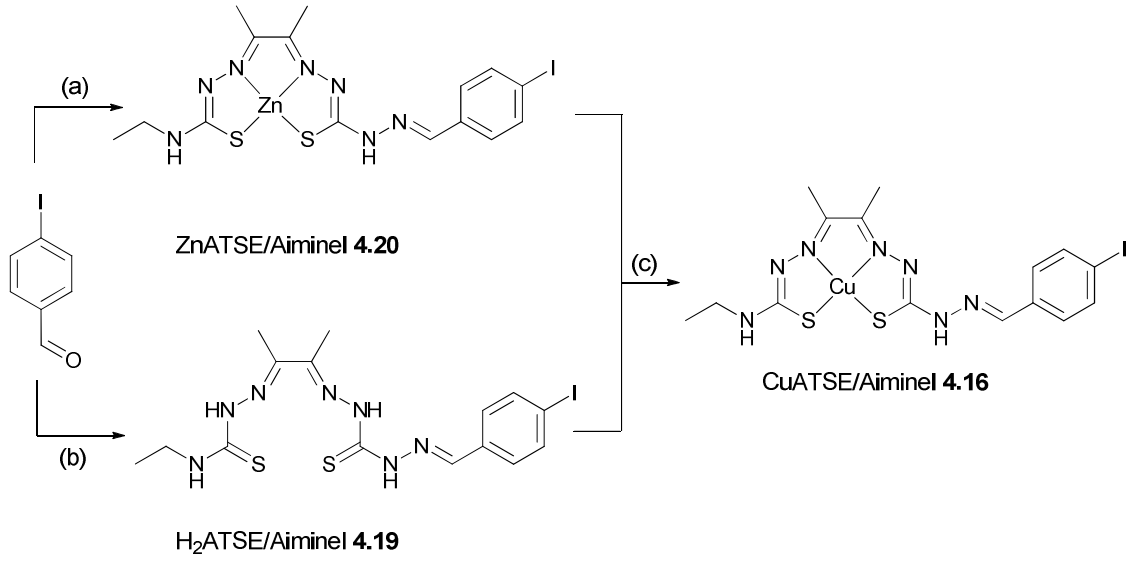

Scheme 14 Synthesis of the imine conjugation product **4.16** *via* the iodinated zinc complex or the ligand (a) ZnATSE/A, MeOH, 50°C, 3 h, 95% (b) H_2ATSE/A, MeOH, rt, overnight, 71% (c) $Cu(OAc)_2 \cdot 2H_2O$, MeOH, 10 min, rt, 84%.

Thus the Zn complex may be a preferable precursor, as heating the hot route can be used to minimise reaction times. Both compounds were fully characterised by NMR, ESI-MS and elemental analysis. Complexation was performed with $CuCl_2$ or $Cu(OAc)_2$. ESI-MS revealed

formation of the product CuATSE/A-imineI (**4.16**) as shown by the desired $[M-H]^-$ and $[M+H]^+$ peaks, however analytical HPLC revealed two peaks. For comparable H_2ATSR/A imine conjugates, two peaks in the HPLC spectrum have previously been attributed to imine *E/Z* isomers.[11] However, the elemental analysis of **4.16** displayed lower than expected values for C and N, indicating that two species may be present. Low C and N values have previously been observed for copper bis(thiosemicarbazonates) and may be indicative of H_2O binding strongly to the complexes even after extensive drying in a vacuum oven.

To investigate further the nature of the Cu-complex formed and to confirm the coordination of Cu(II) to the bis(thiosemicarbazone) ligand, the transmetallation reaction of the zinc complex **4.20** to the corresponding copper complex **4.16** was monitored by UV/vis spectroscopy (Figure 9). Aliquots of 0.1 equiv of $CuCl_2$ were added to a solution of 0.04 mM **4.20** in DMSO and the solution changed from bright orange to red-brown.

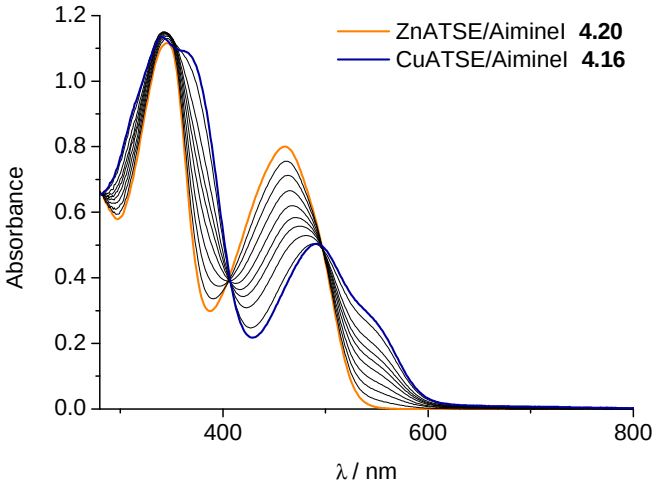

Figure 9 UV titration of **4.20** with $CuCl_2$ in DMSO. The orange line represents the UV/vis spectrum of **4.20**, the brown line is the spectrum of copper complex **4.16** obtained by addition of 10 × 0.1 equiv aliquots (black lines).

Isosbestic points were observed at 281, 406 and 496 nm. This is consistent with a clean transition between the zinc and copper species. The overall shift in absorbance is comparable to that observed for previously reported H_2ATSR/A imine species.[4] The clean transmetallation using sub-stoichiometric amounts of Cu suggest that it should be possible to radiolabel **4.20**.

4.4.3.1 [^{64}Cu]CuATSE/A-imineI

The standard radiolabelling conditions outlined in section 4.2.1.1 were applied. Addition of [^{64}Cu]Cu(OAc)$_2$ to **4.20** afforded [^{64}Cu]**4.16** in 95% RCY as determined by radio-TLC. Pleasingly, a single peak radio-HPLC chromatogram was also obtained.

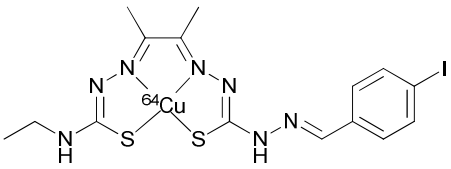

[^{64}Cu]CuATSE/Aimine-I [^{64}Cu]**4.16**

Figure 10 Structure of [^{64}Cu]**4.16**.

Following successful radiolabelling, the log *P* value was determined (log P = 1.62±0.01, see section 4.4.7). Cyclic voltammetry measurements were then performed to investigate whether the ligand modification would adversely affect the Cu(II) to Cu(I) reduction of **4.16**. Unfortunately, the complex did not possess the required redox properties, as shown by an irreversible reduction at -0.525 V. *In vitro* cellular retention assays further revealed no hypoxia selectivity and **4.16** therefore was not pursued for orthogonal radiolabelling. The detailed redox properties and *in vitro* profile are described in section 4.4.6-4.4.8.

4.4.4 Amide bonded derivatives: CuATSE/A-I

Since the fluorinated amide bonded orthogonal tracer **(17)** prepared by Carroll *et al.* displayed favourable physicochemical properties and *in vitro* behaviour, an analogous iodinated derivative was selected next. We chose to use the ATSE/A core instead of its methyl analogue in accordance with the results from Chapter 2 that showed a more facile purification of the ethyl derivative.

4.4.4.1 [^{64}Cu] CuATSE/A-I

Initially, we attempted the reaction of ZnATSE/A with 4-succinimidyl-iodobenzoate (4-SIB, **4.16**)[26] to form **4.22**, due to the prevalence of 4-SIB as a well-known agent for iodination (Scheme 15). As could be expected from reactions of the Zn complex with aromatic activated esters in Chapter 2, the reaction did not go to completion. On heating, it resulted in the formation of side products that could not be adequately removed.

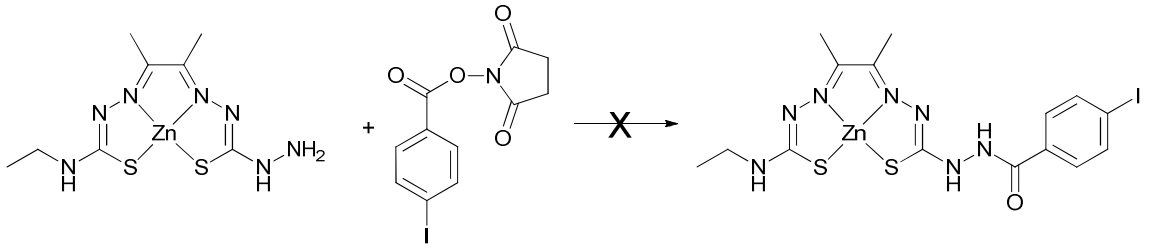

Scheme 15 Attempted synthesis of **4.22** by activated ester conjugation.

Thus we opted for the previously employed peptide coupling strategy using the BOP phosphonium agent and DIPEA in DMF to conjugate the H_2ATSE/A ligand to 4-iodobenzoic acid to afford the iodinated ligand H_2ATSE/A-I (**4.23**, Scheme 16). In an attempt to provide a direct analogue of **(17)**, we also coupled 4-iodobenzoic acid to the methyl ligand H_2ATSM/A (not shown). Surprisingly, the coupling did not go to completion over 4 h at ambient temperature in DMF, whilst coupling of H_2ATSE/A over the same period resulted in the desired iodinated product **4.23**. Copper complexation to give **4.17** was achieved *via* the standard procedure using $Cu(OAc)_2.H_2O$. **4.17** was fully characterised by ESI-MS, HPLC and elemental analysis.

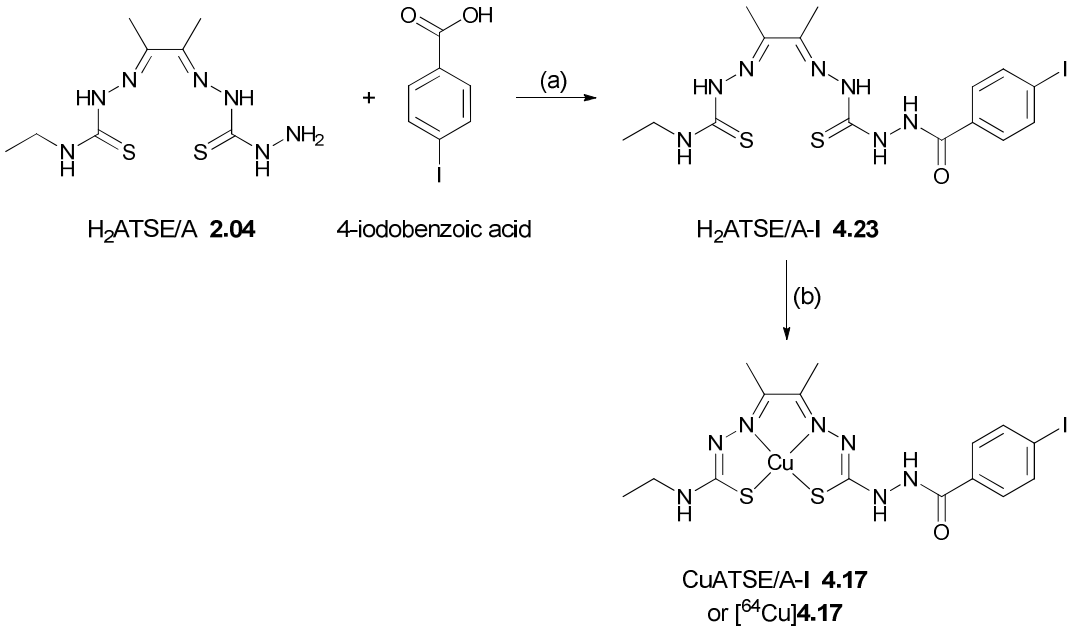

Scheme 16 Synthesis of iodinated derivatives formed *via* amide bond formation. (a) BOP, DIPEA, DMF, rt, 4 h, 93% (b) $Cu(OAc)_2 \cdot H_2O$, MeOH, rt, 30 min, 74% or [^{64}Cu]$Cu(OAc)_2$ DMSO, rt, 5 min, 90% RCY.

^{64}Cu-radiolabelling using the standard conditions proceeded in > 90% RCY and > 97% RCP to afford [^{64}Cu]**4.17** as determined by radio-TLC and radio-HPLC. Before proceeding with the synthesis of the precursor for the orthogonal derivative, the physicochemical properties of **4.17** were determined (log P = 1.50±0.04, $E_{½}$ = - 0.5703 V). [^{64}Cu]**4.17** demonstrated *in vitro* hypoxia selectivity. The results are discussed in detail in sections 4.4.6-4.4.8.

4.4.4.2 Synthesis of stannylated precursors for iododestannylation

Previously, Carroll showed that direct ^{18}F-fluorination attempts on a CuATSM derivative bearing a leaving group were unsuccessful due to substrate decomposition at high temperatures and formation of various fluorinated side products.[31] We postulated that an advantage of iodination over fluorination for the orthogonal labelling would be the possibility of direct electrophilic iodination using a stannylated precursor in combination with a mild oxidising agent discussed in section 4.4.1. Oxidative radioiodination *via* destannylation is commonly carried out in acidic MeOH. To test the stability of the bis(thiosemicarbazone) towards the conditions employed in radioiododestannylation, Cu(ATSM) was incubated in MeOH/AcOH 95:5 for 15 min. HPLC indicated that the complex was not affected. Incubation in an iodogen coated test tube also seemed to have no adverse effect.

We surmised that a stannylated copper bis(thiosemicarbazonato) complex such as CuATSE/A-$SnBu_3$ (**4.26**) could be radioiodinated. The synthesis is of **4.26** is outlined in Scheme 17.

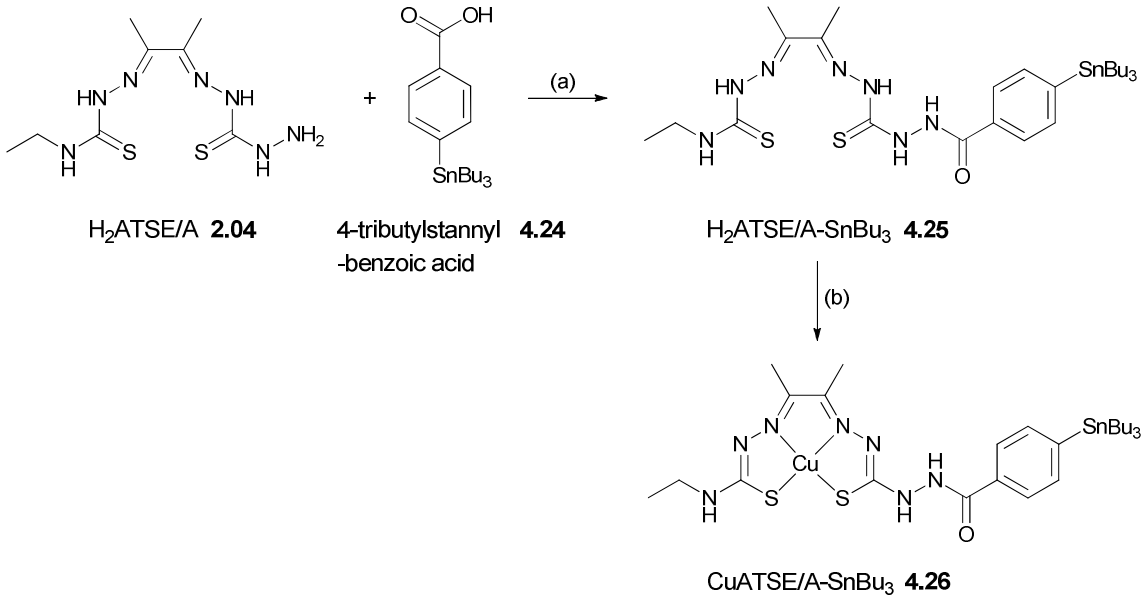

Scheme 17 Synthesis of a stannylated CuATSE/A-$SnBu_3$ complex **4.26** for radioiododestannylation.

Firstly, the tributylstannylbenzoic acid **4.24** was synthesised as previously reported.[32] In order to synthesise the stannylated btsc ligand H_2ATSE/A-$SnBu_3$ (**4.25**), **4.24** was coupled to the H_2ATSE/A proligand using BOP and DIPEA in DMF. The isolated residue was washed with water,

cold MeOH and hexane to remove all phosphonium coupling agent residues and uncoupled tin species to yield **4.25** in 85% yield. ^{13}C NMR and elemental analysis confirmed the purity of **4.25**. The compound displayed low solubility in DMSO and only small amounts could be dissolved for NMR and spectra were acquired over long periods of time. **4.25** was successfully converted to CuATSE/A-$SnBu_3$ (**4.26**) as confirmed by HPLC, ESI-MS and elemental analysis. The analytical data obtained for both the iodinated ligand and copper complex and their stannylated equivalents is summarised in Table 1.

No.	Compound	m/z calc $(M-H)^-$	m/z found	Elemental Analysis C, H, N
4.23	H_2ATSE/A-I	504.0132	504.0138	35.6 (35.7), 3.9 (4.0), 19.3 (19.4)
4.17	CuATSE/A-I	564.9271	564.9271	31.7 (31.8), 3.2 (3.2), 17.3 (17.3)
4.25	H_2ATSE/A-$SnBu_3$	668.2235	668.2232	48.6 (48.5), 7.2 (7.1), 14.8 (14.7)
4.26	CuATSE/A-$SnBu_3$	753.1333*	753.1314	44.6 (44.4), 6.2 (6.2), 13.4 (13.4)

*denotes $(M+Na)^+$

Table 1 ESI-MS and elemental analysis data for the iodinated and stannylated bis(thiosemicarbazones)

Before proceeding with the radiochemical synthesis, the reactivity of **4.26** towards I_2 was investigated (Scheme 18).[33] Due to its low solubility, the stannylated copper complex had to be dissolved in a mixture of DMSO and acetonitrile. After reaction for 15 min at room temperature, about 30% product (not accounting for species-dependent UV intensities) could be detected by HPLC and ESI-MS, validating the feasibility of iododestannylation. Next, **4.26** was incubated with NaI in MeOH/AcOH 95/5 in the presence of Iodogen as oxidising agent.

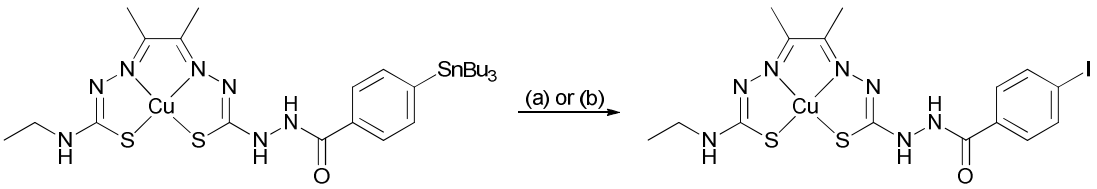

CuATSE/A-$SnBu_3$ **4.26** CuATSE/A-**I 4.17**

Scheme 18 Iododestannylation of CuATSE/A-I *via* (a) I_2, MeCN/DMSO, 30 min, rt, 30% (HPLC) (b) Iodogen, MeOH/AcOH (95:5), trace amounts of product.

Whilst some unidentified side products formed, trace amounts of the desired product **4.17** were identified by spiking with cold reference and analysing the reaction mixture by ESI-MS. To the

best of our knowledge however, there are no reports of cold iodination using iodogen and therefore we considered **4.26** for radioiododestannylation. However, it was observed that despite the low concentration solutions of CuATSE/A-$SnBu_3$ employed, the compound continuously precipitated from solution. Thus it was decided that **4.26** was not an optimal candidate for radioiodination in the first instance and efforts were focused on the CuATSMenI derivative **4.18**.

4.4.5 ^{123}I- and ^{64}Cu-orthogonally labelled complexes based on CuATSM/en

4.4.5.1 CuATSMenI

The derivative CuATSMenI (**4.18**), based on the CuATSM/en motif with the pendant aminoethyl group, was investigated next.

During the synthesis of the fluorinated analogue **4.03**, it was observed that this displayed considerably greater solubility in MeOH and DMSO/H_2O mixtures than the analogous CuATSM/A-F derivative **(17)**. It was therefore anticipated that an ATSM/en based stannylated precursor for radioiododestannylation may possess better solubility than the ATSE/A-based compound **4.26**. Firstly, the iodinated ligand H_2ATSMenI (**4.27**) was synthesised readily using the standard coupling conditions (BOP, DIPEA, DMF) as outlined in Scheme 19.

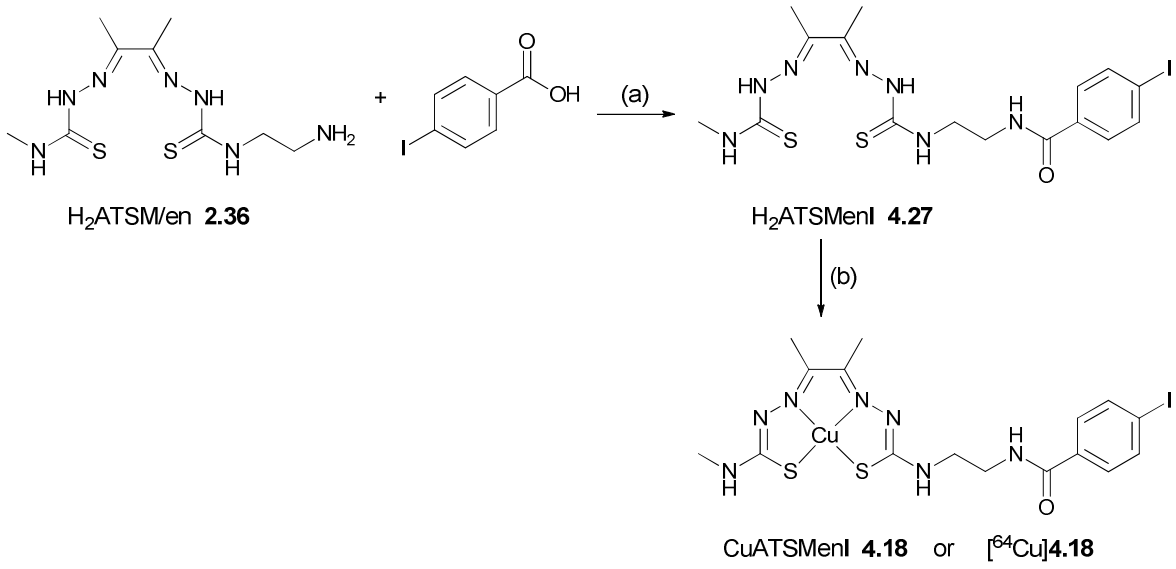

H_2ATSM/en **2.36** H_2ATSMenI **4.27** CuATSMenI **4.18** or [^{64}Cu]**4.18**

Scheme 19 Synthesis of the iodinated derivative CuATSMenI based on the CuATSM/en core motif. (a) BOP, DIPEA, DMF, 4 h, rt, 85% (b) $Cu(OAc)_2 \cdot 2H_2O$, MeOH, 30 min, rt, 74% or [^{64}Cu]$Cu(OAc)_2$, DMSO, 90% RCY (see section 4.4.5.2).

CuATSMenI (**4.18**) was synthesised from **4.27** using $Cu(OAc)_2.2H_2O$ in MeOH. Due to improved solubility, the Cu complex could not be filtered off from a concentrated methanolic solution as for derivatives based on the ATSE/A motif. The solvent had to be removed *in vacuo* and **4.18** was suspended in H_2O before being isolated by filtration. **4.27** and **4.18** were synthesised in 85% and

74% yield respectively and fully characterised. ESI-MS and elemental analysis data for both compounds is shown in Table 2.

No.	Compound	m/z calc $(M+Na)^+$	m/z found	Elemental Analysis C, H, N
4.27	H_2ATSMenI	542.0264	542.0271	36.9 (37.0), 4.1 (4.3), 18.9 (18.9)
4.18	CuATSMenI	602.9404	602.9398	44.6 (44.4), 6.2 (6.2), 13.4 (13.4)

Table 2 ESI-MS and elemental analysis data for the iodinated ATSMen derivatives H_2ATSMenI and its copper complex CuATSMenI.

4.4.5.2 [^{64}Cu]CuATSMenI

[^{64}Cu]**4.18** was synthesised by the general radiolabelling procedure described in section 4.3.1.1, using 150 MBq of [^{64}Cu]Cu(OAc)$_2$. The ^{64}Cu-labelled complex was purified by placing the compound solution onto a Sep-pak-Plus cartridge. Following a 10 mL wash with water, [^{64}Cu]**4.18** was eluted in EtOH and obtained in 90% isolated RCY with a RCP > 98% as determined by radio-TLC and radio-HPLC (Figure 11).

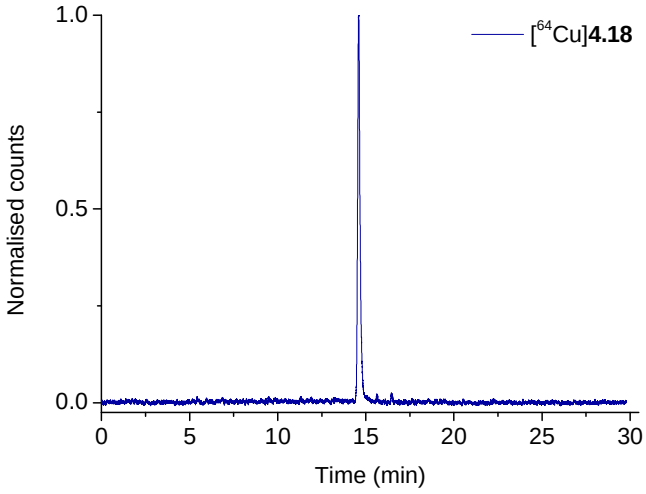

Figure 11 Radio-HPLC trace of [^{64}Cu]CuATSMenI ([^{64}Cu]**4.18**) after reformulation into EtOH

The electrochemical properties and the partition coefficient of the copper complex were determined ($E_{1/2}$ = -0.638 V, log P = 1.52±0.25), revealing that the compound had similar redox properties to the parent Cu(ATSM). Cellular uptake experiments showed that the derivative also maintained *in vitro* hypoxia selectivity. Details of these results are discussed in section 4.4.6-4.4.8.

4.4.5.3 Stannylated precursor (CuATSMenSnBu$_3$) for radioiodination

Synthesis of the stannylated ligand **4.28** and copper complex **4.29**, depicted in Scheme 20, was achieved by peptide coupling of H_2ATSMen to the stannylated acid **4.24** followed by copper complexation, using analogous reaction conditions to those reported for the iodinated derivative.

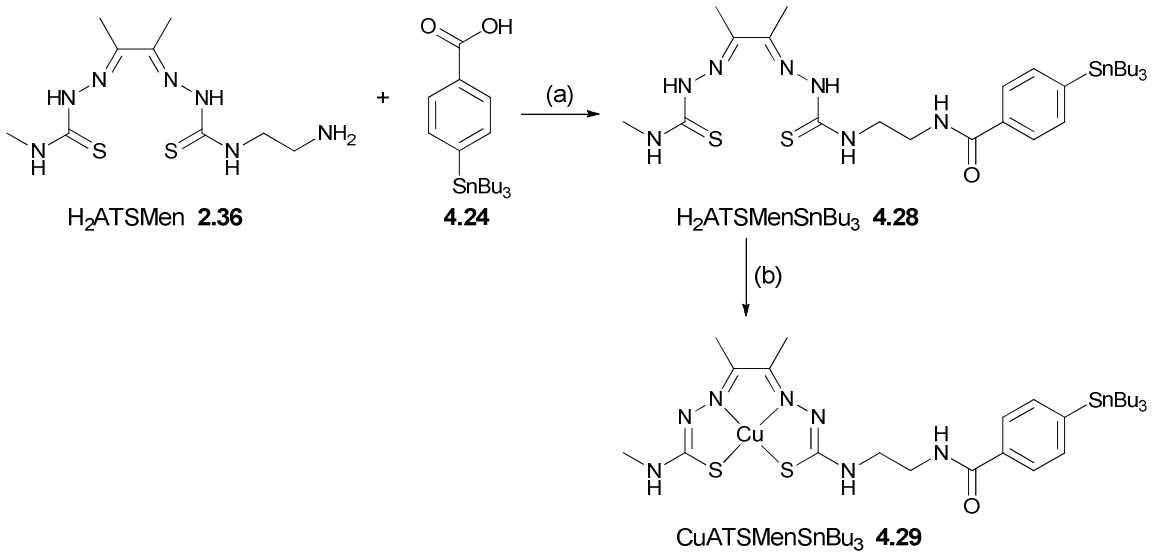

Scheme 20 Synthesis of the stannylated precursors investigated for radioiodination to synthesise [^{123}I]CuATSMenI (a) BOP, DIPEA, DMF, 4 h, rt, 56% (b) $Cu(OAc)_2 \cdot H_2O$, MeOH, rt, 30 min, 68%.

The crude **4.28** was isolated in greater than 95% purity (by HPLC). In contrast to the ATSE/A based derivative **4.26**, the increased solubility of aminoethyl derivatives **4.28** and **4.29** prevented further purification by washing with different solvent systems other than pentane and water. The improved solubility however allowed purification by semi-preparative HPLC using a gradient of MeCN/H_2O. The temperatures involved to remove fully the solvent mixture *in vacuo* yielded impurities in the final product. Careful removal of MeCN *in vacuo* at room temperature, followed by lyophilisation of the H_2O fraction yielded the products in 99% purity as determined by HPLC and elemental analysis.

Figure **12** shows the ^{13}C-NMR spectrum of purified **4.28**.

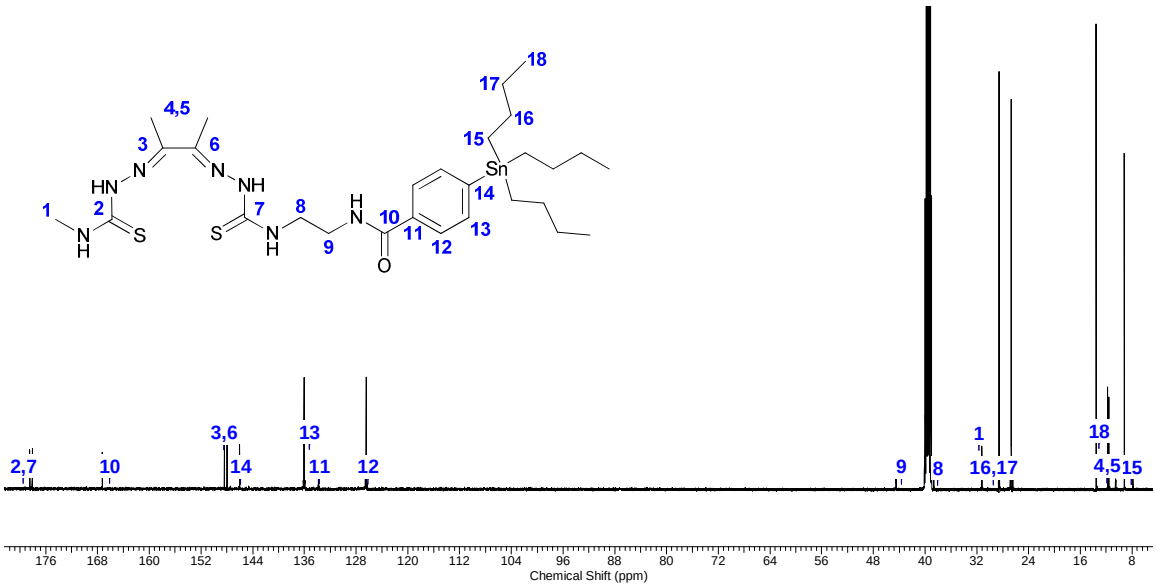

Figure 12 ^{13}C-NMR of H_2ATSMenSnBu$_3$ (**4.28**) in DMSO-d_6.

4.4.5.4 Synthesis of [^{123}I]CuATSMenI

The synthesis of the orthogonally labelled derivative [^{123}I]**4.18** *via* radioiododestannylation of **4.29** was attempted as outlined in Scheme 21. Initially, we tried the radioiodination using iodogen by adaptation of previously reported procedures.[25, 33] For this, a stock solution of 10 mg ml^{-1} of **4.29** in DMSO was diluted into an iodogen coated reaction vial containing MeOH/AcOH and Na^{123}I (1-10 MBq) was added immediately.

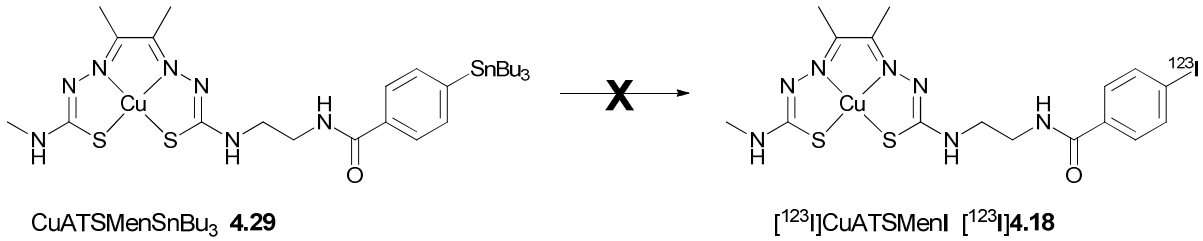

Scheme 21 Attempted synthesis of [^{123}I]**4.18** *via* radioiododestannylation. Conditions: Na^{123}I (1-10 MBq), MeOH/AcOH 95:5 and *either* chloramine T *or* iodogen *or* iodogen (Chizzonite), 2-30 min, rt.

Different reaction times were attempted (2-30 min), but no product could be observed by radio-HPLC. Dissolving **4.29** directly in MeOH/AcOH or reaction in aqueous medium (PBS) both incurred solubility problems and the desired product was not observed. Changing to chloramine-T as the oxidant was also unsuccessful. It was noticeable that the brown copper complex stock

solution turned yellow on addition to the oxidant-coated tube; this had not been noticeable in the more concentrated cold trial reactions. HPLC analysis (UV) indicated that some starting material was remaining but formation of intractable, non-radioiodinated side products also occurred. To determine whether the oxidant was decomposing our metal complex we attempted radioiodination by applying of the Chizzonite method commonly used to radioiodinate sensitive proteins.[34] This indirect approach involves pre-activation of the radioactive iodide in the iodogen tube followed by transfer of the reactive I^+ species to the reaction mixture and avoids contact of the oxidant with the substrate.[34] We activated the iodine and transferred this to the acidic stock solution of **4.29**, but again no product formation was observed. To exclude the possibility of Cu interfering with the labelling, iodination of the stannylated ligand **4.28** was also attempted but this was equally unsuccessful.

The preparation of the radioiodinated activated ester **4.16** is more straightforward than that of its radiofluorinated analogue. Thus we decided to investigate the synthesis of [^{123}I]**4.18** *via* the route employed previously for [^{18}F]**4.03** (section 4.3). To verify the cold chemistry, CuATSMen was reacted with **4.16**[26] and the reaction was monitored by HPLC and ESI-MS (Scheme 22).

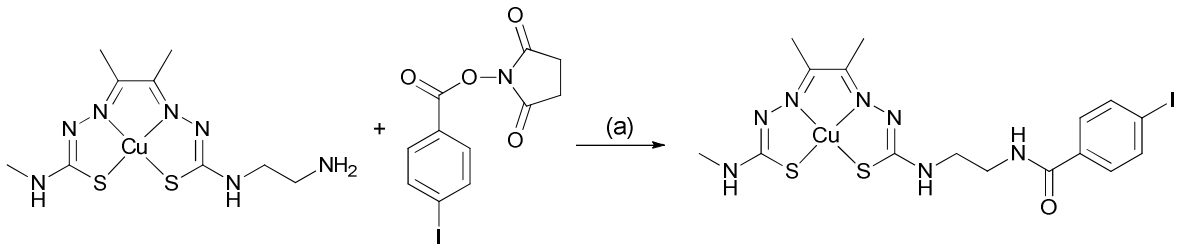

Scheme 22 Synthesis of CuATSMenI (**4.18**) by reaction of CuATSM/en with the activated ester **4.16** (a) for reaction conditions, see Table 3.

The reaction conditions investigated are summarised in Table 3. In contrast to the quantitative conversion of the fluorinated 4-FSB activated ester, the results differed considerably for reaction of CuATSM/en with **4.16**. Complete conversion of activated ester could not be achieved using the copper complex over a range of reaction conditions. Instead, iodobenzoic acid was formed, particularly in the presence of base, as well as other unidentified impurities. Interestingly however,

reacting the ligand **2.36** in DMSO gave full conversion to **4.27** at 45°C after 60 min. Higher temperatures were not investigated to avoid ligand self-cyclisation or decomposition.

Entry	Btsc	Base	Temp.	Time (min)	Solvent	Conversion by HPLC	Side-products
1	CuATSM/en	1 eq Et_3N	60°C	30	DMF	30%	iodobenzoic acid
2	CuATSM/en	DIPEA 1 eq	60°C	60	DMF	30%	iodobenzoic acid +other
3	CuATSM/en	DIPEA 1/8 eq	70°C	120	DMF	65%	iodobenzoic acid
4	CuATSM/en	no	60°C	60	DMF	55%	no
5	CuATSM/en	no	70°C	120	DMF	60%	no
6	CuATSM/en	no	70°C	60	DMSO	20%	iodobenzoic acid
7	CuATSM/en	no	70°C	80	DMSO	20%	iodobenzoic acid
8	CuATSM/en	no	65°C	120	DMF/ PBS	50%	iodobenzoic acid +other
9	H_2ATSM/en	no	45°C	120	DMF	>95%	minor
10	H_2ATSM/en	no	45°C	60	DMSO	>98%	no

Table 3 Summary of conditions tested for reacting 2 equiv of either CuATSM/en or H_2ATSM/en with 4-succinimidyl-iodobenzoate (SIB) to give **4.18** or **4.27** respectively. Conversion of SIB was estimated by HPLC (equimolar injections of CuATSMenI, H_2ATSMenI and SIB gave comparable UV absorptions).

Several procedures have been published for the synthesis of radioiodinated 4-succinimidyl-iodobenzoate, mainly based on radioiododestannylation. To comply with local rules, we chose the radioiododestannylation route by Koziorowski *et al*. that does not require heat or non-aqueous miscible solvents (Scheme 22).[25]

We opted for trimethyltin precursor (*p*MeATE) **4.30** over the tributyl analogue due to reports of better labelling yields.[35, 36] The chosen radioiodination method uses iodobeads® as the oxidant. Significantly, this allowed us to terminate the oxidation easily by removal of the bead, rather than quenching with sodium metabisulfite or a reducing agent which we were concerned might adversely affect the copper bis(thiosemicarbazone). **4.30** was incubated for 5 min in MeOH/AcOH with $Na^{123}I$. The reaction mixture was then diluted with water and passed onto a to a C-18 Sep-pak Light® cartridge to remove any unreacted iodide. [^{123}I]SIB ([^{123}I]**4.16**) was then eluted off the cartridge in 70% RCY using DMSO as the solvent of choice for the conjugation. Some activity was found to remain associated with the Iodobead or remained in the H_2O wash. Small amounts of [^{123}I]4-iodobenzoic acid were detected by HPLC but these did not affect the subsequent

conjugation. A stock solution of H_2ATSMen was added to the activated ester [^{123}I]**4.16** and reacted at 45°C for 60 min which resulted in complete consumption of the ester. Complete reaction of the activated ester was essential before purification by HPLC as the retention times of [^{123}I]**4.16** and the ligand [^{123}I]**4.27** were found to be very similar. Different elution methods did not increase separation. Therefore, removal of any residual unreacted [^{123}I]**4.16** would prove problematic.

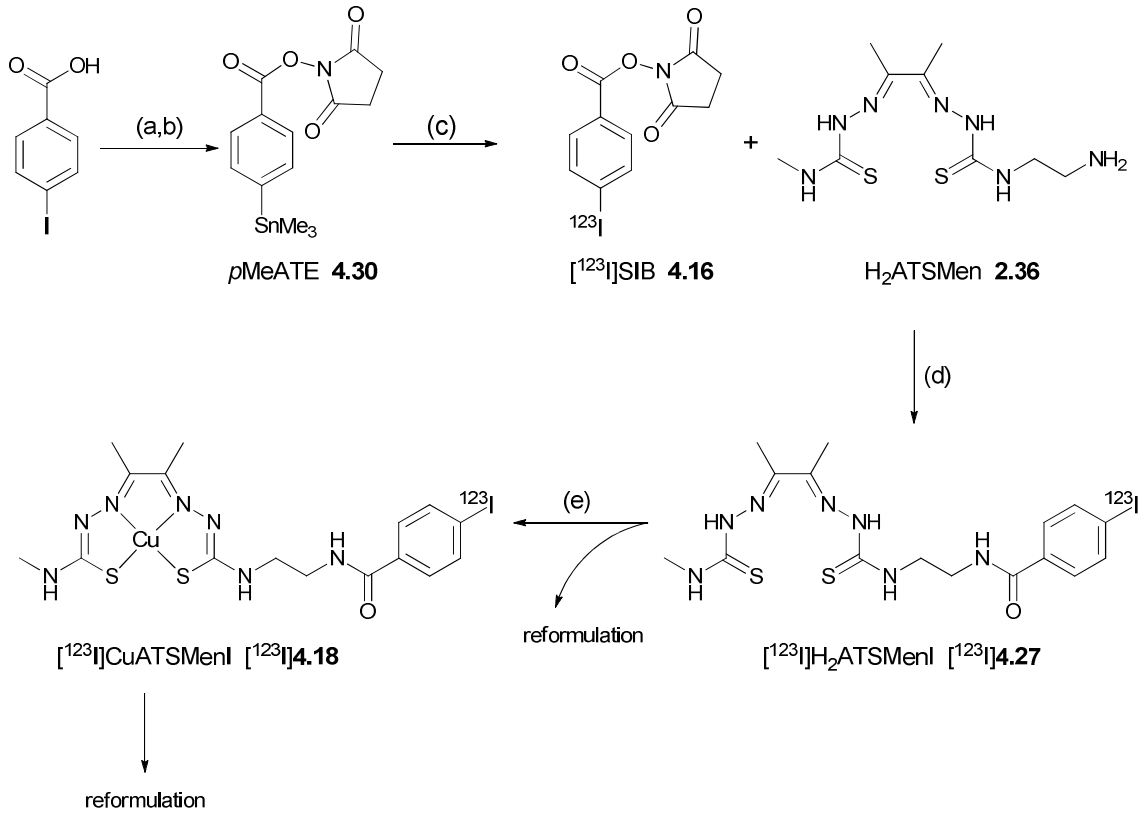

Scheme 23 Synthesis of [^{123}I]**4.16**, [^{123}I]**4.27** and [^{123}I]**4.18** (a) $(CH_3)_6Sn_2$, $(PPh_3)_2Pd(II)Cl_2$, 1,4-dioxane, N_2, 60°C, 90 min (b) Disuccinimidyl-carbonate, pyridine, MeCN, N_2, rt, 4 h (c) Na^{123}I, Iodobeads®, 5% AcOH in MeOH, rt, 5 min (d) DMSO, 45°C, 1h (e) $Cu(OAc)_2 \cdot H_2O$ DMSO/H_2O.

In order to unambiguously confirm product identity, aliquots of the crude reaction mixture were spiked both with cold reference ligand **4.27** and **4.16** to confirm the product identity. The [^{123}I]iodobenzoic acid impurity served as an internal reference.

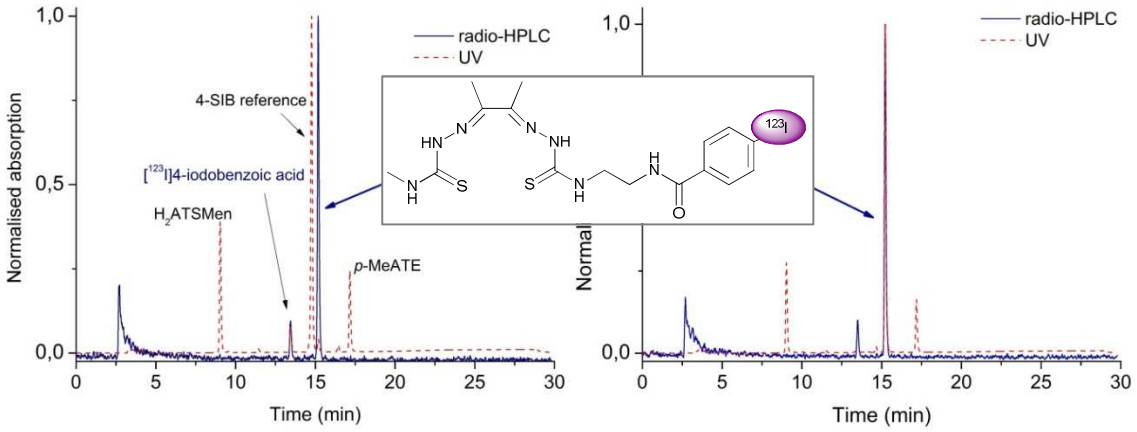

Figure 13 UV/radio-HPLC chromatogram of crude [^{123}I]H_2ATSMenI ([^{123}I]**4.27**) (left) spiked with cold SIB (**4.16**) reference (right) spiked with cold reference H_2ATSMenI

The crude ligand [^{123}I]**4.27** was purified by semi-preparative HPLC and was then reformulated or converted to [^{123}I]**4.18** by addition of excess $Cu(OAc)_2$. Both [^{123}I]**4.27** and [^{123}I]**4.18** were reformulated by passing the HPLC eluent diluted in water onto a C-18 Sep-pak Light cartridge and eluting with EtOH. Copper-complexation causes a decrease in retention time of the bis(thiosemicarbazone) that moves the peak of [^{123}I]**4.18** closer towards any potential [^{123}I]**4.16** residues. Therefore, a ligand aliquot was analysed by HPLC to ensure purity before synthesis of the copper complex, spiking with cold **4.16** (Figure 13 left) and the desired product **4.27** (right) confirm formation of the desired product [^{123}I]**4.27**. The shift of retention time from [^{123}I]H_2ATSMenI to [^{123}I]CuATSMenI further affirms the successful synthesis of both products. Some activity was retained on the column following preparative HPLC. [^{123}I]**4.27** and [^{123}I]**4.18** were isolated in 30 and 40% RCY from Na^{123}I in a total synthesis time of 2.5 h. Figure 14 depicts the radio-HPLC spectra of the reformulated orthogonally ^{123}I and ^{64}Cu-labelled copper bis(thiosemicarbazonato) complexes and the ^{123}I-labelled ligand.

The ethanolic solutions were concentrated under a stream of N_2 gas before addition of saline for intravenous injection in biological studies (< 10% EtOH in 0.9% $NaCl_{(aq)}$).

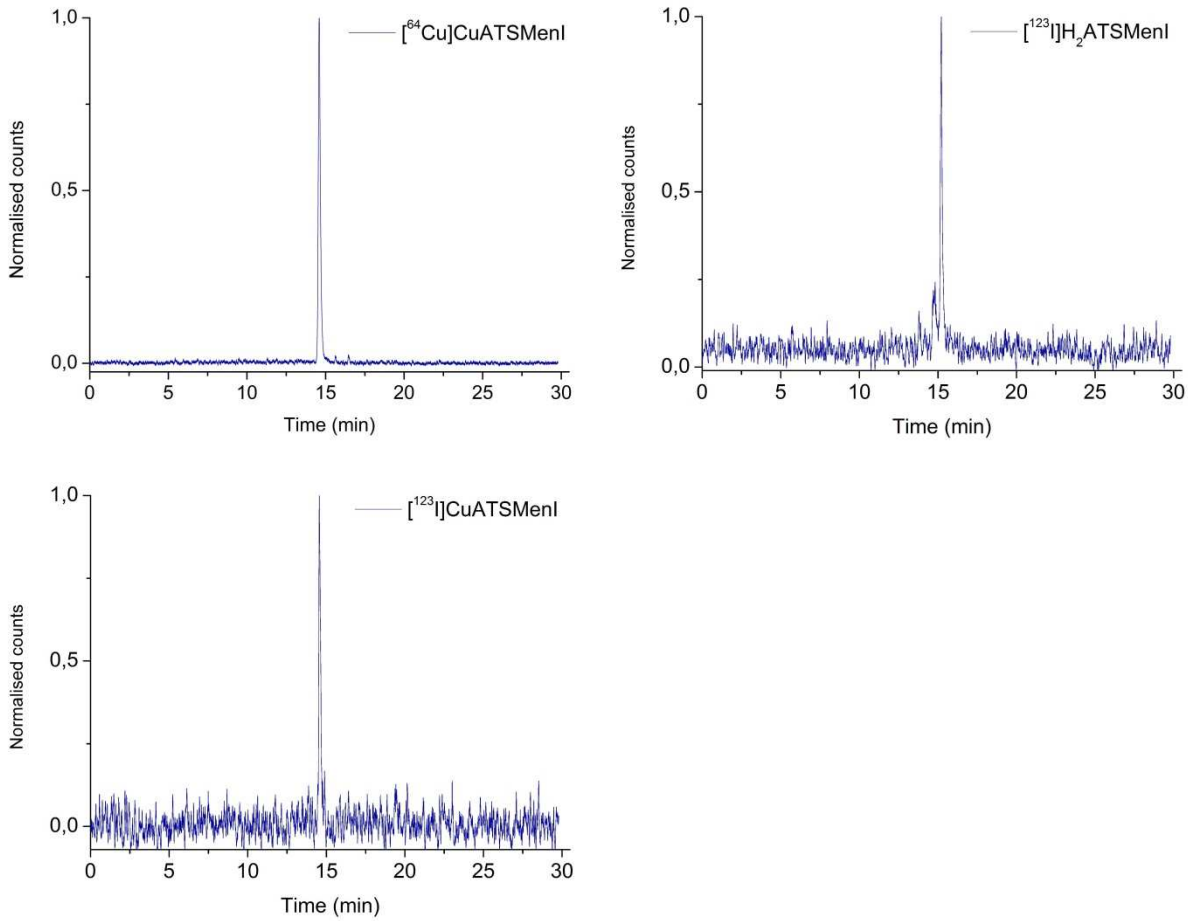

Figure 14 Radio-HPLC spectra of [^{64}Cu]CuATSMenI ([^{64}Cu]**4.18**), [^{123}I]CuATSMenI ([^{123}I]**4.18**) and [^{123}I]H_2ATSMenI ([^{123}I]**4.27**) after purification and reformulation into EtOH.

4.4.6 Electrochemistry

Electrochemical studies were performed on all complexes for a direct comparison to the parent compound CuATSM. As discussed in the introduction, the *in vitro* hypoxia selectivity of CuATSM is thought to be closely related to the Cu(II)/Cu(I) reduction potential. If the reduction potential of the complex is more negative than that of CuATSM (ie < -0.646 V), the reduction may not be biologically accessible in hypoxic cells, or the rate of reoxidation will be greatly enhanced. A more positive potential than that of CuATSM in contrast may lead to uncontrolled reduction, and the compound is deposited non-selectively in all tissues. The reduction potentials of the compounds synthesised in this chapter were recorded in anhydrous DMF using 0.1 M tetrabutylammonium tetrafluoroborate as the electrolyte. Whilst measurements in DMF do not resemble the aqueous biological environment, reduction potentials of copper bis(thiosemicarbazonates) have been recorded in this solvent due to their low solubility. Copper bis(thiosemicarbazonates) with redox potentials in the range -0.58 to -0.65 V (when compared to the SCE) have shown a strong correlation with *in vitro* hypoxia selectivity in cellular uptake assays.[37, 38]

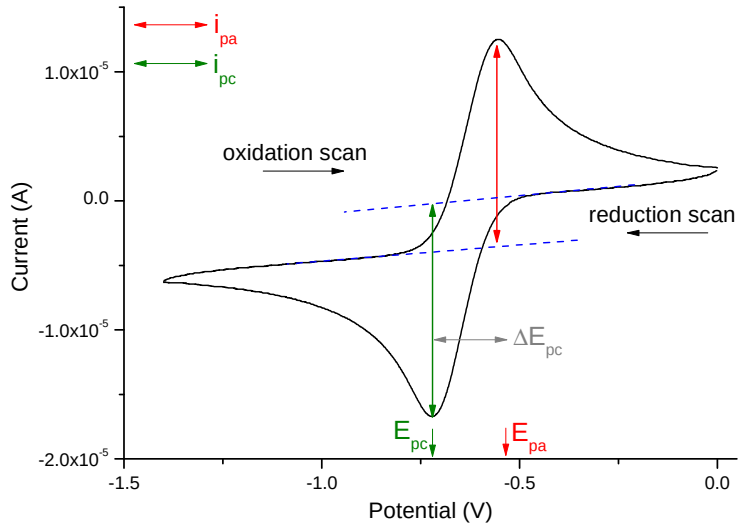

Figure 15 Cyclic voltammogram, illustrating the electrochemical parameters of interest for the Cu(II)/Cu(I) reductive process of **4.18**.

The cyclic voltammetry measurements were carried out using a platinum wire auxiliary electrode, a platinum disc working electrode and silver wire *pseudo* reference electrode. Ferrocene served as an internal reference (Fe(II)/Fe(III): $E_{1/2}$= +0.53 *vs*. SCE). Figure 15 shows the Cu(II)/Cu(I) reduction process of complex **4.18**.

As can be seen in Table 4, complexes **4.03** and **4.18**, were reduced at very similar applied potentials when compared to CuATSM. This confirms previous findings that the pendant aminoethyl arm has little effect on the redox potential of the complex.[13] **4.16** and **4.17** were reduced slightly more easily than the parent compound, indicated by the more positive reduction potentials.

The peak separation between the reductive and oxidative peaks, $\Delta E_{p,}$ gives information about the kinetics of electron transfer. ΔE_p is larger for all derivatised complexes than for CuATSM, the values measured for **4.03** and **4.18** were 0.14 V and 0.16 V respectively and are similar to what has been reported for other hypoxia selective copper-bis(thiosemicarbazonato) complexes, showing that functionalisation through the aminoethyl linker seems to have only minor effect on the overall electron transfer kinetics. The considerably larger peak separation of 0.53 V shown by **4.16** is indicative of particularly slow electron transfer which may be a result of slow electrode transfer kinetics or slower structural reorganisation for the imine complex when going from the planar geometry of the Cu(II) complex to the tetragonally distorted Cu(I) complex.[39]

No.	Compound	$E_{1/2}$/V	$\Delta E_p = E_{pa}-E_{pc}$ (V)[a]	$\lvert i_{pa}\rvert / \lvert i_{pc}\rvert$ [a]	nature of reduction
	CuATSM	-0.646	0.10	0.99	reversible
4.03	CuATSMenF	-0.649	0.1358	0.898	quasi-reversible
4.16	CuATSE/A-imineI	-0.525	0.525	n/a	non-reversible
4.17	CuATSE/A-I	-0.5703	0.275	0.966	reversible
4.18	CuATSMenI	-0.638	0.1648	0.981	reversible

Table 4 Summary of electrochemical data of the fluorinated and iodinated copper complexes synthesised in this chapter. [a] Calculated for a scan rate of 100 mV s^{-1}.

Besides the absolute value and thus biological accessibility of the Cu(II)/Cu(I) reduction, reversibility is another important criterion to determine whether the electrochemical reduction of the functionalised tracers is similar to that of Cu(ATSM).

For a completely reversible couple, the rate of electron transfer is faster than the rate of mass transport and hence the reduction potential, E_{pc}, is independent of the scan rate. The ratio of the peak currents, $|i_{pa}|/|i_{pc}| = 1$ and should be constant at varying scan rates. $|i_{pc}|/\sqrt{}$(scan rate) should also remain constant.

In contrast, for a non-reversible reduction, in the case of electrochemical reversibility, the rate of electron transfer is slower than the rate of mass transfer. Chemical irreversibility occurs when the reduced species cannot undergo oxidation due to a chemical change. The result is a more negative E_{pc} value with increasing scan rate and $|i_{pa}|/|i_{pc}|$ may not be determined due to the absence of an oxidation peak. A quasi-reversible process may also be observed, where the rate of electron transfer and the rate of mass transport have the same order of magnitude, resulting in a reversible process at slower scan rates and irreversibility at higher scan rates. Thus E_{pc} will become more negative with increasing scan rate, $|i_{pa}|/|i_{pc}| < 1$ and $|i_{pc}|/\sqrt{}$(scan rate) may not be constant due to the absence of a linear relationship between i_{pc} and the scan rate.

As can be seen from Table 4, values for **4.03** and **4.17** were 0.898 V and 0.966 V respectively, indicating that the reduction process is not completely reversible but can be viewed as quasi-reversible in line with the parent compound CuATSM which shows a ratio of 0.99.[40] In contrast, **4.18** showed a reduction value of 0.981 V, therefore correlating most closely to CuATSM.

4.4.7 Lipophilicity

Log *P* values (partition coefficients) of all ^{64}Cu-labelled complexes were obtained experimentally as described previously in Chapter 2, by partitioning < 1 MBq of tracer between PBS (pH 7.4) and octanol and sampling each phase.[41] The values, summarised in Table 5, were generally comparable to CuATSM. The imine derivative [^{64}Cu]**4.16** was the most lipophilic complex. Surprisingly, [^{64}Cu]**4.18** was more lipophilic than [^{64}Cu]**4.17**, and also more lipophilic than the fluorinated analogue [^{64}Cu]**4.03**.

No.	Compound	Log P
	[^{64}Cu]CuATSM	1.48
4.03	[^{64}Cu]CuATSMenF	1.46±0.16
4.16	[^{64}Cu]CuATSE/A-imineI	1.62±0.01
4.17	[^{64}Cu]CuATSE/A-I	1.50±0.04
4.18	[^{64}Cu]CuATSMenI	1.52±0.25

Table 5 Experimentally determined log P values of [^{64}Cu]**4.03** and [^{64}Cu]**4.16**-[^{64}Cu]**4.18**. The log P value of [^{64}Cu]CuATSM was taken from reference 42.

4.4.8 Cellular uptake experiments

Following radiochemical synthesis, complexes [^{64}Cu]**4.03**, [^{64}Cu]**4.16**, [^{64}Cu]**4.17** and [^{64}Cu]**4.18**, alongside [^{64}Cu]CuATSM were subjected to time-dependent cellular uptake studies under normoxic and anoxic conditions. The apparatus used for these *in vitro* uptake experiments has been previously described and a full account of the experimental procedure can be found in Chapter 5. The uptake experiments were initially conducted only in HT1080 cells. The intent was a preliminary *in vitro* screening of the ^{64}Cu-labelled analogues to establish whether the hypoxia selectivity was preserved in the functionalised compounds. Suitable candidates could then be selected for the orthogonal labelling. The retention profiles under normoxic and anoxic conditions over 60 min are displayed in Figure 16.The graphs depict the percentage of cellular associated activity with the cells following incubation of the radiolabelled copper complexes in suspension.

All compounds displayed a statistically significant degree of *in vitro* hypoxia selectivity. All showed rapid uptake and reached significant differences between normoxia and hypoxia at 5 min, the maximum differential being reached between 15 and 30 min. When comparing the hypoxic differential to that of [^{64}Cu]CuATSM at 30 min, the observed difference was poorest for the H_2ATSE/A-based derivatives, [^{64}Cu]**4.16** and [^{64}Cu]**4.17** at 14% and 20% respectively. The differential observed for [^{64}Cu]**4.17** was also similar to that reported for [^{64}Cu]**(17)** by Carroll *et al.,*[43] suggesting that the identity of the aromatic halogen has little effect on the *in vitro* hypoxia selectivity. The aminoethyl-based derivatives [^{64}Cu]**4.03** and [^{64}Cu]**4.18** displayed differences of 35% and 40% respectively, and thus compared favourably to [^{64}Cu]CuATSM (41%). This was consistent with previous observations that better hypoxia selectivity can be achieved by using the aminoethyl rather than the hydrazinic exocyclic functionalisation.[3] Interestingly, the differential for [^{64}Cu]**4.16** completely disappeared towards the end of the time-course, this effect could also be observed to a smaller extent for [^{64}Cu]**4.03**.

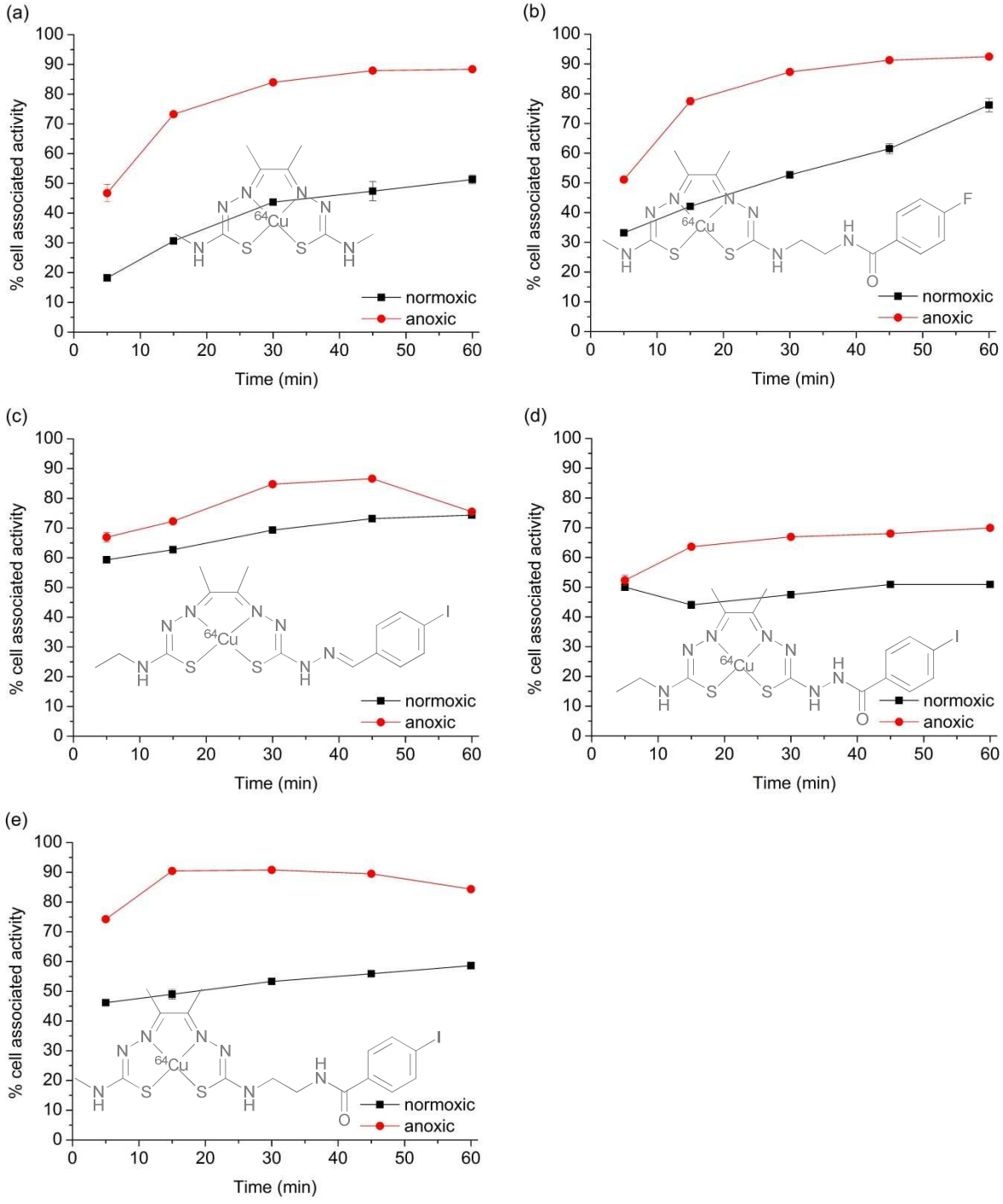

Figure 16 Percentage cellular associated activity of (a)[^{64}Cu]CuATSM (b) [^{64}Cu]CuATSMenF ([^{64}Cu]**4.03**) (c) [^{64}Cu]CuATSE/A-imineI ([^{64}Cu]**4.16**) (d) [^{64}Cu]CuATSE/A-I ([^{64}Cu]**4.17**) (e) [^{64}Cu]CuATSMenI ([^{64}Cu]**4.18**) in HT1080 cells over time incubated either under normoxic (21% O_2, 5% CO_2, balance N_2) or anoxic (5% CO_2, balance N_2) conditions. Errors (standard deviation) are within symbols if not indicated.

Notably, all functionalised compounds displayed a higher normoxic uptake than [^{64}Cu]CuATSM. Previous work within the group has shown that the normoxic uptake is significantly reduced for more hydrophilic derivatives, but higher for more lipophilic derivatives. Compounds **4.03** and **4.16 - 4.18** have comparable or slightly higher lipophilicities than CuATSM and thus these values are in agreement with previous observations.

Overall, it was concluded that CuATSMenI (**4.18**) and to a large extent CuATSE/A-I (**4.16**) and CuATSMenF (**4.03**) displayed *in vitro* hypoxia selectivity that should allow them to serve as suitable mechanistic probes to obtain information about the ligand fate of hypoxia selective bis(thiosemicarbazones).

4.5 Alternative approaches: d_6-CuATSM

The principal aim of the orthogonal labelling experiment was the elucidation of the *in vivo* fate of the ligand. As previously discussed in the introduction, the behaviour of copper bis(thiosemicarbazonato) complexes *in vitro* and *in vivo* is highly dependent on the structure of the ligand. The halogenated probes maintain the methyl groups in the backbone positions and thus do not alter the redox potential significantly and the compounds showed good *in vitro* hypoxia selectivity. However, the orthogonal label presents a significant alteration from the parent compound CuATSM and Green *et al.* report that binding to serum proteins is highly structure dependent.[44-46] Thus the structurally altered ligands may be affected in their binding to serum proteins, transport across the cellular membrane as well as binding and reduction by intracellular reductases.

As the parent compound CuATSM is the focus of interest, a most structurally similar analogue would be desirable. Thus we decided to attempt an orthogonal radiolabelling approach *via* isotopic substitution of hydrogen for deuterium in the ligand backbone. This would maintain the original structure of the parent compound. If successful, a radioactive tritiated version of this derivative could be used for biodistribution, autoradiography and cellular retention experiments. Firstly, butanedione was deuterated *via* reflux in acidic D_2O using previously reported procedures (Scheme 24).[47]

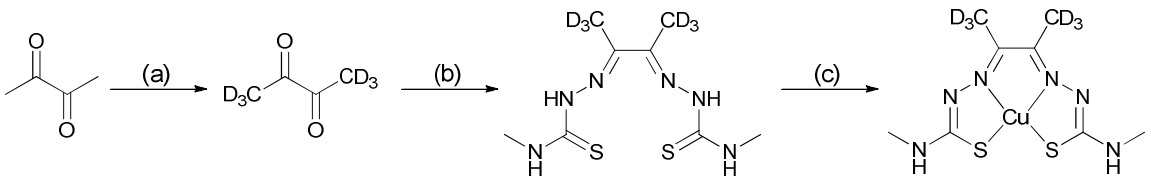

Scheme 24 Synthesis of backbone-deuterated d_6-H_2ATSM and d_6-CuATSM (a) D_2SO_4, D_2O, reflux, 48 h, 2 cycles (b) EtOH, H_2SO_4, 4-methyl-3-thiosemicarbazide, rt, overnight (c) $Cu(OAc)_2.H_2O$, MeOH, rt, 1 h

After two deuteration cycles, comparative ^{1}H and ^{2}H NMR showed 89% d_6-content as determined with respect to the exocyclic methyl group substituent. This was deemed sufficient for a proof-of-principle study.

Subsequently the d_6-ligand **4.31** and copper complex **4.32** were synthesised by adaptation of the previously reported synthetic procedures for H_2ATSM and CuATSM.[48, 49] **4.31** and **4.32** were synthesised and characterised by ESI-MS and ^{1}H and ^{2}H NMR (d_6-H_2ATSM). Figure 17 depicts the high resolution mass spectrum $(M-H)^-$ of **4.32**.

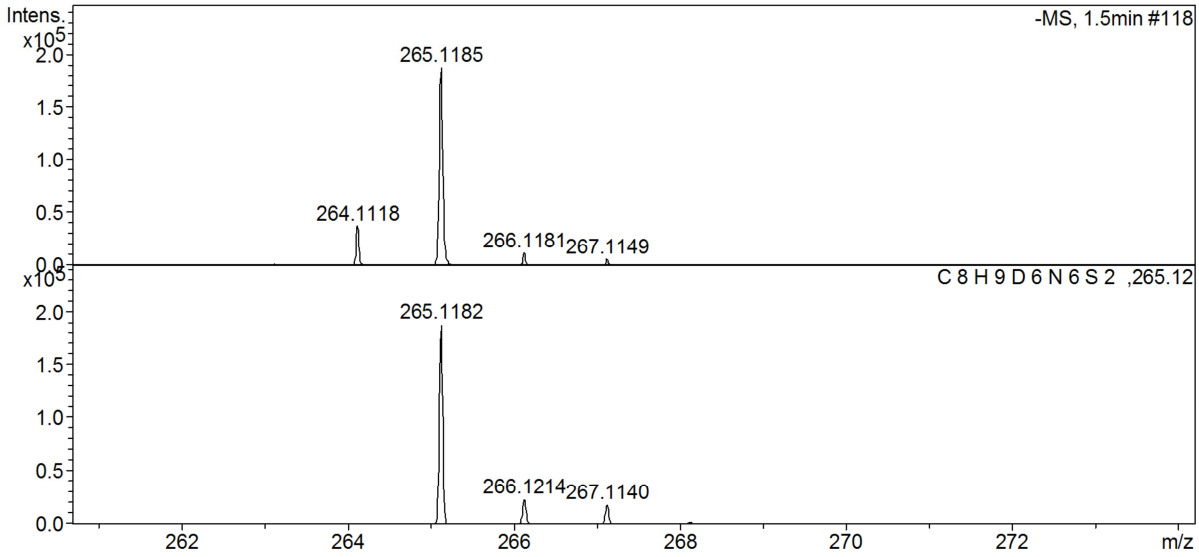

Figure 17 High resolution mass spectrum of d_6-H_2ATSM showing the $(M-H)^-$ ion.

The synthetic procedures shows that it should in theory be feasible to synthesise another isotopologue of CuATSM that employs the radioactive hydrogen isotope tritium.

4.6 Conclusion

A new generation of functionalised copper-bis(thiosemicarbazonates), functionalised with pendant I and F bearing aromatic groups, have been successfully synthesised, characterised and labelled with ^{64}Cu, ^{18}F and ^{123}I. Specifically, the orthogonally labelled derivative [^{18}F]CuATSMenF ([^{18}F]**4.03**) was synthesised on a trial scale as proof-of-principle and a pair of orthogonally labelled iodinated analogues [^{64}Cu]CuATSMenI ([^{64}Cu]**4.18**) and [^{123}I]CuATSMenI ([^{123}I]**4.18**) was successfully obtained.

4.03 and **4.18**, based on the H_2ATSMen aminoethyl motif, displayed the most favourable physicochemical and *in vitro* properties, with the Cu(II)/Cu(I) redox potentials and electrochemical reversibility remaining close to that of the parent CuATSM complex. Preliminary cellular uptake studies in one cell line revealed that all radiocopper-labelled complexes with the exception of [^{64}Cu]CuATSE/A-imineI ([^{64}Cu]**4.16**) maintained hypoxia selectivity *in vitro*. [^{64}Cu]**4.18** possessed the most similar uptake characteristics to [^{64}Cu]CuATSM and displayed the most favourable combined physicochemical- and *in vitro* uptake profile.

Significantly, the radiosynthesis of its orthogonally ^{123}I-labelled counterpart [^{123}I]**4.18** could be scaled-up sufficiently for preclinical work. Hence, [^{123}I]**4.18** and [^{64}Cu]**4.18** were selected as the tracers of choice for further *in vitro* and *in vivo* mechanistic studies to illucidate the mechanism of hypoxia selectivity of this class of compounds.

4.7 References for Chapter 4

1. N. J. Spratt, U. Ackerman, H. J. Tochon-Danguy, G. A. Donnan and D. W. Howells, *Stroke*, 2006, **37**, 1862-1867.
2. P. D. Bonnitcha, A. L. Vavere, J. S. Lewis and J. R. Dilworth, *J. Med. Chem.*, 2008, **51**, 2985-2991.
3. P. D. Bonnitcha, S. R. Bayly, M. B. M. Theobald, H. M. Betts, J. S. Lewis and J. R. Dilworth, *J. Inorg. Biochem.*, 2010, **104**, 126-135.
4. J. P. Holland, F. I. Aigbirhio, H. M. Betts, P. D. Bonnitcha, P. Burke, M. Christlieb, G. C. Churchill, A. R. Cowley, J. R. Dilworth, P. S. Donnelly, J. C. Green, J. M. Peach, S. R. Vasudevan and J. E. Warren, *Inorg. Chem.*, 2007, **46**, 465-485.
5. P. J. Barnard, J. P. Holland, S. R. Bayly, T. J. Wadas, C. J. Anderson and J. R. Dilworth, *Inorg. Chem.*, 2009, **48**, 7117-7126.
6. S. R. Bayly, R. C. King, D. J. Honess, P. J. Barnard, H. M. Betts, J. P. Holland, R. Hueting, P. D. Bonnitcha, J. R. Dilworth, F. I. Aigbirhio and M. Christlieb, *J. Nucl. Med.*, 2008, **49**, 1862-1868.
7. L. Carroll, R. Bejot, R. Hueting, R. King, P. Bonnitcha, S. Bayly, M. Christlieb, J. R. Dilworth, A. D. Gee, J. Declerck and V. Gouverneur, *Chem. Commun.*, 2010, **46**, 4052-4054.
8. G. Vaidyanathan and M. R. Zalutsky, *Nat. Protoc.*, 2006, **1**, 1655-1661.
9. H. M. Betts, DPhil Thesis, University of Oxford, 2009.
10. R. Hueting, M. Christlieb, J. R. Dilworth, E. G. Garayoa, V. Gouverneur, M. W. Jones, V. Maes, R. Schibli, X. Sun and D. A. Tourwe, *Dalton Trans.*, 2010, **39**, 3620-3632.
11. P. D. Bonnitcha.
12. P. D. Bonnitcha, S. R. Bayly, M. B. M. Theobald, H. M. Betts, J. S. Lewis and J. R. Dilworth, *J. Inorg. Biochem.*, **104**, 126-135.
13. M. B. M. Theobald, University of Oxford, 2010.
14. V. Azarian, A. Gangloff, Y. Seimbille, S. Delaloye, J. Czernin, M. E. Phelps and D. H. S. Silverman, *J. Labelled Compd. Radiopharm.*, 2006, **49**, 269-283.
15. J. Marik and J. L. Sutcliffe, *Appl. Radiat. Isot.*, 2007, **65**, 199-203.
16. H. J. Wester and M. Schottelius, *Ernst Schering Res. Found. Workshop*, 2007, **62**, 79-111.
17. G. Tang, X. Tang and X. Wang, *J. Labelled Compd. Radiopharm.*, 2010, **53**, 543-547.
18. M. Glaser, E. Arstad, S. K. Luthra and E. G. Robins, *J. Labelled Compd. Radiopharm.*, 2009, **52**, 327-330.
19. N. Wang, R. Liu, Q. Xu and X. Liang, *Chem. Lett.*, 2006, **35**, 566-567.
20. J. L. H. Eersels, M. J. Travis and J. D. M. Herscheid, *J. Labelled Compd. Radiopharm.*, 2005, **48**, 241-257.
21. M. J. Adam and D. S. Wilbur, *Chem. Soc. Rev.*, 2005, **34**, 153-163.
22. S. Vallabhajosula, *Molecular Imaging for PET and SPECT*, 1 Edition edn., Springer, 2009.
23. G. T. Hermanson and Editor, *Bioconjugate Techniques*, 1995.
24. A. E. Bolton and W. M. Hunter, *Biochem. J.*, 1973, **133**, 529-538.
25. J. Koziorowski, C. Henssen and R. Weinreich, *Appl. Radiat. Isot.*, 1998, **49**, 955-959.
26. B. Dekker, H. Keen, D. Shaw, L. Disley, D. Hastings, J. Hadfield, A. Reader, D. Allan, P. Julyan, A. Watson and J. Zweit, *Nucl. Med. Biol.*, 2005, **32**, 403-413.
27. E. B. Araujo, J. S. Santos, M. T. Colturato, E. Muramoto and C. P. G. Silva, *Appl. Radiat. Isot.*, 2003, **58**, 667-673.
28. D. D. Rossouw, *J. Labelled Compd. Radiopharm.*, 2008, **51**, 48-53.
29. D. R. Collingridge, V. A. Carroll, M. Glaser, E. O. Aboagye, S. Osman, O. C. Hutchinson, H. Barthel, S. K. Luthra, F. Brady, R. Bicknell, P. Price and A. L. Harris, *Cancer Res.*, 2002, **62**, 5912-5919.
30. G. W. Kabalka and R. S. Varma, *Tetrahedron*, 1989, **45**, 6601-6621.
31. L. Carroll, DPhil Thesis, University of Oxford, 2010.
32. C. Gosmini and J. Perichon, *Org. Biomol. Chem.*, 2005, **3**, 216-217.

33. A. Donovan, J. Forbes, P. Dorff, P. Schaffer, J. Babich and J. F. Valliant, *J. Am. Chem. Soc.*, 2006, **128**, 3536-3537.
34. R. Chizzonite, T. Truitt, F. J. Podlaski, A. G. Wolitzky, P. M. Quinn, P. Nunes, A. S. Stern and M. K. Gately, *J. Immunol.*, 1991, **147**, 1548-1556.
35. P. K. Garg, G. E. Archer, Jr., D. D. Bigner and M. R. Zalutsky, *Appl. Radiat. Isot.*, 1989, **40**, 485-490.
36. V. Tolmachev, A. Orlova and H. Lundqvist, *J. Radioanal. Nucl. Chem.*, 2000, **246**, 207-213.
37. P. J. Blower, M. J. Went, K. E. Martin and G. E. Smith, *J. Labelled Compd. Radiopharm.*, 2007, **50**, 354-359.
38. J. L. J. Dearling, J. S. Lewis, G. E. D. Mullen, M. J. Welch and P. J. Blower, *J. Biol. Inorg. Chem.*, 2002, **7**, 249-259.
39. A. R. Cowley, J. R. Dilworth, P. S. Donnelly, E. Labisbal and A. Sousa, *J. Am. Chem. Soc.*, 2002, **124**, 5270-5271.
40. J. P. Holland, P. J. Barnard, D. Collison, J. R. Dilworth, R. Edge, J. C. Green and E. J. L. McInnes, *Chem.--Eur. J.*, 2008, **14**, 5890-5907.
41. E. K. John and M. A. Green, *J. Med. Chem.*, 1990, **33**, 1764-1770.
42. J. P. Holland, University of Oxford, 2008.
43. L. Carroll, DPhil Thesis, University of Oxford 2010.
44. N. E. Basken, C. J. Mathias, A. E. Lipka and M. A. Green, *Nucl. Med. Biol.*, 2008, **35**, 281-286.
45. N. E. Basken and M. A. Green, *Nucl. Med. Biol.*, 2009, **36**, 495-504.
46. N. E. Basken, C. J. Mathias and M. A. Green, *J. Pharm. Sci.*, 2009, **98**, 2170-2179.
47. J. R. Durig, S. E. Hannum and S. C. Brown, *J. Phys. Chem.*, 1971, **75**, 1946-1956.
48. A. R. Cowley, J. Davis, J. R. Dilworth, P. S. Donnelly, R. Dobson, A. Nightingale, J. M. Peach, B. Shore, D. Kerr and L. Seymour, *Chem. Commun.*, 2005, 845-847.
49. B. A. Gingras, T. Suprunchuk and C. H. Bayley, *Can. J. Chem.*, 1962, **40**, 1053-1059.

Chapter 5

In vitro and *in vivo* mechanistic studies on the hypoxia selectivity of Cu(ATSM)

5.1 Overview

The research in this chapter covers *in vitro* and *in vivo* studies using the dual radiolabelling mechanistic approach developed in Chapter 4 to obtain further understanding on the mode of action of hypoxia selective copper bis(thiosemicarbazonato) complexes. The structurally identical pair [^{64}Cu]CuATSMenI and [^{123}I]CuATSMenI were selected as mechanistic probes on the basis of their characteristics compared to the parent compound [^{64}Cu]CuATSM. The selection of suitable experimental parameters for *in vitro* and *in vivo* biological work is described. *In vitro* cellular uptake assays, *in vivo* dynamic PET imaging, nanoSPECT imaging and biodistribution studies were performed alongside the analysis of complex stability and demetallation *in vitro* and *in vivo*. The results obtained for [^{64}Cu]/[^{123}I]CuATSMenI and the proligand [^{123}I]H_2ATSMenI are discussed and compared to those of the parent compound [^{64}Cu]CuATSM and the simple [^{64}Cu]Cu^{2+} salt, administered as [^{64}Cu]$Cu(OAc)_{2(aq)}$

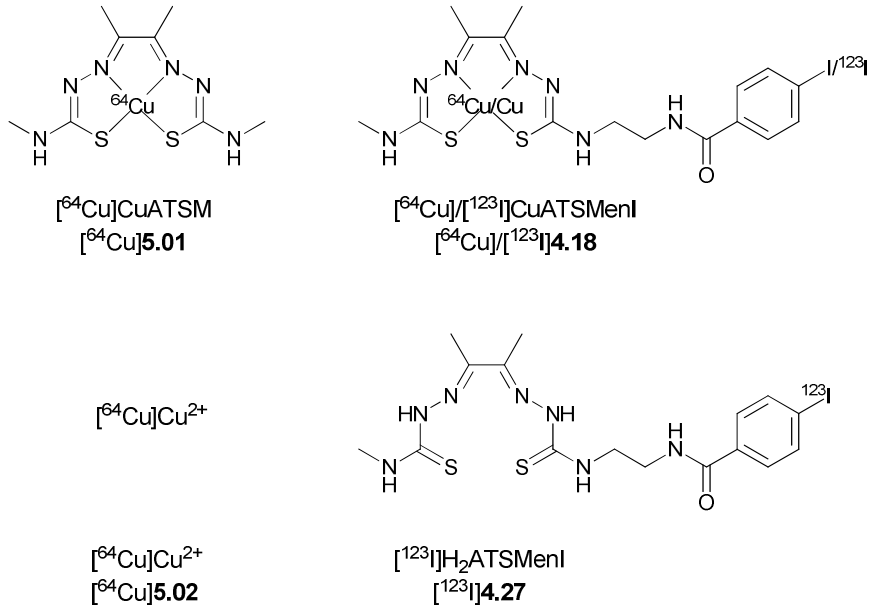

Figure 1 Structure of [^{64}Cu]CuATSM and the orthogonally radiolabelled Cu-bis(thiosemicarbazonato) complexes [^{64}Cu]CuATSMenI and [^{123}I]CuATSMenI and the individual components [^{123}I]H_2ATSMenI and [^{64}Cu]Cu^{2+}.

5.2 Selection of *in vitro* cell line and *in vivo* tumour model

Initially, the human fibrosarcoma cell line HT1080 was selected for *in vivo* imaging studies. The cells have been genetically modified so that HIF upregulates expression of luciferase and addition of luciferin then allows the detection of tumour hypoxia *via* bioluminescence.[1] Whilst HT1080 cells can be grown reliably in culture they proved problematic for use in the *in vivo* hypoxic tumour model. Tumours could not be grown reproducibly and exhibited a lack of growth whilst developing large, necrotic centres. Instead it was decided to implant murine adenocarcinoma NT (CaNT) xenografts. The CaNT tumour is a poorly differentiated non-immunogenic carcinoma (likely of mammary origin) which arose spontaneously in a female CBA/Gy mouse.[2] A disadvantage of this cell line is that it cannot be grown *ex vivo*. Tumour cells for *in vitro* cellular work thus had to be obtained by preparation of single cell suspension from excised tumours.[3] To keep the number of animals sacrificed to a minimum, only selected *in vitro* experiments were carried out with CaNT cells and the majority of the *in vitro* cellular uptake work was performed with HT1080 cells. A significant number of investigations concerning the hypoxia selectivity of Cu(II)ATSM has been performed in the well-documented EMT6 mouse mammary carcinoma cell line *in vitro* and *in vivo*.[4, 5] Solid EMT6 tumours contain a significant hypoxic fraction,[4, 6, 7] but the tumours grow at a faster rate (typically < 10 days) than CaNT tumours which posed problems in coordinating growth with the non-negotiable ^{64}Cu production dates. Hence only selected control *in vivo* experiments were performed in both EMT6 and CaNT tumour models.

5.3 *In vitro* cellular retention studies of orthogonally ^{123}I- and ^{64}Cu-labelled complexes

5.3.1 Apparatus and conditions

The apparatus used for the cellular retention studies was based on that previously reported in order to control temperature, humidity and pO_2 of the cellular medium.[4, 8-10]

In order to determine the oxygen dependence of activity retention, cell suspensions were incubated with the radiolabelled bis(thiosemicarbazonate) complex under anoxic (95% N_2, 5% CO_2) or normoxic (75% N_2, 20% O_2, 5% CO_2) conditions for a period of 60 min. Firstly, cells were harvested by trypsinisation and a single cell suspension (1×10^6 cells/mL) was prepared in DMEM supplemented with 1% (v/v) FBS. Cells were incubated for 30 min at 37°C at the desired oxygen concentration. The labelled complexes were injected into the cell-containing medium and the pO_2 of the suspension was monitored using an Oxylab pO_2 tissue oxygenation throughout the 60 min assay. Triplicate aliquots of cells were removed at 5, 15, 30, 45 and 60 min and the cells were pelleted by centrifugation. The percentage of cellular associated activity was reported as ($counts_{cellpellet}$/($counts_{cellpellet}$+ $counts_{medium}$)*100). For both the ^{64}Cu- and ^{123}I-labelled tracers an identical but cell-free control assay was performed to determine the amount of activity adhering to the Eppendorf tubes. This value was constant at ~5-10% throughout the assay and the values were subtracted from the respective cellular retention figures. In the literature, this assay is commonly referred to as 'cellular uptake assay'. It should be noted that the assay is neither able to distinguish between adherent extracellular, membrane-bound, or intracellular activity nor does it determine the nature of the bound species since no cell lysis or internalisation assays were performed. Hence, cellular retention is referred to here as 'cellular associated activity' rather than cellular uptake.

5.3.2 Verification of cell lines for *in vitro* cellular retention studies

As discussed in Chapter 4.4.8, initial cellular retention studies compared the ^{64}Cu-orthogonally labelled iodinated analogues to the parent [^{64}Cu]CuATSM in HT1080 cells. Before proceeding with further *in vitro* studies, the cellular retention of [^{64}Cu]CuATSM was investigated in both HT1080 and CaNT cells to compare values to those reported in the literature for the EMT6 cell line. Reported retention values for [^{64}Cu]CuATSM in EMT6 range from 15-25% under normoxic and 60-80% under anoxic conditions at 30 min.[4, 11] When repeating the [^{64}Cu]CuATSM retention assay in EMT6 cells in our laboratory, the anoxic/normoxic ratios obtained were slightly lower than in the literature. Retention values of 30% and 60% under normoxic and anoxic conditions respectively were obtained at 30 min (Figure 2).

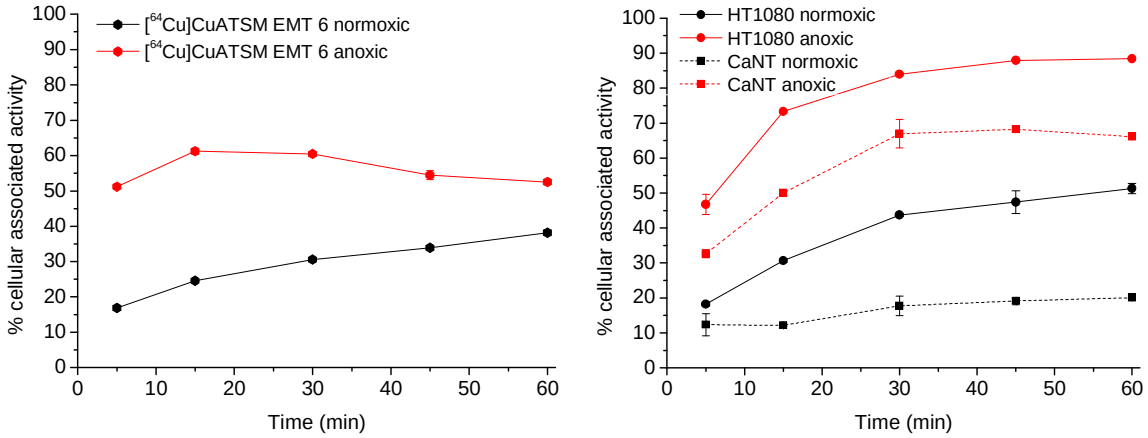

Figure 2 Percentage cellular associated activity of [^{64}Cu]CuATSM in (left) EMT6 and (right) HT1080 and CaNT cell lines over time, incubated either under normoxic (21% O_2, 5% CO_2, balance N_2) or anoxic (5% CO_2, balance N_2) conditions. Errors (standard deviation) are within symbols if not indicated.

Furthermore, an efflux of radioactivity from 30-60 min was observed under anoxia. In CaNT cells, both normoxic and anoxic retention broadly paralleled that observed for EMT6 in the literature,[5] but again there was a slight efflux of activity at later time points. As can be seen from Figure 2, HT1080 cells display higher overall retention of activity under both oxygen regimes compared to CaNT and EMT6 cells. A clear normoxic/anoxic differential of ~30% remained for HT1080. This compared well with 30-40% observed for EMT6 and CaNT.

Next, cellular retention of activity for [^{64}Cu]CuATSMenI was evaluated in CaNT, EMT6 and HT1080 cells. As observed with [^{64}Cu]CuATSM, the anoxic/normoxic differential for [^{64}Cu]CuATSMenI was lower in EMT6 than in CaNT cells (Figure 3) and HT1080 cells (Figure 4). Control assays using the copper ion [^{64}Cu]Cu(OAc)$_2$ (designated henceforth as [^{64}Cu]Cu^{2+}) were also conducted in EMT6, HT1080 and CaNT cells. Compared to [^{64}Cu]CuATSM, [^{64}Cu]Cu^{2+} showed low retention in all cell lines with no significant oxygen dependence in HT1080, a very small (but significant) differential in EMT6 (see Figure 5, section 5.3.3). CaNT cells cannot be grown *ex vivo*, hence [^{64}Cu]Cu^{2+} was also examined in excised CaNT cells *in vitro*. [^{64}Cu]Cu^{2+} again showed low retention (2% under normoxia) but interestingly displayed a normoxic/anoxic differential of 20%.

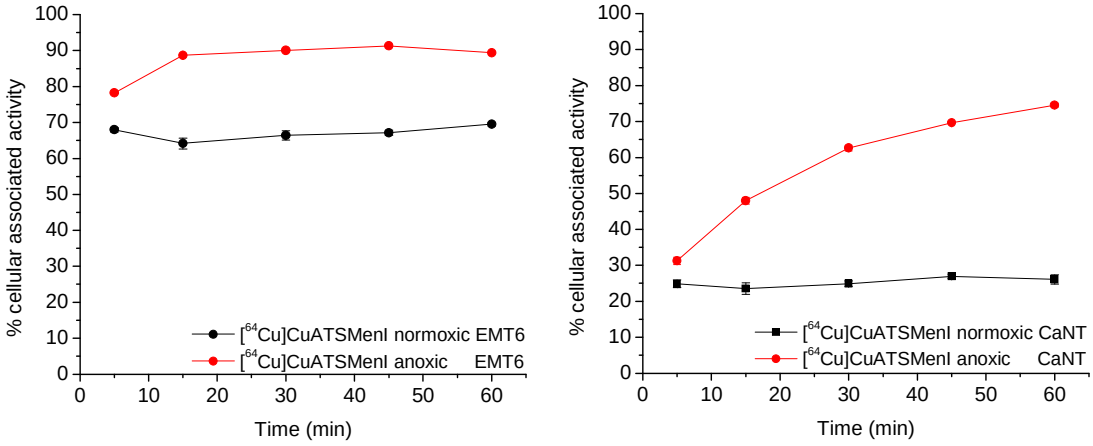

Figure 3 Percentage cellular associated activity of [^{64}Cu]CuATSMenI in (left) EMT6 and (right) CaNT cell lines over time, incubated either under normoxic (21% O_2, 5% CO_2, balance N_2) or anoxic (5% CO_2, balance N_2) conditions. Errors (standard deviation) are within symbols if not indicated.

Overall, the retention assays of [^{64}Cu]CuATSM, [^{64}Cu]CuATSMenI and [^{64}Cu]Cu^{2+} in HT1080, demonstrate that there are cell-line dependent differences for HT1080, CaNT and EMT6 cells. Both ^{64}Cu-labelled complexes however displayed significant retention differentials between anoxic and normoxic incubation in all three cell lines ($p < 0.0001$). Thus HT1080 cells, alongside selected controls in EMT6, were deemed suitable for the majority of *in vitro* studies. This would minimise the use of animals for tumour excision to obtain CaNT cells.

5.3.3 Cellular retention of [^{64}Cu]/[^{123}I]CuATSMenI and [^{123}I]H_2ATSMenI

Cellular retention assays in HT1080 cells were conducted in order to compare the retention of activity for [^{64}Cu]CuATSMenI and its orthogonal partner [^{123}I]CuATSMenI.

As already reported in sections 4.4.8 and 5.3.2, [^{64}Cu]CuATSMenI showed oxygen dependent cellular retention in HT1080. The initial normoxic retention of activity was higher for [^{64}Cu]CuATSMenI than for [^{64}Cu]CuATSM but did not alter much over the course of measurement. As can be seen in Figure 4, for [^{64}Cu]CuATSMenI, normoxic uptake increased from 46.2±0.4% at 5 min to 58.6±1.0% at 60 min, compared to a larger increase from 18.2±0.6% to 51.3±1.5% for the parent [^{64}Cu]CuATSM (Figure 2, section 5.3.2). Interestingly, the anoxic/normoxic ratio for both ^{64}Cu-labelled complexes was higher at the earlier time-points (ca. 15 min) than at the later time-points in HT1080, with maximum values of 2.5 and 1.9 for [^{64}Cu]CuATSM and [^{64}Cu]CuATSMenI respectively.

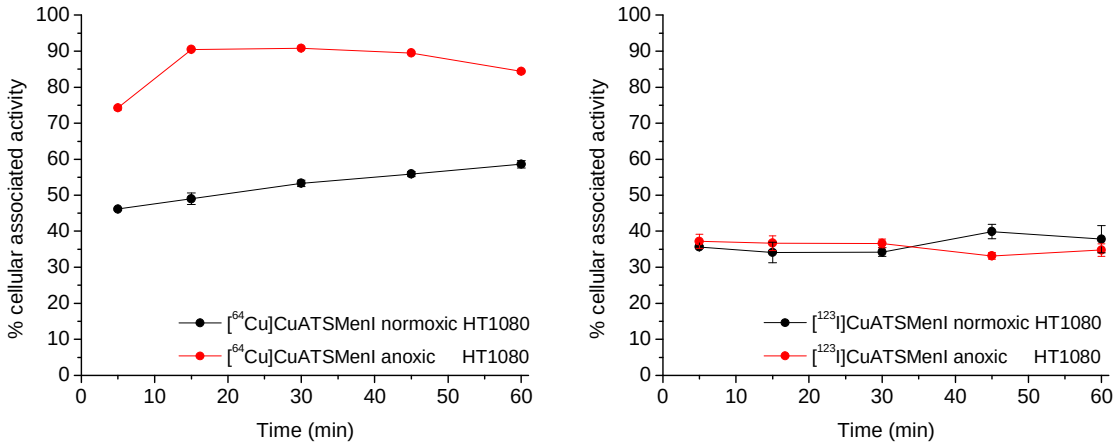

Figure 4 Percentage cellular associated activity of (left) [^{64}Cu]CuATSMenI and (right) [^{123}I]CuATSMenI in HT1080 cells over time, incubated either under normoxic (21% O_2, 5% CO_2, balance N_2) or anoxic (5% CO_2, balance N_2) conditions. Errors (standard deviation) are within symbols if not indicated.

In contrast to its ^{64}Cu-labelled counterpart, [^{123}I]CuATSMenI showed ~35% cellular retention of activity under both normoxic and anoxic conditions. It appears that equilibration for this retention process was fast as this amount of activity was already associated with the cells at the first (5 min) time-point measured (Figure 4, right). The amount retained was also constant over time. A retention profile of [^{123}I]CuATSMenI was also obtained in EMT6 cells, and equally, no significant

difference between normoxic and anoxic retention was observed for [^{123}I]CuATSMenI (Figure 6, for kinetic profiles in EMT6, see Appendix). Cellular associated activity was constant at ~35% over the course of the measurement. Thus it was concluded that [^{123}I]CuATSMenI showed ~35% cellular retention independent of cell line and oxygen concentration (p=0.6331).

In order to obtain further information on the nature of the cellular associated activity, the assay was conducted with the labelled proligand [^{123}I]H_2ATSMenI. As can be seen from Figure 5, no hypoxia selective retention of the ^{123}I-labelled ligand occurred in either HT1080 or EMT6 cells. Between 36-40% of activity was associated with anoxic and normoxic cells at 5 min and no further variation was observed. Interestingly, normoxic retention of [^{123}I]H_2ATSMenI was slightly, but significantly higher than hypoxic retention ($p < 0.001$). When comparing [^{123}I]CuATSMenI and [^{123}I]H_2ATSMenI, retention of activity for the proligand was marginally higher, but not significantly different ($p > 0.32$).

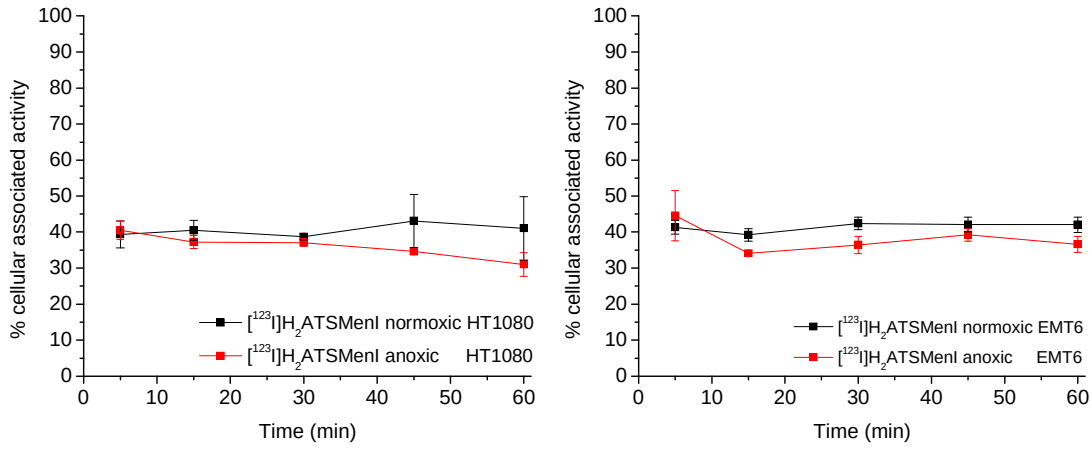

Figure 5 Percentage cellular associated activity of [^{123}I]H_2ATSMenI (left) in HT1080 cells and (right) in EMT6 cells over time incubated either under normoxic (21% O_2, 5% CO_2, balance N_2) or anoxic (5% CO_2, balance N_2) conditions. Errors (standard deviation) are within symbols if not indicated.

Figure 6 summarises the percentage cellular associated activity after 30 min incubation of HT1080 or EMT6 cells with [^{64}Cu]CuATSM, [^{64}Cu]CuATSMenI, [^{123}I]CuATSMenI, the proligand [^{123}I]H_2ATSMenI and [^{64}Cu]Cu^{2+}. The chart illustrates the clear anoxic/normoxic differential for [^{64}Cu]CuATSM and [^{64}Cu]CuATSMenI in both cell lines. The overall retention of activity is

slightly higher for [^{64}Cu]CuATSMenI than for [^{64}Cu]CuATSM, whereas the anoxic/normoxic ratio is slightly higher for [^{64}Cu]CuATSM.

In contrast, the amount of cell-associated activity for both [^{123}I]CuATSMenI and [^{123}I]H_2ATSMenI was broadly similar and independent of oxygen concentration, time or cell line. This suggests that the ligand is not retained by the cells in an oxygen dependent manner. The free metal ion, [^{64}Cu]Cu^{2+}, showed low retention in both cell lines. Interestingly, there was no significant oxygen dependence in HT1080 whilst a small but significant difference was observed in EMT6 ($p < 0.0001$).

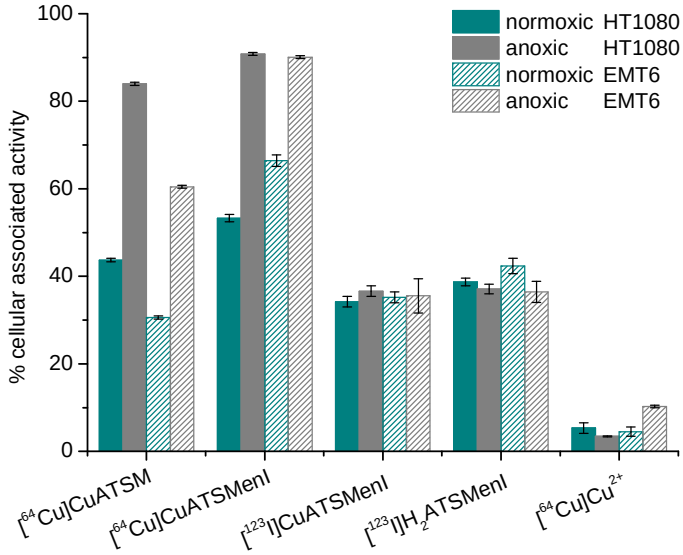

Figure 6 Percentage cellular associated activity of [^{64}Cu]CuATSM, [^{64}Cu]CuATSMenI, [^{123}I]CuATSMenI and [^{123}I]H_2ATSMenI in HT1080 cells at 30 min after incubation under normoxic (21% O_2, 5% CO_2, balance N_2) or anoxic (5% CO_2, balance N_2) conditions. Errors (standard deviation), are within symbols if not indicated.

5.3.4 Temperature dependence

Work carried out by Dr Robert King in parallel to the above experiments suggested that cellular retention/efflux of ^{64}Cu activity following [^{64}Cu]CuATSM incubation may not operate *via* diffusion but could be the result of an active transport mechanism. The temperature dependence of activity retention of [^{64}Cu]CuATSM under normoxic and anoxic conditions was investigated by conducting assays at 4°C, 20°C and 37°C in HeLa cells. As can be seen from Figure 7, normoxic and anoxic retention of activity was markedly reduced at 20°C compared to 37°C. At 4°C, retention of activity

was ~5% under both oxygen tensions (not shown). The assays suggested that selective ^{64}Cu-retention is temperature dependent and could be related to an active transport mechanism.

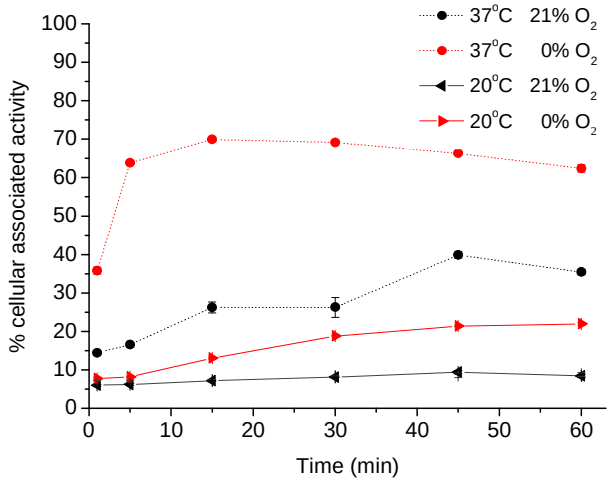

Figure 7 Temperature dependence assays carried out by Dr Robert King. Percentage cellular associated activity of [^{64}Cu]CuATSM in HeLa cells over time incubated either under normoxic (21% O_2, 5% CO_2, balance N_2) or anoxic (5% CO_2, balance N_2) conditions. Errors (standard deviation) are within symbols if not indicated.

5.3.5 Discussion of *in vitro* results

The differences in ^{64}Cu-retention observed for [^{64}Cu]CuATSM and [^{64}Cu]CuATSMenI in the two cell lines may be due to cell-line dependent differences (see Chapter 3.3.3). The kinetics over the time course varied between cell lines. Furthermore, the efflux of activity (Figures 2 and 4) after 30 min under anoxic conditions has previously been observed for R3327-AT cells.[12]

Provided the compounds rentain intact, a common mechanism of uptake/efflux has to operate for [^{64}Cu]CuATSMenI and [^{123}I]CuATSMenI due to their chemically identical nature. The current literature consensus is that the lipophilic [^{64}Cu]CuATSM molecule is able to enter or leave the cell by diffusion. Given the similar HPLC retention time and hence the similar lipophilicities (see Chapter 4), the same mechanism of uptake and efflux (such as diffusion) may operate for [^{123}I]CuATSMenI and [^{123}I]H_2ATSMenI. This may operate independently to the mechanism responsible for selective ^{64}Cu retention from [^{64}Cu]CuATSMenI incubation. The different retention values of [^{64}Cu]CuATSMenI and [^{123}I]CuATSMenI indicate that the ligand is not selectively retained inside the cell and may be able to leave the cell after separation from the copper.

However, under the currently accepted mechanism, normoxic retention of activity should involve primarily the intact complex. Hence retention of activity for [^{64}Cu]CuATSMenI and [^{123}I]CuATSMenI should be similar under normoxia. However, it is significant that normoxic retention of activity for [^{64}Cu]CuATSMenI is higher than for [^{123}I]CuATSMenI and varies with cell line. The similar, lower cellular retention of [^{123}I]CuATSMenI and [^{123}I]H_2ATSMenI may be coincidental, but it is possible that an identical species is retained, for instance the [^{123}I]-labelled free ligand. This would imply that the complex dissociates prior to entering the cell, for instance via dissociation on the membrane, leaving the ligand to be taken up in an oxygen independent process. Further experiments however are needed to illucidate the similar retention observed for [^{123}I]CuATSMenI and [^{123}I]H_2ATSMenI.

The cellular retention assay does not determine the species retained by the cells and does not distinguish whether the activity is bound to the cell surface, in the membrane, or fully internalised. From the cellular uptake experiments presented in this section it is clear however, that the orthogonally labelled ligand of the copper bis(thiosemicarbazone) is not retained inside cells in the same oxygen-dependent manner that is observed for activity resulting from [^{64}Cu]CuATSMenI and [^{64}Cu]CuATSM. Further, the results by King *et al*. suggest that retention of the ^{64}Cu is energy dependent. Before considering further *in vitro* investigations, we examined whether the observed behaviour holds in the *in vivo* setting.

5.4 *In vivo* biodistribution of [^{64}Cu]CuATSM, [^{64}Cu/^{123}I]CuATSMenI and [^{123}I]H_2ATSMenI by imaging and dissection

Following the *in vitro* cellular assays, it was of interest to determine whether the results would translate to the *in vivo* setting, specifically, whether the ligand would show any uptake in hypoxic tumour tissue. Furthermore, we were interested in comparing the biodistribution and uptake kinetics of [^{64}Cu]CuATSM to those of [^{64}Cu]/[^{123}I]CuATSMenI and [^{123}I]H_2ATSMenI.

All *in vivo* animal handling in this chapter was performed by Dr Veerle Kersemans and Dr Bart Cornelissen at the Gray Institute for Radiation, Oncology and Biology, University of Oxford.

5.4.1 Tumour model

Female CBA mice were injected into the rear dorsum with a saline suspension of CaNT cells to induce tumours. Imaging was performed when the tumours reached a geometric mean diameter of 6-8 mm (~3 weeks). The ^{64}Cu- and ^{123}I-labelled imaging agents were prepared freshly on the day of imaging as described in Chapter 4.4.

5.4.2 Anaesthetic protocol

Before commencing with *in vivo* imaging, a common anaesthetic protocol had to be established. As discussed in Chapter 3, Lewis *et al.* previously demonstrated that for 9L glioma bearing rats breathing 100% O_2, tumour uptake of ^{64}Cu activity following [^{64}Cu]CuATSM administration was markedly reduced compared to animals breathing air.[13] Recently Kersemans *et al.* investigated the impact of the anaesthetic protocol on preclinical *in vivo* imaging of tumour hypoxia using [^{18}F]FMISO, [^{64}Cu]CuATSM and [^{99m}Tc]HL91.[14, 15] It was found that both the carrier gas and the anaesthetic caused marked differences in tumour uptake for [^{18}F]FMISO, [^{64}Cu]CuATSM and [^{99m}Tc]HL91, but the effects varied between the three hypoxia tracers. For [^{64}Cu]CuATSM and [^{18}F]FMISO, the tumour-to-muscle ratio (RTM) was lowered when oxygen or anaesthetics, such as isoflurane in air, hypnorm/hypnovel or ketamine/xylazine were administered. For [^{64}Cu]CuATSM, tumour uptake was further reduced when oxygen and anaesthetic were combined (isofluorane in

oxygen). Tumour uptake of [^{99m}Tc]HL91 could only be altered by 100% oxygen breathing and was largely unaffected by anaesthetic drug administration.

Since anaesthesia could not be avoided for the preclinical dynamic imaging of the orthogonally radiolabelled tracers, the anaesthetic protocol was kept constant for all PET and SPECT imaging performed and mice were anaesthetised using an isoflurane/air mixture as the best compromise. In addition, to avoid any confounding effects of anaesthesia, dissection experiments for the ^{64}Cu- and ^{123}I-labelled tracers were also repeated in awake, non-imaging mice breathing room air (biodistributions).

5.4.3 *In-vivo* biodistributions

For *in vivo* biodistributions (organ dose measurements), mice were sacrificed by cervical dislocation 2 h post injection (p.i.) of the tracer. Organs and tissues were harvested and counted in a γ-counter to determine the uptake as percentage of the injected dose per gram, where (% ID/g) = [(activity$_{tissue}$)/(weight$_{tissue}$×activity$_{injected}$)].

Table 1 summarises the biodistribution data for [^{64}Cu]CuATSM, [^{64}Cu/^{123}I]CuATSMenI and [^{123}I]H_2ATSMenI. It can be seen that [^{64}Cu]CuATSM and [^{64}Cu]CuATSMenI show similar uptake values in most organs and tissues. The compounds had marginally different liver uptake with 7.36±0.76 and 6.35±0.80 %ID/g for [^{64}Cu]CuATSM and [^{64}Cu]CuATSMenI respectively ($p = 0.0374$). Heart uptake was slightly lower for [^{64}Cu]CuATSMenI ($p = 0.0011$) and lung uptake was significantly reduced at 3.71±0.4%ID/g for [^{64}Cu[CuATSMenI, compared to 5.6%ID/g observed for [^{64}Cu]CuATSM ($p < 0.0001$). Intestinal and stomach uptake is different for these compounds, although this is likely a result of the mice having *ad lib* access to food and water. The tumour-to-muscle ratios (RTM) were 7.3 and 8.3 for [^{64}Cu]CuATSMenI and [^{64}Cu]CuATSM respectively and were not significantly different ($p = 0.08$), although muscle uptake was slightly lower for [^{64}Cu]CuATSMenI and tumour uptake higher for [^{64}Cu]CuATSM. In both cases, the activity efficiently cleared from the blood *via* hepatobiliary excretion, with only ~ 1% ID/g remaining at 2 h p.i. This value was slightly lower than those observed by Lewis *et al.* (2.2% ID/g at 2.4 h p.i.).[4]

The similar biodistribution profiles of [^{64}Cu]CuATSM and [^{64}Cu]CuATSMenI suggest that exocyclic modification and introduction of the prosthetic group do not greatly influence the biodistribution. [^{64}Cu]CuATSMenI appears to have sufficiently similar properties to [^{64}Cu]CuATSM for it to be a suitable probe for the *in vivo* behaviour of the family of hypoxia selective copper bis(thiosemicarbazonato) complexes.

	[^{64}Cu]CuATSM	[^{64}Cu]CuATSMenI	[^{123}I]CuATSMenI	[^{123}I]H_2ATSMenI
Blood	1.09±0.01	1.03±0.07	0.38±0.06	0.42±0.04
Tumour	2.41±0.59	1.61±0.08	0.56±0.06	0.30±0.01
Muscle	0.33±0.05	0.19±0.02	0.38±0.04	0.23±0.01
Stomach	8.13±3.62	5.80±1.29	2.70±0.2	2.43±0.28
Small intestine	5.44±0.89	8.39±1.13	5.18±0.84	5.18±0.68
Large intestine	10.54±1.5	6.60±1.42	9.86±1.70	8.35±1.52
Fat	0.38±0.05	0.27±0.02	0.29±0.04	0.38±0.01
Spleen	1.54±0.14	1.08±0.06	1.17±0.35	0.34±0.01
Liver	7.36±0.76	6.35±0.80	3.71±0.36	2.79±0.45
Kidneys	5.15±0.60	4.34±0.25	0.93±0.12	0.86±0.31
Heart	1.73±0.32	1.00±0.07	0.62±0.06	0.35±0.03
Lungs	5.60±0.44	3.71±0.40	0.79±0.14	0.61±0.06
Thyroid	-	-	0.34±0.11	0.24±0.02
RTM	7.35±1.13	8.34±0.88	1.50±0.21	1.34±0.06

Table 1 Biodistribution (%ID/g ±SD[†]) of [^{64}Cu]CuATSM, [^{64}Cu]CuATSMenI, [^{123}I]CuATSMenI and [^{123}I]H_2ATSMenI at 120 min p.i. in in female CBA mice bearing CaNT xenografts (dissection only animals). N = 8 [^{64}Cu]CuATSM; n = 5 [^{64}Cu]CuATSMenI; n = 3 [^{123}I]H_2ATSMenI and n = 6 [^{123}I]CuATSMenI.

For biodistribution studies with radioiodinated tracers, *in vivo* deiodination and metabolism by deiodinases was considered to be a possibility. Hence, analysis of the biodistribution data of [^{123}I]CuATSMenI and [^{123}I]H_2ATSMenI first involved examination of the thyroid data. Thyroid uptake was 0.34% and 0.24% ID/g for [^{123}I]CuATSMenI and [^{123}I]H_2ATSMenI respectively, which was comparable to the uptake in reference tissues such as fat and muscle (between 0.29 and 0.38% ID/g). Thus, thyroid uptake was not significantly different from muscle and fat for [^{123}I]CuATSMenI ($p = 0.18$). For [^{123}I]H_2ATSMenI, thyroid uptake was also not significantly different from muscle ($p = 0.17$), but was significantly lower than fat ($p < 0.0001$). These results alleviated any concerns about the *in vivo* stability of the aromatic radioiodine label.

Inspection of the tumour-to-muscle data revealed that tumour uptake is about 5.5-fold lower for [^{123}I]CuATSMenI than its ^{64}Cu-labelled counterpart. Indeed, tumour uptake of [^{64}Cu]CuATSMenI and [^{64}Cu]CuATSM was significantly higher than that observed for [^{123}I]CuATSMenI and

[^{123}I]H_2ATSMenI ($p < 0.0001$). Tumour-to-muscle ratios for [^{123}I]CuATSMenI and [^{123}I]H_2ATSMenI at 2 h p.i. were 1.5±0.21 and 1.3±0.06 respectively and thus not significantly different for the two orthogonally labelled compounds ($p = 0.07$). Retention in non-target organs such as the liver, heart and lungs was much lower for [^{123}I]CuATSMenI and the ^{123}I-labelled ligand than for their ^{64}Cu-labelled counterpart ($p < 0.0001$).

Thus, the *in vivo* biodistributions mirrored the lower *in vitro* retention of the ^{123}I-labelled derivatives observed in cellular retention assays. The results reveal that the activity resulting from the orthogonally labelled ligand is not retained in hypoxic tumours to the same extent as activity administered in the form of the radiocopper complex.

5.4.4 Dynamic PET and SPECT imaging

5.4.4.1 Dynamic PET

In order to compare the kinetics of activity uptake for the set of orthogonally labelled tracers to those of the parent compound, dynamic PET imaging was performed for [^{64}Cu]CuATSM and [^{64}Cu]CuATSMenI; planar dynamic SPECT was employed for [^{123}I]CuATSMenI and [^{123}I]H_2ATSMenI.

For PET/CT imaging, performed on an Inveon PET/CT system (Siemens Preclinical Solutions), mice were anaesthetised and placed supine, head first, in the imaging cradle. A cannula was inserted into the lateral tail vein and following the attenuation CT-scan, 10 MBq of [^{64}Cu]CuATSM or [^{64}Cu]CuATSMenI was injected before 2 h whole body dynamic acquisitions were acquired. The images in Figure 8 show the coronal view of the last frame of the dynamic PET-scans of [^{64}Cu]CuATSM and [^{64}Cu]CuATSMenI. By visual inspection of the images it can be seen that the PET/CT studies qualitatively correspond with the results obtained by dissection.

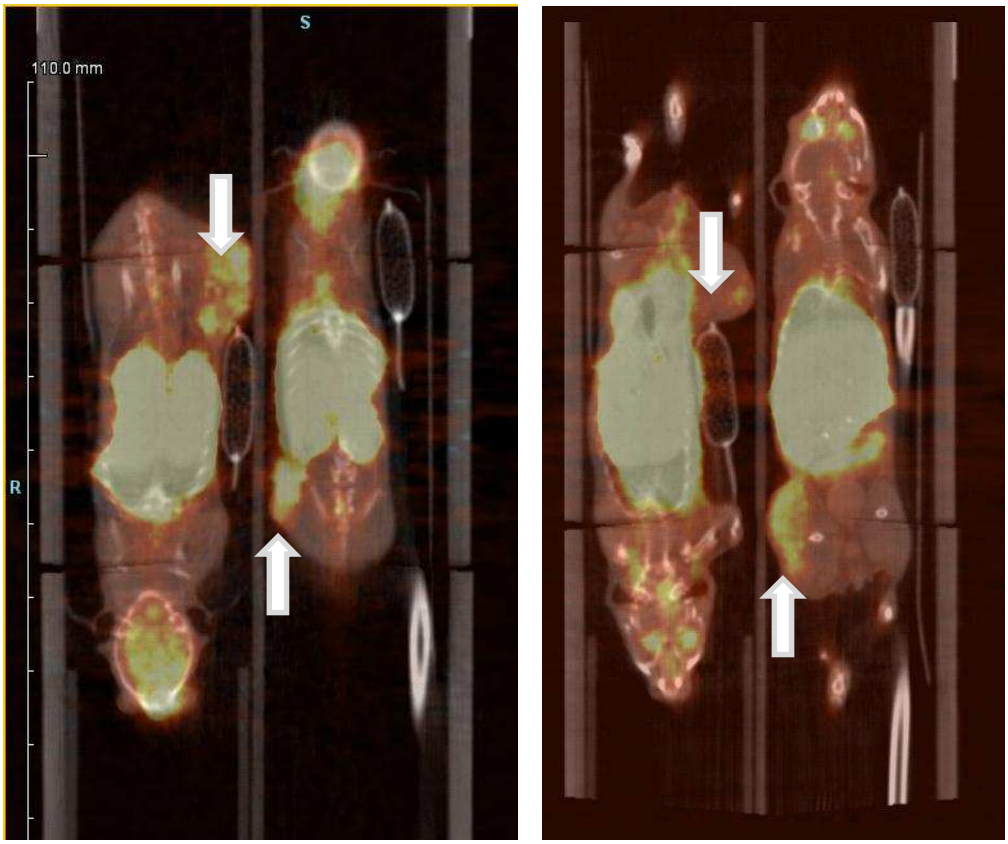

Figure 8 Coronal view of last frame of dynamic PET acquisition of (left) [^{64}Cu]CuATSM and (right) [^{64}Cu]CuATSMenI at 110-120 min p.i. White arrows indicate uptake in the tumour regions.

The majority of activity is taken up in the liver, lungs and the digestive tract. Tumour uptake is clearly visible for both [^{64}Cu]CuATSM or [^{64}Cu]CuATSMenI as indicated by the white arrows. Kinetic analysis to obtain time-activity curves was performed using the Inveon Research Workplace software, version 2.2 as discussed in section 5.4.5.

5.4.4.2 Dynamic SPECT imaging

SPECT imaging was performed on a Bioscan nanoSPECT/CT. The nanoSPECT is capable of collecting kinetic SPECT data, but temporal resolution can only be achieved in 2D and CT is not possible. Planar dynamic imaging was conducted with both [^{123}I]CuATSMenI and the ligand control [^{123}I]H_2ATSMenI. Following induction of anaesthesia, 3 mice were placed simultaneously, supine, head first, on the collimator and a cannula was inserted into their lateral tail vein. Ten MBq of [^{123}I]CuATSMenI or [^{123}I]H_2ATSMenI was injected through the cannula immediately after the 2-hour whole-body scans were initiated. For visualisation purposes, one representative mouse was also chosen for 3D, high resolution SPECT/CT imaging. The mouse was sacrificed using an i.v. overdose of pentobarbitone and was placed supine, head first in the imaging cradle. 3D-SPECT imaging was performed and a CT conducted for anatomical referencing.

Figure 9 depicts a 2D planar dynamic acquisition of [^{123}I]CuATSMenI (left) and a maximum intensity projection of [^{123}I]CuATSMenI (right) at 120 min p.i. Visual analysis shows that uptake in the tumour region was low as indicated by the circles and the white arrow. Most activity is taken up in the liver and intestines.

Image analysis of the 2D and 3D SPECT scans was done by Dr Veerle Kersemans. ROI image analysis of the 2D-dynamic scans was performed using ImageJ. The % injected dose/mm^2, (%ID/mm^2) was calculated and plotted over time. For the 3D SPECT/CT scaning, reconstruction of both CT and SPECT images was achieved using InVivoScope (version 1.42).

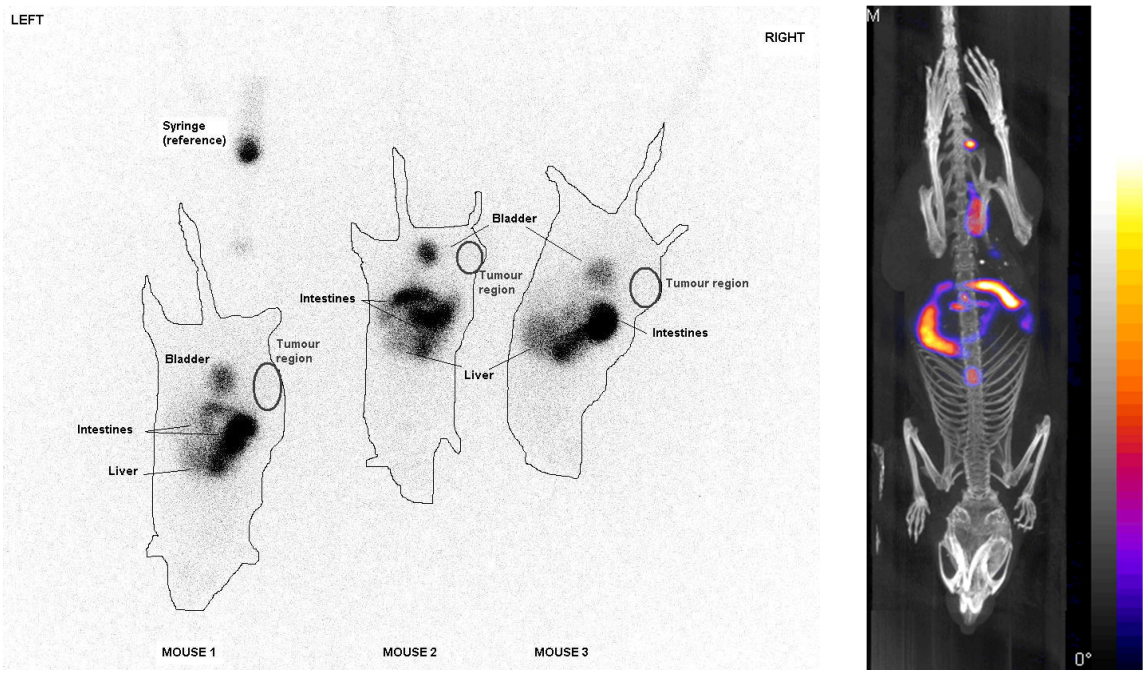

Figure 9 (left) 2D planar dynamic acquisition of [^{123}I]CuATSMenI in CBA mice bearing CaNT tumours at 110-120 min p.i. The labels indicate the uptake in the liver, intestinal regions and the bladder. Circles indicate the tumour regions. (right) Maximum intensity projection of [^{123}I]CuATSMenI at 120 min p.i.

5.4.5 Kinetics of tumour uptake

Using the dynamic PET and SPECT imaging data, time-activity curves can be plotted that show the uptake and distribution of activity over time. Figure 10 depicts the changes in RTM over time from 0 to 120 min p.i. For both [^{64}Cu]CuATSM and [^{64}Cu]CuATSMenI, RTMs increased with time and at approximately 100 min p.i. both compounds reached a steady state. This suggests that the ^{64}Cu activity is accumulated in the tumour tissue over time. In contrast, the RTM values for [^{123}I]CuATSMenI and [^{123}I]H_2ATSMenI settled at 1.5 and 1.3 within the first few minutes of administration.

At 120 min, RTM values were around 6 for [^{64}Cu]CuATSM and 5.5 for [^{64}Cu]CuATSMenI whilst ratios for the ^{123}I-labelled derivatives were around 4 to 4.5-fold lower. Thus kinetic PET and SPECT analysis consolidated the dissection results. The data further reveal similar kinetic profiles for [^{64}Cu]CuATSM and [^{64}Cu]CuATSMenI. Tumour-bound activity is constant for the ^{123}I-labelled complex and ligand.

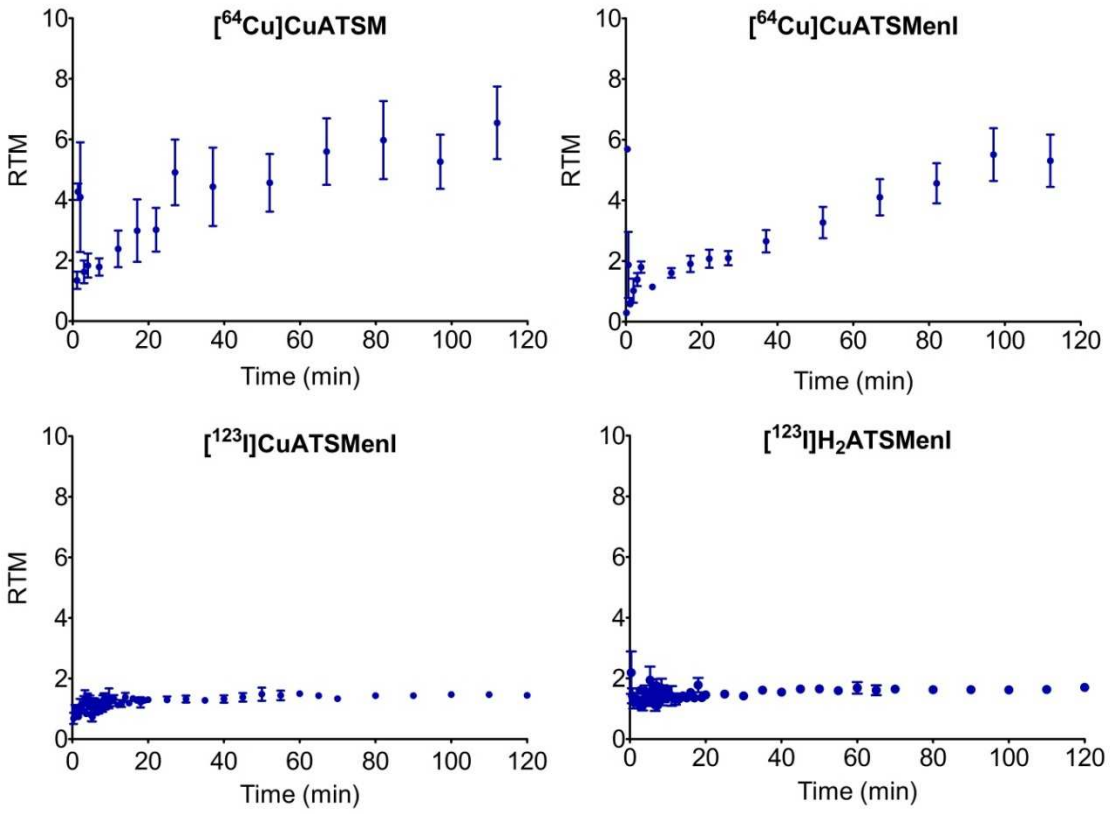

Figure 10 Changes in RTMs from 0 to 120 min p. i. For PET, the time-activity curves were created using volumes of interest (VOIs) composed of several, manually defined regions of interest (ROIs) covering the target area (tumour tissue, muscle tissue). For 2D-SPECT, time-activity curves were created using ROIs covering the target area.

5.4.6 Effect of the anaesthetic

Although similar RTM trends emerged for anaesthetised and dissection-only animals, tumour retention was noticeably lower for mice that underwent imaging. After PET and SPECT imaging, mice were thus sacrificed to obtain %ID/g in tissues and organs for comparison with the dissection-only animals. Figure 11 summarises the tumour-to-muscle ratios for anaesthesised and dissection-only animals, full dissection data for the imaging mice is found in the Appendix. For both [^{64}Cu]CuATSM and [^{64}Cu]CuATSMenI, tumour retention is significantly lower in mice that underwent imaging compared to dissection-only animals ($p = 0.0106$ and 0.0133 respectively). This is in agreement with the previous observations by Kersemans *et al.*[14, 15] For [^{123}I]CuATSMenI, there was a very small but statistically significant decrease in uptake under anaesthetic ($p < 0.01$), whilst tumour retention following [^{123}I]H_2ATSMenI administration was comparable under both protocols ($p = 0.374$).

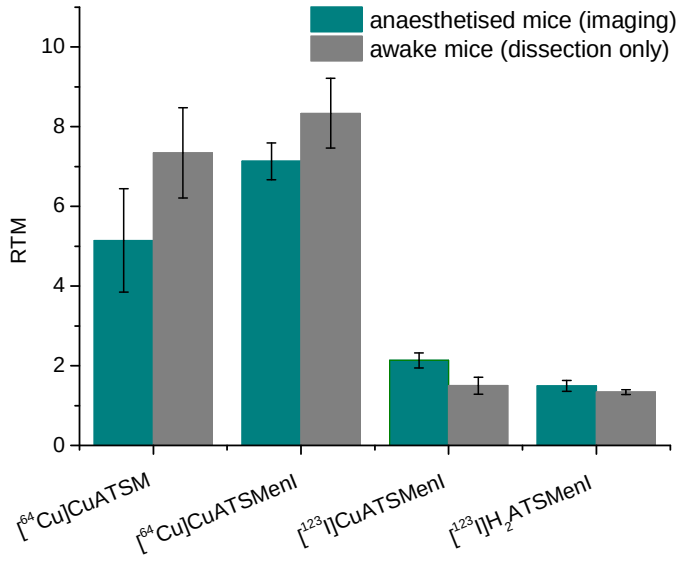

Figure 11 Tumour-to-muscle ratios for [^{64}Cu]CuATSM, [^{64}Cu]CuATSMenI, [^{123}I]CuATSMenI and [^{123}I]H_2ATSMenI determined from organ dose measurements (%ID/g) in animals bearing HT1080 xenografts. 'Anaesthetised mice' refer to values obtained from anaesthetised animals sacrificed after 120 min imaging sessions. 'Awake mice' were injected with the tracer and breathing room air for 120 min following tracer injection.

5.4.7 Implications of *in vivo* results on the fate of the ligand

Biodistributions by imaging and dissection confirmed results from *in vitro* assays and showed that activity administered by labelling the ligand does not seem to accumulate in the tumour tissue to the same extent as activity resulting from [^{64}Cu]CuATSM or [^{64}Cu]CuATSMenI administration.

Under the currently proposed mechanism, the ligand should track the metal into the tumour tissue where Cu is selectively trapped, but the subsequent fate of the ligand is not known. The [^{64}Cu]CuATSMenI and [^{123}I]CuATSMenI orthogonally labelled pair show noticeably different kinetics of tumour uptake, a differing total tumour uptake and different biodistributions to each other. In contrast, *in vivo* profiles of [^{123}I]CuATSMenI and the [^{123}I]H_2ATSMenI ligand control were remarkably similar. The set of *in vivo* experiments supports *in vitro* findings in suggesting that the complex may not remain intact. In addition to the possible causes outlined in 5.3.5, such as dissociation on the cell membrane, *in vivo* this could be a result of metabolic loss of the ^{123}I-label from the ligand. However, the thyroid data confirms the stability of the aromatic carbon-iodine bond. Other processes, such as amide bond cleave could cause *in vivo* metabolism, but this appears

unlikely due to the matching *in vitro* and *in vivo* data. These concerns are further addressed by stability studies in section 5.6.

Considering the possibility that ligand and metal do not track each other *in vivo* and having examined the labelled ligand as a control, it was decided to conduct further *in vivo* control experiments to examine the fate of the metal only.

5.5 Investigation of [^{64}Cu]Cu^{2+} uptake *in vivo*

Dynamic imaging and biodistribution experiments of [^{64}Cu]Cu^{2+} would examine the last individual component of the orthogonally labelled set of tracers for comparison with the data of the parent compound [^{64}Cu]CuATSM, and the orthogonally labelled [^{64}Cu/^{123}I]CuATSMenI and [^{123}I]H_2ATSMenI components. The data could reveal whether the complex remains associated *in vivo* before selective sequestering of the copper ion under hypoxia, or whether the complex dissociates earlier as might be anticipated from the similar *in vitro* and *in vivo* profiles of [^{123}Cu]CuATSMenI and [^{123}I]H_2ATSMenI.

5.5.1 Previous investigations with [^{64}Cu]Cu^{2+}

To date, there has been a lack of *in vivo* studies conducted with [^{64}Cu]Cu^{2+} in hypoxic tumour models. To the best of our knowledge, only a single study by Jalilian *et al.* compared the biodistribution of [^{61}Cu]$CuCl_2$ and [^{61}Cu]CuATSM in mature, male NMRI rats as part of an investigation of [^{61}Cu]CuATSM for fibrosarcoma imaging.[16] The authors reported comparable biodistributions in most organs at 1 and 2 h post injection, although retention of activity in the lung was higher for [^{61}Cu]CuATSM (12% ID/g) than for [^{61}Cu]$CuCl_2$ (0.75% ID/g) and liver accumulation at 1 h p.i. was slightly lower for [^{61}Cu]$CuCl_2$ (0.5%ID/g) than for [^{61}Cu]CuATSM (~1%ID/g). Noteably, [^{61}Cu]$CuCl_2$ studies were only performed in non-fibrosarcoma bearing animals and tumour uptake was not investigated. To date, no published studies have compared the tumour uptake of [^{64}Cu]Cu^{2+} and [^{64}Cu]CuATSM *in vivo*.

5.5.2 *In vivo* biodistributions of [^{64}Cu]Cu^{2+} by imaging and dissection

In vivo biodistributions and dynamic PET imaging of [^{64}Cu]Cu^{2+} in CaNT tumour bearing mice were conducted as described in section 5.3. For this purpose, [^{64}Cu]$Cu(OAc)_2$ was diluted in saline and the pH was adjusted to 7.4 by addition of $NaOH_{(aq)}$ before intravenous administration. Table 2 summarises the biodistribution by dissection (awake) and imaging (anaesthesised) results for [^{64}Cu]Cu^{2+} and [^{64}Cu]CuATSM at 2 h p.i.

The results obtained for the [^{64}Cu]Cu^{2+} component stand out as its biodistribution was comparable to [^{64}Cu]CuATSM. Remarkably, RTM values at 9.3±0.8 for [^{64}Cu]Cu^{2+} were significantly higher than those of [^{64}Cu]CuATSM (7.4±1.1) in dissection-only animals ($p < 0.0001$). For anaesthetised animals following PET, RTM values were reduced for both compounds but the effect was more noticeable for [^{64}Cu]Cu^{2+} where RTM values halved (5.27±0.66) compared to the non-anaesthetised group. As observed for [^{64}Cu]CuATSM and [^{64}Cu]CuATSMenI, intestinal and stomach uptake varied for [^{64}Cu]Cu^{2+} likely due to *ad lib* food and water access. Uptake in other non-target organs was comparable for [^{64}Cu]CuATSM and [^{64}Cu]Cu^{2+}, with exception of higher uptake in the spleen for the free copper ion. Interestingly, blood clearance was more efficient in anaesthetised animals, %ID values were 0.66±0.04% and 0.73±0.05% for [^{64}Cu]Cu^{2+} and [^{64}Cu]CuATSM in imaging mice, compared to 1.28±0.40% and 1.09±0.01% respectively for dissection only animals.

	Dissection only (awake)		Post imaging (anaesthetised)	
	[^{64}Cu]CuATSM	[^{64}Cu]Cu^{2+}	[^{64}Cu]CuATSM	[^{64}Cu]Cu^{2+}
Blood	1.09±0.01	1.28±0.40	0.73±0.05	0.66±0.04
Tumour	2.41±0.59	2.76±0.63	1.41±0.10	1.32±0.09
Muscle	0.33±0.05	0.28±0.07	0.29±0.07	0.25±0.04
Stomach	8.13±3.62	6.67±2.10	5.97±1.49	8.13±6.26
Small intestine	5.44±0.89	7.02±1.34	9.19±1.18	5.45±0.33
Large intestine	10.54±1.5	6.27±2.50	3.92±0.47	3.79±0.87
Fat	0.38±0.05	0.30±0.13	0.45±0.06	0.37±0.09
Spleen	1.54±0.14	2.66±1.01	1.53±0.21	3.33±1.57
Liver	7.36±0.76	9.93±1.75	10.03±1.02	8.43±1.07
Kidneys	5.15±0.60	5.60±0.91	6.03±0.66	4.97±0.98
Heart	1.73±0.32	2.15±1.22	1.28±0.11	0.96±0.09
Lungs	5.60±0.44	6.44±1.62	5.49±0.56	5.20±0.62
RTM	7.35±1.13	9.93±0.79	5.14±1.30	5.27±0.66

Table 2 Biodistribution (%ID/g ±SD) of [^{64}Cu]Cu^{2+} and [^{64}Cu]CuATSM at 120 min p.i. in female CBA mice bearing CaNT xenografts (dissection only animals). Dissection only animals were breathing air for 120 min post injection (n = 8 for [^{64}Cu]CuATSM and [^{64}Cu]Cu^{2+}). Post imaging data was obtained from dissections following 120 min dynamic PET under the isofluorane/air anaesthetic protocol (n = 8 for [^{64}Cu]CuATSM and n = 6 for [^{64}Cu]Cu^{2+}).

Analysis of the dynamic PET data consolidated the similar *in vivo* profile of [^{64}Cu]CuATSM and [^{64}Cu]Cu^{2+}. The time activity curves for [^{64}Cu]CuATSM and [^{64}Cu]Cu^{2+}, as depicted in Figure 12, show similar kinetic behaviour. At approximately 100 min p.i., the RTM of [^{64}Cu]Cu^{2+} reached a steady state as previously observed for [^{64}Cu]CuATSM and [^{64}Cu]CuATSMenI.

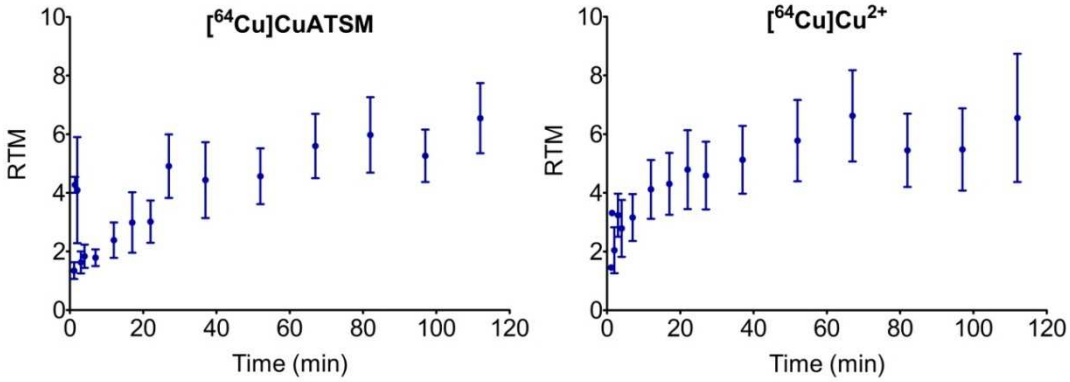

Figure 12 Changes in tumour-to-muscle ratios over time for [^{64}Cu]CuATSM and [^{64}Cu]Cu^{2+} (0-120 min p.i. in anaesthesised CaNT tumour-bearing mice). Time-activity curves were created using volumes of interest (VOIs) composed of several manually defined regions of interest (ROIs) covering the target area (tumour tissue, muscle tissue).

5.5.3 Tumour line dependence

As mentioned in 5.5.1, to the best of our knowledge, no direct comparison between the *in vivo* tumour uptake of [^{64}Cu]CuATSM and [^{64}Cu]Cu^{2+} has been reported to date.

However, [^{64}Cu]Cu^{2+} has been used for imaging human prostate cancer xenografts in mice. Peng *et al.* demonstrated increased [^{64}Cu]Cu^{2+} uptake in PC3 tumours with tissues that had upregulated levels of expression of the human copper transporter (hCtr1).[17] Thus we wanted to ensure that the observed uptake of [^{64}Cu]Cu^{2+} in CaNT was not a phenomenon caused by the tumour model employed.

In order to examine tumour-line specific effects, biodistributions (dissection and dynamic PET) were repeated using EMT6 tumour xenografts as these are widely employed in hypoxia research.[4, 6]

Figure 13 compares the tumour-to-muscle ratios for [^{64}Cu]CuATSM, [^{64}Cu]CuATSMenI and [^{64}Cu]Cu^{2+} in both tumour models. It is evident that [^{64}Cu]Cu^{2+} shows tumour uptake in EMT6.

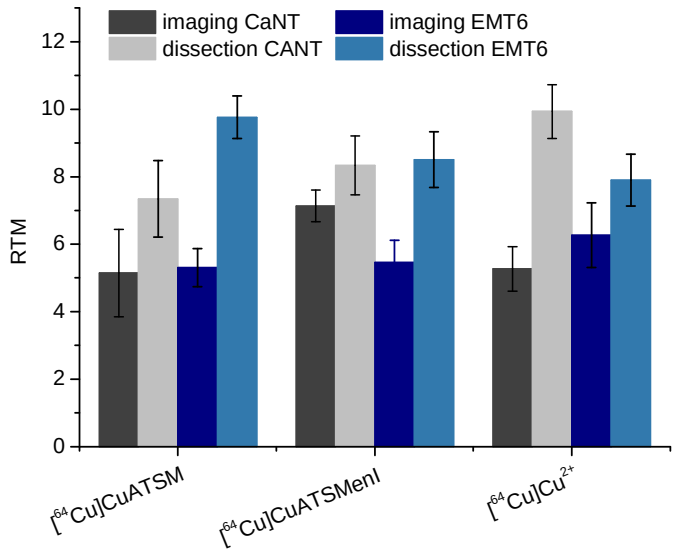

Figure 13 Tumour-to-muscle ratios for [^{64}Cu]CuATSM, [^{64}Cu]CuATSMenI and [^{64}Cu]Cu^{2+} in CaNT and EMT6 tumour bearing CBA mice as determined by organ dose measurements (%ID/g). 'Imaging mice' refer to values obtained from anaesthetised animals sacrificed after 120 min imaging sessions. 'Biodistribution mice' were breathing room air for 120 min following tracer injection.

In dissection only animals, RTMs observed in EMT6 were slightly higher for [^{64}Cu]CuATSM at 9.8±0.63 compared to 7.35±1.13 in CaNT ($p = 0.0014$). RTMs for [^{64}Cu]Cu^{2+} were slightly lower in EMT6 (7.90±0.77) than in CaNT (9.93±0.79) ($p = 0.0013$). For [^{64}Cu]CuATSMenI, RTMs were not significantly different in both tumour models, with ratios of 8.34±0.88 and 8.50±0.82 for CaNT and EMT6 tumour bearing mice respectively ($p = 0.3836$). For all three ^{64}Cu-labelled compounds, the anaesthetic significantly lowered the tumour-to-muscle ratios in EMT6 tumours as previously observed for CaNT. Overall, RTM values for non-anaesthetised animals lie in the region of 7-10 for all the three ^{64}Cu species, whereas those animals receiving isofluorane/air anaesthetic showed ratios ranging between 5-7.

Remarkably similar organ dose measurements and kinetic tumour uptake profiles were observed for [^{64}Cu]CuATSM and [^{64}Cu]Cu^{2+} across 2 tumour lines. Furthermore, tumour uptake following [^{64}Cu]CuATSM, [^{64}Cu]Cu^{2+} and [^{64}Cu]CuATSMenI administration is significantly reduced under the influence of anaesthesia.

5.5.4 Influence of oxygen on tumour uptake of [^{64}Cu]Cu^{2+}

Tumor oxygenation can be altered by changing the inhaled oxygen content and by doing so, Lewis *et al*. showed that tumour retention of ^{64}Cu using [^{64}Cu]CuATSM decreased when animals were breathing 100% oxygen as opposed to air, the implication being that the breathed oxygen content could modulate the extent of hypoxia.[13] As discussed in section 5.4.6, Kersemans *et al.* also observed that besides the use of anaesthetic, oxygen inhalation greatly reduced tumour uptake of activity for [^{64}Cu]CuATSM in CaNT tumour bearing mice.

The similar *in vivo* behaviour of [^{64}Cu]CuATSM and [^{64}Cu]Cu^{2+} prompted us to determine whether oxygen inhalation would influence the tumour uptake of activity for [^{64}Cu]Cu^{2+} similarly. For this purpose, animals were injected with [^{64}Cu]CuATSM or [^{64}Cu]Cu^{2+} and kept awake whilst breathing room air or 100% oxygen, before being sacrificed for organ dose measurements at 120 min p.i. Two additional groups of animals were injected under the influence of inhalation anaesthetics (isofluorane/air or isofluorane/oxygen) to determine whether the combination of inhalation anaesthetics and oxygen would further affect the uptake of activity. Figure 14 depicts the RTM values for [^{64}Cu]Cu^{2+} from organ dose measurements compared to [^{64}Cu]CuATSM. It is clearly visible that for animals breathing oxygen, RTM values for both [^{64}Cu]CuATSM and [^{64}Cu]Cu^{2+} are significantly reduced compared to animals breathing room air.

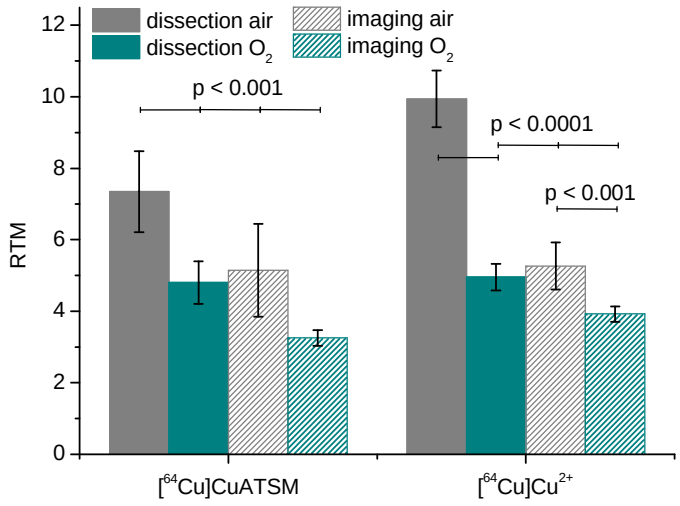

Figure 14 Tumour-to-muscle ratios for [^{64}Cu]CuATSM and [^{64}Cu]Cu^{2+} in CaNT tumour bearing CBA mice as determined by organ dose measurements (%ID/g). 'Imaging mice' refer to values obtained from animals anaesthetised by isoflurane in air or oxygen, sacrificed at the end of the 120 min imaging session. 'Dissection' mice were breathing room air or oxygen for 120 min p.i. before being sacrificed.

Remarkably, the decrease in tumour uptake was more pronounced for [^{64}Cu]Cu^{2+}, its RTM was reduced by more than half (9.93±0.79 to 4.95±0.37) when animals breathed pure oxygen. Tumour uptake of activity for [^{64}Cu]Cu^{2+} was further reduced when isofluorane was supplemented, but similar to [^{64}Cu]CuATSM, this effect was less pronounced than in non-anaesthetised animals.

The % ID/g in other organs was largely unaffected by changing the inhaled gas. As is apparent from Figure 15, a notable change occurred in the lungs, where uptake of activity was reduced for oxygen-breathing animals for both [^{64}Cu]CuATSM and [^{64}Cu]Cu^{2+}. For [^{64}Cu]Cu^{2+} only, inhalation of oxygen reduced liver uptake by ~3.5% ID/g. Some changes occurred in the kidneys, but together with the intestines and stomach (omitted for clarity from Figure 15), these cannot be analysed readily as they are influenced by the animals' unrestricted access to water. Since muscle retention was unaffected by the inhaled gas, RTM variations are due to changes in tumour uptake. Interestingly, measurements of tumour hypoxia *via* Oxylite electrode did not indicate higher tumour oxygenation, but this may be due to sampling errors for the small murine tumours.[18] However, immunohistological EF5 staining indicated a lower amount of tumour hypoxia in mice breathing oxygen compared to those exposed to room air in accordance with previous observations.[18, 19] The results indicate that uptake of [^{64}Cu]Cu^{2+} is dependent on the oxygenation status of the tumour in a similar manner previously observed for [^{64}Cu]CuATSM.

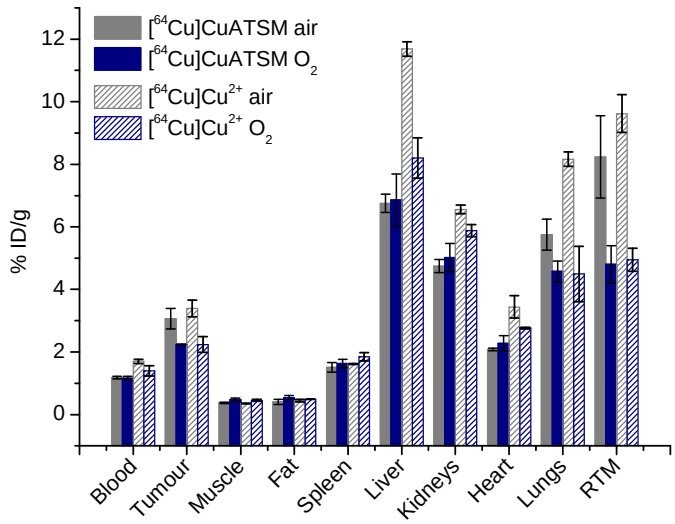

Figure 15 Biodistribution (%ID/g ±SD[†]) of [^{64}Cu]CuATSM and [^{64}Cu]Cu^{2+} at 120 min p.i. in female CBA mice bearing CaNT xenografts. Animals were not anaesthetised and kept in room air or in a 100% oxygen atmosphere. N = 3 for mice breathing oxygen for [^{64}Cu]CuATSM and [^{64}Cu]Cu^{2+}, n = 7 for [^{64}Cu]Cu^{2+} breathing air, n = 8 for [^{64}Cu]CuATSM breathing air.

5.5.5 Differences between [^{64}Cu]CuATSM and [^{64}Cu]Cu^{2+} - first pass kinetics in the liver

The *in vivo* behaviour of [^{64}Cu]Cu^{2+} shows similarities to [^{64}Cu]CuATSM and [^{64}Cu]CuATSMenI in terms of the kinetics of tumour uptake, total dose measurements and oxygen dependence. In contrast, different kinetics of activity uptake in the liver for [^{64}Cu]Cu^{2+} compared to [^{64}Cu]CuATSMenI and [^{64}Cu]CuATSM were found at the early time-points (~ 0-15 min) p.i. Figure 16 depicts time-activity curves of [^{64}Cu]CuATSM, [^{64}Cu]CuATSMenI and [^{64}Cu]Cu^{2+} in the liver and the heart.

For [^{64}Cu]CuATSM, an initial peak can be observed around 12 min before the retention of activity decreases again and levels out, this effect was even more pronounced for [^{64}Cu]CuATSMenI. In contrast, no initial increase is observed for [^{64}Cu]Cu^{2+}, suggesting different uptake kinetics in the liver compared to both copper-bis(thiosemicarbazonato) complexes.

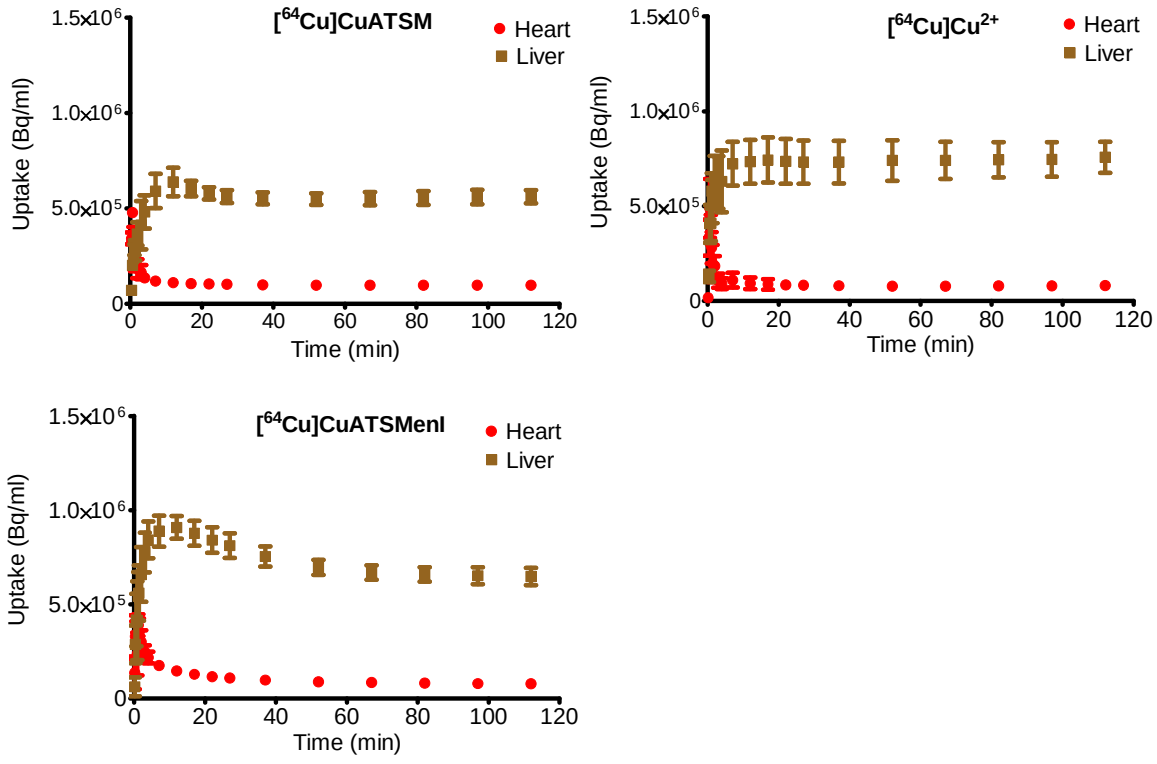

Figure 16 Changes in liver and heart retention for [^{64}Cu]CuATSM, [^{64}Cu]Cu^{2+} and [^{64}Cu]CuATSMenI from 0 to 120 min p.i. Time-activity curves were created using volumes of interest (VOIs) composed of several, manually defined regions of interest (ROIs) covering the target area (heart tissue, kidney tissue).

5.5.6 Implications of *in vivo* results

Besides interrogating whether the ligand enters the cell as part of a hypoxia selective process, the biodistribution data for the [^{64}Cu/^{123}I]CuATSMenI and [^{123}I]H_2ATSMenI compounds and the similar behaviour of [^{64}Cu]Cu^{2+} and [^{64}Cu]CuATSM raised concerns about the *in vivo* stability of the [^{64}Cu]CuATSM and [^{64}Cu]CuATSMenI complexes.

The only significant differences between the salt and copper complexes were the initial kinetics in the liver, suggesting that different ^{64}Cu-species are processed in the liver in the first few minutes p.i. This observation could imply that [^{64}Cu]CuATSM, and more so [^{64}Cu]CuATSMenI, may survive the first pass, despite a possible later dissociation.

A full interpretation of the kinetics in the liver however requires detailed analysis of the ^{64}Cu species present in homogenates of the liver and other organs over a series of time-points and was beyond the scope of this project.

Initially, it seemed important to investigate whether intact [^{64}Cu]CuATSM remains in the blood pool and to gain further information on the species available for tumour uptake. It was decided to examine the species present in blood following intravenous injection by determining the degree of blood-bound demetallation or metabolism in animals injected with [^{64}Cu]CuATSM, [^{64}Cu/^{123}I]CuATSMenI and [^{64}Cu]Cu^{2+}.

5.6 Complex stability (demetallation) studies

5.6.1 Previous serum binding and complex stability studies

Several groups have examined the protein-binding and stability of ^{64}Cu-labelled copper bis(thiosemicarbazonato) complexes by incubation in human serum or animal serum.[9, 10, 20-24] Typically, incubation of the ^{64}Cu-labelled complex in serum at 37°C is followed by analysis with an ethanol precipitation or gel-/ultrafiltration method. In the protein filtration methods, serum aliquots are withdrawn and analysed by gel permeation (or a molecular weight cut off filter in the case of ultrafiltration). Gel filtration of serum plasma allows separation of the high molecular weight serum proteins which pass quickly through the bead-formed gel, from low molecular weight molecules, such as the ^{64}Cu-copper complexes and [^{64}Cu]Cu^{2+}, that are retained in the pores of the beads and consequently elute later.[25] Thus, free, low molecular weight activity is separated from the protein-bound activity fraction. The method does not further resolve the different small molecular weight species, such as chelator-bound or free ^{64}Cu activity in the case of the copper complexes. In the ethanol precipitation method, serum aliquots are withdrawn and mixed with ethanol to cause protein precipitation. The precipitated protein pellet and the ethanol phase are separated, and the amount of protein bound radioactivity is determined by γ-counting.[9, 21] In addition, radio-TLC of the ethanol extract may be used to analyse the separable, non-protein-bound activity. Radio-TLC conditions analogous to those for quality control of the ^{64}Cu-copper bis(thiosemicarbazonato) complexes in Chapter 4.3 and 4.4 may be used to determine the proportions of free and chelator bound ^{64}Cu in the extract.[9] Basken *et al.* studied the structure and species dependence of serum binding for [^{64}Cu]CuATSM, [^{64}Cu]CuPTSM and [^{64}Cu]CuETS. They demonstrated that the amount of activity bound to serum albumins is highly dependent both on the nature of the ^{64}Cu-complex and the albumin species origin.[22-24] Work by McQuade *et al.* and our groups have shown *via* the ethanol precipitation method, that for *in vitro* incubation of [^{64}Cu]CuATSM and related hypoxia selective ^{64}Cu-copper bis(thiosemicarbazonato) complexes in mouse serum, typically ~20% of activity is protein-bound, with the unbound, EtOH-extractable

remainder consisting of intact complex.[8, 9, 21] The nature of the bound activity was assumed to be intact complex in these studies, but has not always been confirmed by experiment in each report.

Mathias *et al.* developed an octanol extraction method to recover quantitatively intact [^{67}Cu]CuPTSM complex from blood samples following *in vitro* incubation.[26] The authors applied this to myocardial perfusion imaging, where they determined the amount of intact CuPTSM in sequential blood samples following i.v. administration of [^{64}Cu]CuPTSM, to correct the arterial blood radioactivity for red blood cell associated activity.[27] Lewis *et al.* extended this method to CuATSM in order to correct the input function from PET images for the presence of dissociation products (ie non-recoverable copper radioactivity) when using [^{64}Cu]CuATSM to image hypoxia in canine myocardium.[28]

With the exception of the canine study by Lewis, it is noticeable that former stability and binding studies have been conducted primarily *in vitro*. We anticipated that analysis of the serum and blood from mice injected with the ^{64}Cu-copper complexes may provide insights into the *in vivo* stability and serum binding of [^{64}Cu]CuATSM and the orthogonal derivatives. These could then be compared to *in vitro* incubations and literature results.

5.6.2 Sampling

Studies were conducted in non-tumour bearing animals to exclude the effect of the tumour. In order to analyse the amount of serum-bound activity in the blood *in vivo*, blood samples were obtained at various time points from female CBA mice that had been injected with 1-2 MBq of [^{64}Cu]CuATSM, [^{64}Cu]CuATSMenI, or [^{64}Cu]Cu^{2+}. The full blood was analysed by octanol extraction immediately after sample collected (see section 5.6.5). To analyse the activity present in the serum plasma fraction, the erythrocyte fraction was separated from the serum plasma by centrifugation, and the plasma was analysed by G25 gel filtration and the ethanol precipitation method.

5.6.3 G25 Protein gel filtrations

Firstly, the retention time of the reference compounds was determined. Samples of [^{64}Cu]CuATSM, [^{64}Cu]CuATSMenI and [^{64}Cu]Cu^{2+} were deposited on G25 mini-columns and eluted with 30 × 100 µL fractions of pH 7.4 PBS. The elution profiles, depicted in Figure 17, revealed that the ^{64}Cu-labelled copper complexes and free [^{64}Cu]Cu^{2+} ion eluted around fraction 20.

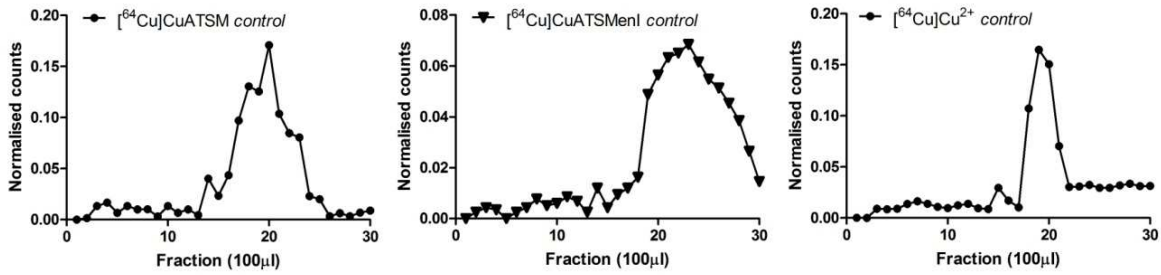

Figure 17 Elution profile of [^{64}Cu]CuATSM, [^{64}Cu]CuATSMenI and [^{64}Cu]Cu^{2+} from a Sephadex 25 size exclusion column, eluted with PBS.

Next, elution profiles of serum plasma fractions from mice injected with [^{64}Cu]Cu^{2+} were obtained (Figure 18). At 5 min post injection, the activity is primarily bound to a higher molecular weight species (fraction 6), before distributing over two bands (fraction 6 and 13) at the later time-points post injection, indicating that the [^{64}Cu]Cu^{2+} becomes bound to two protein fractions of similar size. No unbound [^{64}Cu]Cu^{2+} was observed at any time-point.

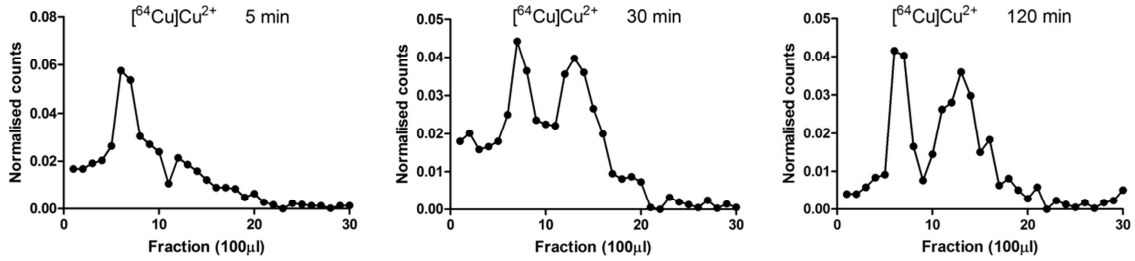

Figure 18 Sephadex G25 column elution profiles of serum fractions from mouse blood samples at 5, 30, and 120 min post injection with [^{64}Cu]Cu^{2+}

The elution profiles of the serum samples from mice injected with [^{64}Cu]CuATSM and [^{64}Cu]CuATSMenI were similar to those for [^{64}Cu]Cu^{2+}. For [^{64}Cu]CuATSM serum samples, most activity eluted around fractions 6 and 13 for 5 and 30 min post injection (Figure 19) whereas at 120 min, activity was primarily in the earlier fraction. Serum samples from mice injected with

[^{64}Cu]CuATSMenI showed similar quantities of activity in fractions 6 and 13 at the 5, 30 and 120 min post injection. For both of the two copper complexes or the copper ion, there was no activity eluted in later fractions that would indicate any non-bound [^{64}Cu]Cu^{2+} or free ^{64}Cu-copper complex. This suggests that all available activity was protein bound. However, the gel filtration assay does not determine the nature of the protein-bound activity.

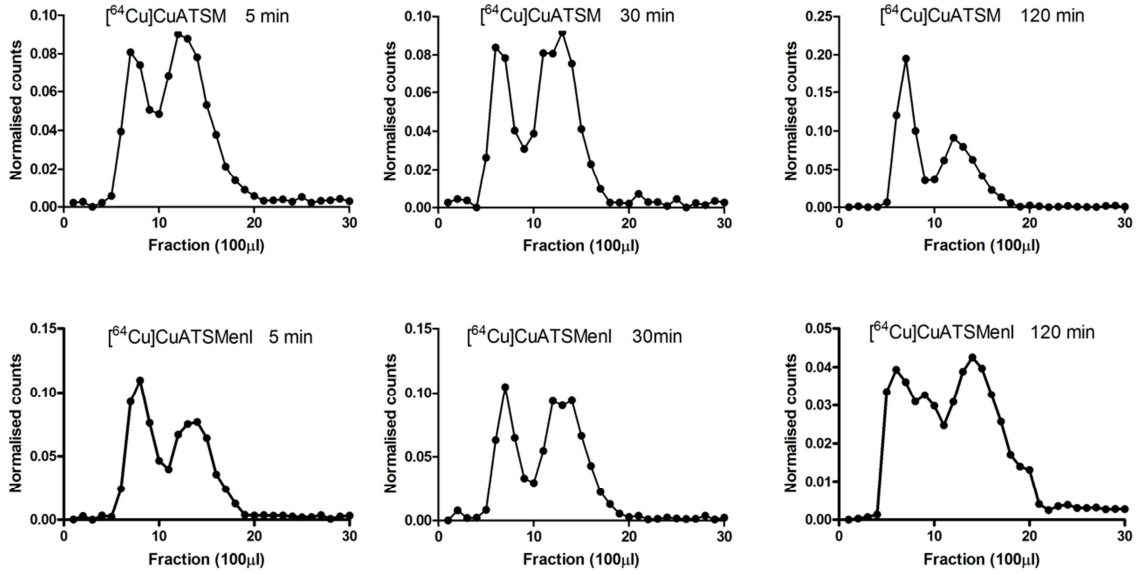

Figure 19 Sephadex G25 column elution profiles of serum fractions from mouse blood samples at 5, 30, and 120 min p.i. with (top) [^{64}Cu]CuATSM and (bottom) [^{64}Cu]CuATSMenI.

In order to compare the *in vivo* behaviour of the complexes to that observed *in vitro*, identical gel filtrations were performed with serum samples that had been incubated with [^{64}Cu]CuATSM, [^{64}Cu]CuATSMenI and [^{64}Cu]Cu^{2+} in fresh mouse serum and blood *in vitro*. Figure 20 shows representative elution profiles at 30 min post incubation at 37°C (elution profiles at 5, 15, and 120 min and those in blood were comparable). Incubation of all three ^{64}Cu-compounds in isolated mouse plasma resulted in 100% protein-associated ^{64}Cu. In contrast to the *in vivo* work, only radioactivity in the first protein region (fraction 6) was observed. As for the *in vivo* work, no unbound activity was eluted. Thus *in vitro* serum incubations resulted in a single protein-bound activity elution and differ from samples obtained from mouse injectates which show two protein bands that bind activity. This may perhaps be attributable to different copper species being present *in vitro* and *in vivo*, showing varying affinities for the different serum proteins.

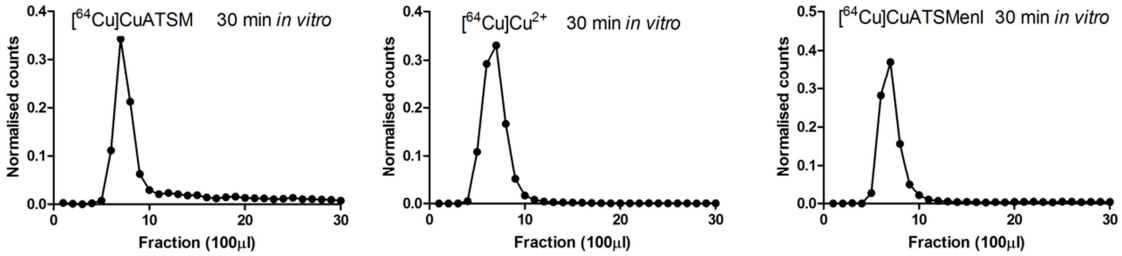

Figure 20 Sephadex G25 column elution profiles of mouse serum incubated at 37°C with [^{64}Cu]CuATSM, [^{64}Cu]Cu^{2+} or [^{64}Cu]CuATSMenI at 30 min post incubation.

5.6.4 Analysis by ethanol precipitation

In the gel filtration experiments, all activity was protein bound. Earlier investigations in our group showed that when using the ethanol precipitation method with serum samples from *in vitro* incubation (5.6.2), intact ^{64}Cu-copper complex is recoverable in the solvent extract. Hence the gel filtration results were complemented with analysis by ethanol precipitation of the serum protein fraction to determine the amount of tightly, protein bound activity in the serum and to identify the nature of any extractable activity *via* radio-TLC. Additionally, it was hoped that including the orthogonally labelled [^{123}I]CuATSMenI would yield information on the nature of the protein bound activity.

Following injection of the [^{64}Cu]Cu^{2+}, [^{64}Cu]CuATSM or [^{64}Cu/^{123}I]CuATSMenI, the serum section was separated from the mouse blood as for the gel filtrations and subjected to ethanol precipitation. Figure 21 (left) depicts the percentage of ^{64}Cu or ^{123}I activity bound to serum plasma at different times p.i. following ethanol precipitation and separation of the protein pellet and supernatant. For [^{64}Cu]CuATSM and [^{64}Cu]CuATSMenI, 48% and 45% of the activity is bound to the protein and not extracted into ethanol at the first time-point. This increases to ~70% at 120 min. Serum of mice injected with [^{64}Cu]Cu^{2+} exhibited similar behaviour, but with around ~10% higher protein binding than the copper complexes. The observed differences between [^{64}Cu]CuATSM, [^{64}Cu]CuATSMenI and [^{64}Cu]Cu^{2+} were not statistically significant at 5-15 min ($p > 0.05$).

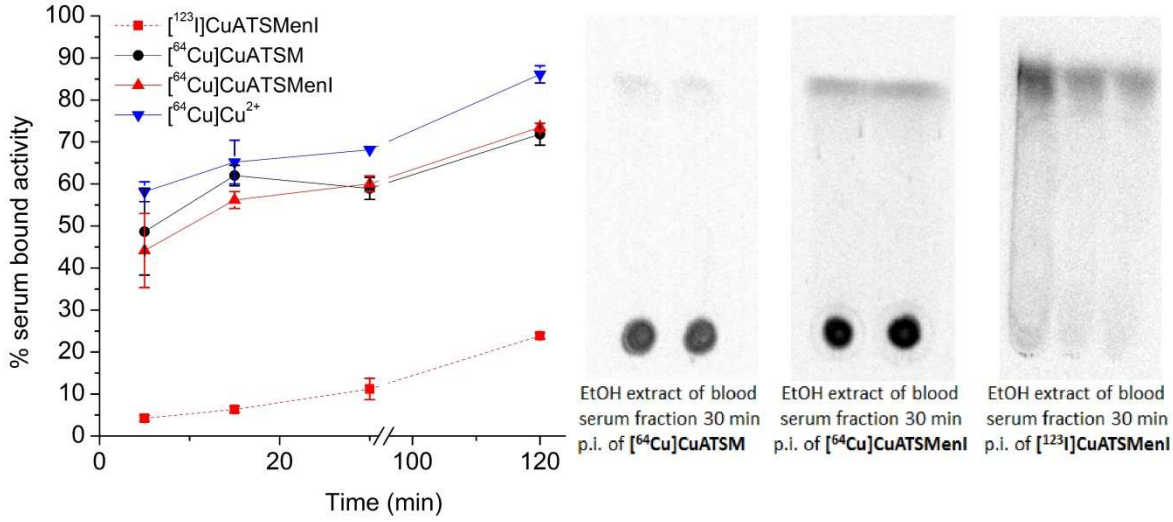

Figure 21 (left) percentage of activity remaining bound to serum proteins after precipitation and extraction with EtOH of serum plasma from in *vivo blood* samples (right) radio-TLC (95:5 EtOAc/MeOH) of ethanol phase of [^{64}Cu/^{123}I]CuATSMenI and [^{64}Cu]CuATSM at 30 min p.i.

In contrast, the orthogonally labelled [^{123}I]CuATSMenI shows much lower binding of activity than its ^{64}Cu-labelled counterpart. Binding only increased from 5-20% over the course of the measurement and was significantly lower than for all the ^{64}Cu species ($p < 0.0001$).

The ethanolic phases were analysed by radio-TLC to determine the nature of the non-bound species. Figure 21 (right) shows representative radio-TLCs for animals injected with [^{64}Cu]CuATSM, [^{64}Cu]CuATSMenI and [^{123}I]CuATSMenI at 30 min p.i. Radio-TLC shows that the extractable activity from serum plasma of mice injected with [^{64}Cu]CuATSMenI, [^{64}Cu]CuATSM and [^{64}Cu]Cu^{2+} is primarily in the form of [^{64}Cu]Cu^{2+} ($R_f = 0$).[1] Ethanol extracts from mice that received [^{123}I]CuATSMenI showed a lipophilic species with a radio-TLC and HPLC retention times corresponding to [^{123}I]CuATSMenI or [^{123}I]H_2ATSMenI (R_f = 0.70 and 0.73, respectively). Radio-TLC could not unambiguously distinguish between [^{123}I]CuATSMenI and [^{123}I]H_2ATSMenI, but no other products were observed that would indicate potential degradation of the ligand itself on this timescale. Hence, the contrasting results for [^{123}I]CuATSMenI with respect to [^{64}Cu]CuATSMenI suggest that the extractable species is [^{123}I]H_2ATSMenI. [^{64}Cu]CuATSM is structurally different to [^{64}Cu]CuATSMenI and Green *et al.* have demonstrated *in vitro* that serum binding of copper bis(thiosemicarbazonates) is highly structure dependent.[22-24]

[1] Cu^{2+} may be extracted into ethanol (ethanol precipitation method) but it does not partition into octanol (octanol extraction method).

Hence, direct extrapolation from the orthogonal pair results to [^{64}Cu]CuATSM may not seem prudent. However, as Figure 21 indicates, the overall quantity of [^{64}Cu]Cu^{2+} extractable from *in vivo* serum was comparable for [^{64}Cu]CuATSM, [^{64}Cu]CuATSMenI and [^{64}Cu]Cu^{2+}, suggesting similar behaviour of [^{64}Cu]CuATSM and [^{64}Cu]CuATSMenI compared to [^{64}Cu]Cu^{2+} *in vivo*. This is in contrast with the amount of radioactivity extracted following *in vivo* administration of [^{123}I]CuATSMenI, which was found to be considerably larger (76% at 120 min p.i.). Combined, the results strongly suggest that the protein-bound species *in vivo* is [^{64}Cu]Cu^{2+}.

As a control experiment, the speciation of [^{64}Cu]CuATSM and [^{64}Cu]CuATSMenI *in vitro* was examined, in order to compare if [^{64}Cu]CuATSMenI, [^{64}Cu]CuATSM (and [^{64}Cu]Cu^{2+}) would display similar behaviour to that previously observed in ethanol precipitation experiments. It was found that for [^{64}Cu]CuATSM and [^{64}Cu]CuATSMenI incubated in fresh serum *in vitro*, 10-15% of radioactivity was associated with precipitated protein after 0-2 h and not extracted into ethanol. This was in agreement with previous results for [^{64}Cu]CuATSM and related [^{64}Cu]Cu-BTSCs, where typically ~20% of activity was protein-bound.[8, 9] Radio-TLC confirmed that the ethanol extractable radioactivity contained only intact ^{64}Cu-complex, in agreement with previous *in vitro* findings (Figure 22 right).[8, 9] For [^{64}Cu]Cu^{+2}, 85-90% of activity was associated with precipitated protein at over the 2 h incubation.

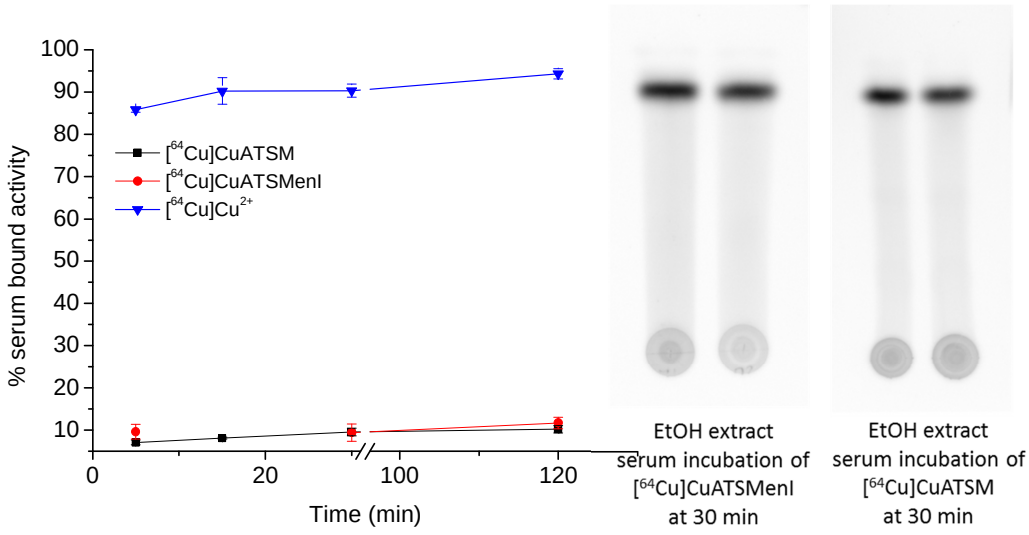

Figure 22 (left) Percentage of activity remaining bound to serum proteins after precipitation and extraction of serum plasma with EtOH (right) Radio-TLC (95:5 EtOAc/MeOH) of ethanol phase of [^{64}Cu]CuATSMenI and [^{64}Cu]CuATSM at 30 min post incubation in serum at 37°C.

Overall, the percentage of serum-bound activity *in vitro* was significantly lower for [^{64}Cu]CuATSM and [^{64}Cu]CuATSMenI than that observed for *in vivo* serum samples. The radio-TLCs of the ethanol extracts from *in vitro* serum incubations demonstrated that the extractable activity was in the form of intact ^{64}Cu-copper complex for both [^{64}Cu]CuATSM and [^{64}Cu]CuATSMenI. This is in contrast to the *in vivo* samples, where no intact compound was observed by radio-TLC. Overall, the amounts of extractable activity for [^{64}Cu]CuATSM and [^{64}Cu]CuATSMenI from *in vivo* blood are comparable to that extractable for [^{64}Cu]Cu^{2+} from both *in vitro* and *in vivo*, providing further evidence that the protein-bound species is copper ion and not intact complex.

5.6.5 Complex stability in blood *via* octanol extraction

Having examined the nature of the radioactivity in the serum fraction, we were further interested to quantify the proportion of intact ^{64}Cu-complex or ^{123}I-complex/ligand in the full blood following i.v. injection by using the previously reported octanol extraction method. It was anticipated that by including the orthogonally-labelled [^{123}I]CuATSMenI, further information on the integrity of the copper complex *in vivo* could be obtained.

Blood samples were obtained from mice sacrificed at various times p.i. and aliquots were immediately vortexed with octanol. The phases were separated by centrifugation and counted in a γ-counter. Radio-TLC controls confirmed that the octanol-extractable radioactivity was in the form of the intact ^{64}Cu-complex.[26, 28] Figure 23 shows the amount of octanol extractable activity at various time-points p.i. Two animals were sacrificed per time-point.

At 5 min p.i. of [^{64}Cu]CuATSM, only 23% of the remaining blood radioactivity was octanol-extractable. This decreased to 3% after 30 min p.i., which was comparable to the background extractable activity observed in mice injected with [^{64}Cu]Cu^{2+} ($p > 0.05$). The values were slightly higher for [^{64}Cu]CuATSMenI, with approximately 35% extractable at 5 min and 15 % from 30-120 min, suggesting a slightly higher stability of [^{64}Cu]CuATSMenI compared to the parent compound. This could also relate to the observed differences in kinetics of liver uptake in section 5.5.4.

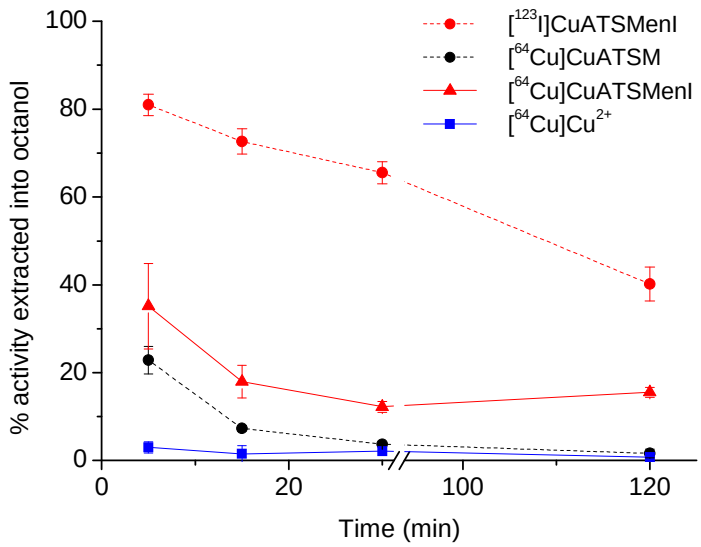

Figure 23 Percentage of octanol extractable activity (w.r.t. the total blood activity) as a function of time

The amount of [^{64}Cu]CuATSM recovered was even lower than that reported for the canine metabolism results from Lewis *et al.* at <15 min (no data available at later time-points), but a direct comparison may be hampered by the differences between canine and murine metabolism. For [^{64}Cu]CuATSMenI, the amount of recoverable activity is slightly higher and remains constant at ~15% from 30 min onwards.

In contrast to the ^{64}Cu-labelled complexes, a significantly larger proportion of activity is extractable for [^{123}I]CuATSMenI, where > 40% of activity was recovered up to 120 min.

Radio-TLC of the octanol extract from [^{123}I]CuATSMenI injected animals was less conclusive than that of the ^{64}Cu-labelled complexes due to the low signals obtained. Despite incubation on super resolution phosphor screens and subsequent evaluation on a digital phosphor imaging autoradiography reader, only a light spot could be seen in the region for [^{123}I]CuATSMenI/H_2ATSMenI and R_f value determination was difficult. However, the chemical equivalence of [^{64}Cu]CuATSMenI and [^{123}I]CuATSMenI and their differing quantitative octanol extraction results corroborate findings from the radio-TLCs of the serum ethanol extracts.

As a control, [^{64}Cu]CuATSMenI, [^{64}Cu]CuATSM and [^{64}Cu]Cu^{2+} were also incubated in fresh mouse blood *in vitro* at 37°C to determine whether the observed decomposition occurred in the bloodpool or whether it resulted from *in vivo* processing.

As can be seen from Figure 24, *in vitro* incubation did not cause a rapid decrease in the amount of octanol extractable activity. Up to 55% and 68% of the intact copper complex were still extractable after 120 min post incubation. Since *in vitro* blood incubation of [^{64}Cu]CuATSM and [^{64}Cu]CuATSMenI did not cause a rapid decrease in the amount of extractable activity, in contrast to what was observed *in vivo*, degradation is likely resulting from *in vivo* decomplexation and Cu sequestration.

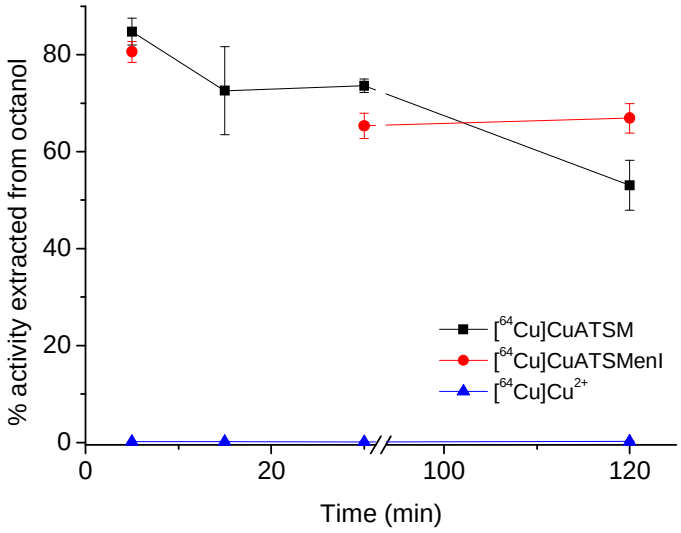

Figure 24 Percentage of octanol extractable activity over time for [^{64}Cu]CuATSM, [^{64}Cu]CuATSMenI and [^{64}Cu]Cu^{2+} following incubation in mouse blood *in vitro*.

5.6.6 Discussion of stability studies

The stability studies further support results from organ dose measurements and kinetics analysis. The fast blood clearance of activity following [^{64}Cu]CuATSM or [^{64}Cu]CuATSMenI injection (~1% at 1h p.i.) and the rapid degradation are contrasted by the dynamic PET imaging data which illustrates that tumour uptake of activity continues much longer (~100 min p.i.) than the suspected *in vivo* life-time of the complex. Taken together, these data suggest that circulating ^{64}Cu available for tumour uptake may not be present as intact ^{64}Cu-copper bis(thiosemicarbazonato) complex, but rather as serum-bound [^{64}Cu]Cu^{2+}.

Stability studies of copper chelators in the literature demonstrated that the main proteins able to transchelate and bind copper ions *in vivo* are serum albumin, transcuprein and superoxide dismutase.[29, 30] Several copper transporters and copper binding proteins are abundant in hepatocytes, epithelial kidney cells and erythrocytes and copper ions are bound by albumin and

transcuprein when passed on into the portal blood.[31] Further, detailed experiments are needed to determine the nature of any demetallation processes *in vivo* that may target [^{64}Cu]CuATSM and cause its decomposition. Furthermore, analysis of the copper binding proteins in the blood and their passage into tumour tissue may be of interest.

5.7 Correlation between activity distribution and tissue hypoxia for [^{64}Cu]CuATSM and [^{64}Cu]Cu^{2+}

The stability studies together with the similar *in vivo* profiles of [^{64}Cu]CuATSM and [^{64}Cu]Cu^{2+} and their oxygen dependent tumour retention all corroborated the hypothesis that circulating [^{64}Cu]Cu^{2+} is responsible for tumour uptake.

We wished to gain further information on the nature of tumour uptake by comparing the spatial distribution of activity in the tumour following injection of [^{64}Cu]Cu^{2+} and [^{64}Cu]CuATSM. In particular, it was of interest to know whether [^{64}Cu]Cu^{2+} uptake would correlate with regional tissue hypoxia in tumour sections as determined by the immunohistochemical markers of hypoxia.

As discussed in Chapter 3.3, for specific tumour lines such as 9L and R3327AT in rats, the correlation of ^{64}Cu with EF5 staining following [^{64}Cu]CuATSM administration has been observed to increase at later time points (16-20 h).[32, 33] Other studies found good correlation in R3230Ac and 9L tumours but not in FSA tumours between regional activity uptake from [^{64}Cu]CuATSM administration and immunohistochemical EF5 staining.[34] Therefore, analysis was performed on tumours excised at both 2 and 16 h p.i.

5.7.1 Biodistributions of [^{64}Cu]CuATSM and [^{64}Cu]Cu^{2+} at 2 and 16 h p.i.

Initially, we compared the biodistribution profiles of [^{64}Cu]CuATSM and [^{64}Cu]Cu^{2+} for mice dissected at 2 h and 16 h p.i. Figure 25 depicts decay corrected organ dose measurements and tumour-to-muscle ratios. Tumour uptake was slightly but significantly lower at 16 h than at 2 h for both [^{64}Cu]CuATSM (RTM = 6.5±0.6 versus 7.35±1.13) and [^{64}Cu]Cu^{2+} (RTM = 5.9±0.5 versus 9.93±0.79) ($p < 0.0001$).

%ID/g values in liver and lungs were also lower for both compounds at the later time-point ($p < 0.0001$). Interestingly, there was a statistically significant difference in blood activity for [^{64}Cu]CuATSM at 2 h and 16 h ($p < 0.0003$) but no differences for [^{64}Cu]Cu^{2+} ($p = 0.3946$).

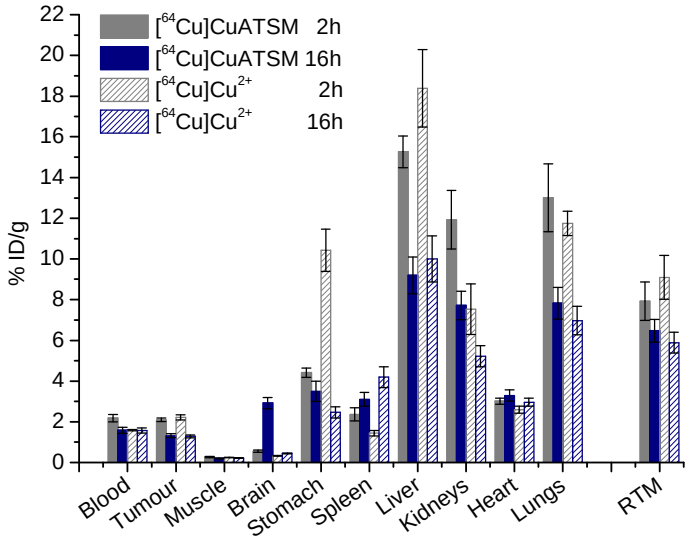

Figure 25 Comparison of biodistribution (%ID/g ±SD) of [^{64}Cu]CuATSM and [^{64}Cu]Cu^{2+} in female CBA mice bearing CaNT xenografts at 2 and 16 h p.i, n = 4 for [^{64}Cu]CuATSM and [^{64}Cu]Cu^{2+}. Animals were awake and breathing air.

5.7.2 Autoradiography and immunohistochemical staining

Autoradiography and immunohistochemical staining was performed by Dr Veerle Kersemans, Dr Bart Cornelissen or Miss Kamila Hussien.

Autoradiography and EF5 immunofluorescence microscopy images were obtained on tumours excised at 2 h and 16 h p.i. for animals administered with [^{64}Cu]CuATSM and [^{64}Cu]Cu^{2+}. Results were compared to data obtained for [^{18}F]FMISO (2 h p.i.) as a control. For this purpose, animals were injected with 10 mM EF5 10 mM intravenously 2 h 30 s, respectively, before being sacrificed. The tumours were resected and immediately placed on dry ice. Autoradiography on 8 µm slices was performed using digital phosphor imaging (Cyclone, PerkinElmer) before the same tumour slice was used for immunohistochemistry. Figure 26 depicts representative autoradiographs of the activity distribution and EF5 immunofluorescence images recorded on the same slice for [^{18}F]FMISO at 2 h p.i. and [^{64}Cu]Cu^{2+} excised at 16 h p.i. EF5 staining confirms that the tumours contain hypoxic regions in both cases.

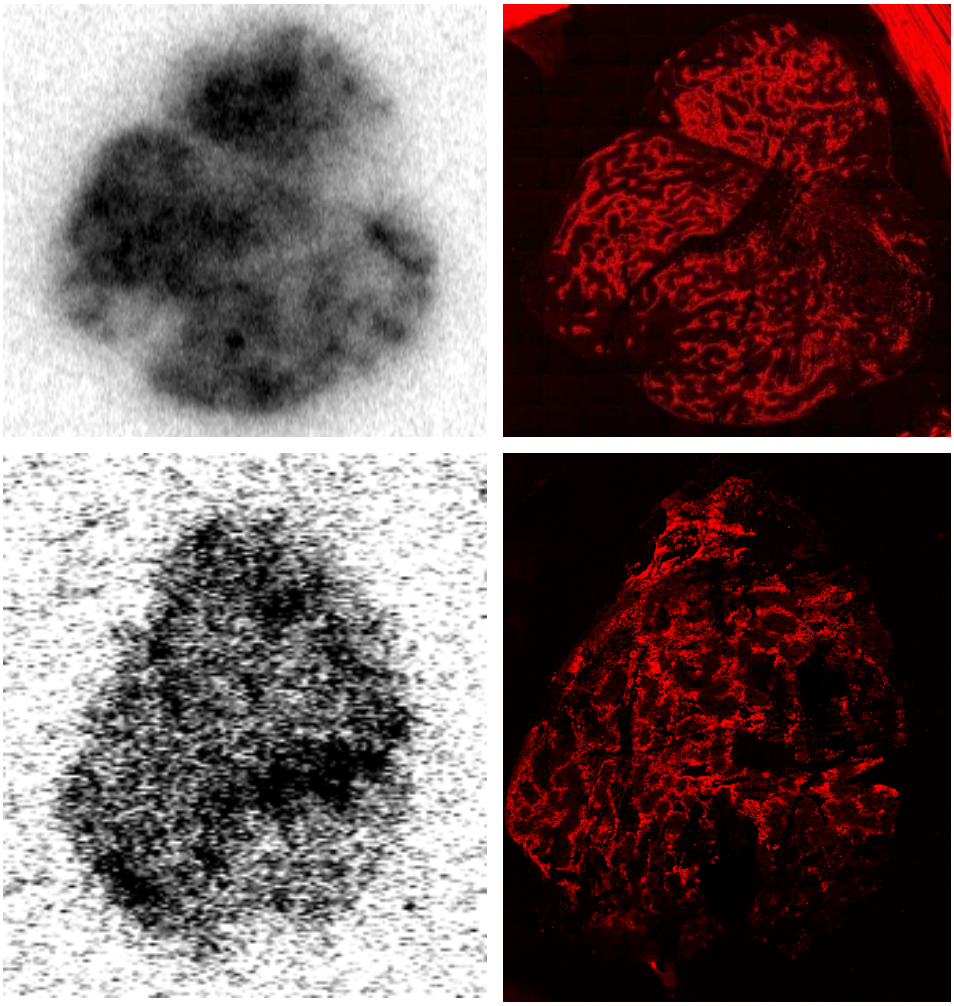

Figure 26 (top, left) autoradiograph of tumour slice showing intratumoural [^{18}F]FMISO distribution at 2 h p.i. (dark = high counts, light = low counts) (right) corresponding EF5 associated immunofluorescence in same slice (bottom, left) autoradiograph of tumour slice showing intratumoural [^{64}Cu]Cu^{2+} distribution at 16 h p.i. (right) EF5 associated immunofluorescence in same tumour slice.

From visual analysis, it appears there is good correlation between the activity distribution for [^{18}F]FMISO and EF5. For [^{64}Cu]Cu^{2+} in contrast it appears from visual analysis that there is no strong spatial correlation between the regions of hypoxia and ^{64}Cu activity distribution. This was similarly the case for [^{64}Cu]CuATSM at 2 h and 16 h p.i. and [^{64}Cu]Cu^{2+} at 2 h p.i. (see Appendix).

5.7.3 Correlation coefficients

Since visual inspection is prone to bias, the spatial correlation of activity from [^{64}Cu]CuATSM, [^{64}Cu]Cu^{2+} and [^{18}F]FMISO with EF5 distribution was quantified by co-registering the autoradiography and fluorescence microscopy images and obtaining correlation coefficients (r). Correlation coefficients (r) were obtained for semi-quantitative assessment of ^{64}Cu and EF5 correlation, using the JACoP plug-in for image J. For this purpose, autoradiography and fluorescence microscopy images were co-registered in a Matlab interface, custom-written by Dr Danny Allen as described in the experimental. The tumour regions were cropped before analysis to exclude the Pap-pen and folded regions. Figure 27 shows the results of the correlation analysis.

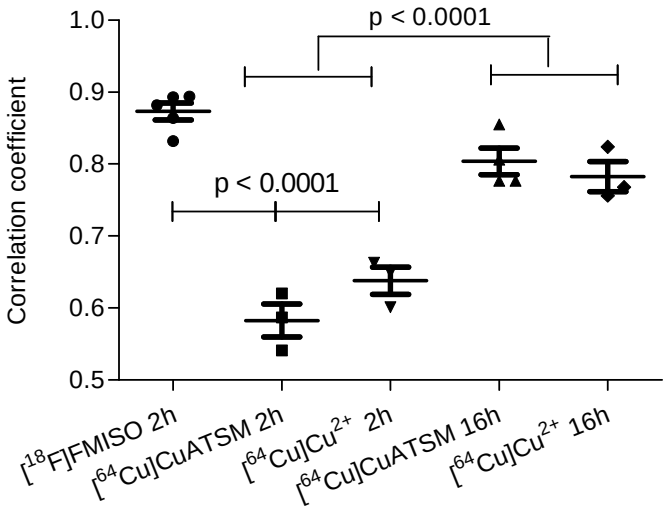

Figure 27 Correlation coefficients describing spatial correlation between autoradiography and EF5 immunofluorescence in tumours excised 2 h or 16 h p.i.

As expected, a significant positive correlation was found between [^{18}F]FMISO and EF5 at 2 h p.i. Little or no spatial correlation between ^{64}Cu distribution and zones of hypoxia, as defined by EF5 immunohistochemistry, was apparent for either [^{64}Cu]CuATSM or [^{64}Cu]Cu^{2+} at 2 h p.i. In contrast, a much higher correlation was found for both [^{64}Cu]CuATSM and [^{64}Cu]Cu^{2+} at 16 h p.i.

5.8 Discussion

Work in this chapter has used the orthogonally labelled probes [^{64}Cu]CuATSMenI and [^{123}I]CuATSMenI to gain further insights into the mechanism of hypoxia selectivity of copper bis(thiosemicarbazonates) and in particular, the ultimate fate of the ligand. Whilst [^{64}Cu]CuATSMenI demonstrated *in vitro* hypoxia selectivity, [^{123}I]CuATSMenI and the labelled ligand [^{123}I]H_2ATSMenI were retained by equal amounts in a non-oxygen dependent manner. This translated to *in vivo*, where similar biodistribution profiles for [^{123}I]CuATSMenI and [^{123}I]H_2ATSMen revealed that the ligand is not retained in the same manner as the ^{64}Cu. Further *in vivo* controls contrasting [^{64}Cu]CuATSM and [^{64}Cu]CuATSMenI to the [^{64}Cu]Cu^{2+} salt demonstrated comparable tumour retention, kinetics of uptake and biodistribution for the radiometal and the labelled complexes. Repeats in EMT6 tumours provided first evidence that this was not a tumour-line dependent phenomenon.

The overall similar *in vivo* behaviour of [^{64}Cu]Cu^{2+} and [^{64}Cu]CuATSM raised concerns about the *in vivo* stability of [^{64}Cu]CuATSM. These were further corroborated by serum binding and stability analysis which indicated that CuATSM undergoes rapid demetallation within a few minutes after i.v. injection. Time-activity curves for [^{64}Cu]Cu^{2+} and [^{64}Cu]CuATSM were similar and tumour uptake continued at time-points where demetallation and stability studies indicated little or no intact Cu-complex in the blood. Hence ^{64}Cu uptake in hypoxic tumours, or at least a large proportion of it, may be due to [^{64}Cu]Cu^{2+} and not [^{64}Cu]CuATSM.

An unexplained aspect of the results obtained is the contrasting uptake of [^{64}Cu]Cu^{2+} *in vitro* and *in vivo*. The metal ion did not show large hypoxic/normoxic differentials in the cell lines *in vitro*. However, the oxygen dependence may be masked by the overall small retention levels. The reasons for these observations are not clear, but the results indicate that direct correlation between *in vitro* and *in vivo* experimentation is therefore not always possible as important differences were observed between the two situations. For instance, copper ions in the blood are not present in their free form *in vivo* but bound to plasma proteins.[35, 36] The *in vitro* cellular retention measurements were obtained under conditions previously employed to allow comparison with other literature

data. Under these conditions, serum albumin concentration in the medium is only 1%, but the level of plasma proteins is significantly higher *in vivo*. A recent review summarising copper transport by hCTr1 points out that *in vitro* results vary widely and immortalised cell lines may respond differently to cells in living tissues.[35] As discussed in the introduction, authors who observed cell and tumour line dependent differences of activity uptake from [^{64}Cu]CuATSM administration have already raised concerns whether the cellular metabolism of copper, in particular the involvement of copper transporters, may be responsible for some of the discrepancies observed.

Another remarkable aspect of the results is the oxygen dependence of [^{64}Cu]CuATSM and [^{64}Cu]Cu^{2+} uptake at 2 h p.i., despite no apparent direct spatial correlation with immunohistochemically hypoxic areas as defined by EF5. It thus appears that the changes in ^{64}Cu retention with oxygen concentration are occurring in non-hypoxic tumour tissue. Indeed, literature accounts on [^{64}Cu]CuATSM present varying results for spatial distribution of activity with immunohistochemical hypoxia (see Chapter 3). The results for our murine models suggest that it may be possible that either part -or all- of the oxygen dependent ^{64}Cu-retention in the tumour following intravenous injection of [^{64}Cu]CuATSM is the result of changes in cellular processing of copper in tumour tissue, mediated by the hypoxic regions in the tumour, rather than purely reflecting the oxygenation status of the tumour.

The influence of hypoxia on the tumour microenvironment however is complex. Work by White *et al.* has shown that hypoxia was able to cause increased copper uptake and Ctr1 transporter expression in macrophages.[37] Overall however, comparatively little is known on the direct influence of tumour hypoxia on copper homeostasis and at this stage, the detailed mechanism of action by which Cu is retained in both hypoxic and non-hypoxic tumor tissues is not established. Collectively, the data suggest that the currently proposed redox trapping mechanism might not provide a complete picture as dismantling of the complex before cell entrance can liberate Cu prior to tumour uptake.

Moreover the results emphasise the importance of determining the identity of radiolabelled compounds post-administration *in vivo* in order to understand fully the factors governing

biodistribution and tumour uptake, thereby facilitating the design of higher performance biomarkers.

5.9 Conclusion

In order to examine the mode of action of biomarkers belonging to the [^{64}Cu]CuATSM family, the copper metal and the ligand were followed *in vitro* and *in vivo* using a pair of [^{123}I/^{64}Cu]-copper bis(thiosemicarbazonates), radiolabelled at the *metal* or at the *ligand*, alongside the labelled proligand, the [^{64}Cu]Cu^{2+} salt and the parent [^{64}Cu]CuATSM. *In vitro* cell studies, *in vivo* biodistribution and PET/SPECT imaging of the complexes and their components in mouse tumour models indicated that the labelled ligand is not retained in an oxygen dependent manner. This rules out the possibility of using ^{18}F- or ^{123}I-radiolabelled Cu-BTSCs as possible hypoxia selective biomarkers. [^{64}Cu]CuATSM and [^{64}Cu]Cu^{2+} demonstrated remarkably similar *in vivo* profiles. Stability studies suggested that the similar behaviour of the complex and the metal are caused by rapid demetallation of the bis(thiosemicarbazone) complex *in vivo*.

The results present new mechanistic insight in the field of hypoxia imaging using CuATSM. The results also unveil the possibility of investigating the directly available simple [^{64}Cu]Cu^{2+} salt as a hypoxia selective radiotracer.

Clinical studies clearly demonstrate a positive correlation between high ^{64}Cu uptake of activity and poor prognosis following PET imaging with [^{64}Cu]CuATSM. However, further experiments are needed to determine the underlining biochemical basis for increased retention of radiocopper in hypoxic tumours.

5.10 References for Chapter 5

1. M. Nogawa, T. Yuasa, S. Kimura, J. Kuroda, K. Sato, H. Segawa, A. Yokota and T. Maekawa, *Cancer Lett.*, 2005, **217**, 243-253.
2. H. B. Hewitt, E. Blake and E. H. Proter, *Br. J. Cancer*, 1973, **28**, 123-135.
3. MACS and M. Biotec, *The gentleMACS Dissociator- Preparation of single cell suspensions from implanted mouse tumours*, Accessed 21st February, 2011, 2011.
4. J. S. Lewis, D. W. McCarthy, T. J. McCarthy, Y. Fujibayashi and M. J. Welch, *J. Nucl. Med.*, 1999, **40**, 177-183.
5. J. L. J. Dearling, J. S. Lewis, G. E. D. Mullen, M. J. Welch and P. J. Blower, *J. Biol. Inorg. Chem.*, 2002, **7**, 249-259.
6. A. J. Franko, *Radiat. Res.*, 1985, **103**, 89-97.
7. J. E. Moulder and S. Rockwell, *Int. J. Radiat. Oncol. Biol. Phys.*, 1984, **10**, 695-712.
8. S. R. Bayly, R. C. King, D. J. Honess, P. J. Barnard, H. M. Betts, J. P. Holland, R. Hueting, P. D. Bonnitcha, J. R. Dilworth, F. I. Aigbirhio and M. Christlieb, *J. Nucl. Med.*, 2008, **49**, 1862-1868.
9. P. D. Bonnitcha, A. L. Vavere, J. S. Lewis and J. R. Dilworth, *J. Med. Chem.*, 2008, **51**, 2985-2991.
10. L. Carroll, R. Bejot, R. Hueting, R. King, P. Bonnitcha, S. Bayly, M. Christlieb, J. R. Dilworth, A. D. Gee, J. Declerck and V. Gouverneur, *Chem. Commun.*, 2010, **46**, 4052-4054.
11. J. L. J. Dearling, J. S. Lewis, G. E. D. Mullen, M. T. Rae, J. Zweit and P. J. Blower, *Eur. J. Nucl. Med.*, 1998, **25**, 788-792.
12. P. Burgman, J. A. O'Donoghue, J. S. Lewis, M. J. Welch, J. L. Humm and C. C. Ling, *Nucl. Med. Biol.*, 2005, **32**, 623-630.
13. J. S. Lewis, T. L. Sharp, R. Laforest, Y. Fujibayashi and M. J. Welch, *J. Nucl. Med.*, 2001, **42**, 655-661.
14. V. Kersemans, R. Huting, P. Allen, J. Dilworth, V. Gouverneur and S. Smart, *Society of Nuclear Medicine Annual Meeting Abstracts*, 2010, **51**, 1184.
15. V. Kersemans, R. Hueting, B. Cornelissen, K. Hussien, P. Allen, N. Falzone, J. Dilworth, V. Gouverneur, R. Muschel and S. Smart, *Society of Nuclear Medicine Annual Meeting Abstracts*, 2011, **52**, 241.
16. A. R. Jalilian, N. Rostampour, P. Rowshanfarzad, K. Shafaii, M. Kamali-Dehghan and M. Akhlaghi, *Acta Pharm.*, 2009, **59**, 45-55.
17. F. Peng, X. Lu, J. Janisse, O. Muzik and A. F. Shields, *J. Nucl. Med.*, 2006, **47**, 1649-1652.
18. V. Kersemans, manuscript in preparation
19. J. Lee, D. W. Siemann, C. J. Koch and E. M. Lord, *Int. J. Cancer*, 1996, **67**, 372-378.
20. J. S. Lewis, J. L. Dearling, J. K. Sosabowski, J. Zweit, P. Carnochan, L. R. Kelland, H. M. Coley and P. J. Blower, *Eur. J. Nucl. Med.*, 2000, **27**, 638-646.
21. P. McQuade, K. E. Martin, T. C. Castle, M. J. Went, P. J. Blower, M. J. Welch and J. S. Lewis, *Nucl. Med. Biol.*, 2005, **32**, 147-156.
22. N. E. Basken, C. J. Mathias, A. E. Lipka and M. A. Green, *Nucl. Med. Biol.*, 2008, **35**, 281-286.
23. N. E. Basken and M. A. Green, *Nucl. Med. Biol.*, 2009, **36**, 495-504.
24. N. E. Basken, C. J. Mathias and M. A. Green, *J. Pharm. Sci.*, 2009, **98**, 2170-2179.
25. A. P. Biotech, *Protein Purification Handbook*, Accessed 16.03.2011, 2011.
26. C. J. Mathias, S. R. Bergmann and M. A. Green, *Nucl. Med. Biol.*, 1993, **20**, 343-349.
27. P. Herrero, J. Markham, C. J. Weinheimer, C. J. Anderson, M. J. Welch, M. A. Green and S. R. Bergmann, *Circulation*, 1993, **87**, 173-183.
28. S. Lewis Jason, P. Herrero, L. Sharp Terry, A. Engelbach John, Y. Fujibayashi, R. Laforest, A. Kovacs, J. Gropler Robert and J. Welch Michael, *J. Nucl. Med.*, 2002, **43**, 1557-1569.
29. L. A. Bass, M. Wang, M. J. Welch and C. J. Anderson, *Bioconjugate Chem.*, 2000, **11**, 527-532.

30. C. A. Boswell, X. Sun, W. Niu, G. R. Weisman, E. H. Wong, A. L. Rheingold and C. J. Anderson, *J. Med. Chem.*, 2004, **47**, 1465-1474.
31. G. Crisponi, V. M. Nurchi, D. Fanni, C. Gerosa, S. Nemolato and G. Faa, *Coord. Chem. Rev.*, 2010, **254**, 876-889.
32. J. A. O'Donoghue, P. Zanzonico, A. Pugachev, B. Wen, P. Smith-Jones, S. Cai, E. Burnazi, R. D. Finn, P. Burgman, S. Ruan, J. S. Lewis, M. J. Welch, C. C. Ling and J. L. Humm, *Int. J. Radiat. Oncol., Biol., Phys.*, 2005, **61**, 1493-1502.
33. C. S. Dence, D. E. Ponde, M. J. Welch and J. S. Lewis, *Nucl. Med. Biol.*, 2008, **35**, 713-720.
34. H. Yuan, T. Schroeder, J. E. Bowsher, L. W. Hedlund, T. Wong and M. W. Dewhirst, *J. Nucl. Med.*, 2006, **47**, 989-998.
35. E. B. Maryon, S. A. Molloy, A. M. Zimnicka and J. H. Kaplan, *BioMetals*, 2007, **20**, 355-364.
36. M. C. Linder, L. Wooten, P. Cerveza, S. Cotton, R. Shulze and N. Lomeli, *Am. J. Clin. Nutr.*, 1998, **67**, 965S-971S.
37. C. White, T. Kambe, Y. G. Fulcher, S. W. Sachdev, A. I. Bush, K. Fritsche, J. Lee, T. P. Quinn and M. J. Petris, *J. Cell Sci.*, 2009, **122**, 1315-1321.

Chapter 6

Experimental Details

6.1 General Instrumentation

Chemicals were obtained from Acros, Aldrich, Alfa Aesar, Apollo Scientific or Bachem unless otherwise stated. All solvents used were HPLC grade. TLC, where applicable, was performed on pre-coated aluminium-backed plates (Merck Kieselgel) and spots were made visible by quenching of UV fluorescence (λ = 254 nm) and/or by staining with potassium permanganate. Flash chromatography was performed according to the method by Still, using silica gel (0.040-0.063 mm; Merck) and air pressure.

NMR spectra were recorded on a Varian Mercury VX300, Bruker DPX 400, AV400 or a Bruker AVANCE AVC500 at frequencies of 300, 400 and 500 MHz for ^{1}H and 75.5, 100 and 126 MHz for ^{13}C respectively, using residual solvent peaks as internal reference.[1]

Nominal mass spectra *(m/z)* were recorded on a Fisons Platform II, under the conditions of positive or negative electrospray ionization (ESI-MS). High resolution mass spectra (HRMS) were recorded by Mr Colin Sparrow or Mr Robin Proctor under ESI conditions on a BrukerMicroTOF (resolution = 5000 FWHM). The lock masses used for calibration were tetraoctylammonium bromide and sodium dodecyl sulphate in positive and negative ion mode respectively.

Elemental analysis of solid compounds for C, H, N was obtained by the microanalysis service of the Inorganic Chemistry Laboratory at the University of Oxford or by Mr Stephen Boyer, London Metropolitan University. Where elementals are not reported, these were Zn or Cu compounds showing consistently low C and N values, indicative of the presence of H_2O. Single peak HPLC traces and high resolution mass spectrometry were obtained for these compounds.

Cyclic voltammetry measurements were performed on a CH Instruments electrochemical analyser, running CHI600A analysis software. Solutions were prepared in anhydrous, deoxygenated DMF, using 0.1M $[NBu_4][BF_4]$ as electrolyte. A platinum disc working electrode, platinum wire auxillary electrode and a silver wire pseudo-reference electrode were used. All potentials are reported relative to the saturated calomel reference electrode (SCE) and were corrected by adding ferrocene

to each experiment, using the reversible, one-electron oxidation of the Fc/Fc^+ couple ($E_{1/2}$ (SCE) = +0.53V in DMF at rt) as internal reference.[2, 3]

Electronic absorption spectroscopy (UV/Vis) was performed using a Perkin-Elmer Lambda 19 spectrometer, running UV Winlab software. Spectra were measured using 1.00 cm quartz cuvettes. Samples were run at a number of concentrations and extinction coefficients were calculated as the gradient of the plot of absorbance vs. concentration.

CW EPR experiments were performed on an X-band Bruker BioSpin GmbH EMX spectrometer equipped with a high sensitivity Bruker probehead and a low-temperature Oxford Instruments CF935 helium-flow cryostat. The magnetic field was calibrated at room temperature with an external 2,2 diphenyl-1-picrylhydrazyl standard (/g/ = 2.0036). X-band CW experiments were conducted at 60 K, with 0.20 mW microwave power, and 2.0 G modulation amplitude at 100 kHz.

Reverse-phase analytical HPLC spectra were recorded on a Gilson 322 instrument or a Dionex Ultimate 3000 system with a C-18 column (Grace Discovery Sciences, 250×4.6mm, 5µ) and UV/vis detection at 254 nm. Gradient methods were as follows:

Method $\mathbf{M_1}$. Solvent A = H_2O + 0.1 % TFA, solvent B = CH_3CN+ 0.1 % TFA, flow rate = 1 mL min^{-1}, gradient (min, % of B): 0, 5; 15, 95; 20, 95; 25, 5; 30, 5.

Method $\mathbf{M_2}$. Solvent A = H_2O, solvent B = CH_3CN, flow rate = 1 mL min^{-1}, gradient (min, % of B): 0, 5; 15, 95; 20, 95; 25, 5; 30, 5.

Reverse-phase radio-HPLC (analytical and preparative) was performed on a Gilson 322 Unipoint HPLC machine equipped with the above C-18 column, UV/vis detection at 254 nm and NaI/PMT detection. Gradient methods were as follows:

Method $\mathbf{RM_1}$. Solvent A = H_2O, solvent B = CH_3CN, flow rate = 1 mL min^{-1}, gradient (min, % of B): 0, 5; 10, 95; 15, 95; 18, 5; 20, 5.

Method **RM_2**. Solvent A = H_2O + 0.1% TFA, solvent B = CH_3CN + 0.1%TFA, flow rate = 1 mL min^{-1}, gradient (min, % of B): 0, 5; 10, 95; 15, 95; 18, 5; 20, 5.

Method **RM_3**. Solvent A = H_2O + 0.1% TFA, solvent B = CH_3CN, flow rate = 1 mL min^{-1}, gradient (min,% of B): 0, 5; 20, 95; 25, 95; 28, 5; 30, 5.

6.2 Radioisotopes

6.2.1 Copper-64

^{64}Cu was purchased from the Wolfson Brain Imaging Centre, Addenbrookes Hospital, Cambridge or from the PET Imaging Centre, St Thomas' Hospital, London, UK. Copper-64 was prepared using a biomedical cyclotron with a nickel-64 target and supplied as [^{64}Cu]$CuCl_2$(aq) in 0.1M HCl (1 GBq). An aqueous solution of copper-64 acetate, [^{64}Cu]$Cu(OAc)_2$, was prepared by diluting 0.2 mL of [^{64}Cu]$CuCl_{2(aq)}$ in 0.1 mol/L HCl with 0.2 mol/L sodium acetate (0.9 mL). This stock solution was used for the radiolabelling experiments.[4]

6.2.2 Fluorine-18

[^{18}F]Fluoride was produced by PETNET Solutions (Mont Vernon Hospital, UK) on a biomedical cyclotron via the $^{18}O(p,n)^{18}F$ reaction. [^{18}F]fluoride was delivered in [^{18}O]water (1-4 GBq, 1-4 mL). The solution was passed through a QMA anion exchange resin cartridge (20 mg, Waters) and [^{18}F]Fluoride was eluted off the charged resin with a solution of Kryptofix 222 (15 mg) and K_2CO_3 (3 mg) in 1 mL acetonitrile/water (8:2). Excess water was removed by azeotropically drying at 120°C under N_2 stream several times with 0.5 mL CH_3CN. The resulting dry complex of K[^{18}F]/Kryptofix 222 was dissolved in 2-4 mL anhydrous CH_3CN and dispensed into reaction vials containing the precursor for subsequent nucleophilic fluorination. Radiochemical yields reported for ^{18}F-fluorinations are non-decay-corrected.

6.2.3 Iodine-123

Non-carrier added $Na^{123}I$ (300 MBq in 0.05 M NaOH) was purchased from GE Healthcare (GE healthcare Limited, UK), typically supplied at a concentration > 500 mCi mL^{-1} with a specific activity of 8.78 $\times 10^{18}$ $Bqmol^{-1}$ and used as supplied.

6.3 Experimental Details for Chapter 2

General Procedure A: Coupling reactions of H_2ATSE/A with carboxylic acid linkers

H_2ATSE/A was suspended in the minimum amount of DMF. The carboxylic acid (1.1 eq), diisopropylethylamine (1.1 eq) and benzotriazole-1-yl-oxy-tris-(dimethylamino)-phosphonium hexafluorophosphate (BOP) (1.1 eq) were added and the mixture was stirred at room temperature for 4 h until a clear solution was formed. H_2O was then added until formation of a white precipitate. The suspension was sonicated, the precipitate collected by filtration and washed with copious amounts of H_2O, EtOH and, if solubility allowed, Et_2O.

General Procedure B: Copper complexation

The proligand and $CuCl_2$ (1.2 eq) or $Cu(OAc)_2 \cdot H_2O$ (1.2 eq) were stirred in a minimum amount of MeOH for 30 min at rt. The solvent was reduced *in vacuo* and H_2O was added. The solid formed was collected by filtration and washed with H_2O and, where solubility allowed, with a few drops of ice-cold Et_2O before being dried *in vacuo.*

6.3.1 Synthetic Chemistry

Diacetyl-2-(4-*N*-methyl-3-thiosemicarbazone) (2.01)[5]

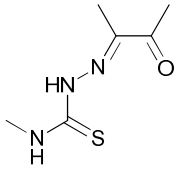

Diacetyl-2-(4-*N*-methyl-3-thiosemicarbazone) was prepared by adaptation of a previously reported procedure.[5] 2,3-Butanedione (4.5 mL, 39.9 mmol) was vigorously stirred in 200 mL of deionized water at 0 °C. 5 Drops of conc. HCl were added followed by the addition of 4-*N*-methyl-3-thiosemicarbazide (3.45 g, 32.8 mmol). A white precipitate quickly formed which after 1 h was collected by filtration, washed thoroughly

with H_2O (3 × 100 mL), dried on filter paper overnight and then dried *in vacuo* to yield the desired product as a white solid (5.19 g, 91%). ^{1}H NMR (300 MHz, DMSO-d_6): δ 10.64 (1H, s, C(=S)N*H*N=), 8.62 (1H, br m, MeN*H*C(=S), 3.05 (3H, d, *J* = 4.6 Hz, C*H*$_3$NH), 2.42 (3H, s, C*H*$_3$C=O), 1.96 (3H, s, C*H*$_3$C=N), ^{13}C NMR (300 MHz, DMSO-d_6): δ 197.5 *C*=O, 178.9 *C*=S, 145.5 *C*=N, 31.4 NH*C*H$_3$, 24.7 *C*H$_3$CO, 9.9 *C*H$_3$CN; LRMS (M-H)$^-$ *m/z* 172.0 (calc. for $C_6H_{10}N_3OS^-$ 172.0)

Diacetyl-2-(4-*N*-ethyl-3-thiosemicarbazone) (2.02)[5]

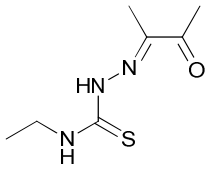

Diacetyl-2-(4-*N*-ethyl-3-thiosemicarbazone) was prepared in the same manner as **2.01**, using 2,3-butanedione (3.58 mL, 41.0 mmol) and 4-*N*-ethyl-3-thiosemicarbazide (4.00 g, 34.0 mmol) to afford the desired product as a white solid (5.59 g, 89%). ^{1}H NMR (200 MHz, DMSO-d_6): δ 10.57 (1H, s, C(=S)N*H*N=), 8.66 (1H, t, *J* = 5.6 Hz, CH$_3$CH$_2$N*H*C(=S)), 3.63 (2H, m, CH$_3$C*H*$_2$NH), 2.42 (3H, s, C*H*$_3$C=O), 1.96 (3H, s, C*H*$_3$C=N), 1.15 (3H, t, *J* = 7.0 Hz, C*H*$_3$CH$_2$NH); ^{13}C NMR (50.3 MHz, DMSO-d_6): δ 197.5 (*C*=O), 178.0 (*C*=S), 145.5 (*C*=N), 38.7 (NH*C*H$_2$), 24.7 (*C*H$_3$(C=O), 14.1 (CH$_2$*C*H$_3$), 10.02 (*C*H$_3$CN); LRMS (ESI$^-$): (M-H)$^-$ 186.1 (calc. for $C_7H_{12}N_3OS^-$ 186.1)

Diacetyl-2-(4-*N*-methyl-3-thiosemicarbazone)-3-(4-*N*-amino-3-thiosemicarbazone) (H_2ATSM/A) (2.03)[5]

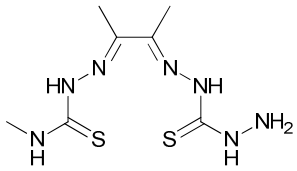

H_2ATSM/A was prepared by adaptation of a previously reported procedure.[5] Thiocarbohydrazide (1.50 g, 14.1 mmol) and 3 drops of conc. HCl were added to EtOH (80 mL) and the suspension was stirred at 40 °C. **2.01** (2.40 g, 13.9 mmol) was added portionwise over 2 h. After the final addition the reaction was heated to 50 °C for 5 hr, during which time a creamy white suspension formed in a clear yellow solution. The mixture was allowed to cool to 20 °C and the solid was collected by filtration, washed with EtOH (2 × 30 mL) and Et_2O (50 mL) before being dried *in vacuo* to afford the desired product as an off-white solid (2.80 g, 77%). ^{1}H NMR (300 MHz, DMSO-d_6): δ 10.23

(2H, s, NHC(S=)N*H*N=), 9.70 (1H, br s, N*H*NH_2), 8.36 (1H, br m, CH_3N*H*N(S=)), 4.96 (2H, s, NHN*H*$_2$), 3.01 (3H, d, *J* = 4.5 Hz, C*H*$_3$NH), 2.19 (3H, s, C*H*$_3$C=N), 2.18 (3H, s, C*H*$_3$C=N); ^{13}C NMR (50.32 MHz, DMSO-d_6) δ 178.4 (CH_3NH(*C*=S)), 175.8 (NH_2NH((*C*=S)); 148.4 (*C*=N); 148.1 (*C*=N); 31.2 ($NHCH_3$), 11.6 (2×*C*H3C=N); LRMS (ESI$^-$): $(M-H)^-$ 260.0 (calc. for $C_7H_{14}N_7S_2^-$ 260.1)

Diacetyl-2-(4-*N*-ethyl-3-thiosemicarbazone)-3-(4-*N*-amino-3-thiosemicarbazone) (H_2ATSE/A) (2.04)[5]

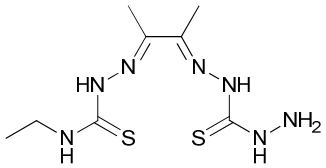

H_2ATSE/A was prepared in the same manner as **2.03** using thiocarbohydrazide (1.37 g, 12.9 mmol), diacetyl-2-(4-*N*-ethyl-3-thiosemicarbazone) (2.4 g, 12.8 mmol) and 3 drops of conc. HCl to afford H_2ATSE/A (3.40 g, 96%) as an off-white solid. ^{1}H NMR (200 MHz, DMSO-*d*$_6$): δ 10.21 (1H, s, NH(C=S)N*H*N=), 10.14 (1H, s, NHC(=S)N*H*N=), 9.70 (1H, br s, N*H*NH_2), 8.40 (1H, t, *J* = 5.9 Hz, CH_3 CH_2N*H*), 4.96 (2H, s, NHN*H*$_2$), 4.59 (2H, m, CH_3C*H*$_2$NH), 2.18 (6H, *two overlapping singlets*, C*H*$_3$C=N), 1.14 (3H, t, *J* = 7.1 Hz, C*H*$_3$$CH_2$NH); ^{13}C NMR (50.32 MHz, DMSO-d_6) δ 177.4 (CH_3NH(*C*=S)), 175.9 (NH_2NH((*C*=S)); 148.4 (*C*=N); 148.1 (*C*=N); 38.5 (CH_3*C*H_2NH), 14.4 (*C*H_3*C*H_2NH), 11.6 (2×*C*H3C=N); LRMS (M-H$^-$) *m/z* 274.1 (calc. for $C_8H_{16}N_7S_2^-$ 274.1), HPLC (M_1) R_t = 8.65 min

Diacetyl-2-(4-*N*-methyl-3-thiosemicarbazonato)-3-(4-*N*-amino-3-thiosemicarbazonato) zinc(II) (ZnATSM/A) (2.05)[5]

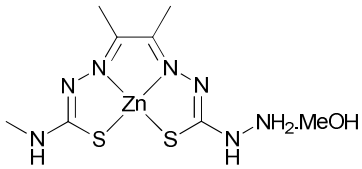

ZnATSM/A was prepared according to a previously reported procedure. H_2ATSM/A (1.90g, 7.3 mmol) was suspended in MeOH (80 mL), $Zn(OAc)_2{\cdot}2H_2O$ (1.91g, 8.7 mmol) was added and the mixture was heated to reflux for 4 h. After cooling, an orange precipitate formed which was isolated by filtration, washed with MeOH (50 mL) and Et_2O (100 mL) and dried *in vacuo* to afford the desired product as an orange solid (2.08g, 80%). ^{1}H NMR (200 MHz, DMSO-*d*$_6$): δ 8.25 (1H, s, N*H*NH_2); 7.23 (1H, br s, CH3N*H*), 4.55 (2H, s, NHN*H*$_2$), 2.82 (3H, d, *J* = 4.5 Hz, C*H*$_3$NH); 2.23

(3H, s, C*H*$_3$C=N); 2.21 (3H, s, C*H*$_3$C=N); ^{13}C NMR (50.32 MHz, DMSO-d$_6$) δ 177.5 (CH3NH*C*=S), 177.3 (NH$_2$NH*C*=S); 146.4 (*C*=N); 146.0 (*C*=N); 48.60 (*C*H$_3$OH coordinating MeOH); 29.3 (*C*H$_3$NH); 14.0 (*C*H3C=N); 13.9 (*C*H$_3$C=N); LRMS (M-H$^-$) *m/z* 322.0 (calc. for $C_7H_{12}N_7S_2Zn^-$ 322.0)

Diacetyl-2-(4-*N*-ethyl-3-thiosemicarbazonato)-3-(4-*N*-amino-3-thiosemicarbazonato) zinc(II) (ZnATSE/A) (2.06)[5]

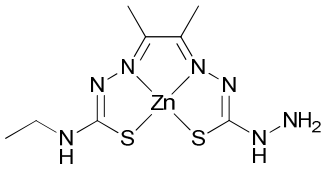

ZnATSE/A was prepared in the same manner as ZnATSM/A, using H$_2$ATSE /A (2.00g, 7.3 mmol) and Zn(OAc)$_2$·2H$_2$O (1.91g, 8.7 mmol) in MeOH (80 mL) to afford the desired product as a yellow solid (2.2 g, 88 %). ^{1}H NMR (300MHz, DMSO-*d*$_6$): δ 8.22 (1H, s, N*H*NH$_2$); 7.28 (1H, br s, CH$_3$CH$_2$N*H*), 4.55 (2H, s, NHN*H*$_2$), 3.36 (3H, m, CH$_3$C*H*$_2$NH, obscured by residual H$_2$O), 2.22 (3H, s, C*H*$_3$C=N), 2.19 (3H, s, C*H*$_3$C=N), 1.10 (3H, t, *J* = 7.2 Hz, C*H*$_3$CH$_2$NH); ^{13}C NMR (50.3 MHz, DMSO-*d*$_6$) δ 178.8 (CH$_3$NH*C*=S), 177.3 (NH$_2$NH*C*=S); 146.5 (*C*=N); 146.1 (*C*=N); 37.0 (NH*C*H$_2$CH$_3$), 14.7 (NHCH$_2$*C*H$_3$), 14.0 (*C*H3C=N), 13.9 (*C*H$_3$C=N); LRMS (M-H$^-$) *m/z* 336.0 (calc. for $C_8H_{14}N_7S_2Zn^-$ 336.0)

Diacetyl-2-(4-*N*-ethyl-3-thiosemicarbazone)-3-[4-*N* (amino)-(4-carboxyphenylmethylidene)-3-thiosemicarbazone] (2.09)

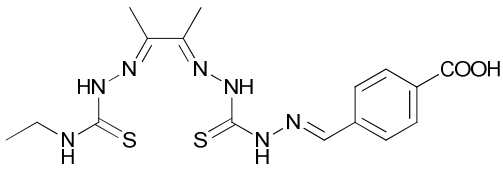

H$_2$ATSE/A (500 mg, 1.82 mmol) was suspended in MeOH (20 mL). 4-Formylbenzoic acid (354 mg, 3.33 mmol) was added and the suspension stirred overnight at rt. The residue was filtered and dissolved in DMF. MeOH was added to induce precipitation of **2.09** (655 mg, 82 %) as a pale yellow solid. ^{1}H NMR (300 MHz, DMSO-*d*$_6$): δ 13.02 (1H, s, COO*H*), 12.31 (1H, s, HC=NN*H*(C=S)NHN=), 10.74 (1H, s, HC=NNH(C=S)N*H*N=), 10.22 (1H, s, EtNH(C=S)N*H*N=), 8.48 (1H, t, *J* = 5.7 Hz, N*H*Et), 8.24 (1H, s, ArC*H*=N), 8.00 (2H, d, *J* = 7.9 Hz, ArC*H*), 7.86 (2H, d, *J* = 7.9 Hz, ArC*H*), 3.62 (2H, m, C*H*$_2$CH$_3$), 2.31 (3H, s, C*H*$_3$C=N), 2.25

(3H, s, C*H*$_3$C=N) 1.15 (3H, t, *J* = 7.3 Hz, CH$_2$C*H*$_3$); ^{13}C NMR (75 MHz, DMSO-*d*$_6$): δ 177.5 (EtNH*C*=S), 174.9 (HC=NNH(*C*=S), 166.8 (*C*O$_2$H), 153.4 (HC=NNH(C=S)NHN=*C*), 147.9 (EtNH(C=S)NHN=*C*), 142.1 (H*C*=NNH) , 137.9 (Ar*C*), 131.7 (Ar*C*), 129.7 (Ar*C*H), 127.2 (Ar*C*H), 38.6 (*C*H$_2$CH$_3$), 14.3 (CH$_2$*C*H$_3$), 11.6 (*C*H$_3$C=NNH(C=S)NHEt), 11.5 (*C*H$_3$C=NNH(C=S)NHNH); HRMS (ESI$^-$): (M-H)$^-$ calcd for $C_{16}H_{20}N_7O_2S_2$ (M-H)$^-$ 406.1125; found 406.1137; HPLC (M$_1$) R$_t$ = 11.85 min; Elemental Analysis Found: C, 47.2; H, 5.1; N, 24.0. $C_{16}H_{21}N_7O_2S_2$ requires: C, 47.2; H, 5.2; N, 24.1%

Diacetyl-2-(4-*N*-ethyl-3-thiosemicarbazone)-3-[4-*N*-(amino)-(2-carboxyphenylmethylidene)-3-thiosemicarbazone] (2.10)

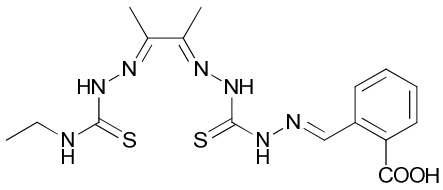

2.10 was prepared according to the procedure described for **2.09** using H_2ATSE/A (0.250 g, 0.91 mmol) and 2-formylbenzoic acid (177 mg, 1.18 mmol) in MeOH (20 mL) to afford **4b** (305 mg, 82%) as a pale yellow solid. ^{1}H NMR (500 MHz, DMSO-*d*$_6$): δ 12.85 (1H, s, COO*H*), 12.31 (1H, s, HC=NN*H*(C=S)NHN=), 10.66 (1H, s, HC=NNH(C=S)N*H*N=), 10.20 (1H, s, EtNH(C=S)N*H*N=), 8.88 (1H, s, ArC*H*=N), 8.46 (1H, t, *J* = 5.7 Hz, N*H*Et), 8.06 (1H, d, *J* = 7.62 Hz, ArCH-4 or ArCH-6), 7.86 (1H, d, *J* = 7.61 Hz, ArCH-3 or ArCH-6), 7.62 (1H, dt, *J* = 7.6 Hz, *J* = 8.5 Hz, ArCH-4 or ArCH-5), 7.52 (1H, dt, *J* = 7.6 Hz, *J* = 8.5 Hz, ArCH-4 or ArCH-5), 3.66-3.57 (2H, m, C*H*$_2$CH$_3$), 2.27 (3H, s, C*H*$_3$C=N), 2.23 (3H, s, C*H*$_3$C=N) and 1.13 (3H, t, *J* = 7.0 Hz, CH$_2$C*H*$_3$); ^{13}C NMR (75 MHz, DMSO-*d*$_6$): δ 179.8 (EtNH*C*=S), 177.9 (HC=NNH(*C*=S), 168.7 (*C*O$_2$H), 149.8 (HC=NNH(C=S)NHN=*C*), 147.9 (EtNH(C=S)NHN=*C*), 142.6 (H*C*=NNH) , 136.7 (Ar*C*), 133.4 (Ar*C*), 129.4 (Ar*C*H), 129.3 (Ar*C*H), 127.8 (Ar*C*H), 124.4 (Ar*C*H) 38.6 (*C*H$_2$CH$_3$), 14.3 (CH$_2$*C*H$_3$), 11.9 (*C*H$_3$C=NNH(C=S)NHEt), 11.6 (*C*H$_3$C=NNH(C=S)NHNH); HRMS (ESI$^-$): (M-H)$^-$ calcd for $C_{16}H_{20}N_7O_2S_2$ (M-H)$^-$ 406.1125, found 406.1123; HPLC (M$_1$) R$_t$ = 12.05 min, Elemental Analysis Found C, 47.1; H, 5.1; N, 24.0. $C_{16}H_{21}N_7O_2S_2$ requires C, 47.2; H, 5.2; N 24.1%

Diacetyl-2-(4-*N*-ethyl-3-thiosemicarbazonato)-3-[4-*N*-(amino)-(4-carboxyphenylmethylidene)-3-thiosemicarbazonato]zinc(II)) (2.11)

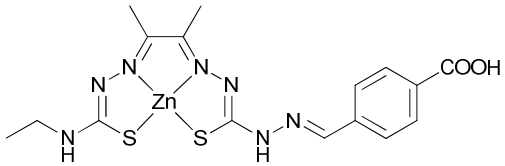

2.09 (70 mg, 0.172 mmol) was suspended in MeOH (5 mL) at rt. $ZnCl_2$ (28 mg, 0.206 mmol) was dissolved in the minimum amount of H_2O and added dropwise. The solution turned yellow immediately and was stirred for 3 h at rt. The solvent was then removed *in vacuo* and H_2O added. The resulting precipitate was filtered off, washed with cold Et_2O and dried *in vacuo* to afford **2.11** (68 mg, 85 %) as an orange solid. ^{1}H NMR (300 MHz, DMSO-d_6): δ 13.05 (1H, s, COOH), 10.75 (1H, s, HC=NN(C=S)N*H*N=) 8.49 (1H, t, *J* = 5.7 Hz, N*H*Et), 8.18-8.16 (1H, m, ArC*H*=N), 8.01-7.98 (2H, m, ArH), 7.87-7.76 (d, *J* = 8.2 Hz, ArH) 3.66-3.57 (2H, m, C*H*$_2$CH$_3$), 2.29 (3H, s, C*H*$_3$C=N), 2.23 (3H, s, C*H*$_3$C=N) and 1.15 (3H, t, *J* = 6.93 Hz, CH$_2$C*H*$_3$); ^{13}C NMR (126 MHz, DMSO-d_6): δ 177.5 (*C*-S), *other* (*C*-S) *not observed*, 167.0 and 168.9 *two isomers* (*C*O$_2$H), (HC=NNH(C=S)NHN=*C*) *not observed*, 147.8 (EtNH(C=S)NHN=*C*), 142.2 (*H*C=NNH) , 137.9 (Ar*C*) 131.8 (Ar*C*), 129.8 (Ar*C*H), 127.3 (Ar*C*H), 38.6 (*C*H$_2$CH$_3$), 14.4 (*C*H$_2$*C*H$_3$), 11.6 and 11.5 (2 × *C*H$_3$C=N); HRMS (ESI$^-$): (M-H)$^-$ calcd for $C_{16}H_{18}N_7O_2S_2Zn^-$ 468.0260; found 468.0267; HPLC (M_1) R_t = 11.75 min

Diacetyl-2-(4-*N*-ethyl-3-thiosemicarbazonato)-3-[4-*N*-(amino)-(2-carboxyphenylmethylidene)-3-thiosemicarbazonato] zinc(II) (2.12)

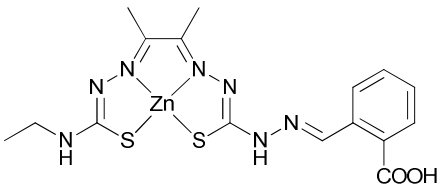

2.10 (70 mg, 0.172 mmol) was suspended in MeOH (5 mL) at rt. $ZnCl_2$ (27.7 mg, 0.206 mmol) was dissolved in the minimum amount of H_2O and added dropwise. The solution turned yellow immediately and was stirred for 3 h at rt. The solvent was then removed *in vacuo* and H_2O added. The resulting precipitate was filtered off, washed with cold Et_2O and dried *in vacuo* to afford the desired product **2.12** (73 mg, 91 %) as an orange solid. ^{1}H NMR (500 MHz, DMSO-d_6): δ 13.12 (1H, s, COO*H*), 10.67 and 10.20 (1H, s, HC=NN(C=S)N*H*N=, 2 isomers 1/2H each), 8.86 (1H, s, ArC*H*=N), 8.47 (1H, t, *J* = 5.7 Hz, N*H*Et), 8.07 (1H, d, *J* =

7.7 Hz, ArCH-3 or -6), 7.88 (1H, d, *J* = 7.7 Hz, 3-ArCH or 6-ArCH), 7.63 (1H, t, *J* = 7.3 Hz, ArCH-4 or H-5), 7.52 (1H, t, *J* = 7.3 Hz, ArCH-4 or H-5), 3.66-3.59 (2H, m, C*H*$_2$CH$_3$), 2.29 (3H, s, C*H*$_3$C=N), 2.23 (3H, s, C*H*$_3$C=N) and 1.15 (3H, t, *J* = 6.9 Hz, CH$_2$C*H*$_3$); ^{13}C NMR (75 MHz, DMSO-*d*$_6$): δ (EtNH*C*=S) *not observed*, 177.4 (HC=NNH(*C*=S), 168.1 (*C*O$_2$H), (HC=NNH(C=S)NHN=*C*) *not observed*, 147.8 (EtNH(C=S)NHN=*C*), 142.5 (*H*C=NNH) , 131.9 (Ar*C*), 131.7 (Ar*C*), 131.0 (Ar*C*H), 130.1 (Ar*C*H), 129.8 (Ar*C*H), 127.0 (Ar*C*H), 38.5 (*C*H$_2$CH$_3$), 14.3 (*C*H$_2$*C*H$_3$), 11.5 (*C*H$_3$C=N), 11.5 (*C*H$_3$C=N); HRMS (ESI$^-$): (M-H)$^-$ calcd for $C_{16}H_{18}N_7O_2S_2Zn^-$ 468.0260; found 468.0259; HPLC (M II) R_t 11.75 min, Elemental Analysis Found C, 40.9; H, 4.1; N, 20.8. $C_{16}H_{19}N_7O_2S_2Zn$ requires C, 40.8; H, 4.1; N, 20.8%

Diacetyl-2-(4-*N*-ethyl-3-thiosemicarbazonato)-3-[4-*N*-(amino)-(4-carboxyphenylmethylidene)-3-thiosemicarbazonato]copper(II) (2.13)

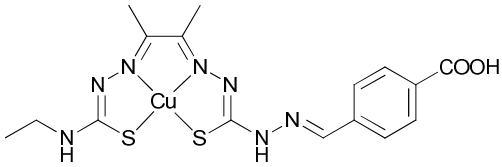

2.13 was prepared following General Procedure B using **2.09** (70 mg, 0.171 mmol) and $CuCl_2$ (28 mg, 0.177 mmol) in MeOH (5 mL) to yield the desired product as a brown solid (73 mg, 91%). HRMS (ESI$^-$): (M-H)$^-$ calcd for $C_{16}H_{18}N_7O_2S_2Cu^-$ 467.0265; found 467.0253; HPLC (M_1) R_t = 12.25 min

Diacetyl-2-(4-*N*-ethyl-3-thiosemicarbazonato)-3-[4-*N*-(amino)-(2-carboxyphenylmethylidene)-3-thiosemicarbazonato]copper(II) (2.14)

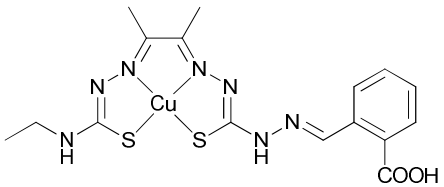

2.14 was prepared following General Procedure B using **2.10** (60 mg, 0.147 mmol) and $CuCl_2$ (23.7 mg, 0.177 mmol) in MeOH (5 mL) to afford the desired product as a dark brown solid (66 mg, 96%). HRMS (ESI$^-$): (M-H)$^-$ calcd for $C_{16}H_{18}N_7O_2S_2Cu^-$ 467.0265; found 467.0255; HPLC (M_1) R_t = 12.05 min; Elemental Analysis Found C, 40.9; H, 4.0; N, 20.9. $C_{16}H_{19}CuN_7O_2S_2$ requires C, 41.0; H, 4.1; N, 20.9%

Diacetyl-2-(4-*N*-ethyl-3-thiosemicarbazone)-3-[4-*N*-(amino)-(4-*tert*butoxycarboxybenzamide)-3-thiosemicarbazone] (2.15)

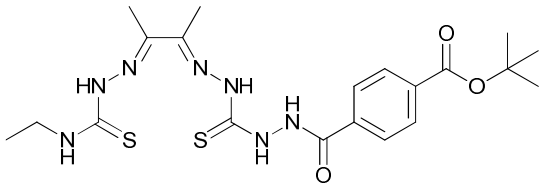

2.15 was synthesized according to General Procedure A, using H_2ATSE/A (300 mg, 1.1 mmol), 4-*tert*-butylbenzoic acid (266 mg, 1.2 mmol), BOP (530 mg, 1.2 mmol) and diisopropylethylamine (209 µL, 1.2 mmol). The product was isolated as an off-white solid (503 mg, 96%). ^{1}H NMR (500 MHz, DMSO-d_6): 10.78 (1H, s, N*H*(C=O)Ar), 10.71 (1H, s, NHNH(C=S)N*H*N=), 10.19 (1H, s, NHN*H*(C=S)NHN=), 10.17 (1H, s, EtNHC=SN*H*N=), 8.45 (1H, t, *J* = 5.8 Hz, N*H*CH_2CH_3), 8.02 (2H, d, *J* = 8.5 Hz, ArCH), 8.01 (2H, d, *J* = 8.5 Hz, ArCH), 3.66-3.59 (2H, m, *J* = 6.9 Hz, C*H*$_2$$CH_3$), 2.27 (3H, s, C*H*$_3$C=N), 2.25 (3H, s, C*H*$_3$C=N), 1.57 (9H, s, CO_2*^{t}Bu*), 1.15 (3H, t, *J* = 7.3 Hz, CH_2C*H*$_3$); ^{13}C NMR (75 MHz, DMSO-d_6): δ 179.8 (NHNH*C*=S), 177.4 (EtNH*C*=S), 166.7 (NHNH*C*=O), 164.9 (*C*O_2^{t}Bu), 149.8 (EtNH(C=S)NHN=*C*), 147.9 (NHNH(C=S)NHN=*C*), 136.7 (Ar*C*CO_2H), 133.9 (Ar*C*(C=O)NH), 129.3 (Ar*C*H), 127.8 (Ar*C*H), 81.3 (*C*$(CH_3)_3$), 38.6 (*C*H_2CH_3), 27.8 (C(*C*H_3)$_3$), 14.4 (CH_2*C*H_3), 11.9 (*C*H_3C=NNH(C=S)NHEt), 11.7 (*C*H_3C=NNH(C=S)NHNH); HRMS (ESI$^-$) $(M+Na)^+$ calcd for$^-$ $C_{20}H_{29}N_7NaO_3S_2$ 502.1666; found 502.1667; HPLC (MII) R_t 13.18 min; Elemental Analysis Found C, 50.0; H, 6.0; N, 20.4. $C_{20}H_{29}N_7O_3S_2$ requires C, 50.1; H, 6.1; N 20.4%

Diacetyl-2-(4-*N*-ethyl-3-thiosemicarbazone)-3-[4-*N*-(amino)-(4-carboxybenzamide)-3-thiosemicarbazone] (2.16)

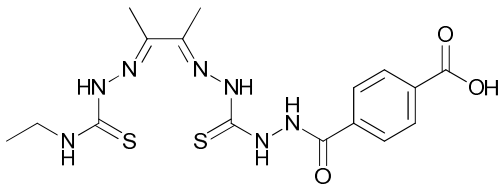

2.15 (500 mg, 1.2 mmol) was suspended in TFA (2 mL) and stirred for 2.5 h at rt. TFA was then removed *in vacuo* and the resulting residue was sonicated in Et_2O, filtered and washed with more Et_2O. The resulting solid was suspended in warm EtOH and sonicated, filtered and dried to afford **2.16** (300 mg, 65 %) as an off-white solid. ^{1}H NMR (500 MHz, DMSO-d_6): δ 13.18 (1H, br s, COOH), 10.78 (1H, br s, N*H*(C=O)Ar), 10.70 (1H, s, NHNH(C=S)N*H*N=), 10.20 (1H, s, NHN*H*(C=S)NHN=), 10.16 (1H, s, EtNHC=SN*H*N=), 8.45

(1H, t, *J* = 5.8 Hz, N*H*Et), 8.07 (2H, d, *J* = 8.5 Hz, ArC*H*), 8.01 (2H, d, *J* = 8.5 Hz, ArC*H*), 3.61 (2H, m, CH_2CH$_3$), 2.27 (3H, s, CH_3C=N), 2.25 (3H, s, CH_3C=N), 1.15 (3H, t, *J* = 7.3 Hz, CH$_2$CH_3); ^{13}C NMR (126 MHz, DMSO-d_6): δ 179.8 (NHNH*C*=S), 177.4 (EtNH*C*=S), 166.7 (NHNH*C*=O), 164.9 (*C*O$_2$H), 149.8 (EtNH(C=S)NHN=*C*), 147.9 (NHNH(C=S)NHN=*C*), 136.7 (Ar*C*CO$_2$H), 133.4 (Ar*C*(C=O)NH), 129.3 (Ar*C*H), 127.8 (Ar*C*H), 38.6 (*C*H$_2$CH$_3$), 14.3 (*C*H$_2$*C*H$_3$), 11.9 (*C*H$_3$C=NNH(C=S)NHEt), 11.6 (*C*H$_3$C=NNH(C=S)NHNH); HRMS (ESI$^-$): (M-H)$^-$ calcd for $C_{16}H_{20}N_7O_3S_2^-$ 422.1075; found 422.1076; HPLC (M_1) R_t = 10.35 min; Elemental Analysis Found C, 45.3; H, 5.0; N, 23.2. $C_{16}H_{21}N_7O_3S_2$ requires C, 45.4; H 5.0; N, 23.2%

Diacetyl-2-(4-*N*-ethyl-3-thiosemicarbazonato)-3-[4-*N*-(amino)-(4-carboxybenzamide)-3 thiosemicarbazonato]copper(II) (2.17)

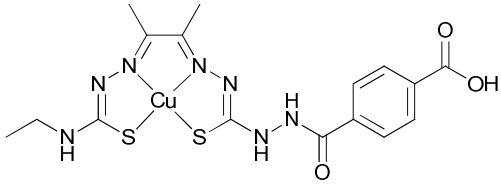

2.17 was prepared following General Procedure B, using **2.16** (38 mg, 0.09 mmol) and $CuCl_2 \cdot H_2O$ (0.1 mmol, 1.1 eq) to afford the desired product as a red-brown solid (37 mg, 85 %). HRMS (ESI$^+$): (M-H)$^-$ calcd for $C_{16}H_{18}CuN_7O_3S_2^-$ 483.0214; found 483.0213; HPLC (M_1) R_t = 10.30 min; Elemental Analysis Found C, 39.6; H, 4.0; N, 20.1. $C_{16}H_{19}CuN_7O_3S_2$ requires C, 39.6; H, 4.0; N, 20.2

Diacetyl-2-(4-*N*-ethyl-3-thiosemicarbazone)-3-[4-*N*-(amino)-4(*N*-(2-*tert*butylacetate)benzamide))-3-thiosemicarbazone (2.18)

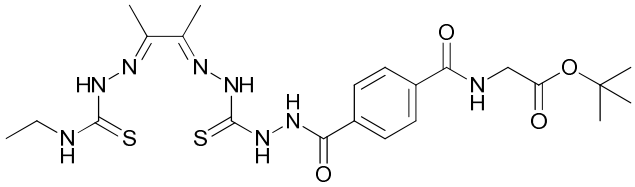

2.18 was synthesised according to General Procedure A using **2.16** (250 mg, 0.59 mmol), glycine *tert*-butyl ester hydrochloride (110 mg, 0.65 mmol), diisopropylethylamine (168 mg, 1.30 mmol) and BOP (288 mg, 0.65 mmol) in DMF (5 mL). The product was isolated as an off-white solid (283 mg, 98%). ^{1}H NMR (500 MHz, DMSO-d_6): δ 10.78 (2H, br s, (C=S)NHN*H*-C=O) and (C=S)N*H*NH-C=O), 10.17 (2H, brs s, 2 × (C=S)-NH-N), 9.00 (1H, t, *J* = 5.8 Hz, N*H*CH$_2$CO$_2^t$Bu), 8.45 (1H, t, *J* = 5.8

Hz, N*H*Et), 8.01 (2H, d, *J* = 8.2 Hz, ArC*H*), 7.98 (2H, d, *J* = 8.5 Hz, ArC*H*), 3.92 (2H, d, *J* = 5.8 Hz, C*H*$_2$CO$_2$^{t}Bu), 3.66-3.57 (2H, m, C*H*$_2$CH$_3$), 2.27 (3H, s, C*H*$_3$C=N), 2.25 (3H, s, C*H*$_3$C=N), 1.43 (9H, s, CO$_2$^{t}*Bu*), 1.15 (3H, t, *J* = 6.6 Hz, CH$_2$C*H*$_3$); ^{13}C NMR (125.8 MHz, DMSO-*d*$_6$): δ 179.7 (NHNH*C*=S), 177.4 (EtNH*C*=S), 168.7 (*C*O$_2$^{t}Bu), 165.8 (*C*ONHCH$_2$), 164.9 (*C*ONHNH), 149.7 (EtNH(C=S)NHN=*C*), 147.9 (NHNH(C=S)NHN=*C*), 136.5 (Ar*C*), 133.4 (Ar*C*), 127.6 (Ar*C*H), 127.3 (Ar*C*H), 80.72 (*C*(CH$_3$), 41.9 (*C*H$_2$CO$_2$^{t}Bu), 38.6 (*C*H$_2$CH$_3$), 27.7 (C(*C*H$_3$), 14.3 (*C*H$_2$*C*H$_3$), 11.9 (*C*H$_3$C=NNH(C=S)NHEt), 11.6 (*C*H$_3$C=NNH(C=S)NHNH); HRMS (ESI$^-$): (M-H)$^-$ calcd for C$_{22}$H$_{31}$N$_8$O$_4$S$_2$$^-$ 535.1915; found 535.1921; HPLC (M$_2$) R$_t$ = 11.8 min; Elemental Analysis Found C, 49.4; H, 6.1; N, 20.9. C$_{22}$H$_{32}$N$_8$O$_4$S$_2$ requires C, 49.2; H, 6.0; N 20.9%

Diacetyl-2-(4-*N*-ethyl-3-thiosemicarbazone)-3-[4-*N*-(amino)-4(*N*-(2-acetic acid)benzamide)-3-thiosemicarbazone (2.19)

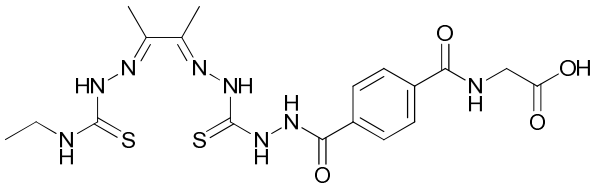

2.18 (280 mg, 0.052 mmol) was suspended in TFA (3 mL) and stirred at rt for 2.25 h. TFA was then removed *in vacuo* and the resulting residue was sonicated in Et$_2$O, filtered and washed with more Et$_2$O and dried to afford the **2.19** (178 mg, 71%) as a pale yellow solid. ^{1}H NMR (500 MHz, DMSO-*d*$_6$): δ 12.59 (brs, COOH), 10.74-10.70 (2H, br s, (C=S)NHN*H*-C=O) and (C=S)N*H*NH-C=O), 10.17 (2H, brs s, 2 × (C=S)-NH-N), 8.99 (1H, t, *J* = 5.8 Hz, N*H*CH$_2$CO$_2$H), 8.45 (1H, t, *J* = 5.8 Hz, N*H*Et), 8.01 (2H, d, *J* = 8.2 Hz, ArC*H*), 7.98 (2H, d, *J* = 8.5 Hz, ArC*H*), 3.96 (2H, d, *J* = 5.8 Hz, C*H*$_2$CO$_2$H), 3.65-3.57 (2H, m, C*H*$_2$CH$_3$), 2.27 (3H, s, C*H*$_3$C=N), 2.25 (3H, s, C*H*$_3$C=N), 1.15 (3H, t, *J* = 6.6 Hz, CH$_2$C*H*$_3$); ^{13}C NMR (125.8 MHz, DMSO-*d*$_6$): δ 179.8 (NHNH*C*=S), 177.4 (EtNH*C*=S), 171.17 (*C*O$_2$H), 165.8 (*C*ONHCH$_2$), 164.9 (*C*ONHNH), 149.7 (EtNH(C=S)NHN=*C*), 147.9 (NHNH(C=S)NHN=*C*), 136.5 (Ar*C*), 135.4 (Ar*C*), 127.6 (Ar*C*H), 127.3 (Ar*C*H), 41.2 (NH*C*H$_2$CO$_2$H) 38.6 (*C*H$_2$CH$_3$), 14.4 (*C*H$_2$*C*H$_3$), 11.9 (*C*H$_3$C=NNH(C=S)NHEt), 11.6 (*C*H$_3$C=NNH(C=S)NHNH); HRMS (ESI$^-$): (M-H)$^-$ calcd for C$_{18}$H$_{23}$N$_8$O$_4$S$_2$$^-$ 479.1289; found 479.1278; HPLC (M$_1$) R$_t$ = 9.48 min; Elemental Analysis Found C, 44.9; H, 5.1; N, 23.4. C$_{18}$H$_{24}$N$_8$O$_4$S$_2$ requires C, 50.0; H, 5.0; N, 23.3%

Diacetyl-2-(4-*N*-ethyl-3-thiosemicarbazonato)-3-[4-*N*-(amino)-4(*N*-(2-acetic acid)benzamide)-3-thiosemicarbazonato]copper(II) (2.20)

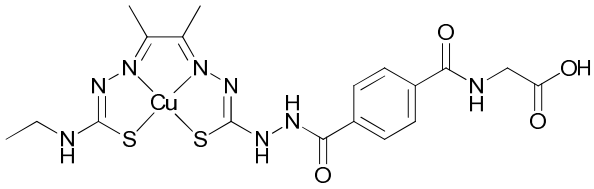

2.20 was prepared following General Procedure B, using **2.19** (60 mg, 0.125 mmol) and $Cu(OAc)_2 \cdot H_2O$ (33 mg, 1.3 eq) to afford the desired product as a black solid (65 mg, 96%). HRMS (ESI^-): $(M-H)^-$ calcd for $C_{18}H_{21}CuN_8O_4S_2^-$ 540.0418; found 540.0429; HPLC (M_1) R_t = 9.07 min

Methyl 2-(4-formylbenzamido) acetic acid (2.21)[6]

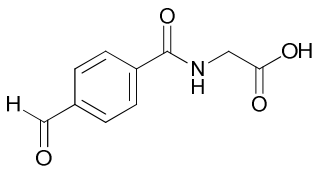

2.21 was synthesised over two steps following a previously reported procedure.[6] A solution of 4-carboxybenzaldehyde (1.79 g, 11.9 mmol), EDCI.HCl (2.28 g, 11.9 mmol) and HOBt (1.61 g, 11.9 mmol) was stirred at room temperature for 20 min. To this was added glycine methyl ester hydrochloride (1.50 g, 11.9 mmol) and DIPEA (2.08 mL, 11.9 mmol) and the reaction mixture was stirred overnight. The solution was washed with water (10 mL), 2M Na_2CO_3 (10 mL) and water (10 mL) and the organic phase was dried over $MgSO_4$ before removal of the solvent *in vacuo*. The crude product was purified by column chromatography (CH_2Cl_2:EtOAc 4:1 - CH_2Cl_2:EtOAc 3:2) to afford methyl 2-(4-formylbenzamido)acetate (1.79 g, 68%) as a white solid. ^{1}H NMR (200 MHz, DMSO-d_6): δ 10.10 (s, 1H, C*H*O), 9.21 (t, 1H, *J* = 6.0 Hz, NH), 8.05 (m, 4H, ArC*H*), 4.06 (d, 2H, *J* = 6.0 Hz, CH_2), 3.67 (s, 3H, OCH_3). The ester (1.0g, 4.50 mmol) was hydrolysed by suspending it in 2.5 M HCl (30 mL) at 60°C for 4 h. The aqueous phase was extracted with ethyl acetate (2× 50 mL) and the organic phase was dried over $MgSO_4$ and concentrated *in vacuo*. Trituration with Et_2O afforded **2.21** (675 mg, 73%) as a white solid. ^{1}H NMR (300 MHz, DMSO-d_6): δ 12.70 (brs, 1H, COO*H*), 10.13 (s, 1H, C*H*O), 9.09 (t, 1H, *J* = 5.0 Hz, N*H*), 8.0 (m, 4H, ArC*H*), 3.90 (d, 2H, *J* = 5.0 Hz, CH_2). ^{13}C NMR (100.6 MHz, DMSO-d_6): δ 193.0 (*C*HO), 171.2 (*C*OOH), 165.8 (*C*ONH), 138.8 (ArC), 137.9 (Ar*C*), 129.5 (Ar*C*H), 128.0 (Ar*C*H), 41.3 (*C*H_2)

Diacetyl-2-(4-*N*-ethyl-3-thiosemicarbazone)-3-[4-*N*-(amino)-methyl 2-(4-formylbenzamido)-acetate)-3-thiosemicarbazone] (2.22)

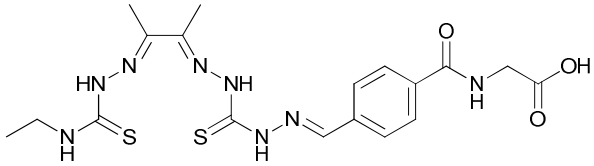

H_2ATSE/A (230 mg, 0.62 mmol) and **2.21** (230 mg, 1.11 mmol) were stirred in MeOH (15 mL) overnight. The suspension was then heated at 50°C for 2h. The solvent was removed *in vacuo* and the solid was washed with cold MeOH (10 mL) and H_2O (10 mL) and dried to afford **2.22** (195 mg, 68%). ^{1}H NMR (500 MHz, DMSO-d_6): δ 12.64 (1H, brs, COOH), 12.3 (s, 1H, N*H*N=CH), 10.75 and 10.23 (2×1H, s, C=SN*H*-N=), 8.94 (1H, t, *J* = 5.7 Hz, N*H*CH_2CO_2H), 8.49 (1H, t, *J* = 5.8 Hz, N*H*Et), 8.26 (1H, brs, NHN=C*H*), 7.95 (2H, d, *J* = 8.2 Hz, ArC*H*), 7.85 (2H, d, *J* = 7.9 Hz, ArC*H*), 3.96 (2H, d, *J* = 5.7 Hz, CH_2CO_2H), 3.66-3.57 (2H, m, CH_2CH_3), 2.31 (3H, s, CH_3C=N), 2.25 (3H, s, CH_3C=N), 1.15 (3H, t, *J* = 7.2 Hz, CH_2CH_3); ^{13}C NMR (126 MHz, DMSO-d_6): δ 177.5 (EtNH*C*=S), 175.1 (*C*=S), 171.3 (*C*O_2H), 165.9 (*C*ONHCH_2), 153.3 (NHNH(C=S)NHN=*C*), 147.8 (EtNH(C=S)NHN=*C*), 142.1 (H*C*=NNH), 136.8 (Ar*C*), 134.8 (Ar*C*), 127.8 (Ar*C*H), 127.1 (Ar*C*H), 41.3 (*C*H_2CO_2H), 38.6 (*C*H_2CH_3), 14.4 (*C*H_2*C*H_3), 11.6 and 11.1 (*C*H_3C=NNH(C=S)NHEt, *C*H_3C=NNH(C=S)NHNH); HRMS (ESI$^+$): $(M+Na)^+$ calcd for $C_{18}H_{24}NaN_8O_3S_2^+$ 487.1305; found 487.1306; Elemental Analysis Found C, 46.6; H, 5.2; N, 24.1. $C_{18}H_{24}N_8O_3S_2$ requires C, 46.5; H, 5.2; N 24.1%

Diacetyl-2-(4-*N*-ethyl-3-thiosemicarbazonato)-3-[4-*N*-(amino)-methyl 2-(4-formylbenzamido)-acetate)-3-thiosemicarbazonato]copper(II) (2.23)

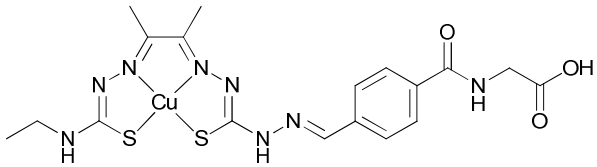

2.23 was prepared following General Procedure B, using **2.22** (30 mg, 0.06 mmol) and $CuCl_2$ (12 mg, 0.07 mmol) to afford the desired product as a black solid (25 mg, 76%). HRMS (ESI$^-$): $(M-H)^-$ calcd for $C_{18}H_{19}CuN_7O_3S_2^-$ 522.0323; found 522.0317; HPLC (M_1) R_t = 10.30 min

H_2ATSM/A-α-Fmoc-L-Glu(O^{t}Bu) (2.26)

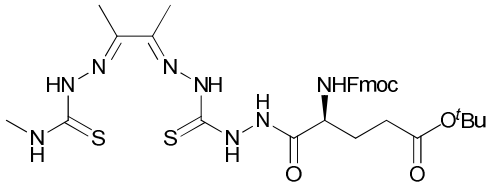

2.26 was prepared according to General Procedure A using H_2ATSM/A (543 mg, 2.08 mmol), Fmoc*L*-GluO^{t}Bu (885 mg, 2.08 mmol), diisopropylethylamine (362 µL, 2.08 mmol) and BOP (920 mg, 2.08 mmol) in DMF (7 mL).The precipitate was then stirred in hot EtOH (5-10 mL) before being filtered off and washed with cold Et_2O (10 mL) to afford 975 mg (70%) of **2.26** as a white solid. ^{1}H NMR (300 MHz, DMSO-d_6): δ 10.60 (1H, s, NHNH(C=S)N*H*N=), 10.25 (1H, s, MeNH(C=S)N*H*N=), 10.20 (1H, s, N*H*NH(C=S)NHN=), 10.02 (1H, s, NHN*H*(C=S)NHN=), 8.40 (d, 1H, *J* = 4.5 Hz, CH_3N*H*), 7.90 (2H, d, *J* = 7.5 Hz, H-4, H-5), 7.75 (2H, m, H-1, H-8), 7.62 (1H, d, *J* = 8.88 Hz, N*H*Fmoc), 7.42 (2H, t, *J* = 7.5 Hz, H-3, H-6), 7.33 (2H, dt, *J* = 7.5 Hz, *J* = 1.4 Hz, H-2, H-7), 4.27-4.17 (4H, m, CH_α, C*H*$_2$Fmoc, H-9), 3.02 (3H, d, *J* = 4.5 Hz, C*H*$_3$NH), 2.37 (2H, t, *J* = 6.6 Hz, CH_γ), 2.23 (3H, s, C*H*$_3$C=N), 2.21 (3H, s, C*H*$_3$C=N), 2.08 (1H, m, CH_β), 1.85 (1H, m, CH_β), 1.14 (9H, s, C(C*H*$_3$)); ^{13}C NMR (75 MHz, DMSO-d_6): δ 179.2 (NHNH*C*=S), 178.4 (EtNH*C*=S), 171.7 (*C*O$_2$^{t}Bu), 170.1 (NHNH*C*O), 155.8 ((*C*=O)Fmoc), 149.7 (NHNH(C=S)NH(*C*=N)), 147.8 MeNH(C=S)NH(*C*=N), 143.8 (Ar*C*), 143.7 (Ar*C*), 140.6 (Ar*C*), 127.6 (C-3, C-6), 127.0 (C-2, C-7), 125.3 (C-1, C-8), 120.1 (C-4, C-5), 79.5 (*C*CH$_3$), 65.7 (*C*H$_2$Fmoc), 52.4 (C_α), 46.6 (C-9), 31.4 (C_γ), 31.2 (NH*C*H$_3$), 27.7 (C(*C*H$_3$)), 27.5 (C_β), 11.8 (*C*H$_3$(C=N)NH(C=S)NHNH), 11.6 (*C*H$_3$(C=N)NH(C=S)NHMe); HRMS (ESI$^+$): (M+Na)$^+$ calcd for $C_{31}H_{40}N_8NaO_5S_2^+$ 691.2455; found 691.2437; HPLC (MII) R_t 14.55 min; Elemental Analysis Found C, 55.6; H, 5.9; N, 16.6. $C_{31}H_{40}N_8O_5S_2$ requires C, 55.7; H, 5.9; N, 16.6%

H_2ATSM/A-α-NH$_2$-*L*-Glu(O^{t}Bu) (2.27)

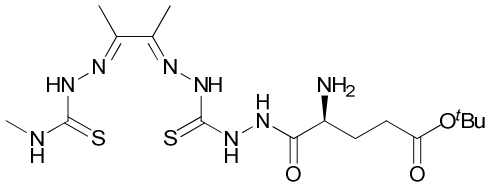

2.27 (100 mg, 0.150 mmol) was stirred in DMF (600 µL) and piperidine (120 µL) for 45 min. The solution was concentrated and H_2O was added until the formation of a white precipitate. The white precipitate was filtered off, washed with ten drops of

H_2O. The aqueous phase was concentrated and Et_2O was added until formation of a precipitate. Filtration and drying under vacuum afforded **2.27** as an off-white solid (40 mg, 60%). ^{1}H NMR (300 MHz, DMSO-d_6): δ 10.20 (4H, superimposed broad singlets, MeNH(C=S)N*H*N=, NHNH(C=S)N*H*N= , N*H*NH(C=S)NHN=, NHN*H*(C=S)NHN=), 8.40 (d, 1H, *J* = 4.7 Hz, CH_3N*H*), 3.33 (*obscured by* H_2O, CH_α) 3.02 (3H, d, *J* = 4.7 Hz, C*H*$_3$NH), 2.37 (2H, t, *J* = 6.6 Hz, C*H*$_\gamma$), 2.23 (3H, s, C*H*$_3$C=N), 2.21 (3H, s, C*H*$_3$C=N), 1.94-1.87 (1H, m, C*H*$_\beta$), 1.75-1.69 (1H, m, C*H*$_\beta$), 1.14 (9H, s, C(C*H*$_3$)); ^{13}C NMR (75 MHz, DMSO-d_6): δ 179.2 (NHNH*C*=S), 178.4 (EtNH*C*=S), 171.7 (*C*O_2tBu), 170.1 (NHNH*C*O), 149.5 (NHNH(C=S)NH(*C*=N)), 147.8 MeNH(C=S)NH(*C*=N), 79.5 (*C*CH_3), 52.5 (C_α), 31.4 (*C*$_\gamma$), 31.2 (NH*C*H_3), 27.7 (C(*C*H_3)), 27.5 (*C*$_\beta$), 11.8 (*C*H_3(C=N)NH(C=S)NHNH), 11.6 (*C*H_3(C=N)NH(C=S)NHMe); HRMS (ESI$^+$): $(M+H)^+$ calcd for $C_{16}H_{31}N_8O_3S_2^+$ 447.1955; found 447.1964; HPLC (M_2) R_t = 12.40 min; Elemental Analysis Found C, 42.9; H, 6.8; N, 25.0. $C_{16}H_{30}N_8O_3S_2$ requires C, 43.0; H, 6.8; N, 25.1%

H_2ATSM/A-α-Fmoc-*L*-Glu(OH) (2.28)

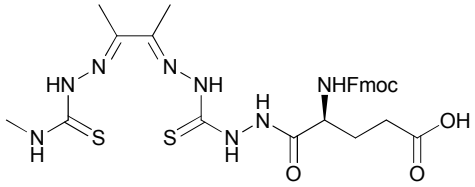

2.26 (400 mg, 0.60 mmol) was stirred in TFA (3 mL) at rt for 3 h. The solvent was then evaporated *in vacuo*. Et_2O was added and the suspension sonicated before evaporating to dryness. The residue was stirred in warm EtOH (5 mL) and left to cool before being filtered, washed with Et_2O and dried *in vacuo* to afford **2.28** (216 mg, 59%) as a white solid. ^{1}H NMR (300 MHz, DMSO-d_6): δ 10.61 (1H, s, NHNH(C=S)N*H*N=), 10.25 (1H, s, MeNH(C=S)N*H*N=), 10.20 (1H, s, N*H*NH(C=S)NHN=), 10.03 (1H, s, NHN*H*(C=S)NHN=), 8.41 (q, 1H, *J* = 4.6 Hz, CH_3N*H*), 7.89 (2H, d, *J* = 7.5 Hz, H-4, H-5), 7.75 (2H, m, H-1, H-8), 7.65 (1H, d, *J* = 8.2 Hz, N*H*Fmoc), 7.42 (2H, t, *J* = 7.5 Hz, H-3, H-6), 7.33 (2H, t, *J* = 7.0 Hz, H-2, H-7), 4.27-4.17 (4H, m, CH_α, C*H*$_2$Fmoc, H-9), 3.03 (3H, d, *J* = 4.6 Hz, C*H*$_3$NH), 2.42 (2H, t, *J* = 6.6 Hz, CH_γ), 2.23 (3H, s, C*H*$_3$C=N), 2.21 (3H, s, C*H*$_3$C=N), 2.10 (1H, m, C*H*$_\beta$), 1.89 (1H, m, C*H*$_\beta$); ^{13}C NMR (75 MHz, DMSO-d_6): δ 179.3 (NHNH*C*=S), 178.5 (EtNH*C*=S), 174.1 (*C*O_2H), 170.4 (NHNH*C*O), 155.9 ((*C*=O)Fmoc), 149.8 (NHNH(C=S)NH(*C*=N)), 147.9 MeNH(C=S)NH(*C*=N),

143.9 (Ar*C*), 143.8 (Ar*C*), 140.7 (Ar*C*), 127.7 (C-3, C-6), 127.1 (C-2, C-7), 125.4 (C-1, C-8), 120.2 (C-4, C-5), 65.8 (*C*H_2Fmoc), 52.6 (C_α), 46.7 (C-9), 31.3 (C_γ), 30.4 (NH*C*H_3), 27.5 (C_β), 11.8 (*C*H_3(C=N)NH(C=S)NHNH), 11.6 (*C*H_3(C=N)NH(C=S)NHMe); HRMS (ESI^+): $(M+H)^+$ calcd for $C_{27}H_{33}N_8O_5S_2^+$ 613.2010; found 613.1989; HPLC (M_1) R_t = 12.45 min; Elemental Analysis Found C, 52.9; H, 5.2; N, 18.2 $C_{27}H_{32}N_8O_5S_2$ requires C, 52.9; H, 5.3; N, 18.3%

CuATSM/A-α-*L*-FmocGlu(OH) 2.29

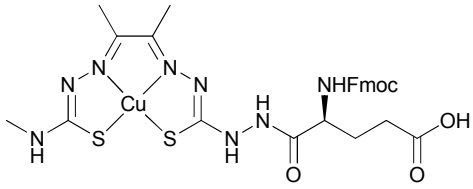

$Cu(OAc)_2 \cdot H_2O$ (12 mg, 0.059 mmol) was dissolved in H_2O (1 mL) and added dropwise to a stirring suspension of **2.28** (30 mg, 0.048 mmol) in MeOH (5 mL). The suspension turned brown immediately and was left to stir for 1 h. The solvent was then removed *in vacuo* and H_2O was added, the residue was filtered, washed with cold Et_2O and dried *in vacuo* to afford **2.29** (25 mg, 77%) as a dark brown solid. HPLC (M_1) R_t =12.40 min, HRMS (ESI^-): $(M-H)^-$ calcd for $C_{27}H_{29}CuN_8O_5S_2^-$ 672.1004; found 672.0983; Elemental Analysis Found C, 48.0; H, 4.6; N,16.6. $C_{27}H_{30}CuN_8O_5S_2$ requires C, 48.1; H, 4.5; N, 16.6%

H_2ATSM/A-α-NH-Biotin-*L*-Glu(O^{t}Bu) (2.30)

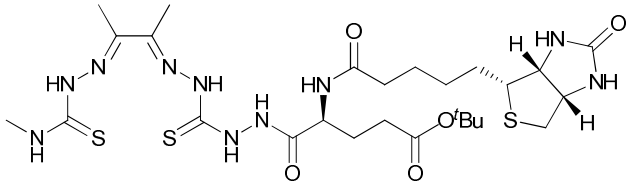

2.30 was synthesised according to General Procedure A using **2.27** (40 mg, 0.089 mmol), biotin (23 mg, 0.09 mmol), diisopropylethylamine (16 µL, 0.09 mmol) and BOP (42 mg, 0.09 mmol) in DMF (5 mL). The product was isolated as a beige solid (38.2 mg, 63%). ^{1}H NMR (300 MHz, DMSO-d_6): δ 10.58 (1H, s, NHNH(C=S)N*H*N=), 10.23 (1H, s, MeNH(C=S)N*H*N=), 10.17 (1H, s, N*H*NH(C=S)NHN=), 10.00 (1H, s, NHN*H*(C=S)NHN=), 8.41 (d, 1H, *J* = 4.5 Hz, CH_3N*H*), 7.89 (2H, d, *J* = 7.5 Hz, H-4, H-5), 7.75 (2H, m, H-1, H-8), 7.99 (1H, d, *J* = 8.5 Hz, N*H*biotin), 6.41 and 6.35 (2×1H, s, C*H*NHC=O), 4.45 (1H, dd, *J* = 13.8 Hz, *J* = 8.5 Hz, NHNH(C=O)C*H*), 4.30-4.13 (2H, m, 2×CHN*H*(C=O), 3.09 (1H, m, CH_2C*H*SCH_2), 3.02 (3H, d, *J* = 4.6 Hz, CH_3NH), 2.81 (1H,

dd, *J* =12.6 Hz, *J* = 5.2 Hz, 1×SC*H*$_2$CH), 2.54 (1H, m, obscured by DMSO, 1×SC*H*$_2$CH),2.36-2.31 (2H, CH$_2$C*H*$_2$CO$_2$^{t}Bu), 2.23 (3H, s, C*H*$_3$C=N), 2.21 (3H, s, C*H*$_3$C=N), 2.15-2.13 (2H, m, (C=O)C*H*$_2$(CH$_2$)$_3$), 2.04-1.24 (8H,m, (C=O)CH$_2$(C*H*$_2$)$_3$ and C*H*$_2$CH$_2$CO$_2$^{t}Bu), 1.40 (9H,s, CO$_2$^{t}*Bu*); ^{13}C NMR (75 MHz, DMSO-*d*$_6$): δ 179.2 (NHNH*C*=S), 178.5 (EtNH*C*=S), 172.0 (CO), 171.7 (*C*O$_2$^{t}Bu), 170.1 (NHNH*C*O), 162.7 (NH(C=O)NH), 149.8 (NHNH(C=S)NH(*C*=N)), 147.9 MeNH(C=S)NH(*C*=N), 79.6 (CO$_2$*C*(CH$_3$)$_3$), 61.0 (CH*C*HNH(C=O)), 59.2 (SCH$_2$*C*HNH(C=O)), 55.4 (*C*HS), 50.0 (*C*HCH$_2$CH$_2$CO$_2$^{t}Bu), 34.8 (NH(C=O)*C*H$_2$(CH$_2$)$_3$), 28.1 (*C*H$_2$), 28.0 (*C*H$_2$), 27.8 (CO$_2$C(*C*H$_3$)$_3$, 25.2 (*C*H$_2$), 11.8 (*C*H$_3$(C=N)NH(C=S)NHNH), 11.7 (*C*H$_3$(C=N)NH(C=S)NHMe); HRMS (ESI$^+$): (M+Na)$^+$ calcd for $C_{26}H_{44}N_{10}NaO_5S_3^+$ 695.2550; found 695.2554; HPLC (M_2) R_t = 11.26 min; Elemental Analysis Found C, 46.4; H, 6.5; N, 20.9. $C_{26}H_{44}N_{10}O_5S_3$ requires C, 46.4; H, 6.6; N, 20.8%

CuATSM/A-α-N-Biotin-*L*-Glu(O^{t}Bu) (2.31)

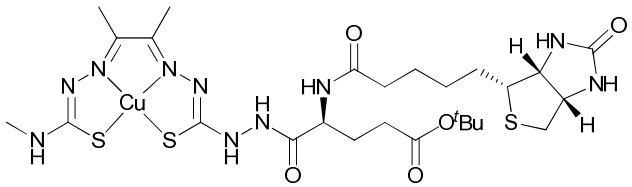

2.31 was prepared following General Procedure B, using **2.30** (38 mg, 0.056 mmol) and Cu(OAc)$_2$·H$_2$O (14 mg, 1.2 eq) to afford the desired product as a black solid (40 mg, 96%). HRMS (ESI$^+$): (M+Na)$^+$ calcd for $C_{26}H_{42}CuN_{10}NaO_5S_3^+$ 756.1690; found 756.1691; HPLC (M_2) R_t = 11.84 min

For compounds **2.36** and **2.38**, see experimental details for Chapter 4.

H$_2$ATSE/A-Almaleimide (2.40)

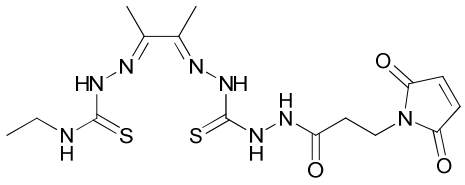

H$_2$ATSE/A (65 mg, 0.24 mmol) was suspended in the minimum amount of DMF. 3-Maleimidopropionic acid (44 mg, 0.26 mmol), diisopropylethylamine (45µL, 0.26 mmol) and benzotriazole-1-yl-oxy-tris-(dimethylamino)-phosphonium hexafluorophosphate (BOP) (115 mg, 0.26 mmol) were added and the mixture was stirred at room temperature for 4 h until a clear solution was formed. H$_2$O was then added until formation of a precipitate. The suspension

was sonicated, the precipitate collected by filtration, washed with copious amounts of H_2O and dried *in vacuo* to afford **2.40** as an off-white solid (95 mg, 94 %). The isolated compound was ~95% pure as determined by HPLC and NMR. Aliquots of the sample were purified to >99% purity by preparative HPLC and lyophilisation. ^{1}H NMR (500 MHz, DMSO-d_6): δ 10.70 (1H, s, NHNH(C=S)N*H*N=), 10.18 (1H, s, NHN*H*(C=S)NHN=), 10.15 (1H, s, EtNHC=SN*H*N=), 9.91 (1H,s, NHN*H*CO) 8.43 (1H, t, *J* = 5.8 Hz, N*H*Et), 7.01 (2H, s, N(C=O)C*H*), 3.65 (2H, t, *J* = 7.6 Hz, (C=O)CH_2C*H*$_2$), 3.60 (2H, m, C*H*$_2$$CH_3$), 2.5 (2H, (C=O)C*H*$_2$$CH_2$, obscured by DMSO), 2.23 (3H, s, C*H*$_3$C=N), 2.20 (3H, s, C*H*$_3$C=N), 1.14 (3H, t, *J* = 7.3 Hz, CH_2C*H*$_3$) ; ^{13}C NMR (126 MHz, DMSO-d_6): δ 179.2 (NHNH*C*=S), 177.4 (EtNH*C*=S), 170.7 (*C*=O), 168.3 (C=O), 149.6 (EtNH(C=S)NHN=*C*), 147.8 (NHNH(C=S)NHN=*C*), 134.6 (N((C=O)*C*H)$_2$), 38.7 ((C=O)*C*H$_2$$CH_2$), 33.5 (*C*H$_2$), 31.7 (*C*H$_2$), 38.6 (*C*H$_2$$CH_3$), 14.3 ($CH_2$*C*H$_3$), 11.8 (*C*H$_3$C=NNH(C=S)NHEt), 11.6 (*C*H$_3$C=NNH(C=S)NHNH); HRMS (ESI$^+$): $(M+Na)^+$ calcd for $C_{15}H_{22}NaN_8O_3S_2^+$ 449.1148; found 449.1137; HPLC (M_1) R_t = 9.72 min; Elemental Analysis Found C, 42.2; H, 5.2; N, 26.2. $C_{15}H_{22}N_8O_3S_2$ requires C, 42.2; H 5.2; N, 26.3%

CuATSE/A-ALmaleimide (2.41)

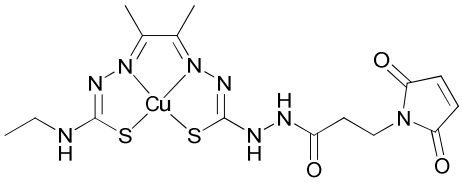

2.41 (31 mg, 0.07 mmol) and Cu(OAc)$_2$.H_2O (17mg, 0.84 mmol) were stirred in the minimum amount of MeOH for 5 min at rt. The solvent was removed at room temperature *in vacuo*. The remaining solid was washed with water and dried under vacuum. to afford the title compound as a brown solid (25 mg, 71%). HRMS (ESI$^+$): $(M+Na)^+$ calcd for $C_{15}H_{20}CuNaN_8O_3S_2^+$ 510.0288; found 510.0283; Elemental Analysis Found C, 37.0; H, 4.1; N, 22.8. $C_{15}H_{22}CuN_8O_3S_2$ requires C, 36.9; H 4.1; N, 23.0%

H_2ATSE/A-ARmaleimide (2.42)

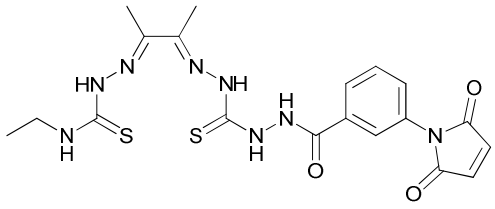

H_2ATSE/A (200 mg, 0.72 mmol) was suspended in the minimum amount of anhydrous DMF. 3-Maleimidobenzoic acid (173.5 mg, 0.79 mmol), diisopropylethylamine (139 µL, 0.79 mmol) and benzotriazole-1-yl-oxy-tris-(dimethylamino)-phosphonium hexafluorophosphate (BOP) (353 mg, 0.79 mmol) were added and the mixture was stirred at room temperature for 4 h until a clear solution was formed. H_2O was then added until formation of a precipitate. The suspension was sonicated, the precipitate collected by filtration, washed with copious amounts of H_2O and dried *in vacuo* to afford **2.42** as a pale yellow solid (347 mg, 98 %). The isolated compound was >95% pure as determined by HPLC and NMR. Aliquots of the sample were purified to >99% by preparative HPLC followed by lyophilisation. ^{1}H NMR (500 MHz, DMSO-d_6): 10.71 (1H,s, NH), 10.69 (1H, s, NH), 10.19 (1H, s, NHN*H*(C=S)NHN=), 10.17 (1H, s, EtNHC=SN*H*N=), 8.45 (1H, t, *J* = 5.8 Hz, N*H*Et), 7.96-7.88 (1H, m, ArC*H*), 7.88 (1H, m, ArC*H*), 7.66-7.63 (1H, m, ArC*H*), 7.58-7.56 (1H, m, ArC*H*), 7.22 (2H, s, N(COC*H*)$_2$), 3.63-3.58 (2H, m, CH_2CH$_3$), 2.27 (3H, s, CH_3C=N), 2.24 (3H, s, CH_3C=N), 1.15 (3H, t, *J* = 7.3 Hz, CH$_2$CH_3); ^{13}C NMR (126 MHz, DMSO-d_6): δ 179.8 (NHNH*C*=S), 177.4 (EtNH*C*=S), 169.8 (NHNH*C*=O), 164.6 (N(*C*OCH$_2$)$_2$), 149.8 (EtNH(C=S)NHN=*C*), 147.9 (NHNH(C=S)NHN=*C*), 134.8 (N(*C*OCH$_2$)$_2$), 133.7 (ArC), 131.8 (Ar*C*), 129.1 (ArC), 126.5 (ArC), 126.2 (ArC), 38.6 (*C*H$_2$CH$_3$), 14.4 (*C*H$_2$*C*H$_3$), 11.9 (*C*H$_3$C=NNH(C=S)NHEt), 11.7 (*C*H$_3$C=NNH(C=S)NHNH); HRMS (ESI$^+$): (M+CH$_3$OH+Na)$^+$ calcd for $C_{20}H_{26}NaN_8O_4S_2^+$ 529.1411; found 529.1412; Elemental Analysis Found C, 48.0; H, 4.6; N, 23.7. $C_{19}H_{22}N_8O_3S_2$ requires C, 48.1; H 4.7; N, 23.6%

CuATSE/A-ARmaleimide (2.43)

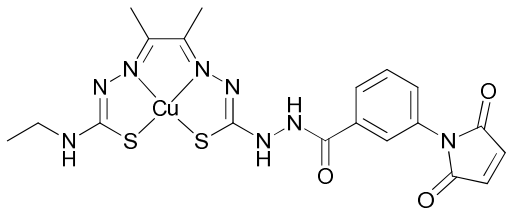

2.42 (20 mg, 0.04 mmol) and $Cu(OAc)_2.H_2O$ (10 mg, 0.05 mmol) were stirred in a minimum amount of MeOH for 5 min at rt. MeOH was removed at room temperature *in vacuo*. The residue was washed with water and dried to afford **2.43** as a brown solid (17.3 mg, 65%). HRMS (ESI^-): $(M-H)^-$ calcd for $C_{19}H_{19}CuN_8O_3S_2^-$ 534.0323; found 534.0322; Elemental Analysis Found C, 37.65; H, 3.76; N, 17.39. $C_{19}H_{20}CuN_8O_3S_2$ requires C, 42.57; H 3.76; N, 20.90%

Diacetyl-*bis*(4-(2-adamantyl)thiosemicarbazone) (2.49)

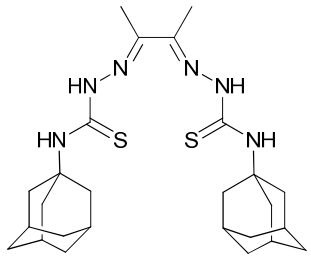

4-(2-Adamantyl)thiosemicarbazide (**2.48**) (500 mg, 2.22 mmol) was dissolved in EtOH (50 mL) and butane-2,3-dione (96 µL, 1.10 mmol) and concentrated H_2SO_4 (5 drops) were added. The reaction stirred at room temperature for 16 h. The white precipitate formed was filtered, rinsed with water and EtOH and dried *in vacuo* to afford **2.49** (593 mg, 54%) as a white solid. ^1H NMR (200 MHz, DMSO-d_6): δ 7.46 (2H, s, NHC(S=)N*H*N=), 8.40 (2H, s, ADN*H*), 2.30 (6H, s, NHC(C*H*$_2$)$_3$), 2.16 (6H, CNC*H*$_3$), 2.07 (12H, s, C*H*$_2$), 1.71 (6H, s, NHC(CH$_2$)$_3$C*H*); ^{13}C NMR (50.3 MHz, DMSO-d_6): δ 175.3 (*C*=S), 145.0 (*C*=N), 54.8 (NH*C*(CH$_2$)$_3$), 41.3 (NHC(*C*H$_2$)$_3$CH), 36.7 (*C*H$_2$), 31.2 (NH*C*H$_3$), 30.0 (*C*H), 10.8 (*C*H$_3$(C=N)); HRMS (ESI^+): $(M+Na)^+$ calcd for $C_{26}H_{40}NaN_6S_2^+$ 523.2648; found 523.2624; Elemental Analysis Found C, 62.4; H, 8.1; N, 16.7. $C_{26}H_{40}N_6S_2$ requires C, 62.4; H 8.1; N, 16.8%

Diacetyl-*bis*(4-(2-adamantyl)thiosemicarbazonato) zinc(II) (2.50)

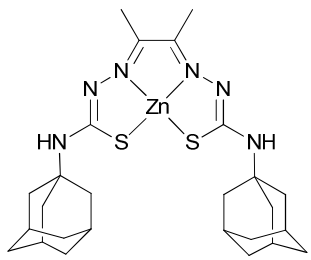

2.49 (100 mg, 0.20 mmol) was suspended in CH_3Cl:MeOH 7:3 (10 mL) and $Zn(OAc)_2{\cdot}2H_2O$ (53 mg, 0.24 mmol) was added. The reaction was stirred at 50°C for 2 h, and the solvent was removed *in vacuo*. The residue was washed with H_2O and a few drops of cold

MeOH to afford **2.50** as a bright yellow solid (89 mg, 79%). HRMS (ESI^+): $(M+Na)^+$ calcd for $C_{26}H_{38}N_6NaS_2Zn^+$ 585.1783; found 585.1179; Elemental Analysis Found C, 55.5; H, 6.7; N, 14.8. $C_{26}H_{38}N_6S_2Zn$ requires C, 55.4; H 6.8; N, 14.9%.

6.3.2 Crystallography for 2.50

X-ray crystallography experiments were performed by Dr Michael Jones and Dr Amber Thompson. The crystal was mounted using the oil drop technique, in perfluoropolyether oil at 150(2) K with a Cryostream N_2 open-flow cooling device.[7] Single crystal X-ray diffraction data were collected using graphite monochromated Mo-Kα radiation (λ = 0.71073 Å) using a Nonius KappaCCD diffractometer. Series of ω-scans were generally performed to provide sufficient data in each case to a maximum resolution of 0.77 Å. Data collection and cell refinement were carried out using DENZO-SMN.[8] Intensity data were processed and corrected for absorption effects by the multi-scan method, based on multiple scans of identical and Laue equivalent reflections using SCALEPACK (within DENZO-SMN). Structure solution was carried out with direct methods using the program SuperFlip[9] within the CRYSTALS software suite.[10] In general, coordinates and anisotropic displacement parameters of all non-hydrogen atoms were refined separately. Hydrogen atoms were generally visible in the difference map and were treated in the usual manner.[11] PLATON/SQUEEZE[12-14] was used leaving a void from which the electron density was removed. A full table of the cif is found in the Appendix and the cif may be found on the CD affixed in the inside back cover of this thesis.

Formula	$C_{26}H_{38}N_6S_2Zn \cdot DMSO$
Mr (g/mol)	624.27
Crystal system	Monoclinic
Space group	*C 2/c*
a (Å)	57.2108(8)
b (Å)	6.9230(1)
c (Å)	36.0993(6)
α (°)	90
β (°)	100.1154(5)

γ (°)	90
Volume	14075.6(4)
Dx (g/cm^3)	1.212
Z prime	2
μ (mm^{-1})	0.904
F000	5440.0
h,k,l max	68,8,43
Total reflections	74697
Unique reflections	12549
Parameters refined	703
T max	25.360
Tmin/Tmax	0.880, 0.980
Goodness of fit	1.023
R	0.0738

6.3.3 Radiochemistry

6.3.3.1 ^{64}Cu-radiolabelling (small scale) of 2.09, 2.16, 2.19, 2.22, 2.40 and 2.42 (<10 MBq)

A standard 1 mg mL^{-1} solution of the relevant ligand was prepared in DMSO. ^{64}Cu-radiolabelled complexes were prepared by reacting 20 µL of [^{64}Cu](OAc)$_2$(aq) (<10 MBq) with 50 µL of the ligand standard solution and 150 µL DMSO. Reaction mixtures were briefly stirred at room temperature before 25 µL of the reaction solution was analysed by reverse-phase radio-HPLC. Analysis was performed using a Gilson Unipoint HPLC machine equipped with a C-18 column. [^{64}Cu]**2.13**, [^{64}Cu]**2.17**, [^{64}Cu]**2.20** and [^{64}Cu]**2.23** as well as [^{64}Cu]**2.41** and [^{64}Cu]**2.43** were prepared in this manner. All complexes were radiolabelled at room temperature.

6.3.3.2 Log P measurements

5 µL of ^{64}Cu-labelled complex (<1 MBq) was added to a mixture of 0.5 mL octanol and 0.5 mL PBS. The mixture was vortexed for 1 min and then centrifuged for 5 min at 2000 rpm. A 50 µL sample of each layer was taken and counted in a γ-counter. Measurements for each compound were performed in triplicate and Log *P* were calculated as follows:

$$\text{Log } P = \left[\frac{\text{counts (octanol)}}{\text{counts (PBS)}}\right]$$

6.3.4 Bombesin Conjugates

6.3.4.1 Synthesis

The synthesis of the Bombesin analogues were performed manually as previously described,[15, 16] by solid-phase peptide synthesis on a Fmoc Rink Amide resin (Novabiochem). The synthesis was carried out in a 2.5 mL plastic syringe fitted with a PE frit (MultiSynTech GmbH, Germany) with a maximum of 50 mg Fmoc-Rink Amide resin per syringe. The Fmoc group was removed by treatment with 25% 4-methylpiperidine in DMF (2 × 10 min), the resin was washed with 3 × DMF,

3 × ^{i}PrOH and 3 × DMF. Unless mentioned otherwise, all couplings were carried out in duplicate (2 × 90 min) with 4 eq Fmoc-amino acid, 4 eq DIC and 4 eq HOBt in DMF.

A stock solution of HOBt in DMF was used to dissolve the amino acid ([AA] = 0.5 mM). After each coupling the resin was washed with 3 × DMF, 3 × ^{i}PrOH and 3 × DMF. The completion of each coupling was checked with the NF31 colour test. Chelators **2.16** (2 eq) and **2.19** (2 eq) were coupled in a single coupling to β^{3}hAsp using 2 eq of BOP, 2 eq diisopropylethylamine (8 h) or 2 eq DIC and 2 eq HOBt (3 h) respectively. At the end of the synthesis the resin was washed several times with CH_2Cl_2 and Et_2O and dried *in vacuo* before cleavage.

For cleavage from the resin, a mixture of thioanisole (TA)/ethanedithiol (EDT) 7:3 was added as scavenger to the TFA solution. The resin-bound ligand-peptide conjugate (0.2 mmol) was shaken in 900 µL TFA and 100 µL TA/EDT in a syringe fitted with a glass frit for 3.5 h. The filtrate was added dropwise to ice-cooled Et_2O (10 mL) and the mixture was left in an ice-bath for 15 min before centrifugation for 5 min. The Et_2O was decanted and the solid resuspended in Et_2O, left to settle in the ice-bath and centrifuged again. This operation was repeated twice more to eliminate all remaining TFA and scavengers. The resulting precipitate was dried, dissolved in CH_3CN/H_2O with 5 % DMSO and lyophilised.

Analytical HPLC for BBS-conjugates was performed on a Waters Breeze™ HPLC system with UV detection (215 nm) using an RP-column (Supelco Discovery Bio Wide Pore, C 18, 5 µm, 250 mm × 4.6 mm). Gradient 1: 3% B to 100 %B in 30 min, flow rate 1 mL min^{-1}, the gradient was finished by washing with 100% B. (solvent B = 0.1% TFA in CH_3CN).

Analysis was performed by coupling the mass spectrometer to a Waters system equipped with a UV detector (Waters, 215nm), a manual injector and Waters 600E pump. The runs were performed on an RP-column (Supelco Discovery Bio Wide Pore, C 18, 5 µm, 250 mm × 4.6 mm) at a flow rate of 1mL min^{-1}. The outlet of the HPLC column passed through a splitter with a split ratio of 1/10.

Preparative HPLC was carried out on a Gilson System fitted with a reverse phase C18 Column, Supelco Discovery Bio Wide Pore, 10 m, 250 mm x 21.2 mm, flow rate 20 mL min^{-1}.

6.3.4.2 Radiolabelling and octanol/water partition coefficients of ATSM-BBS conjugates

20 µL of 1mM stock solution ATSM-BBS1 (**2.32**) or ATSM-BBS2 (**2.33**) in DMSO were transferred into 280 µL of 0.25M ammonium acetate at pH 5.5. 2.5 µL $^{64/67}$Cu (equivalent to 0.045µg Cu) was added and the solution was shaken for 30 min at room temperature. The labelling was purified on a Sep-Pak™ C_{18} or Chromafix® C_{18}ec. by washing with 2 mL H_2O and eluting with 2×1 mL EtOH/H_2O 9:1.

The octanol/water partition coefficients were determined at pH 7.4 by adding 5 µL of radiolabelled [^{64}Cu]**2.34** and [^{64}Cu]**2.35** in PBS to a vial containing 1.2 mL of 1:1 octanol:PBS. Vortex mixing for 1 min was followed by centrifugation at 10000 rpm for 5 min. 40 µL from each separated layer were sampled into a pre-weighed vial and measured in a γ-counter. Counts per unit weight of sample were calculated and log D values were obtained using the formula log D = log (counts in 1 g of octanol/counts in 1 g of water).

6.3.4.3 Cell Culture (PC3)

The human prostate adenocarcinoma cell line PC3 was purchased from the European Collection of Cell Culture (ECACC, Salisbury, UK). Cells were maintained in DMEM GLUTAMAX-I (Invitrogen) supplemented with 1-10% FCS, 100 IU/mL penicillin G sodium, 100 µg/mL streptomycin sulphate and 0.25µg/mL amphotericin B (Bioconcept). Cells were cultured at 37°C in an atmosphere containing 5% CO_2. The cells were subcultured weekly after detaching them with trypsin/EDTA 0.25 % (Invitrogen).

6.3.4.4 Binding Assays

The binding assays were carried out as previously reported.[17] All experiments were carried out twice in triplicate. PC-3 cells were placed in 48-well plates (250,000 cells/well). A protease inhibitor containing binding buffer was used (50 mM HEPES, 125 mM NaCl, 7.5 mM KCl, 5.5 mM $MgCl_2$, 1 mM EGTA, 5 g/l BSA, 2 mg/l chymostatin, 100 mg/l soybean trypsin inhibitor and 50 mg/l bacitracin). Cells were incubated at 37°C with 15,000-25,000 cpm of [^{125}I-Tyr^4]BBS per well and increasing concentrations (0-3000nM) of the non-labelled ATSM-BBS analogues. After 1 h incubation the cells were rinsed twice with cold PBS. Cells with bound activity were solubilised by adding 2 × 400 µl of 1 M NaOH at 37°C. The final suspension was measured in a γ-counter. IC_{50} values were calculated by nonlinear regression analysis using GraphPad Prism.

6.3.4.5 Internalisation Assays

The internalisation assays were carried out as previously reported.[17] PC-3 cells at confluence were placed in 6-well plates at ~10^6 cells/well. Cells were incubated with ~1 kBq of the $^{64/67}$Cu-labelled analogues in culture medium at a total volume of 1 mL/well for 5, 15, 30, 60 and 120 min at 37°C to allow binding and internalisation. Non-specific internalisation was determined in the presence of 1 µM non-labelled BBS(7-14). After each incubation time, cells were washed three times with PBS to remove any unbound peptide. Surface-bound activity was removed by two 5 min acid washes (50 mM glycine-HCl, 100 mM NaCl, pH 2.8, 600 µL per well) at room temperature. Cells containing internalised activity were then solubilised by adding 2 × 600 µL 1 M NaOH/well. Surface bound and internalised activity were measured in a γ-counter. The data reported refers to the specific internalisation after subtracting the non-specific binding and are given as a percentage of the total activity added per milligram of protein.

6.3.4.6 Biodistribution studies

Female CD-1 nu/nu mice 6-8 week-old (Charles River Laboratories, Sulzfeld, Germany) were subcutaneously injected with 8 × 106 PC-3 cells. Three weeks after tumour implantation, the mice

received i.v. 100 kBq [$^{64/67}$Cu]CuATSM-BBS2. At 1 and 24 h p.i., the animals were killed by cervical dislocation. Blood and different organs were collected, weighed, and the radioactivity measured in a γ-counter. Results are presented as percentage of injected dose per gram of tissue (%ID/g). To determine the specificity of the *in vivo* uptake, one group of mice received a co-injection of 100 μg of unlabelled BBS(1-14) and the radiolabelled analogue and were sacrificed at 1 h p.i.

6.3.5 C2Ac conjugation and radiolabelling

Radiolabelling, serum stability and red blood cell binding assays of the [^{64}Cu]**2.41**-C2Ac conjugate were carried out by Dr Richard Tavaré.

6.3.5.1 C2Ac protein

The C2Ac was provided by Dr Richard Tavaré.[18]

2.40-C2Ac and 2.42-C2Ac Conjugates

C2Ac was conjugated to **2.40** and **2.42** by adaptation of a previously reported procedure for Fluorescein-5-maleimide conjugates of C2Ac.[18] One millilitre of C2Ac (2 mg mL^{-1} in PBS) was mixed with a 3-fold molar excess of **2.40** or **2.42** dissolved in 100 µL of DMSO and incubated at room temperature for 4 h. Excess unconjugated chelator was removed by size exclusion chromatography using a PD-10 column pre-equilibrated with PBS. Fractions were monitored by UV absorbance at 280 nm and analysed by LC-MS.

6.3.5.2 Direct ^{64}Cu-labelling of 2.40-C2Ac conjugate

140 MBq of [^{64}Cu]Cu(OAc)$_2$ (in 1 M ammonium acetate, pH 6.2) was added to 50 µg of **2.40**-C2Ac in 50 µL of PBS and incubated at room temperature for 120 min before radiolabeling efficiency was determined by radio-TLC (Lablogic, UK) using 10% ammonium acetate:methanol (1:1) as the mobile phase. The radiolabelled conjugate was purified by passing the protein through a PD-10 column (Sephadex G-25, GE healthcare). The labelling efficiency was calculated by comparing the amount of activity associated with the eluted protein fraction versus the unbound, low molecular weight radioactivity using a dose calibrator (CRC-25R, Capintec, US).

6.3.5.3 Conjugation of C2Ac with pre-labelled [^{64}Cu]2.41

2.40 (10 µg in 10 µL of DMSO) was radiolabelled with 165 MBq of [^{64}Cu]Cu(OAc)$_2$ in ammonium acetate (400 µL) and purified on a C-18 cartridge before being reformulated into EtOH (600 µL) using standard procedures.[19, 20] The eluent was concentrated under a stream of nitrogen

(~10 µL) and 100 µL of C2Ac (1 mg mL^{-1}) was added. The pH was adjusted to 8 and the reaction was left to stand for 70 min. The radiolabelled conjugate [^{64}Cu]**2.41**-C2Ac was then purified by PD-10 chromatography and the labelling efficiency determined as above.

6.3.5.4 Stability in PBS

100 µL of [^{64}Cu]**2.41**-C2Ac isolated in PBS from PD-10 purification (radiolabelled either *via* the pre- or or postlabelling method) was incubated at 37°C. Samples were taken at 1, 2 and 20 h and analysed by radio-TLC or SDS-PAGE followed by electronic autoradiography (Cyclone phosphorimager, Perkin-Elmer, UK). Radio-TLC was performed using a mobile phase of 10% ammonium acetate:methanol (1:1) and plates were monitored using a radio-TLC scanner (Lablogic, UK). Stability was calculated as the area under the [^{64}Cu]**2.41**-C2Ac peak (R_f = 0) versus the area under the remaining chromatograph).

6.3.5.5 Serum stability

100 µL of [^{64}Cu]**2.41**-C2Ac (radiolabelled via the pre-labelling method) was incubated in 400 µL human serum (Sigma, Poole, UK) and incubated at 37°C. At 1, 2, 6 and 20 h samples were taken and analysed as described for PBS incubations above.

6.4 Experimental details for Chapter 4

6.4.1 Synthetic Chemistry

General Procedure C: Coupling reactions of H_2ATSM/en with halogenated carboxylic acid. H_2ATSM/en was suspended in the minimum amount of DMF. The carboxylic acid (1.1 eq), diisopropylethylamine (1.1 eq) and benzotriazole-1-yl-oxy-tris-(dimethylamino)-phosphonium hexafluorophosphate (BOP) (1.1 eq) were added and the mixture was stirred at room temperature for 4 h until a clear solution was formed. H_2O was then added until formation of a white precipitate. The suspension was sonicated, the precipitate collected by filtration and washed with copious amounts of H_2O and a few drops of ice-cold EtOH and ice-cold Et_2O.

General Procedure D: Copper complexation

The proligand and $Cu(OAc)_2 \cdot H_2O$ (1.2 eq) were stirred in the minimum amount of MeOH for 30 min at rt. The solvent was removed *in vacuo* and ice cold H_2O was added. The suspension was briefly sonicated and the solid formed was collected by filtration and washed with a few drops of ice-cold EtOH before being dried *in vacuo*.

Boc-ethylenediamine (4.04)[21]

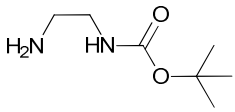

Boc-ethylenediamine was prepared following a previously reported procedure.[21] Di-tbutyldicarbonate (8.74 g, 40.0 mmol) was dissolved in chloroform (200 mL). This was slowly added to ethylene diamine (28 mL, 428 mmol) in 400 mL chloroform at 0°C. The mixture was allowed to warm up to room-temperature overnight during which time a white precipitate formed. The mixture was washed with brine (5 × 100 mL), H_2O (100 mL) and the organic phase was dried over $MgSO_4$. The solvent was removed *in vacuo* to afford the product as a clear, colourless oil (5.67 g, 88 %). ^{1}H NMR (400MHz, DMSO-d_6): δ ^{1}H NMR ($CDCl_3$): δ 5.00 (1H, broad, N*H*Boc), 3.14 (2H, m, NH_2CH_2), 2.77 (2H, m, CH_2NH), 1.42 (9H, s, Boc), 1.13 (2H, broad, NH_2). ^{13}C NMR (300 MHz, DMSO-d_6) δ 156.2 (*C*=O); 79.06

(*C*CH_3); 43.4 (CH_2), 41.82 (*C*H_2); 28.3 (C*C*H3); LRMS ($M+H^+$) *m/z* 161.1 (calc. for $C_7H_{17}N_2O_2^+$ 161.1)

Methyl-*N*-(2-^{t}butoxycarbonylaminoethyl)dithiocarbamate (4.05)[22]

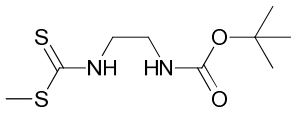

4.05 was prepared following a previously reported procedure.[22] Carbon disulphide (1.90 mL, 31.59 mmol) was added dropwise to a stirring solution of boc-ethylenediamine (5.06 g, 31.58 mmol) and Et_3N (4.41 mL, 31.64 mmol) in EtOH (100 mL) whilst maintaining room temperature with a water bath. After stirring for 1½ h, iodomethane (1.97 mL, 31.64 mmol) was added and the resulting mixture stirred for a further 1¾ h. The solvent was removed *in vacuo* and the residue suspended in ethyl acetate. This was washed with 1M HCl (100 mL), saturated sodium bicarbonate solution (100 mL) and H_2O (100 mL). The organic phase was dried ($MgSO_4$) and solvent removed *in vacuo* to give **4.05** as an off-white solid (7.05 g, 89%). ^{1}H NMR (200 MHz, $CDCl_3$): δ 8.33 (1H, broad, N*H*(C=S), 4.94 (1H, broad, N*H*Boc), 3.73 (2H, m, C*H*$_2$NH(C=S), 3.36 (2H, m, C*H*$_2$NHBoc), 2.53 (3H, s, C*H*$_3$S), 1.39 (9H, s, Boc); ^{13}C NMR (300 MHz, DMSO-d_6): δ 199.8 (C=S), 158.3 (C=O), 80.97 (*C*CH_3), 50.11 (*C*H_2NH(C=S)), 39.1 (*C*H_2NHBoc), 28.8 (C*C*H_3), 18.4 (*C*H_3S); LRMS $(M-H)^-$ *m/z* 249.1 (calc. for $C_9H_{17}N_2O_2S_2^-$ 249.1)

4-*N*-(2-^{t}butoxycarbonylaminoethyl)-3-thiosemicarbazide (4.06)[22]

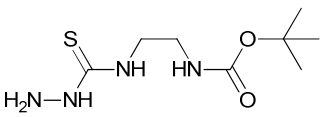

4.06 was synthesised according to a previously reported procedure.[22] A solution of methyl-*N*-(2-^{t}butoxycarbonylaminoethyl)dithiocarbamate (7.00 g, 27.85 mmol) and hydrazine hydrate (2.2 mL, ca. 38.50 mmol) were dissolved in EtOH (100 mL) and heated under reflux for 2½ hrs. The solvent was removed *in vacuo* and the residue redissolved in $CHCl_3$. This solution was passed onto a plug of silica, washed with $CHCl_3$ and washed through with MeOH. The MeOH fraction was evaporated to give an oil which solidifies on standing (6.58 g, 99%). ^{1}H NMR (200MHz, $CDCl_3$): δ 7.8 (1H, broad, N*H*NH_2), 7.48 (1H, broad, CH_2N*H*C=S), 4.99 (1H, broad, CH_2N*H*Boc), 3.76 (2H, broad, NHN*H*$_2$), 3.69 (2H, m, C*H*$_2$NHC=S), 3.32 (2H, m, C*H*$_2$NHBoc), 1.45 (9H, s, Boc); ^{13}C NMR (300 MHz, $CDCl_3$) δ 182.3

(C=S), 156.5 (C=O), 79.5 (*C*CH_3), 44.2 (*C*H_2), 40.1 (*C*H_2), 28.3 (C*C*H_3); LRMS (M-H)$^-$ *m/z* 233.1 (calc. for $C_8H_{17}N_4O_2S^-$ 233.1)

Diacetyl-2-(4-*N*-methyl-3-thiosemicarbazone)-3-(4-*N*-^{t}butylethylcarbamate-3-thiosemicarbazone) (H_2ATSM/en-Boc) (4.07)[22]

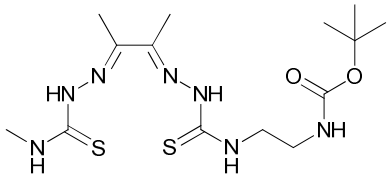

H_2ATSM/en-Boc was synthesised following a previously reported procedure.[22] 4-*N*-(2-^{t}butoxycarbonylaminoethyl)-3-thiosemi-carbazide (2.5 g, 10.7 mmol) was suspended in ethanol (30 mL) and stirred at 50°C. Diacetyl-2-(4-*N*-methyl-3-thiosemicarbazone) (1.83 g, 10.6 mmol) was added in portions over 30 min. After the final addition, 2 drops of conc. HCl was added and the reaction heated at 80°C for 3 h. The solution was left to cool and a white precipitate was collected by filtration, washed with cold ethanol (2 × 20 mL) and diethyl ether (1 × 10 mL), and dried *in vacuo* to afford **4.07** as a white solid (3.1 g, 72%). ^{1}H NMR (200 MHz, DMSO-d_6): δ 10.30 (1H, s, S=CN*H*N), 10.28 (1H, s, S=CN*H*N), 8.45 (1H, m, CH_3N*H*C=S), 8.37 (1H, m, CH_2N*H*C=S), 7.02 (1H, t, *J* = 5.1 Hz, N*H*Boc), 3.62-3.59 (2H, m, C*H*$_2$NHC=S), 3.20-3.17 (2H, m, C*H*$_2$NHBoc), 3.02 (3H, d, *J* = 4.8 Hz, NHC*H*$_3$), 2.22 (6H, s, 2× N=CC*H*$_3$), 1.37 (9H, s, Boc); ^{13}C NMR (300 MHz, DMSO-d_6) δ 178.5 (*C*=S), 178.0 (*C*=S), 156.2 (*C*=O), 148.3 (N=*C*), 147.8 (N=*C*), 77.9 (*C*CH_3), 44.0 (NHC*H*$_2$CH_2), 38.3 (NHCH_2C*H*$_2$), 31.2 (*C*H_3NH), 28.2 (C*C*H_3) 11.7 (*C*H_3C=N), 11.6 (*C*H_3C=N); LRMS (M-H$^-$) *m/z* 388.2 (calc. for $C_{14}H_{26}N_7O_2S_2^-$ 388.2)

Diacetyl-2-(4-*N*-methyl-3-thiosemicarbazone)-3-(4-*N*-ethylamine-3-thiosemicarbazone) (H_2ATSM/en) (2.36)[22]

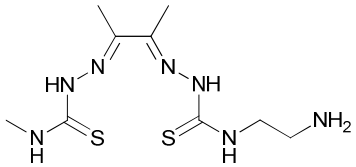

H_2ATSM/en was synthesised following a previously reported procedure.[22] TFA (2 mL) was added to **4.07** (3 g, 7.7 mmol) and the solution was stirred for 90 min at room temperature. The solvent was removed *in vacuo* and saturated $NaHCO_3$ was added slowly, dropwise, until a white suspension was formed. After stirring for 15 min at room temperature, the solid was filtered off,

washed with H_2O (2 × 20 mL), a few drops of cold EtOH and Et_2O (2 × 20 mL) before being dried *in vacuo* to afford H_2ATSMen (1.8 g, 75%) as an off-white solid. ^{1}H NMR (400 MHz, DMSO-d_6 with added TFA): δ 10.50 (1H, s, S=CN*H*N), 10.25 (1H, s, S=CN*H*N), 8.50 (1H, q, J = 6.7Hz, CH_3N*H*C=S), 8.40 (1H, t, J = 4.4 Hz, CH_2N*H*C=S), 7.87 (3H, brs, NH_3^+), 3.85-3.80 (2H, m, C*H*$_2$NHC=S), 3.08-3.01 (2H, m, C*H*$_2$$NH_3^+$), 2.22 (6H, s, 2× N=CC*H*$_3$); ^{13}C NMR (125.8 MHz, DMSO-d_6): δ 178.5 (*C*=S), 178.5 (*C*=S), 148.9 (N=*C*), 147.8 (N=*C*), 44.0 (NHC*H*$_2$$CH_2$), 38.0 ($NHCH_2$C*H*$_2$), 31.2 (*C*$H_3$NH), 11.7 (*C*$H_3$C=N), 11.6 (*C*$H_3$C=N); LRMS ($M+H^+$) *m/z* 290.1 (calc. for $C_9H_{20}N_7S_2^+$ 290.1)

Diacetyl-2-(4-*N*-methyl-3-thiosemicarbazone)-3-(4-*N*-ethylamine-3-thiosemicarbazonato)-zinc(II) (ZnATSM/en) (2.38)[23]

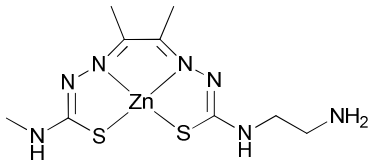

To a stirring suspension of H_2ATSM/en (0.250 g, 0.859 mmol) in methanol (15 mL) was added $Zn(OAc)_2{\cdot}H_2O$ (0.230 g, 0.594 mmol) and a dark yellow solution formed. This was heated under reflux for 3 h during which time a yellow precipitate formed. The precipitate was collected by filtration, washed with MeOH and dried *in vacuo*. Triethylamine (~1 mL) was added to the filtrate followed by an excess of water and a yellow precipitate formed which was collected by filtration, washed with cold MeOH (10 mL) and dried *in vacuo*. Both solids were the desired product **2.38** (0.290 g, 80%). ^{1}H NMR (300 MHz, DMSO-d_6): δ ppm 7.32 (1H, brs, N*H*CH_2CH_2), 7.16 (1H, brs, N*H*CH_3), 3.27 (2H, m, C*H*$_2$$CH_2NH_2$) 2.82 (3H, d, J = 3.5 Hz, CH_3NH) 2.42 (2H, br., C*H*$_2$$NH_2$), 2.22 (3H, s, C*H*$_3$C=N), 2.14 (3H, s, C*H*$_3$C=N). LRMS $(M+H)^+$ *m/z* 352.0 (calc. for $C_9H_{18}N_7S_2Zn^+$ 352.0); HPLC (M_1) R_t = 5.8 min

Diacetyl-2-(4-*N*-methyl-3-thiosemicarbazone)-3-(4-*N*-ethylamine-3-thiosemicarbazonato)-copper(II) (CuATSM/en)[23] (4.08)

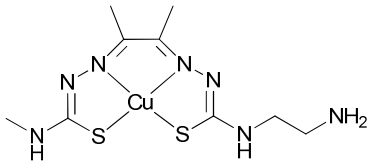

To a stirring suspension of H_2ATSM/en (0.250 g, 0.865 mmol) in methanol (10 mL) was added $Cu(OAc)_2 \cdot H_2O$ (0.181 g, 0.908 mmol) and the mixture stirred at room temperature for 1 h. A brown precipitate was collected by filtration, washed with MeOH and Et_2O then dried *in vacuo* (0.198 g, 65%). LRMS $(M+H)^+$ *m/z* 351.0 (calc. for $C_9H_{18}CuN_7S_2$ 351.0). HPLC (M_1) R_t = 5.38 min

H_2ATSMenF (4.09)

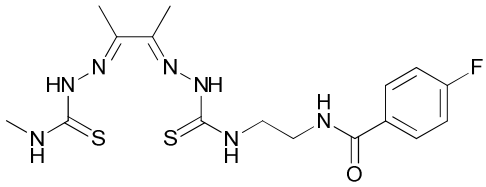

4.09 was synthesised according to General Procedure C using H_2ATSMen (150 mg, 0.52 mmol), 4-fluorobenzoic acid (88 mg, 0.57 mmol), diisopropylethylamine (74 mg, 0.57 mmol) and BOP (230 mg, 0.57 mmol) in DMF (1.5 mL). The product was isolated as a white solid (145 mg, 70 %). ^{1}H NMR (400 MHz, DMSO-d_6): δ 10.30, 10.23 (2H, s, 2 × (C=S)-N*H*-N), 8.71 (1H, t, *J* = 5.20 Hz, N*H*C=O), 8.59 (1H, t, *J* = 5.20 Hz, CH_2N*H*C=S), 8.39-8.36 (1H, m, CH_3N*H*C=S), 7.94-7.91 (2H, m, 2× ArC*H*(C=O)), 7.31-7.28 (2H, m, 2×ArC*H*), 3.77-3.73 (2H, m, C=SNHC$H_2$$CH_2$), 3.53-3.50 (2H, m, C=SNHCH$_2$CH_2), 3.02 (3H, d, *J* = 4.5 Hz NHCH_3), 2.22 (3H, s, CH_3C=N), 2.21 (3H, s, CH_3C=N); ^{13}C NMR (125.8 MHz, DMSO-d_6): δ 178.5 (*C*=S), 178.1 (*C*=S), 165.9 (*C*=O), 163.9 (d, Ar*C*F, *J* = 248 Hz), 148.4 (N=*C*), 147.9 (N=*C*), 130.7 ((C=O)Ar*C*H), 129.2 (d, *J* = 22 Hz, Ar*C*H), 115.2 (d, *J* = 10.0 Hz, Ar*C*HF), 44.2 (CH_2NH(C=O)), 38.7 ((C=S)NHCH_2), 31.2 (*C*H_3NH), 11.8 (*C*H_3C=N), 11.6 (*C*H_3C=N); HRMS (ESI^+): $(M+Na)^+$ calcd for $C_{16}H_{22}FN_7NaOS_2^+$ 434.1203; found 434.1201; Elemental Analysis Found C, 46.6; H, 5.4; N, 23.8. $C_{16}H_{22}FN_7OS_2$ requires C, 46.7; H, 5.4; N 23.8%

CuATSMenF (4.03)

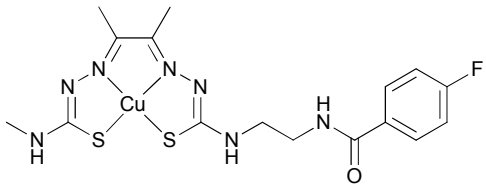

4.03 was prepared following General Procedure D, using H_2ATSMenF (40 mg, 0.10 mmol) and $Cu(OAc)_2 \cdot H_2O$ (24 mg, 0.12 mmol) to afford the desired product as a brown solid (37 mg, 81%). HRMS (ESI$^-$): $(M-H)^-$ calcd for $C_{16}H_{19}CuFN_7OS_2^-$ 471.0378; found 471.0376; HPLC (M_1) R_t = 9.07 min, Elemental Analysis Found C, 35.5; H, 3.3; N, 16.5. $C_{16}H_{20}CuFN_7OS_2$ requires C, 40.6; H, 4.2; N 20.7%

Succinimidyl-4-fluorobenzoate (FSB, 4.10)[24]

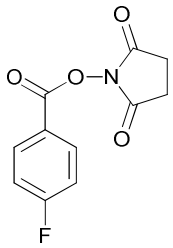

4.10 was synthesised according to a previously reported procedure. 4-Fluorobenzoic acid (547 mg, 3.90 mmol) was dissolved in anhydrous acetonitrile (20 mL). To this was added dissucinimidyl carbonate (1 g, 3.90 mmol) and pyridine (316 µL, 3.90 mmol) and the solution was stirred at room temperature for 90 min. The solvent was evaporated and the crude product was purified by flash column chromatography EtOAc:Hexane (1:1) to afford the desired product as a white crystalline solid (520 mg, 56 %). ^{1}H NMR (400 MHz, DMSO-d_6): δ 8.24-8.13 (2H, m, ArC*H*), 7.55-7.42 (2H, m, ArC*H*), 2.90 (4H, s, N(COCH_2)$_2$); ^{13}C NMR (50.3 MHz, DMSO-d_6): δ 170.3 (N(*C*OCH$_2$)$_2$), 166.3 (d, *J* = 255.1 Hz, Ar*C*F), 160.9 (Ar*C*O$_2$), 133.26 (d, *J* = 10.3 Hz, Ar*C*H), 121.1 (Ar*C*), 116.9 (d, *J* = 22.1 Hz, Ar*C*H), 25.6 (N(CO*C*H$_2$)$_2$)

Ethyl 4(-trimethylammonium triflate)benzoate (4.11)[25, 26]

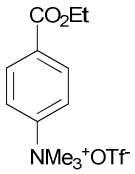

4.11 was synthesised following a previously reported procedure.[25, 26] Ethyl-4-(dimethylamino)benzoate (1.9 g, 9.8 mmol) was dissolved in Et_2O (20 mL) and methyl triflate (0.8 mL, 7.0 mmol) and the solution was stirred for 2 h after which time a precipitate had formed. The crude product was filtered off and washed with excess Et_2O. Recrystallisation from CH_2Cl_2 afforded **4.11** as a white, crystalline solid (2.0 g, 57%). ^{1}H NMR (200 MHz, DMSO-d_6): δ 8.19-8.09 (4H, m, ArC*H*), 4.36 (2H, q, *J* = 7.2 Hz, CH_2CH$_3$), 3.64 (9H, s,

N(CH_3)$_3$), 1.34 (3H, t, J = 7.2 Hz, CH_2CH_3); ^{13}C NMR (50.3 MHz, DMSO-d_6): δ 164.4 (CO_2Et), 150.5 (ArCNMe_3), 131.4 (ArC), 130.7 (ArCH), 121.3 (ArCH), 61.4 (CH_2CH_3), 56.4 (N(CH_3)$_3$), 61.4 (CH_2CH_3)

4-Formyl-*N,N,N*-trimethyl benzaminium trifluoromethane sulfonate (4.14)[27]

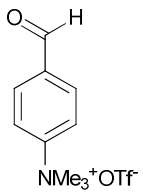

4.14 was synthesised following a previously reported procedure.[27] 4-Dimethylaminobenzaldehyde (1.5 g, 10.0 mmol) was dissolved in dry CH_2Cl_2 under argon atmosphere. To this was added, dropwise, methyl trifluoromethane sulfonate (1.22 mL) and the mixture was stirred at rt overnight. The solution was concentrated to 20 mL *in vacuo* at ambient temperature. The concentrated solution was then added, dropwise, to ice cold Et_2O (200 mL). the granular precipitate was filtered and washed with Et_2O (3× 50 mL) and dried *in vacuo* to afford **4.14** as a white solid (0.8 g, 76%). ^{1}H NMR (400 MHz, DMSO-d_6): δ (1H, s, CHO), 8.22-8.19 (2H, m, ArCH), 8.17-8.13 (2H, m, ArCH), 3.66 (9H, s, N(CH_3)$_3$); ^{13}C NMR (50.3 MHz, DMSO-d_6): δ 192.2 (CHO), 151.1 (ArCNMe_3), 136.8 (ArC), 131.0 (ArCH), 121.7 (ArCH), 56.4 (N(CH_3)$_3$)

***S*uccinimidyl-4-iodobenzoate (SIB, 4.15)**[28]

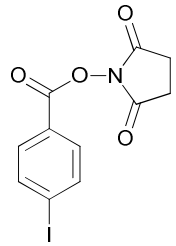

4.15 was synthesised according to a previously reported procedure. To a solution of 4-iodobenzoic acid (2.5 g, 10.2 mmol) in dry CH_2Cl_2 (30 mL) was added dicyclohexylcarbodiimide (3.0 g, 14.5 mmol) and N-hydroxysuccinimide (1.3 g, 11.3 mmol). The solution was left to stir for 24 h and the precipitated dicyclohexylurea was filtered off. The filtrate was evaporated *in vacuo* to yield a crude solid which was suspended in 20 mL of 1:1 CH_2Cl_2:hexane and then filtered. The insoluble solid was heated in MeOH to yield the desired product (1.3 g, 37%) as a white crystalline solid. ^{1}H NMR (400 MHz, DMSO-d_6): δ 8.06 (2H, d, J = 8.2 Hz, 2×(C=O)ArCH), 7.83 (2H, J = 8.2 Hz, 2×ArCH), 2.89 (4H, s, N(C=O)$_2$(CH_2)$_2$); ^{13}C NMR (100.6 MHz, DMSO-d_6): 170.2 ((C=O)(CH_2)$_2$), 161.6 (ArC(C=O)), 138.6 (ArCHI), 131.3 (ArCH), 123.8 (ArC) 104.9 (ArCI), 25.6 (CH_2))

ZnATSE/A-imineI (4.20)

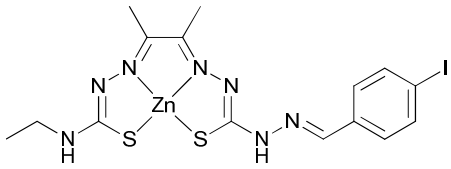

ZnATSE/A (200 mg, 0.54 mmol) was suspended in MeOH (40 mL) and purged under N_2 atmosphere for 15 min. 4-Iodobenzaldehyde (150 mg, 0.65 mmol) was added and the mixture was heated at 55°C under N_2 atmosphere for 5h. The solution was left to cool and the solvent volume was reduced *in vacuo* before the solid was isolated by filtration, washed with cold MeOH and and dried *in vacuo* to afford **4.20** as a bright orange solid (283 mg, 95%). ^{1}H NMR (300 MHz, DMSO-d_6): δ 11.31 (1H, s, HC=NN*H*(C=S)NHN=), 8.05 (1H, m, ArC*H*=N), 7.77 (2H, d, *J* = 8.5 Hz, ArH), 7.41 (2H, d, *J* = 8.5 Hz, ArH), obscured by residual H_2O peak 3.39-3.36 (2H, m, CH_2CH$_3$ obscured by residual H_2O peak), 2.27 (3H, s, CH_3C=N), 2.21 (3H, s, CH_3C=N) and 1.15 (3H, t, *J* = 6.9 Hz, CH$_2$CH_3), N*H*Et not observed; ^{13}C NMR (75 MHz, DMSO-d_6): δ 148.5 (N=*C*), 140.3 (H*C*=NNH), 137.5 (Ar*C*H), 134.9 (Ar*C*), 128.2 (Ar*C*H), 95.1 (Ar*C*I), 38.6 (*C*H$_2$CH$_3$), 14.1 (CH$_2$*C*H$_3$), 11.6 (*C*H$_3$C=NNH(C=S)NHEt), (*C*H$_3$C=N*)* not observed, (*C*=*S*) not observed; HRMS (ESI$^+$): (M+H)$^+$ calcd for $C_{15}H_{19}IN_7S_2Zn^+$ 551.9474; found 551.9468; Elemental Analysis Found C, 32.4; H, 3.3; N, 17.5. $C_{15}H_{18}IN_7S_2Zn$ requires C, 32.6; H, 3.3; N 17.7%

H_2ATSE/A-imineI (4.19)

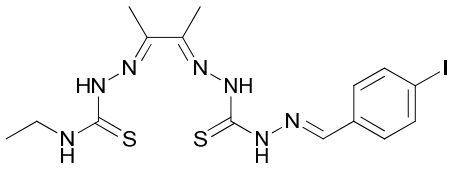

H_2ATSE/A (150 mg, 0.55 mmol) was suspended in MeOH (20 mL). 4-Iodobenzaldehyde (177 mg, 0.763 mmol) was added and the suspension was stirred overnight at rt. An additional 20 mL of MeOH was added and the solid was filtered off, washed with CH_2Cl_2 (10 mL), Et_2O (10 mL) and dried under vacuum to afford **4.19** as a white solid (190 mg, 71%). ^{1}H NMR (300 MHz, DMSO-d_6): δ 11.4 (1H, s, HC=NN*H*(C=S)NHN=), 10.69 (1H, s, HC=NNH(C=S)N*H*N=), 10.21 (1H, s, EtNH(C=S)N*H*N=), 8.47 (1H, t, *J* = 5.6 Hz, N*H*Et), 8.13 (1H, brs, ArC*H*=N), 7.83 (2H, d, *J* = 7.9 Hz, ArC*H*), 7.54 (2H, d, *J* = 7.9 Hz, ArC*H*), 3.61 (2H, m, CH_2CH$_3$), 2.29 (3H, s, CH_3C=N), 2.24 (3H, s, CH_3C=N), 1.15 (3H, t, *J* = 7.2 Hz, CH$_2$CH_3); ^{13}C NMR (75 MHz, DMSO-d_6): δ 177.5 (EtNH*C*=S), 174.6 (HC=NNH(*C*=S), 153.2

(HC=NNH(C=S)NHN=*C*), 147.8 (EtNH(C=S)NHN=*C*), 142.6 (H*C*=NNH), 137.7 (Ar*C*H), 133.4 (Ar*C*), 129.04 (Ar*C*H), 97.2 (Ar*C*I), 38.6 (*C*$H_2$$CH_3$), 14.4 ($CH_2$*C*$H_3$), 11.6 (*C*$H_3$C=NNH(C=S)NHEt), 11.1 (*C*H_3C=NNH(C=S)NHNH); HRMS (ESI^+): $(M+Na)^+$ calcd for $C_{15}H_{20}IN_7NaS_2^+$ 512.0148; found 512.0158; HPLC (M_1) R_t = 11.85 min; Elemental Analysis Found C, 36.9; H, 4.0; N, 20.0. $C_{15}H_{20}IN_7S_2$ requires C, 36.8; H, 4.1; N 20.0%

CuATSE/A-imineI (4.15)

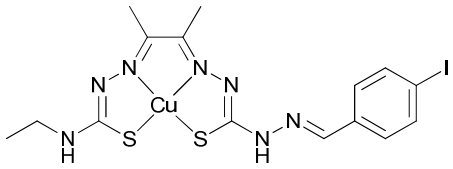

4.15 was prepared following General Procedure B, using **4.20** (30 mg, 0.05 mmol) and $CuCl_2$ (10 mg, 0.06 mmol) to afford the desired product as a brown solid (25 mg, 84%). HRMS (ESI^-): $(M-H)^-$ calcd for $C_{15}H_{17}CuIN_7S_2^-$ 548.9333; found 548.9332. HPLC (M_1) R_t = 13.5 min Elemental Analysis Found C, 30.7; H, 2.6; N, 15.6. $C_{15}H_{18}CuIN_7S_2$ requires C, 32.7; H, 3.3; N 17.8%

H_2ATSE/A-I (4.23)

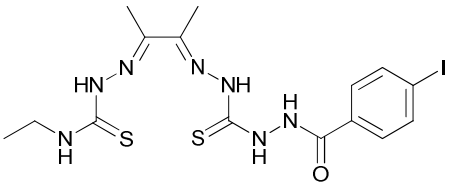

4.23 was synthesised according to General Procedure A using H_2ATSE/A (200 mg, 0.73 mmol), 4-iodobenzoic acid (198 mg, 0.80 mmol), diisopropylethylamine (103 mg, 0.80 mmol) and BOP (353 mg, 0.80 mmol) in DMF (4 mL). The product was isolated as an off-white solid (340 mg, 93%). ^{1}H NMR (500 MHz, DMSO-d_6): δ 10.68 (2H, br s, N*H*(C=O)Ar, NHNH(C=S)N*H*N=), 10.16 (2H, s, NHN*H*(C=S)NHN=, EtNHC=SN*H*N=), 8.44 (1H, t, *J* = 5.7 Hz, N*H*Et), 7.92 (2H, d, *J* = 8.5 Hz, ArC*H*), 7.69 (2H, d, *J* = 8.5 Hz, ArC*H*), 3.60 (2H, m, C$H_2$$CH_3$), 2.26 (3H, s, C$H_3$C=N), 2.23 (3H, s, C$H_3$C=N), 1.15 (3H, t, *J* = 7.3 Hz, CH_2CH_3) ; ^{13}C NMR (126 MHz, DMSO-d_6): δ 179.8 (NHNH*C*=S), 177.4 (EtNH*C*=S), 164.9 (NHNH*C*=O), 149.8 (EtNH(C=S)NHN=*C*), 147.9 (NHNH(C=S)NHN=*C*), 137.4 (Ar*C*H), 132.4 (Ar*C*(C=O)NH), 129.4 (Ar*C*H), 99.51 (Ar*C*I), 38.6 (*C*$H_2$$CH_3$), 14.4 ($CH_2$*C*$H_3$), 11.9 (*C*$H_3$C=NNH(C=S)NHEt), 11.7 (*C*H_3C=NNH(C=S)NHNH); HRMS (ESI^-): $(M-H)^-$ calcd for $C_{15}H_{19}IN_7OS_2^-$ 504.0132; found

504.0138; HPLC (M_1) R_t = 12.47 min; Elemental Analysis Found C, 35.6; H, 3.9; N, 19.3. $C_{15}H_{20}IN_7OS_2$ requires C, 35.7; H, 4.0; N 19.4%

CuATSE/A-I (4.17)

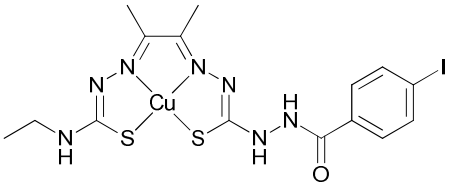

4.17 was prepared following General Procedure B, using **4.23** (60 mg, 0.12 mmol) and $Cu(OAc)_2 \cdot H_2O$ (26 mg, 0.14 mmol) to afford the desired product as a brown solid (56 mg, 74%). HRMS (ESI^-): $(M-H)^-$ calcd for $C_{15}H_{17}CuIN_7OS_2^-$ 564.9271; found 564.9278; HPLC (M_1) R_t = 12.47 min; Elemental Analysis Found C, 31.7; H, 3.2; N, 17.3. $C_{15}H_{18}CuIN_7OS_2$ requires C, 31.8; H, 3.2; N 17.3%

Tributylstannylbenzoic acid (4.24)

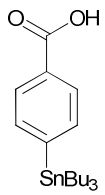

Ethyl 4-(tributylstannyl)benzoate was synthesised following a previously reported procedure.[29] Briefly, a solution of $CoBr_2$ (380 mg, 1.75 mmol), allyl chloride (200 mg, 2.62 mmol) and zinc dust (1.43g, 21.8 mmol) in acetonitrile (10mL) was stirred at room temperature, and activated by 100 µL of trifluoroacetic acid. The mixture was stirred for 5 min and the temperature increased. To this solution were added 4-ethylbromobenzoate (2.0 g, 8.7 mmol) and tributyltinchloride (3.13 g, 9.6 mmol) and the mixture was stirred for 1h. Saturated NH_4Cl solution was added for hydrolysis and the mixture was extracted with Et_2O to give the crude arylstannane. A silica short plug (pentane) gave the ethyl 4-(tributylstannyl) (3.04 g, 80%) as a colourless clear oil. ^{1}H NMR (300 MHz, DMSO-d_6): δ 7.98 (2H, d, *J* = 8.2 Hz, 2×ArC*H*), 7.56 (2H, d, *J* = 8.2 Hz, 2×ArC*H*), 4.38 (2H, q, *J* = 7.0 Hz, CH_2CH$_3$), 1.57-1.49 (6H, m), 1.42-1.27 (9H, m),1.12-1.06 (6H, m), 0.89 (9H, t, *J* = 7.0 Hz). To ethyl 4-(tributylstannyl)benzoate (1.5g, 3.4 mmol) in THF/H_2O (30 mL/20 mL) was added LiOH.H_2O (570 mg, 13.6 mmol) and the solution was heated to reflux for 20 h. After acidification with 2M HCl, the solution was extracted with Et_2O and the solvent was removed *in vacuo* to afford tributylstannylbenzoic acid (1.4 g, 99%) as a colourless oil. ^{1}H NMR (400 MHz, DMSO-d_6): δ 12.87 (1H, brs, COO*H*), 7.87 (2H, d, *J* = 7.5 Hz,

2×ArC*H*), 7.57 (2H, d, *J* = 7.5 Hz, 2×ArC*H*), 1.53-1.47 (6H, m), 1.38-1.32 (6H, m), 1.08-1.04 (6H, m), 0.89 (9H, t, *J* = 7.0 Hz); ^{13}C NMR (125.8 MHz, DMSO-d_6): δ 167.6 (C=O), 148.5 (ArC), 136.3 (Ar*C*H), 130.4 (Ar*C*), 128.3 (Ar*C*H), 28.5 (*C*H_2), 26.7 (*C*H_2), 13.52 (Sn(CH$_2$)$_3$*C*H$_3$), 9.23 (3×Sn*C*H$_2$), LRMS (ESI$^-$): (M-H)$^-$ calcd for $C_{19}H_{31}OSn^-$ 411.1; found 411.1

H_2ATSE/A-ArSnBu$_3$ (4.25)

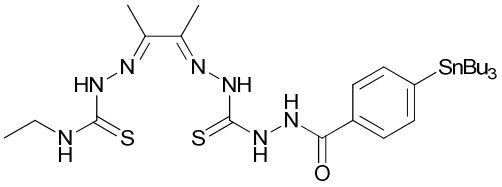

4.25 was synthesised according to General Procedure A using H_2ATSE/A (200 mg, 0.73 mmol), 4-(tributylstannyl)benzoic acid (338 mg, 0.80 mmol), diisopropylethylamine (100 mg, 0.80 mmol) and BOP (353 mg, 0.80 mmol) in DMF (4 mL). After H_2O was added the resulting suspension was sonicated, the precipitate was filtered off and washed with pentane before being dried *in vacuo* to afford **4.25** as an off-white solid (410 mg, 85%). ^{1}H NMR (400 MHz, DMSO-d_6): δ 10.65 and 10.57 (2H, br s, N*H*(C=O)Ar, NHNH(C=S)N*H*N=), 10.16 (2H, s, NHN*H*(C=S)NHN=, EtNHC=SN*H*N=), 8.45 (1H, t, *J* = 5.6 Hz, N*H*Et), 7.85 (2H, m, ArC*H*), 7.58 (2H, m, ArC*H*), 3.61 (2H, m, C*H*$_2$CH$_3$), 2.27 (3H, s, C*H*$_3$C=N), 2.24 (3H, s, C*H*$_3$C=N), 1.56-1.48 (6H, m, SnCH$_2$(C*H*$_2$)$_2$CH$_3$), 1.37-1.25 (6H, m SnCH$_2$(C*H*$_2$)$_2$CH$_3$), 1.15 (3H, t, *J* = 7.1 Hz, CH$_2$C*H*$_3$) 1.10-1.06 (6H, SnC*H*$_2$), 0.87-0.83 (6H, m, SnCH$_2$(CH$_2$)$_2$C*H*$_3$); ^{13}C NMR (101 MHz, DMSO-d_6): δ 179.8 (NHNH*C*=S), 177.5 (EtNH*C*=S), 160.3 (NHNH*C*=O), 148.0 and 146.7 (EtNH(C=S)NHN=*C*, NHNH(C=S)NHN=*C*), 136.2 (Ar*C*H), 132.6 (Ar*C*(C=O)NH), 126.7 (Ar*C*H), 38.7 ((C=S)NHC*H*$_2$), 28.6 (SnCH$_2$(*C*H$_2$)$_2$CH$_3$), 26.7 (SnCH$_2$(*C*H$_2$)$_2$CH$_3$), 14.4 (CH$_2$*C*H$_3$), 13.6 (SnCH$_2$(CH$_2$)$_2$*C*H$_3$), 11.9 (*C*H$_3$C=N), 11.7 (*C*H$_3$C=N), 9.3 (Sn*C*H$_2$(CH$_2$)$_2$CH$_3$); Ar*C*Sn not observed; HRMS (ESI$^-$): (M-H)$^-$ calcd for $C_{27}H_{46}N_7OS_2Sn^-$ 668.2235; found 668.2232; Elemental Analysis Found C, 48.6; H, 7.2; N, 14.8. 4$C_{27}H_{47}N_7OS_2Sn$ requires C, 48.5; H, 7.1; N 14.7%

CuATSE/A-SnBu$_3$ (4.26)

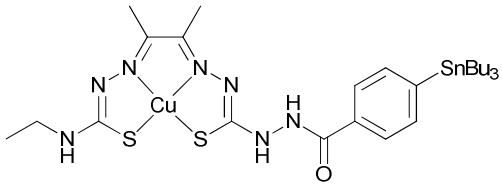

4.26 was synthesised according to General Procedure B, using H_2ATSE/A-SnBu$_3$ (80 mg, 0.12 mmol) and Cu(OAc)$_2$·H$_2$O (29 mg, 0.14 mmol) to afford the desired product as a black solid (56 mg, 76%). HRMS (ESI$^+$): (M+Na)$^+$ calcd for $C_{27}H_{45}CuN_7NaOS_2Sn^+$ 753.1333; found 753.1314; Elemental Analysis Found C, 44.6; H, 6.2; N, 13.4. $C_{27}H_{45}CuN_7OS_2Sn$ requires C, 44.4; H, 6.2; N 13.4%

H$_2$ATSMenI (4.27)

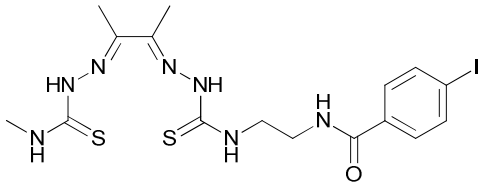

4.27 was synthesised according to General Procedure C using H_2ATSMen (200 mg, 0.69 mmol), 4-iodobenzoic acid (110 mg, 0.76 mmol), diisopropylethylamine (98 mg, 0.76 mmol) and BOP (336 mg, 0.76 mmol) in DMF (2 mL). The product was isolated as a white solid (304 mg, 85%). ^{1}H NMR (400 MHz, DMSO-*d*$_6$): δ 10.30 and 10.23 (2H, s, 2 × (C=S)-N*H*-N), 8.74 (1H, s, N*H*C=O), 8.58 (1H, s, N*H*C=S), 8.38 (N*H*C=S), 7.85 (2H, d, *J* = 8.2 Hz, 2× ArC*H(C=O)*), 7.63 (2H, d, *J* = 8.2 Hz, 2×ArC*H*), 3.75-3.74 (2H, m, C=SNHC*H*$_2$CH$_2$), 3.71-3.50 (2H, m, C=SNHCH$_2$C*H*$_2$), 3.03 (3H, d, *J* = 4.5 Hz NHC*H*$_3$), 2.22 (3H, s, C*H*$_3$C=N), 2.21 (3H, s, C*H*$_3$C=N); ^{13}C NMR (125.8 MHz, DMSO-*d*$_6$): δ 178.5 (*C*=S), 178.1 (*C*=S), 166.2 (*C*=O), 148.4 (N=*C*), 147.9 (N=*C*), 137.1 ((C=O)Ar*C*H), 133.6 (Ar*C*), 129.2 (Ar*C*H), 98.9 (Ar*C*I), 44.0 (C*H*$_2$NH(C=O)), 38.7 ((C=S)NHC*H*$_2$), 31.2 (*C*H$_3$NH), 11.7 (*C*H$_3$C=N), 11.6 (*C*H$_3$C=N); HRMS (ESI$^+$): (M+Na)$^+$ calcd for $C_{16}H_{22}IN_7NaOS_2^+$ 542.0264; found 542.0271; HPLC (M$_1$) R$_t$ = 11.8 min; Elemental Analysis found C, 36.87; H, 4.14; N, 18.94. $C_{16}H_{22}IN_7OS_2$ requires C, 37.0; H, 4.27; N 18.88%

CuATSMenI (4.18)

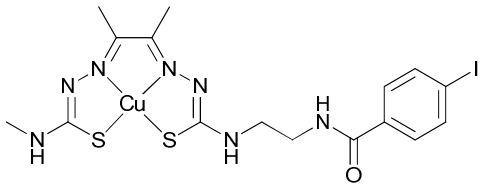

4.18 was prepared following General Procedure D, using **4.27** (60 mg, 0.116 mmol) and $Cu(OAc)_2 \cdot H_2O$ (28 mg, 0.13 mmol) to afford the desired product as a brown solid (50 mg, 74%). HRMS (ESI^+): $(M+Na)^+$ calcd for $C_{16}H_{20}CuIN_7NaOS_2^+$ 602.9404; found 602.9398; HPLC (M_1) R_t = 9.07 min; Elemental Analysis Found C, 32.93; H, 3.36; N, 16.79. $C_{16}H_{20}CuIN_7OS_2$ requires C, 33.08; H, 3.47; N 16.88%

H_2ATSMen-ArSnBu_3 (4.28)

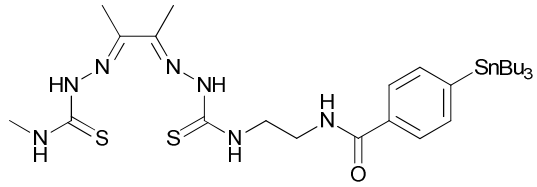

4.28 was synthesised according to General Procedure C using H_2ATSMen (200 mg, 0.69 mmol), 4-iodobenzoic acid (110 mg, 0.76 mmol), diisopropylethylamine (98 mg, 0.76 mmol) and BOP (336 mg, 0.76 mmol) in DMF (2 mL). The crude product was washed with pentane and H_2O and dried *in vacuo* to afford the desired product as a white solid (176 mg, 55%). The product was isolated in 95% purity (by HPLC) and can further be purified to >99% purity by preparative HPLC using an MeCN/H_2O gradient system. ^{1}H NMR (400 MHz, DMSO-d_6): δ 10.30 and 10.23 (2H,s, 2 × (C=S)-N*H*-N), 8.69-8.61 (2H, m, NHC=S), 8.41-8.36 (1H, m, N*H*C=O), 7.79-7.76 (2H, m, 2× ArC*H*(C=O)), 7.54-7.51 (2H, d with Sn satellites, *J* = 8.2 Hz, 2×ArC*H*Sn), 3.77-3.71 (2H, m, C=SNHCH_2CH$_2$), 3.71-3.50 (2H, m, C=SNHCH$_2$CH_2), 3.03 (3H, d, *J* = 4.5 Hz, NHCH_3), 2.25 (3H, s, CH_3C=N), 2.21 (3H, s, CH_3C=N), 1.56-1.44 (6H, m, SnCH$_2$(CH_2)$_2$CH$_3$), 1.35-1.20 (6H, m SnCH$_2$(CH_2)$_2$CH$_3$), 1.09-1.03 (6H, m, SnCH_2), 0.86-0.81 (6H, m, SnCH$_2$(CH$_2$)$_2$CH_3); ^{13}C NMR (125.8 MHz, DMSO-d_6): δ 178.5 (*C*=S), 178.1 (*C*=S), 167.3 (*C*=O), 148.4 (N=*C*), 148.0 (N=*C*), 147.0 (Ar*C*Sn), 136.1 (Ar*C*HSn), 133.8 (Ar*C*), 126.5 (Ar*C*H), 44.5 (CH_2NH(C=O)), 38.7 ((C=S)NHCH_2), 31.2 (*C*H$_3$NH), 28.57 (SnCH$_2$(*C*H$_2$)$_2$CH$_3$), 26.65 (SnCH$_2$(*C*H$_2$)$_2$CH$_3$), 13.55 (SnCH$_2$(CH$_2$)$_2$*C*H$_3$), 11.7 (*C*H$_3$C=N), 11.6 (*C*H$_3$C=N), 9.21 (Sn*C*H$_2$(CH$_2$)$_2$CH$_3$); HRMS (ESI^-): $(M-H)^-$ calcd for $C_{28}H_{48}N_7OS_2Sn^-$ 682.2391; found 682.2400; Elemental Analysis Found C,

49.4; H, 7.1; N,14.3. $C_{28}H_{49}N_7OS_2Sn$ requires C, 49.3; H, 7.2; N 14.4%

CuATSMenSnBu$_3$ (4.29)

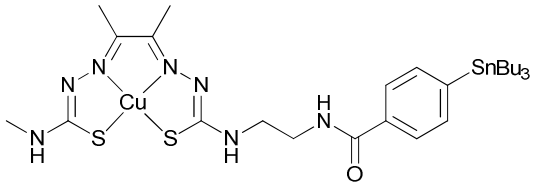

$CuATSMenSnBu_3$ was synthesised following General Procedure D, using $H_2ATSMenSnBu_3$ (80 mg, 0.12 mmol) and $Cu(OAc)_2 \cdot H_2O$ (28 mg, 0.14 mmol) to afford the desired product as a red-brown solid (68 mg, 81%). HRMS (ESI^+): $(M+Na)^+$ calcd for $C_{28}H_{47}CuN_7NaOS_2Sn^+$ 767.1490; found 767.1507; Elemental Analysis Found C, 32.4; H, 3.2; N, 17.6. $C_{28}H_{47}CuN_7OS_2Sn$ requires C, 32.6; H, 3.3; N 17.7%

4-Trimethylstannyl)benzoic acid (4.30a)[30]

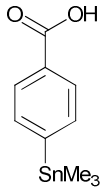

4-(Trimethylstannyl)benzoic acid was synthesised following a previously reported procedure.[30] To a round-bottom flask under nitrogen containing 4-iodobenzoic acid (1.0 g, 4 mmol) in degassed 1,4-dioxane (80 mL) were added hexamethyldistannane (2 mL, 4.8 mmol) and 20 mg bis-(triphenylphosphine)-palladium(II)-dichloride (20 mg, 0.03 mmol). The solution was stirred at 60°C for 90 min. After removal of the solvent *in vacuo* the crude mixture was purified by flash chromatography column (30×200 mm) using an EtOAc:hexane gradient (100% hexane-60% hexane:40% EtOAc) to yield 4-(trimethylstannyl)benzoic acid (1.0g, 87 %) as a white crystalline solid. ^{1}H NMR (400 MHz, DMSO-d_6): δ 8.06 (2H, d, J = 8.0 Hz, (C=O)ArCH_2), 7.64 (2H, d with Sn satellites, J = 8.0 Hz, SnArCH_2), 0.35 (9H, s with Sn satellites, SnCH_3); ^{13}C NMR (100.6 MHz, DMSO-d_6): 172.6 (*C*=O), 151.0 (Sn*C*), 135.9 (SnArCH), 129.3 and 129.0 (*C*CO_2H and Ar*C*H), -9.5 (Sn*C*H_3); LRMS ($M-H^-$) *m/z* 284.9 (calc. for $C_{10}H_{13}O_2Sn^-$ 285.0)

_N_-succinimidyl-4-(trimethylstannyl)benzoic acid (p-MeATE) (4.30)[30]

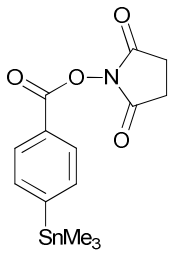

_N_-Succinimidyl 4-(trimethylstannyl)benzoic acid was synthesised following a previously reported procedure.[30] To a dry round-bottom flask containing dry acetonitrile (15 mL) was added 4-(trimethylstannyl)benzoic acid (535 mg, 1.88 mmol), pyridine (182 µL, 2.26 mmol), and di(_N_-succinimidyl) carbonate (579 mg, 2.26 mmol). The mixture was stirred for 4 h at room temperature and the solvent was removed *in vacuo*, also at room temperature. Flash column chromatography of the crude product eluted with an EtOAc:hexane gradient (80% hexane: 20% EtOAc -50% hexane:50% EtOAc) afforded _N_-succinimidyl 4-(trimethylstannyl)benzoic acid (616 mg , 86 %) as a white crystalline solid. ^{1}H NMR (400 MHz, DMSO-d_6): δ 8.06 (2H, d, J = 8.1 Hz, (C=O)ArCH_2), 7.66 (2H, d with Sn satellites, J = 8.1 Hz, SnArCH_2), 2.91 (4H, s, N(C=O)$_2$(CH$_2$)$_2$), 0.35 (9H, s with Sn satellites, SnCH_3); ^{13}C NMR (100.6 MHz, DMSO-d_6): 169.3 ((*C*=O)(CH$_2$)$_2$), 162.2 (ArC(*C*=O)), 153.05 (Sn*C*), 136.2 (SnArCH), 129.2 (Ar*C*H), 124.6 (Ar*C*(C=O)), 25.7 (*C*H$_2$) -9.5 (Sn*C*H$_3$)

d_6-Butanedione (4.31)[33]

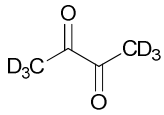

d_6-Butanedione was synthesized by adaptation of a previously reported procedure.[33] 2,3-Butanedione (12 mL) was stirred under N_2 atmosphere over anhydrous $MgSO_4$. 11 mL of the liquid was then refluxed for 48 h with 30 mL of D_2O made approximately 0.5 N with D_2SO_4. The biacetyl was then distilled out of the solution and dried. After 2 such exchanges 2.5 mL (23 %) of deuterated biacetyl were obtained. Comparative ^{1}H NMR using CH_2Br_2 as an internal standard showed 89 % of the d_6-, 9.5 % of the d_5- and 1.5 % of the d_4-deuterated species to be present. ^{1}H NMR (500 MHz, $CDCl_3$): δ 4.92 (2H, s, CH_2Br_2, *internal standard*), 2.27 (0.015H, t, J = 2.44 Hz, d_4), 2.25 (0.11 H, q, J = 2.20 Hz, d_5); ^{2}H NMR (500 MHz, $CDCl_3$): δ 2.28 (CD_3), HRMS (FI$^+$) calcd for $C_4D_6O_2$ 92.0744; found 92.0744

d_6-Diacetyl-*bis*(4-*N*-methyl-3-thiosemicarbazone) (d_6-H_2ATSM) (4.32)[31]

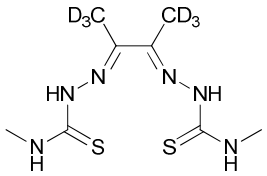

4-Methyl-3-thiosemicarbazide (1.56 g, 14.8 mmol) was dissolved in MeOD (15 mL) and d_6-butane-2,3-dione (700 µL, 7.41 mmol) and concentrated H_2SO_4 (5 drops) were added. The reaction stirred at room temperature for 16 h. The white precipitate was filtered, rinsed with water and EtOH and dried *in vacuo* to afford d_6-H_2ATSM (1.81 g, 84%) as a white solid.[32] ^{1}H NMR (300 MHz, DMSO-d_6): δ 10.20 (2H, s, NHC(S=)N*H*N=), 8.37 (2H, d, *J* = 5.8 Hz, 2 × CH_3N*H*); ^{13}C NMR (50.3 MHz, DMSO-d_6): δ 178.5 (*C*=S), 148.5 (*C*=N), 31.3 (NH*C*H_3), 11.3 (q, *C*D_3(C=N)). ^{2}H NMR (153 MHz, DMSO) δ 2.28 (m, CD_3) low intensity splitting suggest some evidence for the residual amount of protonated species, HRMS (ESI$^-$): $(M-H)^-$ calcd for $C_8H_9D_6N_6S_2^-$ 265.1182; found 265.1185; a residual signal at δ 2.14 indicates 0.1H of d_5 species

d_6-Diacetyl-*bis*(*N*4-methyl-3-thiosemicarbazonato) copper(II) (d_6-CuATSM) (4.33)

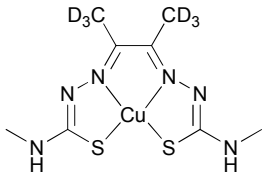

4.32 (0.50 g, 1.9 mmol) was suspended in MeOD (25 mL) and $CuOAc)_2 \cdot H_2O$ (0.42 g, 2.09 mmol) was added. The reaction was stirred at room temperature for 4 h, and the red-brown precipitate was filtered, and rinsed with MeOH and Et_2O. (0.50 g, 82%). HRMS (FI^+) $(M+H)^+$ calc. for $C_8D_6H_8CuN_6S_2$ 328.0467, found 328.0337. HPLC (M_2) R_t = 13.75 min

6.4.2 Radiochemical Synthesis

[^{18}F]4-fluorobenzaldehyde ([^{18}F]FBA) ([^{18}F]4.01)[27]

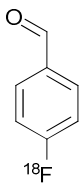

[^{18}F]4.01 was synthesised on an automated Scintomics synthesis unit by adapting a previously reported procedure. To the dry K^{18}F/Kryptofix 222 complex (2000 MBq) was added 4-formyl-*N*,*N*,*N*-trimethyl benzenaminium trifluoromethane sulfonate (12 mg) in 0.3 mL anhydrous DMSO and the reaction was heated for 15 min at 90°C. The reaction was then diluted with water (5 mL) and passed through a C-18 Sep-Pak Plus®. The cartridge was washed with H_2O (5 mL) and then eluted with MeOH (2 mL). C-18 Sep-Pak purification yielded 130 MBq

of pure [^{18}F]FBA (non-decay-corrected RCY = 10 %) in MeCN as analysed by radio-TLC (MeCN:H_2O 95:5) and radio-HPLC.

[^{18}F]- *N*-succinimidyl 4-fluorobenzoate ([^{18}F]FSB, [^{18}F]4.10)[34]

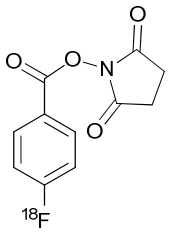

[^{18}F]4.10 was synthesised on an automated Scintomics synthesis unit from [^{18}F]FBA by adapting a previously reported procedure. To $PhI(OAc)_2$ (28 mg in 0.2 mL MeCN) was added [^{18}F]FBA in MeCN (1 mL) and *N*-hydroxy-succinimide (50 mg in 0.5 mL MeCN). The reaction was kept at 0°C for 15 min followed by 5 min at room temperature. The solution was passed onto a C-18 Semi-Prep Column for preparative HPLC (isocratic 80:20 H_2O:MeCN) and reformulation into MeCN afforded 18 MBq of [^{18}F]FSB (20% RCY non-decay corrected from [^{18}F]FBA). HPLC (RM_1) R_t = 8.9 min

[^{18}F]CuATSMenF ([^{18}F]4.03)

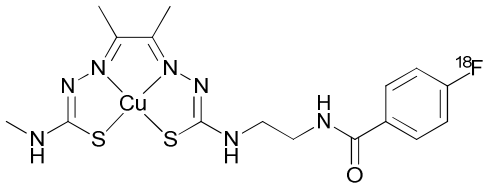

To CuATSMen (1.3 mg in 300 µL DMSO) was added [^{18}F]FSB and 4 µL of Et_3N. The reaction was stirred at 80°C for 15 min. Subsequent analysis by radio-TLC (EtOAc:MeOH 95:5) and radio-HPLC showed complete conversion of the active ester and formation of a single product. Comparison with the cold reference HPLC trace confirmed this to be [^{18}F]**4.03**. HPLC (RM_1) R_t = 8.1 min

[^{123}I]-succinimidyl-iodobenzoate ([^{123}I]SIB) ([^{123}I]4.16)

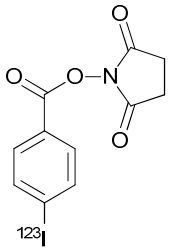

[^{123}I]**4.16** was synthesised by adaptation of a previously reported procedure.[30] Briefly, to 50 µL of 1mg mL^{-1} *p*MeATE in MeOH/AcOH (95:5) was added 50 µL MeOH/AcOH (95:5) and 10 µL $Na^{123}I$ (130-200 MBq). The stock vial was rinsed with an additional 10 µL EtOH to retrieve any remaining activity. To this was added 1 iodination bead (Pierce® Iodination Bead, Thermo Scientific) and the solution was left to stand for 15 min. The reaction was terminated by separation from the iodination bead; the solution was pulled into a syringe containing 5 mL H_2O and loaded onto a pre-conditioned C-18 Sep-pak

Light® cartridge (Waters, Milford, MA). The cartridge was washed with 3 mL H_2O and eluted with DMSO (100 µL void volume, then 500 µL DMSO containing ([^{123}I]SIB, 90-140 MBq, 70 % RCY). The product was analysed by radio-TLC (EtOAc:Hex, 1:1) and radio-HPLC. HPLC (RM_3) R_t = 14.8 min

[^{123}I]H_2ATSMenI ([^{123}I]4.27)

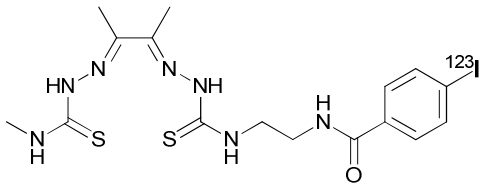

To [^{123}I]**4.16** (138 MBq) in 500 µL DMSO was added an excess of H_2ATSMen (200 µg, 20 µL of 10 mg mL^{-1} in DMSO) and the reaction was allowed to react at 45°C for 1h in a closed vessel. The reaction mixture was then purified by semi-preparative HPLC (C18 column, Discovery Sciences) using gradient Method RM_3. The fraction containing the product (61 MBq) was diluted with 3 mL H_2O and loaded onto a pre-conditioned C-18 Sep-Pak Light® and eluted with EtOH (700 µL) to afford [^{123}I]H_2ATSMenI (57 MBq, 30 % RCY from Na^{123}I). The product was analysed by radio-TLC and radio-HPLC (> 95% RCP). In addition, the product identity was confirmed by spiking an aliquot of the radiotracer with a small amount of the cold reference compound (8µg) and comparing the UV and radio-HPLC tracers. HPLC (RM_3) R_t = 15.3 min

[^{123}I]CuATSMenI ([^{123}I]4.18)

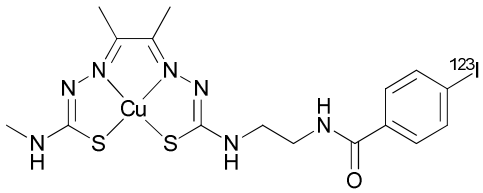

To [^{123}I]**4.16** (90 MBq, produced from 120 MBq Na^{123}I) in 500 µL DMSO was added an excess of H_2ATSMen (200 µg, 20 µL of 10 mg mL^{-1} in DMSO) and the reaction was allowed to react at 45°C for 1 h in a sealed vessel. The reaction mixture was then purified by reversed-phase, semi-preparative HPLC (C18 column, Discovery Sciences) using gradient method RM_3. To the fraction containing [^{123}I]H_2ATSMenI (48 MBq) was added 20 µL of $Cu(OAc)_2.H_2O$ (10 mg mL^{-1} in DMSO) and the solution was left to stand for 10 min before being diluted with 3 mL H_2O and loaded onto a pre-conditioned C-18 Sep-Pak light, washed with 2 mL H_2O to remove any remaining Cu^{2+} and eluted with EtOH (700 µL) to afford [^{123}I]CuATSMenI (48

MBq, 40 % RCY from $Na^{123}I$). The product was analysed by radio-TLC and radio-HPLC (> 97% RCP). In addition, the product identity was confirmed by spiking an aliquot of the radiotracer with a small amount of the cold reference compound (8 µg) and comparing the UV and radio-HPLC tracers. HPLC (RM_3) R_t = 14.5 min

**Retention times were found to vary slightly with injection volumes. Due to the similar retention times of [^{123}I]SIB and [^{123}I]H_2ATSMenI and [^{123}I]CuATSMenI, aliquots of each batch were not only spiked with the reference compound, but also with the active ester precursors to unambiguously check the compound identity before biological work. [^{123}I]SIB can clearly be distinguished from [^{123}I]H_2ATSMenI, but due to the intermediate retention time of [^{123}I]CuATSMenI, an aliquot of [^{123}I]H_2ATSMenI was analysed before proceeding to formation of the copper complex.*

[^{64}Cu]CuATSM and [^{64}Cu]**4.18** were prepared by reaction of the bis(thiosemicarbazone) ligand with [^{64}Cu]$Cu(OAc)_2$ (100-150 MBq) and reformulated into EtOH following C-18 light Sep-pak light purification. The radiochemical purity of the complexes was determined by radio-TLC on silica gel plates using ethyl acetate/methanol (95:5) as the mobile phase. The specific activity of the administered tracers was in the range of 2-5 MBq/µg of labeling precursor.

[^{64}Cu]CuATSM was prepared in 90 % isolated RCY and > 98% RCP. R_t = 11.3 min

[^{64}Cu]**4.18** was synthesised 90 % isolated RCY and >98% RCP. R_t = 14.5 min

[^{64}Cu]**4.16** and [^{64}Cu]**4.17** were prepared on a small scale (< 10 MBq) as described in section 6.3.3.1 in > 90% RCY and > 95% and > 99% RCP respectively.

6.5 Experimental details for Chapter 5

6.5.1 Synthesis

Diacetyl-*bis*(4-*N*-methyl-3-thiosemicarbazone) (H_2ATSM) (5.01a)[31]

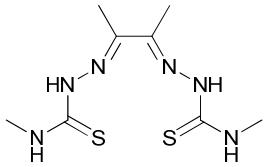

4-Methyl-3-thiosemicarbazide (1.55 g, 14.8 mmol) was dissolved in EtOH (15 mL) and butane-2,3-dione (700 µL, 7.41 mmol) and concentrated H_2SO_4 (5 drops) were added. The reaction stirred at room temperature for 16 h. The white precipitate was filtered, rinsed with water and EtOH.[32] Recrystallisation from DMSO/H_2O afforded H_2ATSM (1.70 g, 81%) as a white solid. ^{1}H NMR (300 MHz, DMSO-d_6): δ 10.26 (2H, s, NHC(S=)N*H*N=), 8.41 (2H, d, *J* = 5.8 Hz, 2 × CH_3N*H*), 2.14 (6 H, CH_3); ^{13}C NMR (50.3 MHz, DMSO-d_6): δ 178.5 (*C*=S), 148.0 (*C*=N), 31.2 (NH*C*H_3), 11.6 (*C*H_3(C=N)); LRMS (ESI+): $(M+Na)^+$ m/z 283.1 (calc. for $C_8H_{16}N_6NaS_2^+$ 283.1)

Diacetyl-*bis*(N4-methyl-3-thiosemicarbazonato) copper(II) (CuATSM) (5.01)

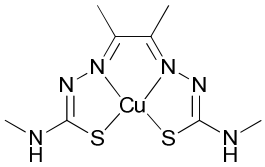

H_2ATSM (0.50 g, 1.9 mmol) was suspended in MeOH (25 mL) and $Cu(OAc)_2{\cdot}H_2O$ (0.42 g, 2.09 mmol) was added. The reaction was stirred at room temperature for 4 h, and the red-brown precipitate was filtered, and rinsed with MeOH and Et_2O. (0.50 g, 82%). LRMS (ESI^+) $(M+H)^+$ *m/z* 322.0 (calc. for $C_8H_{14}CuN_6S_2$ 322.0) $[M + H]^+$. HPLC (M_2) R_t = 13.75 min.

6.5.2 Cell culture

EMT6 and HT1080 cells were cultured obtained from ATCC and used within 6 months of resuscitation from frozen stock. Cells were grown as monolayers in Dulbecco's Modified Eagle's Medium (DMEM) (Sigma, UK) supplemented with 10% foetal bovine serum (HyClone, USA), L-glutamine (2 mM), 100 units/mL penicillin and 100 µg/mL streptomycin (all from Sigma Aldrich, UK). Cells were maintained at a temperature of 37 °C in a 5% CO_2 humidified atmosphere and

grown to ~ 95% confluence, (at which point they were split 1:10 using 2.5% Trypsin (GIBCO) at 37 °C, 5% CO_2).

The CaNT tumour is a poorly differentiated non-immunogenic mammary carcinoma, probably of mammary origin, which arose spontaneously in a female CBA/Gy mouse.[35] The CaNT tumour cell line cannot be grown *ex vivo*. Hence, single cell suspensions for *in vitro* cellular uptake assays were prepared from implanted CaNT mouse tumours by Dr Veerle Kersemans and Dr Bart Cornelissen, using a gentleMACS™ dissociator by following protocol "2.2.2- Preparation of single cell suspensions from mouse mPAC pancreatic" of the manufacturer's instructions.[36] 5mm^3 sections of tumour were transferred to gentleMACS C Tube containing 5 mL of RPMI1640. 150 µL Collagenase I and 150 µL Dispase II were added and the closed tube was incubated at 37°C for 20 min using the MACSmix Tube Rotator. Next, the gentleMACS program **m_impTumor_04** on the gentleMACS dissociator is run prior to a second 20 min incubation period. 2 µL of DNase I solution is added to the tube and the **m_impTumor_04** programme is repeated. Next, the sample is resuspended and the cell suspension is applied to a 70 µm mesh size cell strainer placed on a 50mL tube. The cell strainer is washed with 5 mL of PEB buffer and the final volume of the solution is made up to 50mL. The cell suspension is centrifuged at 300×g for 10 min and the supernatant is aspirated. Finally the cells are resuspended to the required volume of DMEM medium (supplemented as described above) for cellular uptake assays.

6.5.3 *In vitro* cellular uptake assays (% cellular associated activity)[19, 37, 38]

The apparatus and protocols used for these *in vitro* experiments are based on those previously described.[19, 37, 38] Experiments were performed on HeLa human cervical carcinoma, EMT6 mouse mammary carcinoma, HT1080 human fibrosarcoma and CaNT cell lines. EMT-6 and HT1080 cells were cultured *in vitro* and CaNT tumour cells were obtained as described above. Prior to performing *in vitro* cellular uptake assays, it was confirmed that cell viability was > 90 % using the trypan blue exclusion assay. As internalisation assays were not performed, the experiment determines the amount of cellular associated activity, but is unable to distinguish between surface bound, membrane bound or internalised activity.

A suspension of cells (15 mL, 1×10^6 cells/mL) was equilibrated in a three-necked, glass round-bottom flask at 37°C under anoxic (95% N_2, 5% CO_2) or normoxic (75% N_2, 20% O_2, 5% CO_2) conditions by passing a continuous flow of warm, humidified gas over the cells, with all remaining variables kept constant. The medium was identical to that employed in cell culture, but supplemented with only 1% fetal bovine serum. After 30 min, when the vessels had reached equilibrium (probed with an Oxford Optronics Oxylab pO_2 tissue oxygenation monitor) 0.5-1 MBq of the radiotracer was added. Samples (1 mL) were removed by use of a long needle syringe at 5, 15, 30, 45 and 60 min, and three 300-μL portions of each sample were dispensed into Eppendorf tubes. The tubes were spun to pellet the cells, and the supernatant liquid was removed. The activities of the cell pellet and of the supernatant liquid were measured with a γ-counter (Hidex Triathler). The amount of ^{64}Cu or ^{123}I activity associated with the cells (pellet) as a percentage of the total activity injected was calculated (counts pellet/(pellet + supernatant)*100) and plotted. As a control, the compounds were put through an identical experiment in the absence of cells to assess the amount of ^{64}Cu or ^{123}I activity adhering to the plastic Eppendorf tubes. This value was subtracted from each data point.

6.5.4 *In vivo* studies

All *in vivo* experimental animal work was performed by Dr Veerle Kersemans and Dr Bart Cornelissen.

6.5.4.1 Animals

Animal studies were performed in accordance with the Animals Scientific Procedures Act of 1986 (UK). Mice were maintained at 21°C with a controlled 12 h light/dark cycle in a specific-pathogen-free animal colony and water and food was available *ad lib* during the experiments.

6.5.4.2 Tumour model

Tumor and normal tissue uptake of ^{64}Cu or ^{123}I-labelled compounds was determined in female CBA mice (17-20 g) (Charles River). The murine adenocarcinoma (CaNT) tumour line cannot be grown *ex vivo* (vide infra). Fifty µL of a crude cell suspension, prepared by mechanical dissociation of an excised CaNT tumor from a donor animal, was injected. Imaging was performed when tumours had reached approximately 6-8 mm in diameter. The EMT-6 tumor model was generated as described by Lewis *et al.*[37]

6.5.4.3 Anaesthesia/Tissue oxygen modulation

Anaesthesia was induced and maintained using isoflurane in room air or in oxygen. Non-anaesthetised mice for dissection-only controls were kept in room air or in a 100% oxygen atmosphere. The hypoxic status of the tumors was confirmed using both the OxyLite probe (Oxford Optronix Ltd) and EF5 IHC as described below.

6.5.4.4 Dynamic PET imaging

PET imaging was performed using the Inveon PET/CT system (Siemens Preclinical Solutions). Mice were anaesthetised and a cannula was inserted into the lateral tail vein. Following the attenuation CT-scan, 10 MBq of ^{64}Cu-labelled compound was injected and 2 h whole-body dynamic acquisitions were performed. Throughout the imaging session, mice were maintained at

37°C and respiration rate was monitored (60-100 respirations/min). Image analysis was performed using the Inveon Research Workplace software (IRW, version 2.2).

6.5.4.5 Dynamic SPECT imaging

Planar SPECT imaging was performed using the nanoSPECT/CT system (Bioscan) equipped with an Ultra High Resolution (UHR) parallel hole collimator. Anaesthesia was induced, 4 mice were placed simultaneously on the collimator and a cannula was inserted into their lateral tail vein. Ten MBq of [^{123}I]CuATSMenI or [^{123}I]H_2ATSMenI was injected immediately after the 2 h whole-body dynamic scans were initiated. ROI image analysis was performed using ImageJ. Subsequently, for visualisation purposes only, one representative mouse was sacrificed to perform 3D high resolution SPECT/CT imaging (9x1 mm pinhole apertures, 100,000 counts/projection, 24 projections and a pitch of 1.5). CT was conducted for anatomical referencing. Reconstruction of both CT and SPECT images was achieved using InVivoScope (version 1.42).

6.5.4.6 Dissections

Immediately following imaging, mice were sacrificed and organs, tissues and tumor were removed, washed and weighed. The blood was collected and weighed. The radioactivity of the samples was counted using an auto gamma-counting system (Wizard, Perkin Elmer). The amount of radioactivity in the organs and tissues was calculated as percentage of the injected dose per gram (%ID/g).

$$\%ID/g = [(activity_{tissue})/(weight_{tissue} \times activity_{injected})*100]$$

In order to avoid confounding effects of anaesthesia, dissection experiments were repeated in awake non-imaging mice.

6.5.4.7 Autoradiography and immunohistochemistry (IHC)

Tumour hypoxia was confirmed by immunohistological staining for EF5 (2-(2-nitro-1*H*-imidazol-1-yl)-*N*-(2,2,3,3,3-pentafluoropropyl)acetamide). For EF5 studies, mice were administered with 10 mM EF5 in 0.9% saline i.v. 2 h prior to tumour excision (EF5 was obtained from Dr. Cameron Koch, University of Pennsylvania, PA). The same tumour slice was used for autoradiography and EF5 IHC.[39] Tumour Sections were stored in 1% paraformaldehyde at 4ºC and images were acquired within 2 days of staining. Fluorescence detection was performed at x10 magnification with an upright motorised Nikon Eclipse 90i system (Nikon, UK), fitted with a motorised stage and equipped with cooled charge-coupled Hamamatsu ORCA-ER camera and acquisition software.

The spatial correlation of ^{64}Cu activity distribution and EF5 was quantified by co-registering autoradiography and fluorescence microscopy images using a rigid transformation based on a set of manually defined landmarks. Landmark placement was facilitated by a custom written matlab interface provided by Dr Danny Allen. The resulting image transformation was applied using the standard matlab functions 'cp2tform' and 'imtransform'." Correlation coefficients (r) were derived by using the JACoP plug-in for Image J (methods of Manders for spatial intensity correlation analysis and Costes for automatic thresholding).[40]

6.5.5 Stability studies

***In vitro* stability studies**

Samples of non-tumour-bearing CBA mouse blood were collected by heart puncture into heparin-coated vials. Aliquots of 500-800 µL of blood were incubated with 0.2-0.5 MBq of the required ^{64}Cu-copper complex at 37°C for 5-120 min. To determine the amount of intact complex, samples were analysed using octanol extraction, as described below. In some cases, vials were centrifuged to obtain plasma. *In vitro* plasma incubation experiments were carried out as previously described.[19, 38, 41] Briefly, 0.5 MBq of the required ^{64}Cu-labelled copper complex was incubated with 500 µL fresh mouse plasma at 37°C for 5-120 min. To determine the amount and species of

protein-bound $^{64}Cu/^{123}I$, 50 µL aliquots were withdrawn from the serum at various time-points and analysed using ethanol extraction/precipitation, as described below.

***In vivo* stability studies**

Female, non-tumour-bearing CBA mice were injected intravenously with 1-2 MBq of the required ^{64}Cu- or ^{123}I-labelled copper complex. 500-800 µL of blood was collected by heart puncture into heparin-coated vials at various time points after injection (n = 2 per time point). Whole blood was analysed by octanol extraction as described below. In order to analyse the species in the plasma, the vials were spun (4000 rpm, 4°C, 5 min) and the supernatant (serum) was isolated and analysed using ethanol extraction, as described below.

6.5.5.1 Protein binding and stability (ethanol extraction)

Aliquots of 50 µL serum were added to 200 µL ethanol to precipitate proteins. The mixture was centrifuged until formation of a protein pellet and the supernatant was removed. The pellet was washed with 200 µL ethanol and re-centrifuged. The combined supernatants and the pellet were counted in a γ-counter to determine the percentage of protein bound activity. The supernatant was further analysed by radio-TLC (95:5 EtOAc/MeOH) or radio-HPLC to determine the amount of intact ^{64}Cu-copper complex and ^{123}I-copper complex/ligand present and detect the presence of metabolites. Digital autoradiography was performed on developed radio-TLC using super resolution phosphor screens (Type SR, Perkin Elmer) and a CyclonePlus phosphor imager (PerkinElmer).

6.5.5.2 Stability in blood (octanol extraction)

Octanol extraction methods were based on those previously described.[42, 43] To determine the amount of intact, octanol-extractable compound, 50 µL of whole blood was immediately added to 750 µL of octanol and vortexed for 1 min. The mixture was centrifuged (14,000 rpm, 5 min), the octanol phase aspirated and the octanol and pellet were counted in a γ-counter. The percentage of octanol-extractable activity, i.e. the amount of intact ^{64}Cu-copper complex or ^{123}I-complex/ligand

was determined. The octanol phase was further analysed by radio-TLC (95:5 EtOAc/MeOH) to confirm that the extractable activity was in the form of ^{64}Cu-copper complex or ^{123}I-complex/ligand. Developed TLC plates were processed as above.

6.6 References for Chapter 6

1. H. E. Gottlieb, V. Kotlyar and A. Nudelman, *J. Org. Chem.*, 1997, **62**, 7512-7515.
2. N. G. Tsierkezos, *J. Solution Chem.*, 2007, **36**, 289-302.
3. S. R. Jacob, Q. Hong, B. A. Coles and R. G. Compton, *J. Phys. Chem. B*, 1999, **103**, 2963-2969.
4. P. Burke, O. Golovko, J. C. Clark and F. I. Aigbirhio, *Inorg. Chim. Acta*, 2010, **363**, 1316-1319.
5. J. P. Holland, F. I. Aigbirhio, H. M. Betts, P. D. Bonnitcha, P. Burke, M. Christlieb, G. C. Churchill, A. R. Cowley, J. R. Dilworth, P. S. Donnelly, J. C. Green, J. M. Peach, S. R. Vasudevan and J. E. Warren, *Inorg. Chem.*, 2007, **46**, 465-485.
6. S.-A. Poulsen, *J. Am. Soc. Mass Spectrom.*, 2006, **17**, 1074-1080.
7. J. Cosier and A. M. Glazer, *J. Appl. Crystallogr.*, 1986, **19**, 105-107.
8. Z. Otwinowski and W. Minor, *Methods Enzymol.*, 1997, **276**, 307-326.
9. L. Palatinus and G. Chapuis, *J. Appl. Crystallogr.*, 2007, **40**, 786-790.
10. P. W. Betteridge, J. R. Carruthers, R. I. Cooper, K. Prout and D. J. Watkin, *J. Appl. Crystallogr.*, 2003, **36**, 1487.
11. R. I. Cooper, A. L. Thompson and D. J. Watkin, *J. Appl. Crystallogr.*, 2010, **43**, 1100-1107.
12. P. Vandersluis and A. L. Spek, *Acta Crystallographica Section A*, 1990, **46**, 194-201.
13. A. L. Spek, *J. Appl. Crystallogr.*, 2003, **36**, 7-13.
14. A. L. Spek, Utrech, The Netherlands, Editon edn., 1998.
15. V. Maes, E. Garcia-Garayoa, P. Blaeuenstein and D. Tourwe, *J. Med. Chem.*, 2006, **49**, 1833-1836.
16. E. Garcia Garayoa, C. Schweinsberg, V. Maes, D. Ruegg, A. Blanc, P. Blauenstein, D. A. Tourwe, A. G. Beck-Sickinger and P. A. Schubiger, *Q. J. Nucl. Med. Mol. Imaging*, 2007, **51**, 42-50.
17. E. Garcia Garayoa, D. Ruegg, P. Blauenstein, M. Zwimpfer, I. U. Khan, V. Maes, A. Blanc, A. G. Beck-Sickinger, D. A. Tourwe and P. A. Schubiger, *Nucl. Med. Biol.*, 2007, **34**, 17-28.
18. R. Tavare, R. Torres Martin De Rosales, P. J. Blower and G. E. D. Mullen, *Bioconjugate Chem.*, 2009, **20**, 2071-2081.
19. P. D. Bonnitcha, A. L. Vavere, J. S. Lewis and J. R. Dilworth, *J. Med. Chem.*, 2008, **51**, 2985-2991.
20. R. Hueting, M. Christlieb, J. R. Dilworth, E. G. Garayoa, V. Gouverneur, M. W. Jones, V. Maes, R. Schibli, X. Sun and D. A. Tourwe, *Dalton Trans.*, 2010, **39**, 3620-3632.
21. C. Dardonville, C. Fernandez-Fernandez, S.-L. Gibbons, G. J. Ryan, N. Jagerovic, A. M. Gabilondo, J. J. Meana and L. F. Callado, *Bioorg. Med. Chem.*, 2006, **14**, 6570-6580.
22. P. D. Bonnitcha, S. R. Bayly, M. B. M. Theobald, H. M. Betts, J. S. Lewis and J. R. Dilworth, *J. Inorg. Biochem.*, 2010, **104**, 126-135.
23. M. B. M. Theobald, DPhil Thesis, University of Oxford, 2010.
24. V. Azarian, A. Gangloff, Y. Seimbille, S. Delaloye, J. Czernin, M. E. Phelps and D. H. S. Silverman, *J. Labelled Compd. Radiopharm.*, 2006, **49**, 269-283.
25. S. Guhlke, H. H. Coenen and G. Stoecklin, *Appl. Radiat. Isot.*, 1994, **45**, 715-727.
26. R. Bejot, A. M. Elizarov, E. Ball, J. Zhang, R. Miraghaie, H. C. Kolb and V. Gouverneur, *J. Labelled Compd. Radiopharm.*, 2011, **54**, 117-122.
27. G. Vaidyanathan and M. R. Zalutsky, *Nat. Protoc.*, 2006, **1**, 1655-1661.
28. B. Dekker, H. Keen, D. Shaw, L. Disley, D. Hastings, J. Hadfield, A. Reader, D. Allan, P. Julyan, A. Watson and J. Zweit, *Nucl. Med. Biol.*, 2005, **32**, 403-413.
29. C. Gosmini and J. Perichon, *Org. Biomol. Chem.*, 2005, **3**, 216-217.
30. J. Koziorowski, C. Henssen and R. Weinreich, *Appl. Radiat. Isot.*, 1998, **49**, 955-959.
31. H. M. Betts, DPhil Thesis, University of Oxford, 2009.
32. M. Christlieb and J. R. Dilworth, *Chem.--Eur. J.*, 2006, **12**, 6194-6206.
33. J. R. Durig, S. E. Hannum and S. C. Brown, *J. Phys. Chem.*, 1971, **75**, 1946-1956.

34. M. Glaser, E. Arstad, S. K. Luthra and E. G. Robins, *J. Labelled Compd. Radiopharm.*, 2009, **52**, 327-330.
35. H. B. Hewitt, E. Blake and E. H. Proter, *Br. J. Cancer*, 1973, **28**, 123-135.
36. MACS and M. Biotec, *The gentleMACS Dissociator- Preparation of single cell suspensions from implanted mouse tumours*, Accessed 21st February, 2011.
37. J. S. Lewis, D. W. McCarthy, T. J. McCarthy, Y. Fujibayashi and M. J. Welch, *J. Nucl. Med.*, 1999, **40**, 177-183.
38. S. R. Bayly, R. C. King, D. J. Honess, P. J. Barnard, H. M. Betts, J. P. Holland, R. Hueting, P. D. Bonnitcha, J. R. Dilworth, F. I. Aigbirhio and M. Christlieb, *J. Nucl. Med.*, 2008, **49**, 1862-1868.
39. J. Lee, D. W. Siemann, C. J. Koch and E. M. Lord, *Int. J. Cancer*, 1996, **67**, 372-378.
40. S. Bolte and F. P. Cordelieres, *J. Microsc.*, 2006, **224**, 213-232.
41. P. McQuade, K. E. Martin, T. C. Castle, M. J. Went, P. J. Blower, M. J. Welch and J. S. Lewis, *Nucl. Med. Biol.*, 2005, **32**, 147-156.
42. C. J. Mathias, S. R. Bergmann and M. A. Green, *Nucl. Med. Biol.*, 1993, **20**, 343-349.
43. S. Lewis Jason, P. Herrero, L. Sharp Terry, A. Engelbach John, Y. Fujibayashi, R. Laforest, A. Kovacs, J. Gropler Robert and J. Welch Michael, *J. Nucl. Med.*, 2002, **43**, 1557-1569.

Appendix

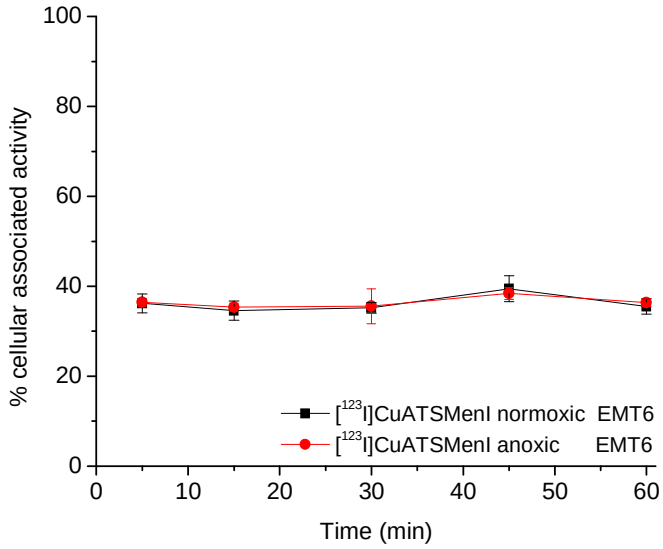

Figure A1 Percentage cellular associated activity of [^{123}I]CuATSMenI in EMT6 cells over time, incubated either under normoxic (21% O_2, 5% CO_2, balance N_2) or anoxic (5% CO_2, balance N_2) conditions. Errors (standard deviation) are within symbols if not indicated.

%ID/g	[^{64}Cu]CuATSM imaging (air)	[^{64}Cu]CuATSMenI imaging (air)	[^{123}I]CuATSMenI imaging (air)	[^{123}I]H_2ATSMenI imaging (air)	[^{64}Cu]Cu^{2+} imaging (air)
Blood	0.73±0.05	0.68±0.08	1.1±0.86	1.31±0.05	0.66±0.04
Tumour	1.41±0.10	1.44±0.12	0.69±0.50	0.50±0.05	1.33±0.09
Muscle	0.29±0.07	0.20±0.01	0.30±0.25	0.34±0.00	0.26±0.04
Stomach	5.97±1.49	4.12±0.53	1.40±3.82	1.49±0.59	7.11±6.26
Small intest.	9.19±1.18	14.11±0.87	12.23±14.74	0.78±0.03	5.38±0.33
Large intest.	3.92±0.47	3.31±0.42	2.38±3.81	0.99±0.30	3.59±0.87
Fat	0.45±0.06	0.42±0.03	0.54±0.61	0.59±0.06	0.36±0.09
Spleen	1.53±0.21	1.25±0.08	3.02±3.60	0.88±0.02	3.03±1.57
Liver	10.03±1.02	7.69±0.81	8.59±7.66	0.83±0.08	8.44±1.07
Kidneys	6.03±0.66	4.55±0.45	3.32±2.90	2.59±0.46	5.01±0.98
Heart	1.28±0.11	0.98±0.10	0.95±0.76	1.01±0.02	0.97±0.09
Lungs	5.49±0.56	5.16±1.13	2.20±1.26	1.43±0.15	5.28±0.62
Thyroid	-		0.57±0.50	0.59±0.02	-
Ratio T/M	5.14±1.30	7.13±0.46	2.27±2.00	1.49±0.14	5.16±0.66

Table A1 Biodistribution data (%ID/g ±SD) of [^{64}Cu]CuATSM (n=4), [^{64}Cu]Cu^{2+} (n=3), [^{64}Cu]CuATSMenI (n=4), [^{123}I]CuATSMenI (n=2), [^{123}I]H_2ATSMenI (n=2), at 120 min p.i. in female CBA mice bearing CaNT tumors that were anaesthetised with isofluorane/air for 120 min dynamic PET/SPECT imaging sessions.

%ID/g	[^{64}Cu]CuATSM imaging (air)	[^{64}Cu]CuATSM dissection (air)	[^{64}Cu]Cu^{2+} imaging (air)	[^{64}Cu]Cu^{2+} dissection (air)
Blood	0.52±0.05	0.77±0.06	0.58±0.03	0.89±0.09
Tumour	1.00±0.05	2.37±0.18	1.42±0.20	2.04±0.13
Muscle	0.19±0.01	0.24±0.01	0.23±0.02	0.26±0.02
Stomach	3.91±0.45	4.05±1.12	6.73±0.53	3.47±0.43
Small intestine	7.72±0.48	4.64±0.54	6.63±0.73	4.93±0.21
Large intestine	3.14±0.24	10.55±1.07	4.28±0.66	5.73±0.65
Fat	0.26±0.02	0.23±0.03	0.40±0.07	0.18±0.02
Spleen	1.38±0.05	1.32±0.16	1.18±0.15	1.60±0.21
Liver	10.40±1.36	6.63±0.29	9.73±1.32	8.46±0.55
Kidneys	5.16±0.42	4.19±0.54	6.00±1.01	5.12±0.60
Heart	1.05±0.09	1.32±0.05	1.01±0.10	1.73±0.17
Lungs	4.76±0.34	4.90±0.45	5.18±0.41	5.34±0.57
RTM	5.30±0.57	9.76±0.63	6.27±0.96	7.90±0.77

Table A2 Biodistribution data (%ID/g ±SD) of [^{64}Cu]CuATSM (n=4 imaging, n=4 dissection) and [^{64}Cu]Cu^{2+} (n=4 imaging, n=6 dissection) at 120 min p.i. in female CBA mice bearing EMT6 tumours that were anaesthetised with isofluorane/air (imaging) or breathing room air (dissection) for 120 min p.i.

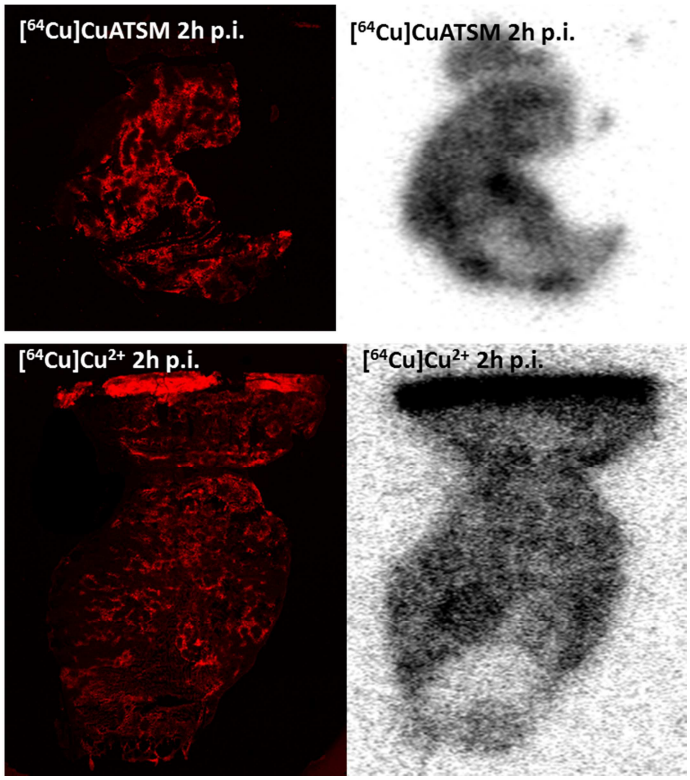

Figure A2 Representative images of ^{64}Cu activity distribution and hypoxia in CaNT tumors for [^{64}Cu]CuATSM and [^{64}Cu]Cu^{2+} at 2 h p.i., as measured by autoradiography and EF5 immunostaining. Autoradiography (right) and EF5 immunostaining (left) were performed on the same section. EF5 stained

hypoxic areas are indicated by red, high intensity in autoradiographs is indicated by dark areas. The spatial correlation coefficients between autoradiography and EF5 staining images are reported in Chapter 5.

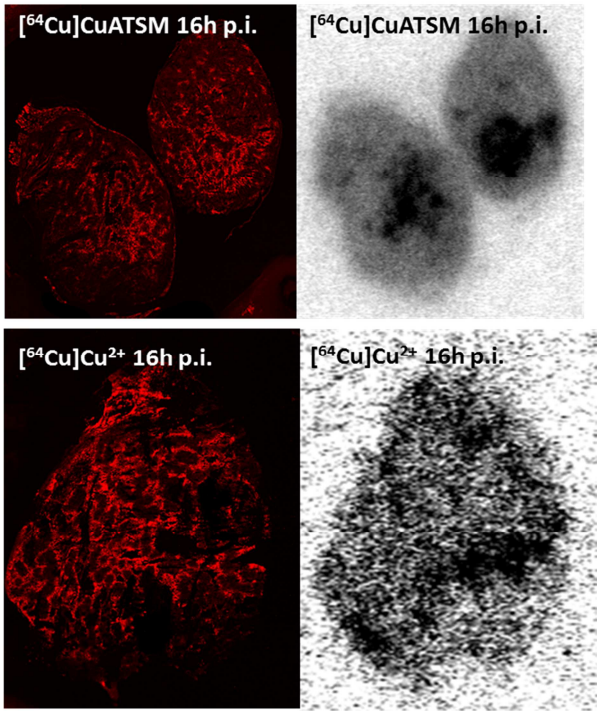

Figure A3 Representative images of ^{64}Cu activity distribution and hypoxia in CaNT tumours for [^{64}Cu]CuATSM and [^{64}Cu]Cu^{2+} at 16 h p.i., as measured by autoradiography and EF5 immunostaining. Autoradiography (right) and EF5 immunostaining (left) were performed on the same section.